UNIVERSITY OF CALIFORNIA,
IRVINE

Assembly and Coassembly of Peptides Derived from β-Sheet Regions of β-Amyloid

DISSERTATION

submitted in partial satisfaction of the requirements
for the degree of

DOCTOR OF PHILOSOPHY

in Chemistry

by

Nicholas L. Truex

Dissertation Committee:

Professor James S. Nowick, Chair

Professor Greg Weiss

Professor Robert Spitale

2017

DEDICATION

In memory of my mother,

Michelle L. Truex

TABLE OF CONTENTS

LIST OF FIGURES

LIST OF TABLES

Page

ACKNOWLEDGMENTS

I would like to start by expressing my deep gratitude to my advisor, Professor James S. Nowick. I truly appreciate his selfless devotion to my education in a wide variety of scientific areas, including organic chemistry, amyloid biochemistry, and complex equilibria, and to my training in ^{1}H NMR spectroscopy, X-ray crystallography, and numerous biophysical techniques. I also really appreciate how much I learned during our writing meetings while working on manuscripts, and I am particularly fond of the many imaginative conversations we had during those meetings. Without his incredible training and creative input, the research described in this dissertation would not have been possible.

I would like to thank the faculty and staff at UC Irvine, who have also been a major part of my Ph.D. education and training. In particular, I would like to thank Dr. Phil Dennison and Professor Melanie Cocco for their assistance with NMR spectroscopy and for their friendship throughout my graduate career. I would also like to thank the other members of my thesis committee, Professors Greg Weiss and Rob Spitale. I really appreciate their commitment to my degree.

I would like to thank my colleagues in the Nowick laboratory–both past and present–for fostering an intellectually stimulating research environment over the past five years. I am particularly grateful to the three students who joined the Nowick lab in the same year as me, Yilin Wang, Adam Kreutzer, and Kevin Chen. In addition, I am thankful for the guidance and friendship from former student, Pin-Nan Cheng. I am also thankful for the helpful assistance with my projects from undergraduate students Katie Ferrick and Khalil Bassam.

I would like to thank my family for their love and support, my mother and father, Lew and Michelle, and my three siblings, Bethany, Alexandria, and Gabe. I am very thankful we have stayed close to each other, even though we have barely seen each other over the last 10 years. I am also thankful for how we have managed to continue to live on, even after the passing of our dear mother.

I would finally like to thank my fiancé, Winny Oo, for being patient with my work schedule and for believing in me when I did not. I am profoundly moved by her continued love and support. She has filled my life with so much joy throughout these past three years that we have known each other.

CURRICULUM VITAE

Department of Chemistry
University of California, Irvine
1102 Natural Sciences II
Irvine, CA 92697-2025

E-mail: nltruex@gmail.com
Tel: (317) 372-5786

EDUCATION

Ph.D., Chemistry, University of California, Irvine	2012 – 2017
B.S., Chemistry, Purdue University	2007 – 2011

RESEARCH EXPERIENCE

Graduate Student with Professor James S. Nowick, U.C. Irvine	2012 – 2017
Undergraduate Researcher with Professor Ei-ichi Negishi, Purdue	2008 – 2012
Summer Intern, Eli Lilly and Company	2008 – 2010

PUBLICATIONS (an asterisk * indicates the corresponding author)

7. Wang, Y.; **Truex, N.L.**; Nowick, J.S.* Effects of Charge and Hydrophobicity on the Oligomerization of a Peptide Derived from IAPP. *Bioorganic Med. Chem.* **2017**, DOI: 10.1016/j.bmc.2017.10.001.

6. **Truex, N.L.**; Nowick, J.S.* Transmembrane Proteins: Amyloids Hidden in Plain Sight? *Biochemistry*, **2017**, 56, 4735–4736.

5. Wang, Y.; Kreutzer, A.G.; **Truex, N.L.**; Nowick, J.S.* A Tetramer Derived from Islet Amyloid Polypeptide. *J. Org. Chem.* **2017**, *82*, 7905–7912.

4. **Truex, N.L.**; Nowick, J.S.* Coassembly of Peptides Derived from β-Sheet Regions of β-Amyloid. *J. Am. Chem. Soc.* **2016**, *138*, 13891–13900.

3. **Truex, N.L.**; Wang, Y.; Nowick, J.S.* Assembly of Peptides Derived from β-Sheet Regions of β-Amyloid. *J. Am. Chem. Soc.* **2016**, *138*, 13882–13890.

2. Yoo, S.; Kreutzer, A.G.; **Truex, N.L.**; Nowick, J.S.* Square Channels formed by a peptide derived from transthyretin. *Chem. Sci.* **2016**, *7*, 6946–6951.

1. Xu, S.; **Truex, N.L.**; Swathi, M.; Negishi, E.-I.* Pd-Catalyzed Cross-Coupling Reactions Exhibiting Catalyst Turnover Numbers Exceeding One Million. *Arkivoc* **2012**, *7*, 242.

CONFERENCE PRESENTATIONS (an underline indicates the presenter)

6. "Assembly and Coassembly of Peptides Derived from β-Sheet Regions of β-Amyloid" **Truex, N.L.**; Wang, Y.; Nowick, J.S. Presented at the 2016 Graduate Research Symposium of the ACS Division of Organic Chemistry, Bryn Mawr, PA, July 28–31, 2016.

5. "Effect of Hydrophobicity and Charge in the Oligomerization of Amyloidogenic Peptides and the Design of a pH-Switchable Oligomer" Wang, Y.; **Truex, N.L.**; Wali, H.A.M.; Nowick, J.S. Presented at the 45th Western Regional Meeting of the American Chemical Society, San Marcos, CA, November 6–8, 2015.

4. "A β-Hairpin Derived from Transthyretin 106–121 that Forms Square Hydrophobic Channels" Yoo, S.; **Truex, N.L.**; Kreutzer, A.G.; Nowick, J.S. Presented at the 45th Western Regional Meeting of the American Chemical Society, San Marcos, CA, November 6–8, 2015.

3. "Mimicry and Study of Amyloidogenic Peptides with Macrocyclic β-Sheet Models" Ferrick, K.R.; **Truex, N.L.**; Nowick, J.S. Presented at the 44th National Organic Chemistry Symposium, Philadelphia, PA, June 28–July 2, 2015; paper T41.

2. "Assembly of Peptides Derived from the Central and C-Terminal Regions of β-Amyloid" **Truex, N.L.**; Nowick, J.S. Presented at the 2015 Data Science Initiative Summer Fellows Program, Irvine, CA, May 29, 2015.

1. "Molecular Recognition between Chemical Models of β-Amyloid Peptides." **Truex, N.L.**; Wang, Y.; Dong, V.; Nowick, J.S. 2013. Presented at the 246th National Meeting of the American Chemical Society, Indianapolis, IN, September 8–12, 2013.

EXPERIMENTAL SKILLS

Peptide Synthesis, Organic Synthesis, Organometallic Synthesis, NMR Spectroscopy, Mass Spectrometry, HPLC Chromatography, Circular Dichroism (CD), Infrared Spectroscopy (IR), UV-Vis Spectroscopy, Dynamic Light Scattering (DLS), SDS-PAGE, Analytical Ultracentrifugation.

TEACHING EXPERINCE

Teaching Assistant, Department of Chemistry, University of California, Irvine

Chem 1C, General Chemistry	2017
Chem 51B, Organic Chemistry	2015
Chem 203, Organic Spectroscopy (Graduate Course)	2014, 2015
Chem 51C, Organic Chemistry	2014, 2015
Chem 1LD, Organic Chemistry Laboratory	2014
Chem 51LB, Organic Chemistry Laboratory	2014
Chem 52LA, Honors Organic Chemistry Laboratory	2013
Chem 193, CalTeach Research Methods	2013
Chem 1C, General Chemistry	2012, 2013

Get FIT! Faculty in Training Program with Associate Professor Suzanne A. Blum

Chem 203, Organic Spectroscopy (Graduate Course)	2014

HONORS AND AWARDS

Allergan Graduate Fellowship	2016
Michael Zach Award	2016 – 2017
In recognition of the most promising future faculty member at UC Irvine on the basis of research and teaching.	
Regents' Dissertation Fellowship Award	2017

DEPARTMENT CONTRIBUTIONS

NMR Facility Fellow	2016

PROFESSIONAL AFFILIATIONS

American Chemical Society, member	2013 – 2017

ABSTRACT OF THE DISSERTATION

Assembly and Coassembly of Peptides Derived from β-Sheet Regions of β-Amyloid

By

Nicholas L. Truex

Doctor of Philosophy in Chemistry

University of California, Irvine, 2017

Professor James S. Nowick, Chair

Interactions among β-sheets are critical in driving the aggregation of the β-amyloid peptide (Aβ) to form oligomers and fibrils in Alzheimer's disease. Two main regions of this 40- or 42-residue peptide are known to adopt β-sheet structure and promote aggregation: the central region and the C-terminal region. The central region comprises the hydrophobic pentapeptide LVFFA ($A\beta_{17–23}$), and the C-terminal region comprises the hydrophobic undecapeptide AIIGLMVGGVV ($A\beta_{30–40}$) or the hydrophobic tridecapeptide AIIGLMVGGVVIA ($A\beta_{30–42}$). This dissertation is devoted to studies of the assembly and coassembly of peptides derived from the central and C-terminal regions of Aβ, which are critical in the formation of oligomers and fibrils in Alzheimer's disease pathology.

Chapters 2 and 3 of this dissertation describe a two-part investigation of peptides derived from the central and C-terminal regions of Aβ. The first part, called "Assembly of Peptides Derived from β-Sheet Regions of β- Amyloid", introduces two macrocyclic β-sheet peptides that contain residues 17–23 (LVFFAED) from the central region and residues 30–36 from the C-terminal region, and elucidates how each peptide self-assembles in aqueous solution. ^{1}H NMR spectroscopy shows that the peptides assemble to form tetramers. Incorporation of a single isotopic label into each peptide and ^{15}N-edited NMR spectroscopy facilitated the identification and quantification of the monomers

and tetramers. Molecular modeling further elucidates the structures of the tetramers. These studies provide insights into the peptide interactions and supramolecular assembly of an important peptide in an important amyloid disease.

The second part, called "Coassembly of Peptides Derived from β-Sheet Regions of β-Amyloid", asks how the macrocyclic β-sheet peptides coassemble upon mixing. This question is important because the two regions generally segregate in most fibril structures of Aβ but coassemble in the oligomers. The two macrocyclic β-sheet peptides form a complex mixture homotetramers and heterotetramers upon mixing. ^{15}N-Editted NMR spectroscopy shows that three heterotetramers form in addition to the homotetramers. Job's method of continuous variation and nonlinear least-squares fitting to help establish the identity of each heterotetramer, and also reveal a surprising preference for one particular heterotetramer. These studies illustrate the role of molecular recognition in amyloid assembly and push the boundaries for experimental studies involving complex supramolecular equilibria.

For the remainder of this dissertation, the focus of the research shifts to a study on macrocyclic β-sheets that contain *N*-methyl blocking groups, rather than Hao. These studies were intended to conclude ongoing efforts to characterize analogues of peptides derived from $A\beta_{17–36}$. These analogues were studied by X-ray crystallography and ^{1}H NMR spectroscopy, and also with biophysical and biological techniques. DOSY NMR studies revealed these peptides oligomerize in solution, which have not been observed previously by other biophysical techniques. Additional NMR experiments, and corroboratory analytical ultracentrifugation studies, are needed to further establish this finding. These studies show that evaluating the oligomers N-methyl peptides is possible by ^{1}H NMR spectroscopy. These efforts to correlate solution-phase biophysical techniques with ^{1}H NMR spectroscopy may prove useful to other members the Nowick lab.

CHAPTER 1

An Overview of using Chemical Model Systems to Study Amyloid Aggregation

INTRODUCTION

In this chapter, I attempt to give a literature summary of research that has helped inspire this dissertation. Although the following chapters contain their own research summaries, the current chapter provides wider context. The topics discussed in this chapter are divided into five sections. The first section gives a broad overview of peptide and protein aggregation in amyloid diseases, which is followed by a similar section that focuses primarily on the aggregation of the β-amyloid peptide (Aβ) in the pathology of Alzheimer's disease. The third section introduces chemical model systems derived from amyloidogenic peptides and proteins, and explains advantages in studying these model systems. The fourth section introduces the chemical model systems that are studied in the following chapters of this dissertation, which are called macrocyclic β-sheet peptides. The concluding section describes several discoveries that I made during the first year of my graduate studies at UC Irvine and provides context for the studies described in the following chapters of this dissertation.

1. PEPTIDE AND PROTEIN AGGREGATION IN AMYLOID DISEASES

Amyloid aggregation is the unifying theme of all amyloidogenic diseases, and is emerging as an important part of the protein energy landscape.[1,2,3] Over 60 peptides or proteins have been identified thus far that can aggregate to form amyloid oligomers and fibrils. Many of these amyloids are important in the pathology of amyloid diseases, such as β-amyloid (Aβ) in Alzheimer's disease, α-synuclein in Parkinson's disease, and hIAPP in type II diabetes.[1,3] Other amyloids appear to have vital biological roles. A growing body of work suggests that amyloids are important in protein storage, cell-to-cell communication, and biofilm formation.[1,4] As additional new amyloids are identified and characterized, other important properties will undoubtedly be discovered.

Characterizing the structures of amyloid oligomers and fibrils is the bedrock for elucidating their roles in biology and disease.[1,5] The structures of many amyloid fibrils have been established by solid-state NMR spectroscopy, and more recently by cryo-electron microscopy, for several full-length amyloidogenic peptides or proteins, including $A\beta_{1-40}$,[6,7,8] $A\beta_{1-42}$,[9,10,11,12] hIAPP,[13] α-synuclein,[14] and Tau.[15] These fibrils are typically composed of parallel β-sheets that assemble in an elongated fashion, and then twist together. Although amyloid fibrils are generally nontoxic aggregates, fibril formation usually results in the loss of function of the peptide or protein involved.

Amyloid oligomers formed by most peptides and proteins are damaging to cells, regardless of whether the corresponding protein is associated with the pathology of a known disease.[3] Oligomerization results in a heterogeneous mixture of intermediates that are difficult to characterize by high-resolution techniques, such as NMR spectroscopy or X-ray crystallography. Most efforts to characterize the oligomers have focused on evaluating their size and secondary structure, which have offered little information on their high-resolution structures. At this time, a high-resolution structure has not been determined for any oligomer of a full-length amyloidogenic peptide or protein. As a result, little is known about the precise roles of the oligomers in amyloid diseases.

2. Aβ AGGREGATION IN ALZHEIMER'S DISEASE

Aβ in the pathology of Alzheimer's disease is generated as a 40- or 42- residue peptide that aggregates to form amyloid oligomers and fibrils. Even though the fibrils have been associated with the progression of the disease pathology for over a century, the oligomers have emerged over the last two decades as the primary species that promote neurodegeneration. The

characterization of Aβ oligomers and fibrils represents the forefront of understanding the mechanisms by which they form and contribute to Alzheimer's disease pathology.

Aβ oligomers adopt a heterogeneous mixture of aggregates that are difficult to characterize and study.[16,17] Mixtures of Aβ oligomers composed of dimers, trimers, tetramers, hexamers, and even dodecamers have been observed by gel electrophoresis,[18] atomic force microscopy,[19] fluorescence lifetime imaging,[20] ion mobility mass spectrometry,[21] and by other methods. Information on the secondary structure of these oligomers has been obtained by making use of circular dichroism spectroscopy,[22] electron paramagnetic resonance,[23] two-dimensional infrared spectroscopy,[24] conformation-specific antibodies,[2,22,25] and affibody proteins.[26,27] These biophysical techniques show that Aβ adopts antiparallel β-sheets within the oligomers, and may even favor a β-hairpin conformation. Figure 1.1 shows a β-hairpin conformation of $A\beta_{1-40}$ that has been isolated and stabilized by an affibody protein.

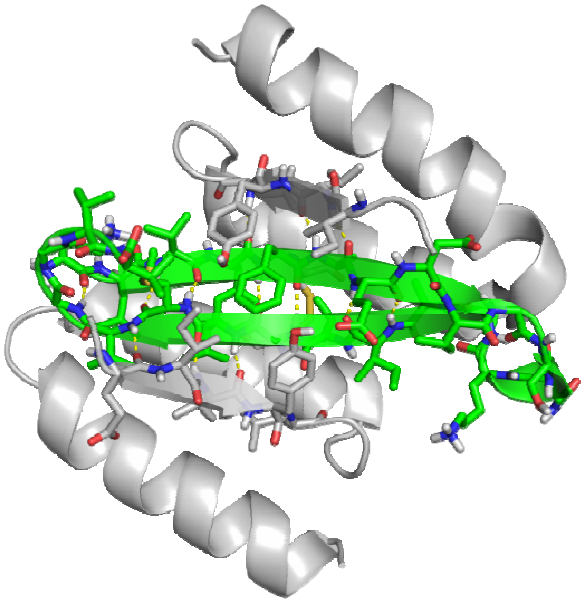

Figure 1.1. β-Hairpin conformation of $A\beta_{1-40}$ (green) with an affibody protein (PDB ID: 2OTK).

Further aggregation of Aβ results in the formation of amyloid fibrils. The structures of these fibrils are important, because they reveal key regions of the peptide that can adopt β-sheet

structure. These β-sheet-structured regions in Aβ fibrils may also favor β-sheets in Aβ oligomers. The fibril structures of $A\beta_{1-40}$ typically favor extended parallel β-sheet structures in which the central region and C-terminal regions laminate together, with a U-shaped turn in between (Figure 1.2A).[6] This fibril structure of $A\beta_{1-40}$ is discussed in more detail in Chapter 2. The structures of $A\beta_{1-42}$ fibrils also form parallel β-sheets, but these structures tend to be more compact (Figure 1.2B).[10,11,12]

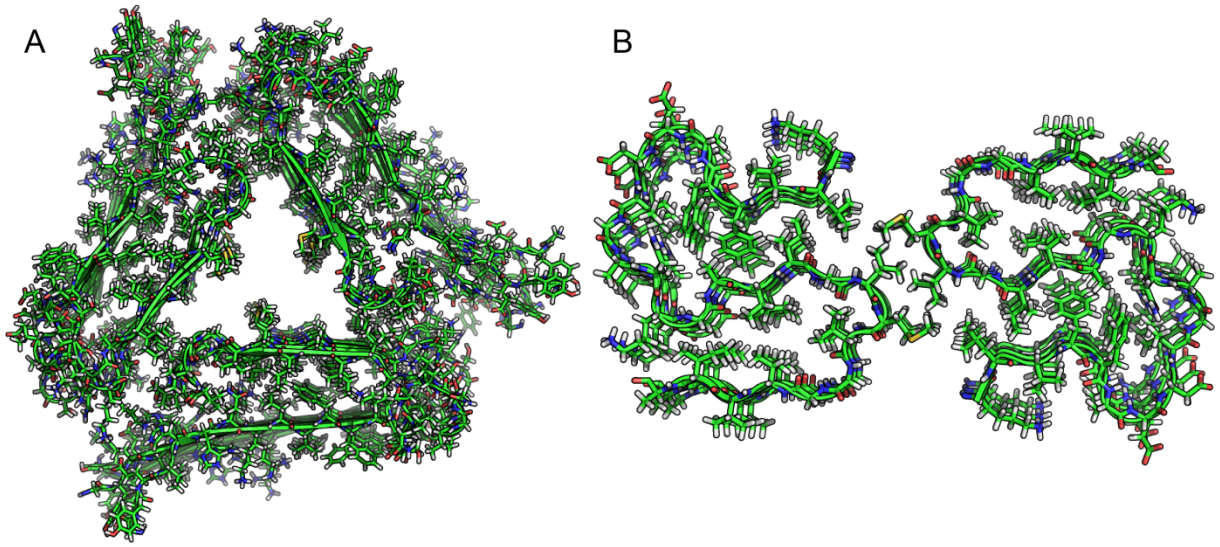

Figure 1.2. Solid-state NMR structures of fibrils formed by $A\beta_{1-40}$ (A, PDB ID: 2LMQ) and $A\beta_{1-42}$ (B, PDB ID: 2NAO).

3. CHEMICAL MODEL SYSTEMS

The heterogeneity and polymorphism of amyloid oligomers, and even some fibrils, continues to limit their isolation and characterization to this day. These challenges have led to designs and studies of chemical model systems that contain smaller amyloidogenic fragments. These chemical model systems are peptide scaffolds composed of one or two peptide strands, which contain key amyloidogenic regions from a peptide or protein. These regions are often identified as those that favor β-sheet structure in the fibrils. These regions may also be identified through evaluating the aggregation propensity of peptide sequences by either experimental[28,29,30,31] or computational techniques.[32,33,34,35] Incorporation of these amyloidogenic

regions into a chemical model system facilitates the characterization and study of these regions within a well-behaved system.

The advantage to studying these chemical model systems is the information they can provide: high-resolution structures of amyloid-like oligomers and fibrils. X-ray crystallography has revealed the structures of amyloid-like oligomers and fibrils of chemical model systems derived from Aβ,[30,36,37,38] Tau,[36] α-synuclein,[39] hIAPP,[40,41] transthyretin,[42] αB-crystallin,[43] β_2-microglobulin,[44] prion protein,[45] and many other amyloidogenic peptides and proteins. ^{1}H NMR spectroscopy studies have also provided information on the solution-phase assembly of chemical model systems derived from Aβ[46,47,48,49,50] and hIAPP.[41,51] These chemical model systems adopt structures of amyloid-like oligomers or fibrils that, in many cases, appear to resemble the oligomers or fibrils of their corresponding full-length peptide or protein.

Correlating structure with function is important for evaluating the biological significance of these chemical model systems. Solution-phase biophysical and biological studies have shown that some chemical model systems can mimic the biophysical and biological properties of their corresponding full-length peptide or protein, such as oligomerization and toxicity.[37,43,52] These studies can also reveal themes and patterns associated with the molecular pathology of Alzheimer's disease and other amyloid diseases.

4. MACROCYCLIC β-SHEET PEPTIDES

The Nowick laboratory has designed and introduced several chemical model systems to study the folding and oligomerization of β-sheets. These chemical model systems are called macrocyclic β-sheet peptides. The peptides contain turn and template units, which promote folding and prevent uncontrolled aggregation. Although the Nowick laboratory introduced these

peptides in 2007 as simple mimics of β-sheet folding and dimerization,[53,54] these peptides have since been redesigned multiple times for studies of amyloid oligomers and fibrils.

In 2007, the Nowick laboratory introduced macrocyclic β-sheet peptides **1**.[54] These peptides **1** contain a heptapeptide strand (upper strand) for displaying peptide fragments, two δ-linked ornithine ($^{\delta}$Orn) units, and a template strand (lower strand) with two tripeptide mimics, called Hao (Figure 1.3A).[55,56] The $^{\delta}$Orn units connect the upper and lower strands, which permits β-sheet folding of these strands. The two Hao units promote the assembly of these peptides, but also block uncontrolled aggregation. Peptides **1** later inspired the Nowick laboratory to design and study the larger macrocyclic β-sheet peptides **2**, which contain a nonapeptide strand in the upper strand (Figure 1.3B).[48,57,58]

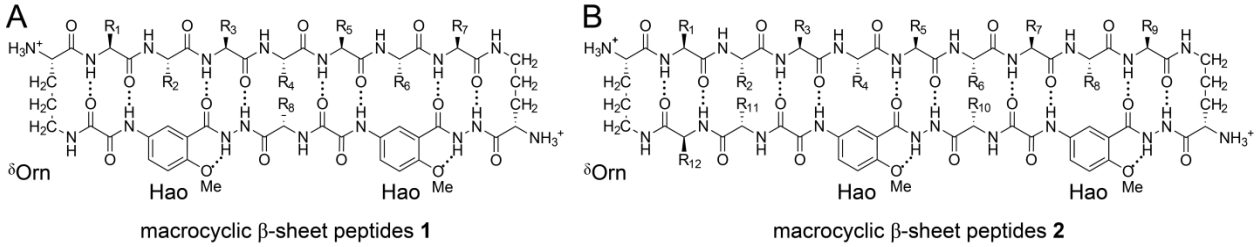

Figure 1.3. Macrocyclic β-sheet peptides **1**, showing the heptapeptide strand in the upper strand and the two Hao units in the template strand (A). Macrocyclic β-sheet peptides **2**, showing the nonapeptide strand and the two Hao units (B).

^{1}H NMR and X-ray crystallography studies have shown that macrocyclic β-sheet peptides **1** and **2** can oligomerize to form dimers, tetramers, and other higher-order oligomers. In a study of an analogue of peptide **1** derived from the protein G variant NuG2, ^{1}H NMR showed that this peptide forms hydrogen-bonded dimers that stack to form a sandwich-like tetramer.[54] X-ray crystallography further established the structure of the hydrogen-bonded dimer. Figure 1.4A shows the crystal structure of the dimer of peptide **1**.[59] ^{1}H NMR studies of an analogue of peptide **2** derived from $A\beta_{15–23}$ showed that this peptide can also forms hydrogen-bonded dimers, which further

assemble to form a tetramer.[48] X-ray crystallography also showed a different tetramer morphology of peptide **2**.[57] Figure 1.4B shows the crystal structure of a cruciform tetramer formed by peptide **2**.

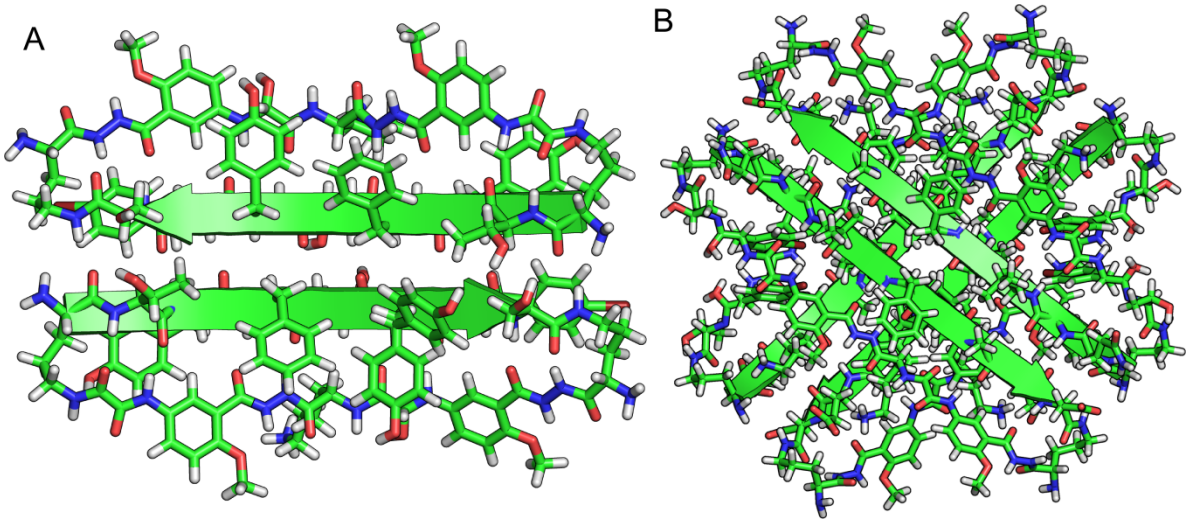

Figure 1.4. X-ray crystallographic structure of a dimer formed by a macrocyclic β-sheet peptide **1** derived from the protein G variant NuG2 (A, PDB ID: 3NI3). X-ray crystallographic structure of a cruciform tetramer formed by a macrocyclic β-sheet peptide **2** derived from $A\beta_{15–23}$ (B, PDB ID: 4IVH).

While studying peptides **1** and **2**, the Nowick laboratory worked on designing improved macrocyclic β-sheets that better mimic β-sheet folding and assembly. In 2012, the Nowick laboratory introduced macrocyclic β-sheet peptides **3** for delaying the aggregation of full-length Aβ (Figure 1.5A).[60] Peptides **3** are similar to peptides **2**, except that they contain only a single Hao in the template strand, rather than two. The four residues (R_8–R_{11}) that flank Hao add the ability to tune the hydrophobicity and charge of these peptides. The Nowick laboratory envisioned peptides **3** would exhibit enhanced folding and assembly over the predecessor peptides, **1** and **2**.

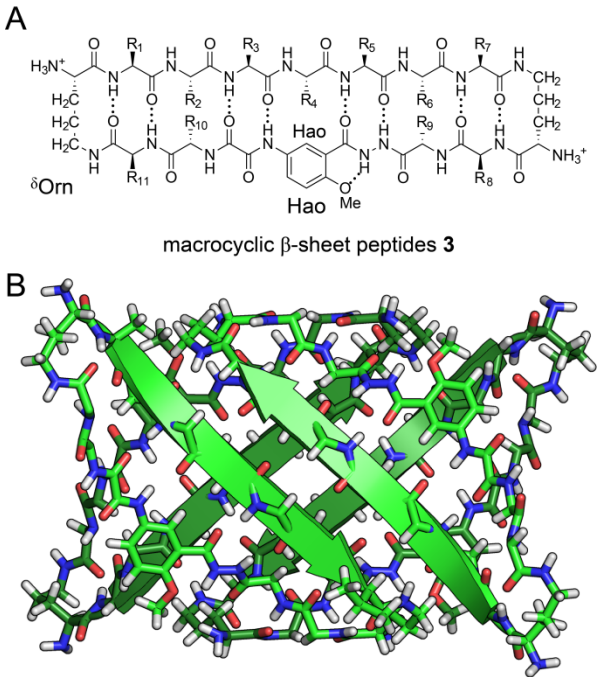

Figure 1.5. Macrocyclic β-sheet peptides **3**, showing the heptaptide strand and the single Hao unit in the template strand. X-ray crystallographic structure of a tetramer formed by a macrocyclic β-sheet peptide **3** derived from $A\beta_{30–36}$ (B, PDB ID: 3T4G).

The Nowick laboratory characterized analogues of peptides **3** derived from Aβ, hIAPP, and other amyloidogenic peptides by X-ray crystallography and NMR spectroscopy. X-ray crystallography studies showed that an analogue derived from $A\beta_{30-36}$ can assembles to form amyloid-like oligomers. These oligomers consist of hydrogen-bonded dimers that further assemble to form a barrel-shaped tetramer (Figure 1.5B).[36,60] ^{1}H NMR spectroscopy showed that peptides **3** exhibit enhanced β-sheet folding over the predecessor peptides **1** and **2**. Although these studies of peptide **3** folding showed promise for using ^{1}H NMR spectroscopy to characterize oligomers, the oligomers that formed were not well defined. As a result, hydrophilic residues were placed at position R_8 and R_{11}, which typically prevented oligomerization altogether.

In 2013, the Nowick laboratory began to develop macrocyclic β-sheets that do not contain any Hao units.[61] These efforts led to the design of macrocyclic macrocyclic β-sheet peptides **4** (Figure 1.6).[38] These peptides contain heptapeptide strands in the upper and lower

strands (R_1–R_7 and R_8–R_{14}). Peptides **4** also contain an *N*-methyl (*N*-Me) group, rather than Hao, to block uncontrolled aggregation.[37,38,39,42,44,62,63]

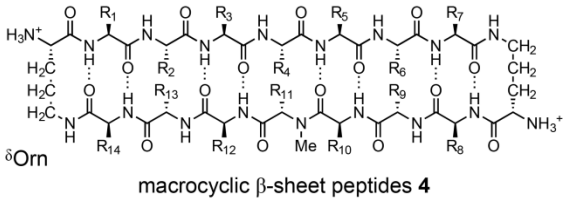

Figure 1.6. Macrocyclic β-sheet peptides **4**, showing the two heptaptide strands (upper and lower strands) and the *N*-Me group.

In 2014, the Nowick lab published X-ray crystallographic structures of several analogues of peptides **4** derived from $A\beta_{17–36}$.[38] The crystal structures showed that these peptides can **4** form triangular trimers, hexamers, and dodecamers (Figure 1.7). These oligomers assemblies inspired our laboratory to design several subsequent analogues derived from Aβ,[37,62] β_2-microglobulin,[44] α-synuclein,[39] and transthyretin.[42] X-ray crystallographic studies of these peptides show that they also assemble to form various sizes and morphologies of dimers, trimers, hexamers, dodecamers, and other higher-order oligomers. Solution-phase biophysical and biological studies of these peptides have also begun to show relationships between structure and toxicity of trimers and higher-order oligomers. These findings may reflect the structures and the toxicities of oligomers that full-length Aβ can form.

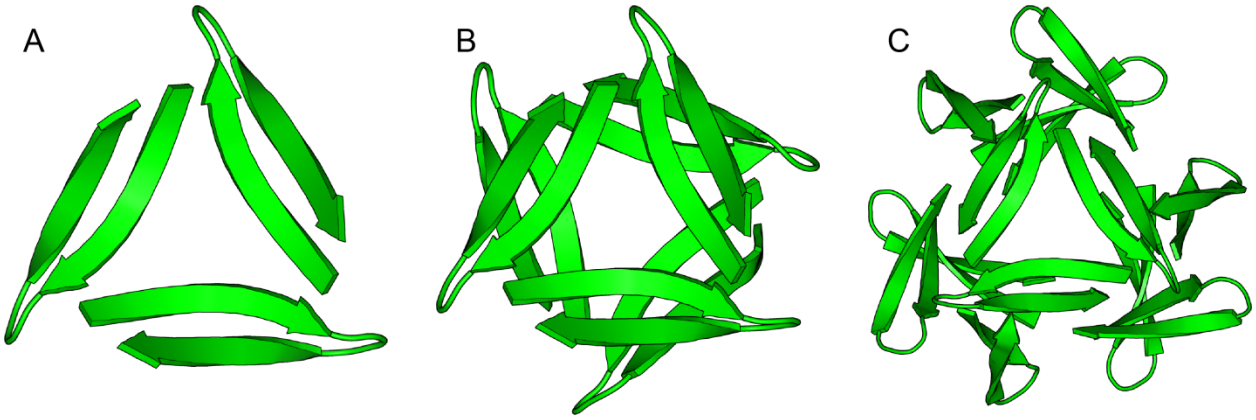

Figure 1.7. X-ray crystallographic structure of a trimer, hexamer, and dodecamer of formed by an analogue of macrocyclic β-sheet peptide **4** derived from $A\beta_{17–36}$ (A-C, PDB ID: 4NTR).

5. MY DISSERTATION RESEARCH

In the summer of 2012 before starting my graduate studies at UC Irvine, I made two discoveries with macrocyclic β-sheet peptides **3** during a rotation in the Nowick laboratory. I found that macrocyclic β-sheet peptides **3** indeed form well-defined oligomers in solution, which had not been observed previously. I also found that two homologues of peptides **3**, which were derived from $A\beta_{17\text{-}23}$ (LVFFAED) and $A\beta_{30\text{-}36}$ (AIIGLMV), can assemble and coassemble in solution. During the course of my graduate studies, I confirmed these findings by ^{1}H NMR spectroscopy, which ultimately resulted in two first-author publications[46,47] and are described in Chapters 2 and 3 of this dissertation. These findings also had a major influence on the publications[41,51] and dissertation of my colleague, Yilin Wang.

For the remainder of my graduate career, I shifted the focus of my research to study peptides **4**. These studies focus on characterizing analogues of peptides **4** derived from $A\beta_{17\text{–}36}$. In Chapter 4, I describe my efforts to characterize these analogues by X-ray crystallography and ^{1}H NMR spectroscopy, and also with biophysical and biological techniques.

REFERENCES

1. Chiti, F.; Dobson, C. M. *Annu. Rev. Biochem.* **2006**, *75*, 333–366.
2. Glabe, C. G. *J. Biol. Chem.* **2008**, *283*, 29639–29643.
3. Knowles, T. P.; Vendruscolo, M.; Dobson, C. M. *Nat. Rev. Mol. Cell Biol.* **2014**, *15*, 384–396.
4. Otzen, D.; Nielsen, P. H. *Cell. Mol. Life Sci.* **2008**, *65*, 910–927.
5. Riek, R.; Eisenberg, D. S. *Nature* **2016**, *539*, 227–235.
6. Paravastu, A. K.; Leapman, R. D.; Yau, W.-M.; Tycko, R. *Proc. Natl. Acad. Sci. U.S.A.* **2008**, *105*, 18349–18354.
7. Qiang, W.; Yau, W. M.; Luo, Y.; Mattson, M. P.; Tycko, R. *Proc. Natl. Acad. Sci. U.S.A.* **2012**, *109*, 4443–4448.
8. Gremer, L.; Scholzel, D.; Schenk, C.; Reinartz, E.; Labahn, J.; Ravelli, R. B. G.; Tusche, M.; Lopez-Iglesias, C.; Hoyer, W.; Heise, H.; Willbold, D.; Schroder, G. F. *Science* **2017**, *358*, 116–119.
9. Lührs, T.; Ritter, C.; Adrian, M.; Riek-Loher, D.; Bohrmann, B.; Döbeli, H.; Schubert, D.; Riek, R. *Proc. Natl. Acad. Sci. U.S.A.* **2005**, *102*, 17342–17347.
10. Xiao, Y.; Ma, B.; McElheny, D.; Parthasarathy, S.; Long, F.; Hoshi, M.; Nussinov, R.; Ishii, Y. *Nat. Struct. Mol. Biol.* **2015**, *22*, 499.
11. Colvin, M. T.; Silvers, R.; Ni, Q. Z.; Can, T. V.; Sergeyev, I.; Rosay, M.; Donovan, K. J.; Michael, B.; Wall, J.; Linse, S.; Griffin, R. G. *J. Am. Chem. Soc.* **2016**, *138*, 9663–9674.
12. Walti, M. A.; Ravotti, F.; Arai, H.; Glabe, C. G.; Wall, J. S.; Bockmann, A.; Guntert, P.; Meier, B. H.; Riek, R. *Proc. Natl. Acad. Sci. U.S.A.* **2016**, *113*, E4976–E4984.
13. Luca, S.; Yau, W.-M.; Leapman, R.; Tycko, R. *Biochemistry* **2007**, *46*, 13505–13522.

14. Tuttle, M. D.; Comellas, G.; Nieuwkoop, A. J.; Covell, D. J.; Berthold, D. A.; Kloepper, K. D.; Courtney, J. M.; Kim, J. K.; Barclay, A. M.; Kendall, A.; Wan, W.; Stubbs, G.; Schwieters, C. D.; Lee, V. M.; George, J. M.; Rienstra, C. M. *Nat. Struct. Mol. Biol.* **2016**, *23*, 409–415.

15. Fitzpatrick, A. W. P.; Falcon, B.; He, S.; Murzin, A. G.; Murshudov, G.; Garringer, H. J.; Crowther, R. A.; Ghetti, B.; Goedert, M.; Scheres, S. H. W. *Nature* **2017**, *547*, 185–190.

16. Benilova, I.; Karran, E.; De Strooper, B. *Nat. Neurosci.* **2012**, *15*, 349–357.

17. Teplow, D. B. *Alzheimers Res. Ther.* **2013**, *5*, 1–39.

18. Ono, K.; Condron, M. M.; Teplow, D. B. *Proc. Natl. Acad. Sci. U.S.A.* **2009**, *106*, 14745–14750.

19. Harper, J. D.; Wong, S. S.; Lieber, C. M.; Lansbury Jr, P. T. *Chemistry & Biology* **1997**, *4*, 119–125.

20. Esbjörner, Elin K.; Chan, F.; Rees, E.; Erdelyi, M.; Luheshi, Leila M.; Bertoncini, Carlos W.; Kaminski, Clemens F.; Dobson, Christopher M.; Kaminski Schierle, Gabriele S. *Chemistry & Biology* **2014**, *21*, 732–742.

21. Bernstein, S. L.; Dupuis, N. F.; Lazo, N. D.; Wyttenbach, T.; Condron, M. M.; Bitan, G.; Teplow, D. B.; Shea, J. E.; Ruotolo, B. T.; Robinson, C. V.; Bowers, M. T. *Nat. Chem.* **2009**, *1*, 326–331.

22. Murakami, K.; Tokuda, M.; Suzuki, T.; Irie, Y.; Hanaki, M.; Izuo, N.; Monobe, Y.; Akagi, K.-i.; Ishii, R.; Tatebe, H.; Tokuda, T.; Maeda, M.; Kume, T.; Shimizu, T.; Irie, K. *Sci. Rep.* **2016**, *6*, 29038.

23. Gu, L.; Liu, C.; Guo, Z. *J. Biol. Chem.* **2013**, *288*, 18673–18683.

24. Cerf, E.; Sarroukh, R.; Tamamizu-Kato, S.; Breydo, L.; Derclaye, S.; Dufrene, Y. F.; Narayanaswami, V.; Goormaghtigh, E.; Ruysschaert, J. M.; Raussens, V. *Biochem. J.* **2009**, *421*, 415–423.

25. Lesne, S.; Koh, M. T.; Kotilinek, L.; Kayed, R.; Glabe, C. G.; Yang, A.; Gallagher, M.; Ashe, K. H. *Nature* **2006**, *440*, 352–357.

26. Hoyer, W.; Gronwall, C.; Jonsson, A.; Stahl, S.; Hard, T. *Proc. Natl. Acad. Sci. U.S.A.* **2008**, *105*, 5099–5104.

27. Sandberg, A.; Luheshi, L. M.; Söllvander, S.; Pereira de Barros, T.; Macao, B.; Knowles, T. P. J.; Biverstål, H.; Lendel, C.; Ekholm-Petterson, F.; Dubnovitsky, A.; Lannfelt, L.; Dobson, C. M.; Härd, T. *Proc. Natl. Acad. Sci. U.S.A.* **2010**, *107*, 15595–15600.

28. Liu, R.; McAllister, C.; Lyubchenko, Y.; Sierks, M. R. *J. Neurosci. Res.* **2004**, *75*, 162–171.

29. Colletier, J. P.; Laganowsky, A.; Landau, M.; Zhao, M.; Soriaga, A. B.; Goldschmidt, L.; Flot, D.; Cascio, D.; Sawaya, M. R.; Eisenberg, D. *Proc. Natl. Acad. Sci. U.S.A.* **2011**, *108*, 16938–16943.

30. Sawaya, M. R.; Sambashivan, S.; Nelson, R.; Ivanova, M. I.; Sievers, S. A.; Apostol, M. I.; Thompson, M. J.; Balbirnie, M.; Wiltzius, J. J.; McFarlane, H. T.; Madsen, A. O.; Riekel, C.; Eisenberg, D. *Nature* **2007**, *447*, 453–457.

31. Nelson, R.; Sawaya, M. R.; Balbirnie, M.; Madsen, A. O.; Riekel, C.; Grothe, R.; Eisenberg, D. *Nature* **2005**, *435*, 773–778.

32. Goldschmidt, L.; Teng, P. K.; Riek, R.; Eisenberg, D. *Proc. Natl. Acad. Sci. U.S.A.* **2010**, *107*, 3487–3492.

33. Sormanni, P.; Aprile, F. A.; Vendruscolo, M. *J. Mol. Biol.* **2015**, *427*, 478–490.

34. Fernandez-Escamilla, A. M.; Rousseau, F.; Schymkowitz, J.; Serrano, L. *Nat. Biotechnol.* **2004**, *22*, 1302–1306.

35. Maurer-Stroh, S.; Debulpaep, M.; Kuemmerer, N.; Lopez de la Paz, M.; Martins, I. C.; Reumers, J.; Morris, K. L.; Copland, A.; Serpell, L.; Serrano, L.; Schymkowitz, J. W.; Rousseau, F. *Nat. Methods* **2010**, *7*, 237–242.

36. Liu, C.; Zhao, M.; Jiang, L.; Cheng, P. N.; Park, J.; Sawaya, M. R.; Pensalfini, A.; Gou, D.; Berk, A. J.; Glabe, C. G.; Nowick, J.; Eisenberg, D. *Proc. Natl. Acad. Sci. U.S.A.* **2012**, *109*, 20913–20918.

37. Kreutzer, A. G.; Spencer, R. K.; McKnelly, K. J.; Yoo, S.; Hamza, I. L.; Salveson, P. J.; Nowick, J. S. *Biochemistry* **2017**, *56*, 6061–6071.

38. Spencer, R. K.; Li, H.; Nowick, J. S. *J. Am. Chem. Soc.* **2014**, *136*, 5595–5598.

39. Salveson, P. J.; Spencer, R. K.; Nowick, J. S. *J. Am. Chem. Soc.* **2016**, *138*, 4458–4467.

40. Wiltzius, J. J.; Sievers, S. A.; Sawaya, M. R.; Cascio, D.; Popov, D.; Riekel, C.; Eisenberg, D. *Protein Sci.* **2008**, *17*, 1467–1474.

41. Wang, Y.; Kreutzer, A. G.; Truex, N. L.; Nowick, J. S. *J. Org. Chem.* **2017**, *82*, 7905–7912.

42. Yoo, S.; Kreutzer, A. G.; Truex, N. L.; Nowick, J. S. *Chem. Sci.* **2016**, *7*, 6946–6951.

43. Laganowsky, A.; Liu, C.; Sawaya, M. R.; Whitelegge, J. P.; Park, J.; Zhao, M.; Pensalfini, A.; Soriaga, A. B.; Landau, M.; Teng, P. K.; Cascio, D.; Glabe, C.; Eisenberg, D. *Science* **2012**, *335*, 1228–1231.

44. Spencer, R. K.; Kreutzer, A. G.; Salveson, P. J.; Li, H.; Nowick, J. S. *J. Am. Chem. Soc.* **2015**, *137*, 6304–6311.

45. Apostol, M. I.; Perry, K.; Surewicz, W. K. *J. Am. Chem. Soc.* **2013**, *135*, 10202–10205.

46. Truex, N. L.; Wang, Y.; Nowick, J. S. *J. Am. Chem. Soc.* **2016**, *138*, 13882–13890.

47. Truex, N. L.; Nowick, J. S. *J. Am. Chem. Soc.* **2016**, *138*, 13891–13900.

48. Pham, J. D.; Demeler, B.; Nowick, J. S. *J. Am. Chem. Soc.* **2014**, *136*, 5432–5442.

49. Lendel, C.; Bjerring, M.; Dubnovitsky, A.; Kelly, R. T.; Filippov, A.; Antzutkin, O. N.; Nielsen, N. C.; Hard, T. *Angew. Chem., Intl. Ed.* **2014**, *53*, 12756–12760.

50. Yu, L.; Edalji, R.; Harlan, J. E.; Holzman, T. F.; Lopez, A. P.; Labkovsky, B.; Hillen, H.; Barghorn, S.; Ebert, U.; Richardson, P. L.; Miesbauer, L.; Solomon, L.; Bartley, D.; Walter, K.; Johnson, R. W.; Hajduk, P. J.; Olejniczak, E. T. *Biochemistry* **2009**, *48*, 1870–1877.

51. Wang, Y.; Truex, N. L.; Vo, N. D. P.; Nowick, J. S. *Bioorg. Med. Chem.* **2017**, Just Published.

52. Kreutzer, A. G.; Yoo, S.; Spencer, R. K.; Nowick, J. S. *J. Am. Chem. Soc.* **2017**, *139*, 966–975.

53. Woods, R. J.; Brower, J. O.; Castellanos, E.; Hashemzadeh, M.; Khakshoor, O.; Russu, W. A.; Nowick, J. S. *J. Am. Chem. Soc.* **2007**, *129*, 2548–2558.

54. Khakshoor, O.; Demeler, B.; Nowick, J. S. *J. Am. Chem. Soc.* **2007**, *129*, 5558–5569.

55. Nowick, J. S.; Chung, D. M.; Maitra, K.; Maitra, S.; Stigers, K. D.; Sun, Y. *J. Am. Chem. Soc.* **2000**, *122*, 7654–7661.

56. Nowick, J. S.; Brower, J. O. *J. Am. Chem. Soc.* **2003**, *125*, 876–877.

57. Pham, J. D.; Chim, N.; Goulding, C. W.; Nowick, J. S. *J. Am. Chem. Soc.* **2013**, *135*, 12460–12467.

58. Pham, J. D.; Spencer, R. K.; Chen, K. H.; Nowick, J. S. *J. Am. Chem. Soc.* **2014**, *136*, 12682–12690.

59. Khakshoor, O.; Lin, A. J.; Korman, T. P.; Sawaya, M. R.; Tsai, S. C.; Eisenberg, D.; Nowick, J. S. *J. Am. Chem. Soc.* **2010**, *132*, 11622–11628.

60. Cheng, P. N.; Liu, C.; Zhao, M.; Eisenberg, D.; Nowick, J. S. *Nat. Chem.* **2012**, *4*, 927–933.

61. Spencer, R.; Chen, K. H.; Manuel, G.; Nowick, J. S. *Eur. J. Org. Chem.* **2013**, 3523–3528.

62. Salveson, P. J.; Spencer, R. K.; Kreutzer, A. G.; Nowick, J. S. *Org. Lett.* **2017**, *19*, 3462–3465.

63. Kreutzer, A. G.; Hamza, I. L.; Spencer, R. K.; Nowick, J. S. *J. Am. Chem. Soc.* **2016**, *138*, 4634–4642.

CHAPTER 2

Assembly of Peptides Derived from β-Sheet Regions of β-Amyloid

INTRODUCTION

Interaction among β-sheets is the two-edged sword in protein structure, imparting folding and stability but also driving misfolding and aggregation. While folding is typically associated with normal biological function, aggregation is associated with the pathology of Alzheimer's disease and other amyloid diseases, including Parkinson's disease and type II diabetes.[1] In Alzheimer's disease, the β-amyloid peptide (Aβ) aggregates to form oligomers and fibrils that characterize the disease pathology.[2]

Elucidation of the oligomers and fibrils is critical to understanding how Aβ aggregates and counteracting the harmful effects. The fibrils mark the thermodynamic end point of Aβ aggregation and accumulate as the disease progresses.[3] Several high-resolution structures have been reported of the Aβ fibrils, which typically adopt parallel β-sheet structure.[4,5] The oligomers are thought to be primarily responsible for neurodegeneration, causing synaptic dysfunction in neurons.[6] The oligomers are metastable and heterogeneous, and thus are difficult to study by high-resolution structural techniques.

Two key regions of Aβ favor β-sheet formation and promote aggregation: the central region and the C-terminal region.[7] The central region contains $A\beta_{17–21}$ (LVFFA). The two phenylalanine residues therein are especially important in nucleating and propagating the formation of Aβ aggregates.[8] The C-terminal region comprises residues AIIGLMVGGVV (for $A\beta_{1–40}$) or AIIGLMVGGVVIA (for $A\beta_{1–42}$). These successive hydrophobic residues also promote aggregation.[9]

The central and C-terminal regions of Aβ are thought to assemble in a different fashion in the fibrils than in the oligomers. In fibrils formed by $A\beta_{1–40}$, the two regions of the peptide can assemble to form layered parallel β-sheets connected by a U-shaped turn: one layer consists of

the central region and the other consists of the C-terminal region.[4,5] Figure 2.1 illustrates a layered β-sheet structure formed by $A\beta_{1\text{-}40}$.[4c] These layered fibril structures can further assemble in twos and threes to form fibrils that exhibit two-fold or three-fold symmetry. In the oligomers, the central and C-terminal regions are thought to coassemble in an antiparallel fashion to form β-hairpins, which assemble to form the oligomers.[10] These regions may also promote the assembly of Aβ to form higher-order oligomers.

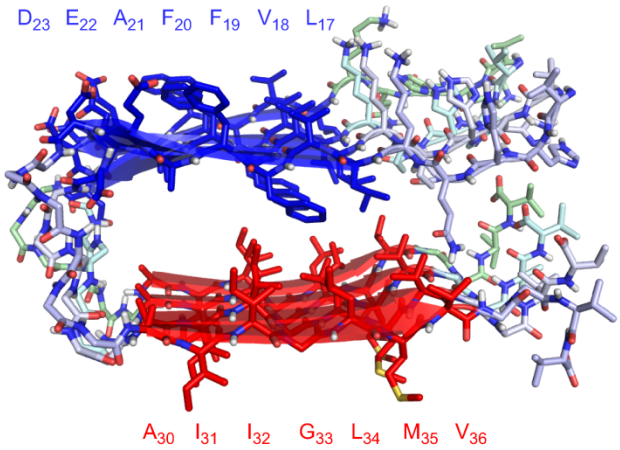

Figure 2.1. Layered β-sheet structure formed by $A\beta_{1\text{–}40}$ within β-amyloid fibrils (PDB ID: 2LMQ).

In 2012, our research group introduced macrocyclic β-sheet peptides **1** as a model system to investigate the assembly of amyloidogenic peptides and proteins (Figure 2.2).[11] Peptides **1** consist of a heptapeptide strand ($R_{1\text{–}7}$), a template strand, and two turn units. The heptapeptide strand displays amyloidogenic peptide sequences. The template strand contains the unnatural amino acid Hao and four additional residues ($R_{8\text{–}11}$) that help promote β-sheet structure. Hao is a tripeptide mimic that templates β-sheet hydrogen bonding and blocks uncontrolled aggregation.[12] The δ-linked ornithine ($^{\delta}$Orn) turn units on each side connect the two strands and allow β-sheet folding.[13] Our research group incorporated hydrophilic residues at positions R_8 and/or R_{11} to minimize oligomerization.

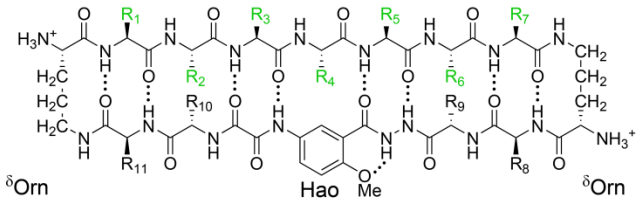

macrocyclic β-sheet peptides **1**

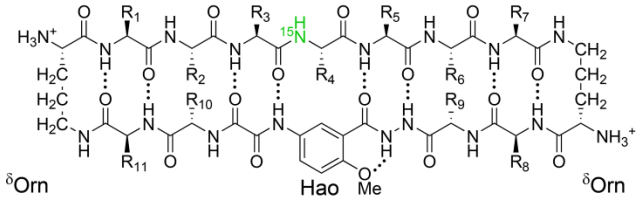

macrocyclic β-sheet peptides [^{15}N]**1**

Figure 2.2. Macrocyclic β-sheet peptides **1**, illustrating the heptapeptide strand (upper strand), the template strand (lower strand), and the two $^{\delta}$Orn turn units. Macrocyclic β-sheet peptides [^{15}N]**1**, illustrating the ^{15}N isotopic label at the R_4 position.

In this two-part investigation, I incorporated residues from the central and C-terminal regions of Aβ into peptides **1** to ask whether these regions prefer to coassemble or to segregate.[14] To promote the formation of well-defined oligomers, I incorporated hydrophobic residues into positions R_8 and R_{11}. The first part—the current chapter—determines how the two peptides assemble in aqueous solution. The second part—the accompanying chapter—determines whether the two peptides exhibit a special preference to coassemble when mixed.[14] This question is important because the two regions generally segregate in the fibrils but coassemble in the oligomers.

To facilitate these studies, I incorporated ^{15}N isotopic labels into peptides **1**. Peptides [^{15}N]**1** contain a single ^{15}N isotopic label at the R_4 position in the center of the heptapeptide strand (Figure 2.2). These peptides are readily prepared from commercially available ^{15}N-labeled amino acids using solid-phase peptide synthesis. The ^{15}N isotopic label provides a simple and effective spectroscopic probe to monitor assembly and coassembly by ^{1}H,^{15}N NMR spectroscopy.

RESULTS AND DISCUSSION

Design of Peptides Derived from the Central and C-Terminal Regions of Aβ. I incorporated residues LVFFAED ($A\beta_{17–23}$) and AIIGLMV ($A\beta_{30–36}$) into peptides **1**, to give peptides **1a** and **1b**. I designed the peptides with a distinct hydrophobic surface to promote assembly by incorporating isoleucine residues at positions R_8 and R_{11} of the template strand. I also designed the peptides with a hydrophilic surface to promote solubility and prevent uncontrolled aggregation by incorporating lysine residues at positions R_9 and R_{10} of the template strand.

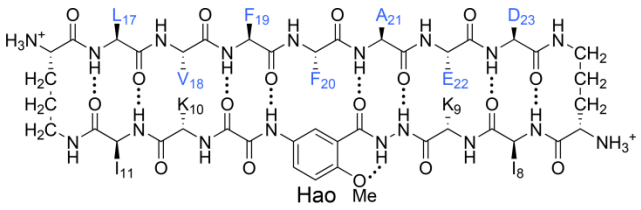

macrocyclic β-sheet peptide **1a**

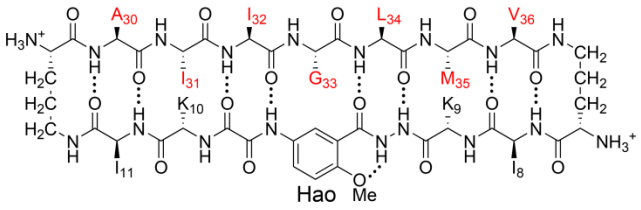

macrocyclic β-sheet peptide **1b**

^{1}H NMR studies show that peptides **1a** and **1b** assemble to form sandwich-like tetramers in aqueous solution.[16] The tetramers consist of two β-sheet dimers that stack like slices of bread. The dimers are stabilized by hydrogen-bonding interactions between the amide backbones of the heptapeptide strands; the tetramers are stabilized by hydrophobic interactions between the hydrophobic surfaces of the dimers. The following subsections describe the elucidation of the tetramers by NMR spectroscopy.

DOSY Shows That Peptides 1a and 1b Form Tetramers. Our laboratory has previously used DOSY NMR studies and corroboratory analytical ultracentrifugation (AUC)

experiments to establish that related macrocyclic β-sheet peptides form tetramers.[17] DOSY NMR studies of peptides **1a** and **1b** show that these macrocyclic β-sheets also form tetramers (Table 2.1). The DOSY spectrum of peptide **1a** at 0.15 mM shows two sets of resonances: one set from the monomer, with a diffusion coefficient of 20.4 x 10^{-11} m^2/s; the other set from the tetramer, with a diffusion coefficient of 12.6 x 10^{-11} m^2/s. At 8.0 mM, the spectrum shows only the latter set of resonances with a diffusion coefficient of 11.8 x 10^{-11} m^2/s. The DOSY spectrum of peptide **1b** at 1.0 mM shows resonances from the monomer, with a diffusion coefficient 19.4 x 10^{-11} m^2/s, and the spectrum at 16.0 mM shows resonances from the tetramer, with a diffusion coefficient of 11.9 x 10^{-11} m^2/s.

Table 2.1. Diffusion coefficients (*D*) of peptides 1a and 1b in D_2O at 298 K

	$MW_{monomer}$[a] (Da)	$MW_{tetramer}$[a] (Da)	conc. (mM)	*D* (10^{-11} m^2/s)	oligomer state
1a	1767	7068	0.15	20.4 ± 1.7	monomer
			0.15	12.6 ± 1.6	tetramer
			8.0	11.8 ± 1.0	tetramer
1b	1643	6572	1.0	19.4 ± 1.7	monomer
			16.0	11.9 ± 1.1	tetramer

[a]Molecular weight calculated for the neutral (uncharged) peptide.

The ratio of diffusion coefficients of a tetramer and monomer is typically 0.6.[18] DOSY studies show that the oligomers of peptides **1a** and **1b** have diffusion coefficients of about 12 x 10^{-11} m^2/s and the monomers have diffusion coefficients of about 20 x 10^{-11} m^2/s. The ratio of the diffusion coefficients (0.6) is consistent with a tetramer.[19]

Elucidation of the Peptide 1a Tetramer. Peptide **1a** forms a tetramer that consists of two β-sheet dimers. The ^1H NMR spectrum of peptide **1a** at 8 mM in D_2O at 298 K shows one predominant set of resonances (Figure 2.3a).[20] These resonances are associated with the tetramer. The resonances are disperse and exhibit distinct spectral features that reflect well-defined β-sheet structure: Seven of the 11 α-protons appear downfield of 5 ppm. The methyl proton resonance of A_{21} appears at 0.5 ppm. The aromatic proton resonances of F_{19} appear upfield of 7 ppm (6.3 to

6.5 ppm). The ^{1}H NMR spectrum of peptide **1a** at 0.15 mM in D_2O at 298 K shows resonances associated with both the monomer and the tetramer (Figure S2.1). The resonances of the monomer lack the distinct spectral features of the tetramer.

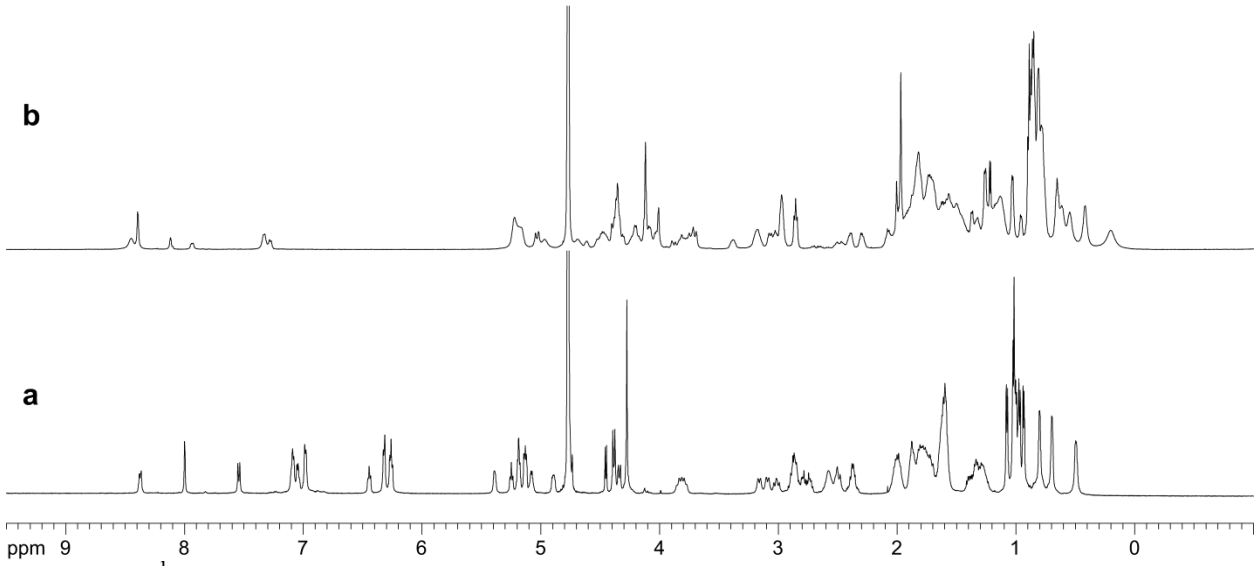

Figure 2.3. ^{1}H NMR spectra of (a) peptide **1a** and (b) peptide **1b** at 8.0 mM in D_2O at 600 MHz and 298 K.

The magnetic anisotropy of the diastereotopic δ-proton resonances of the $^{\delta}$Orn turn units reflects β-sheet folding in peptides **1** and related macrocyclic β-sheets.[10a,12] In a well-folded macrocyclic β-sheet, the diasterotopic *pro-S* δ-protons appear about 0.6 ppm downfield of the *pro-R* δ-protons. In the tetramer of peptide **1a**, the *pro-S* δ-protons appear 0.63 and 0.74 ppm downfield of the *pro-R* δ-protons. In the monomer, the *pro-S* δ-protons of peptide **1a** appear 0.30 and 0.39 ppm downfield of the *pro-R* δ-protons. The magnetic anisotropies of these proton resonances indicate that the monomer is moderately folded, while the tetramer is well folded.

The NOESY spectrum of peptide **1a** shows strong NOEs associated with the β-sheet folding and assembly of the tetramer. The spectrum shows a network of five strong NOEs

associated with β-sheet folding: between the α-protons of V_{18} and K_{10}, the α-protons of E_{22} and K_9, the α-proton of F_{20} and the proton at the 6-position of the unnatural amino acid Hao ($HaoH_6$), and the α- and δ-protons of the $^{\delta}$Orn turn units (Figure S2.2). The spectrum shows two additional NOEs associated with β-sheet dimerization, between the α-protons of L_{17} and D_{23} and between the α-protons of F_{19} and A_{21} (Figure S2.2a). Figure 2.4 illustrates the dimer of peptide **1a** consistent with these interlayer NOEs.

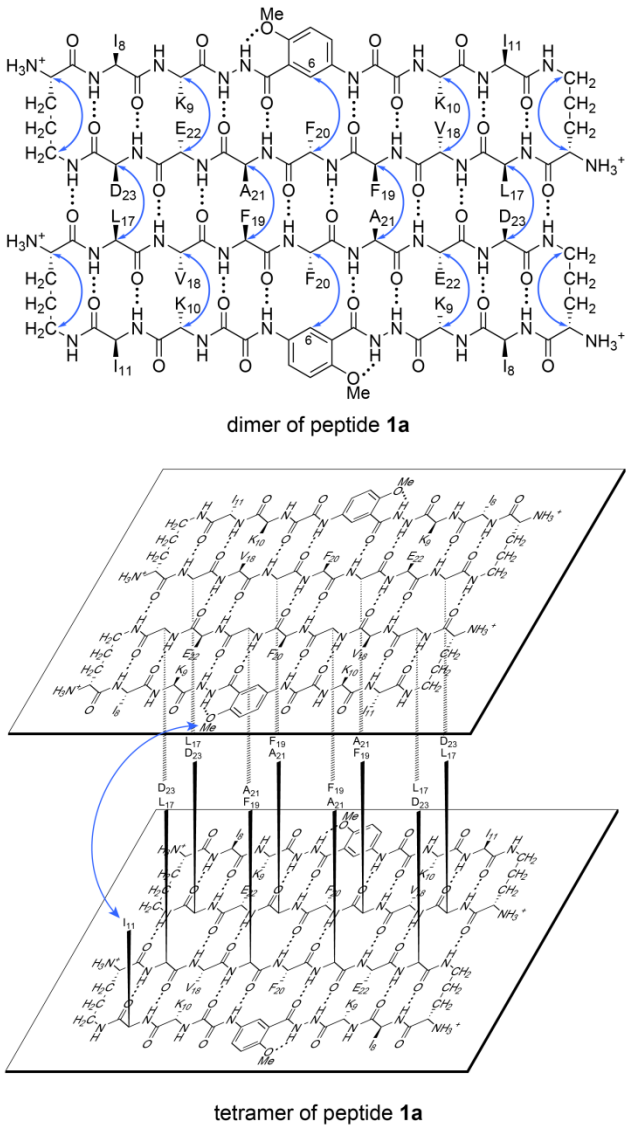

Figure 2.4. Dimer and tetramer of peptide **1a**. Hydrogen-bonded dimer subunit (upper). Blue arrows illustrate intramolecular and intermolecular NOEs observed in the NOESY spectrum. Sandwich-like tetramer consisting of two hydrogen-bonded dimers (lower). The blue arrow illustrates the interlayer NOEs observed in the NOESY spectrum. The tetramer exhibits four-fold symmetry and four I_{11}–Hao_{OMe} interactions, even though only one arrow is shown.

The NOESY spectrum shows additional NOEs associated with the stacking of two dimers to form a sandwich-like tetramer. The spectrum shows a pattern of NOEs between the methoxy protons of Hao (Hao_{OMe}) and the side-chain protons of I_{11}, and additional NOEs between the protons at the 3- and 4-positions of Hao ($HaoH_3$ and $HaoH_4$) and the δ-methyl protons of I_{11}

(Figure S2.3). Figure 2.4 illustrates the stacking of the two dimers of peptide **1a** consistent with these interlayer NOEs.

Elucidation of the Peptide 1b Tetramer. Peptide **1b** forms a similar tetramer, which also consists of two β-sheet dimers. The tetramer is considerably less stable than that formed by peptide **1a** and is in equilibrium with substantial amounts of monomer at millimolar concentrations (Figure S2.4). The ^{1}H NMR spectrum of peptide **1b** at 8.0 mM in D_2O at 298 K shows two sets of resonances. These resonances appear in a 3:2 ratio of intensities, with the predominant set associated with the tetramer and the smaller set associated with the monomer (Figure 2.3b). The resonances are broadened, reflecting chemical exchange between the tetramer and the monomer on a ca. hundred-millisecond time scale. The resonances associated with the tetramer exhibit several distinct spectral features that reflect well-defined β-sheet structure: Five of the 11 α-proton resonances appear downfield of 5 ppm. The methyl proton resonances of L_{34} are shifted upfield of 0.5 ppm (0.38 and 0.12 ppm). The *pro-S* δ-proton resonances of the $^{\delta}$Orn turn units appear 0.65 and 0.69 ppm downfield of the *pro-R* δ-proton resonances.

The monomer of peptide **1b** lacks these distinct spectral features. The *pro-S* δ-proton resonances of the $^{\delta}$Orn turn units appear 0.16 and 0.19 ppm downfield of the *pro-R* δ-proton resonances. The magnetic anisotropies of these proton resonances indicate that the monomer is poorly folded. In contrast to peptide **1a**, the monomer of peptide **1b** predominates at low millimolar concentrations. At concentrations below 1 mM, the spectrum shows almost exclusively the monomer and virtually no tetramer.

The NOESY spectrum of peptide **1b** shows strong NOEs associated with β-sheet folding and weaker NOEs associated with β-sheet assembly. The spectrum shows a network of five strong NOEs associated with β-sheet folding: between the α-protons of I_{31} and K_{10}, the α-protons

of M_{35} and K_9, the *pro-R* α-proton of G_{33} and the $HaoH_6$ proton, and the α- and δ-protons of the $^{\delta}$Orn turn units (Figure S2.5). The spectrum shows an additional NOE associated with β-sheet dimerization, between the α-protons of I_{32} and L_{34} (Figure S2.5a). The spectrum does not show a well-defined NOE crosspeak between the α-protons of A_{30} and V_{36}. The absence of a well-defined crosspeak may reflect broadening of the resonances through chemical exchange with the monomer and overlap with an exchange crosspeak, or it may reflect a lack of close contact between the two protons. Figure 2.5 illustrates the β-sheet folding and dimerization of peptide **1b** consistent with these NOEs.

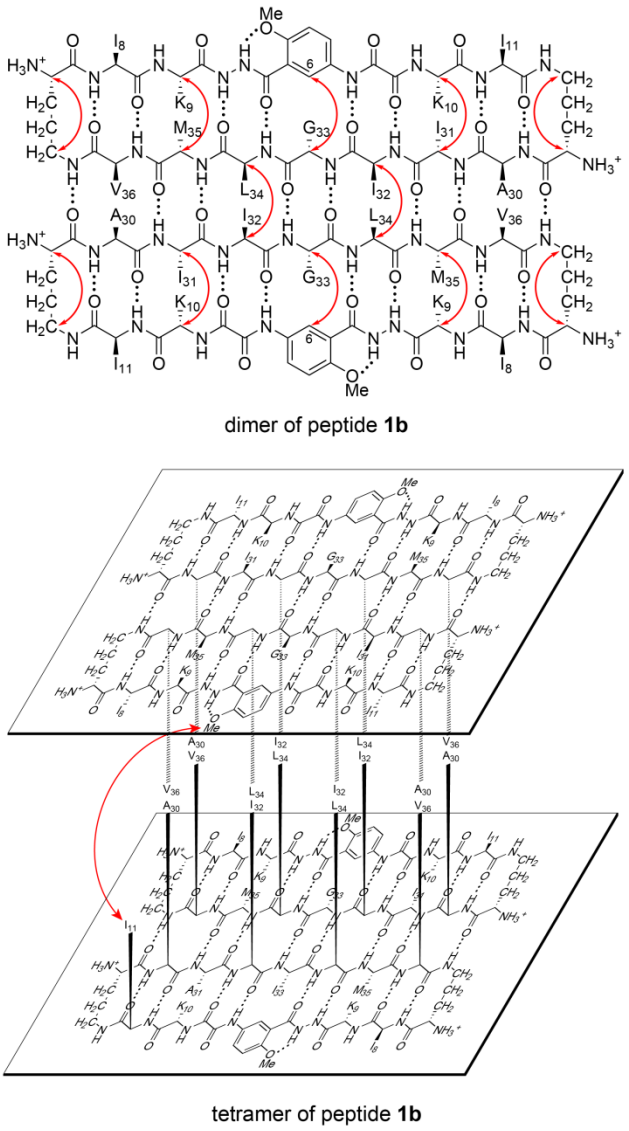

Figure 2.5. Dimer and tetramer of peptide **1b**. Hydrogen-bonded dimer subunit (upper). Red arrows illustrate intramolecular and intermolecular NOEs observed in the NOESY spectrum. Sandwich-like tetramer consisting of two hydrogen-bonded dimers (lower). The red arrow illustrates the interlayer NOEs observed in the NOESY spectrum. The tetramer exhibits four-fold symmetry and four I_{11}–Hao_{OMe} interactions, even though only one arrow is shown.

The NOESY spectrum shows additional NOEs associated with the stacking of two dimers to form a sandwich-like tetramer. Like peptide **1a**, peptide **1b** exhibits a pattern of NOEs between the Hao protons and the I_{11} side-chain protons, and an additional NOE between $HaoH_3$ and the δ-methyl protons of I_{11} (Figure S2.6). Figure 2.5 illustrates the stacking of the two dimers of peptide **1b** consistent with these interlayer NOEs.

^{1}H,^{15}N HSQC Studies of the Tetramers Formed by Peptides [^{15}N]1a and [^{15}N]1b. I studied ^{15}N-labeled homologues of peptides **1a** and **1b** by ^{1}H,^{15}N HSQC to identify and quantify the tetramers. ^{1}H,^{15}N HSQC is a mainstay in NMR spectroscopy of proteins, but is also useful for peptides. ^{15}N-Isotopic labeling and the dispersion provided by the f_1 (^{15}N) dimension resolves mixtures of peptides far better than is possible by homonuclear techniques.

I prepared peptides [^{15}N]**1a** and [^{15}N]**1b**, which each contain a single ^{15}N-labeled amino acid in the center of the heptapeptide strand. Peptide [^{15}N]**1a** contains an ^{15}N-labeled phenylalanine; peptide [^{15}N]**1b** contains an ^{15}N-labeled glycine. The ^{15}N isotopic label provides a spectroscopic probe for each species containing the ^{15}N-labeled peptide.

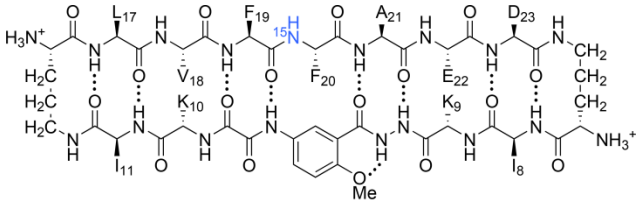

macrocyclic β-sheet peptide [^{15}N]**1a**

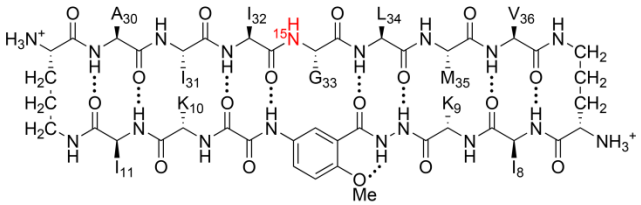

macrocyclic β-sheet peptide [^{15}N]**1b**

The ^{1}H,^{15}N HSQC spectrum of peptide [^{15}N]**1a** in 9:1 H_2O/D_2O at 8.0 mM and 293 K shows two crosspeaks; the ^{1}H,^{15}N HSQC spectrum of peptide [^{15}N]**1b** also shows two crosspeaks (Figure 2.6). The spectrum of peptide [^{15}N]**1a** shows a weak crosspeak associated with the monomer and a strong crosspeak associated with the tetramer; these crosspeaks are designated *1* and *2*, respectively. The spectrum of peptide [^{15}N]**1b** shows crosspeaks of comparable intensities associated with the monomer and tetramer; these crosspeaks are designated *3* and *4*, respectively. Table 2.2 summarizes the chemical shifts of these crosspeaks.

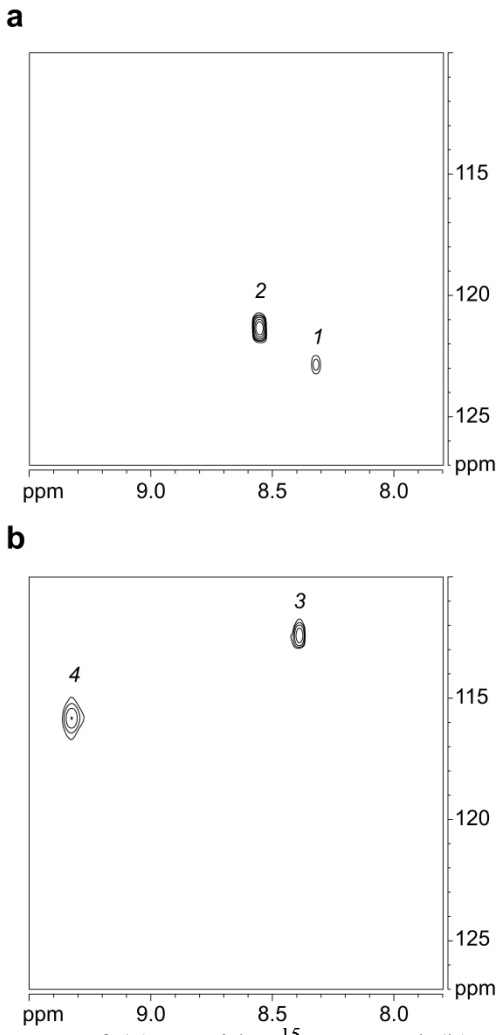

Figure 2.6. $^{1}H,^{15}N$ HSQC spectra of (a) peptide [^{15}N]**1a** and (b) peptide [^{15}N]**1b** at 8.0 mM in 9:1 H_2O/D_2O at 600 MHz and 293 K.

Table 2.2. Chemical shifts of peptides [^{15}N]1a and [^{15}N]1b[a]

crosspeak	δ F_{20}		δ G_{33}		species
	^{1}H	^{15}N	^{1}H	^{15}N	
1	8.32	122.3	–	–	A monomer
2	8.56	121.3	–	–	A_4 tetramer
3	–	–	8.39	112.5	B monomer
4	–	–	9.33	115.8	B_4 tetramer

[a] $^{1}H,^{15}N$ HSQC spectra were recorded at 8.0 mM in 9:1 H_2O/D_2O at 293 K.

In the accompanying chapter, I combine ^{15}N-labeling and $^{1}H,^{15}N$ NMR spectroscopy to identify and characterize the seven different species that form upon mixing peptides [^{15}N]**1a** and [^{15}N]**1b**.[15]

^{15}N-Edited NOESY. I used peptides [^{15}N]**1a** and [^{15}N]**1b** to corroborate the pairing of the dimers within the tetramers. I recorded ^{1}H,^{15}N NOESY-HSQC spectra with typical NOESY parameters in both ^{1}H dimensions (f_1 and f_3), but with only one increment in the ^{15}N dimension (f_2). The result is an ^{15}N-edited NOESY spectrum that shows only NOEs involving the ^{15}NH protons and requires no more time than a regular NOESY spectrum.

The NH protons of an antiparallel β-sheet typically give a pattern of four key NOEs associated with β-sheet folding and interstrand interaction. Two of the NOEs reflect β-sheet folding: a weaker intraresidue NOE to the α-proton and a stronger interresidue NOE to the α-proton of the adjacent residue. Figure 2.7 illustrates these close contacts and shows typical distances (3.0 Å and 2.2 Å, respectively). Two of the NOEs reflect interstrand interaction: an NOE to the α-proton diagonally across in the non-hydrogen-bonded pair, and another NOE to the NH proton diagonally across in the hydrogen-bonded pair. Figure 2.7 also illustrates these close contacts and shows typical distances (3.2 Å and 3.3 Å, respectively). The magnitude of the interresidue NOE should be much stronger than the magnitude of the interstrand NOEs, because the NOE intensities decrease with distance to the inverse sixth power.

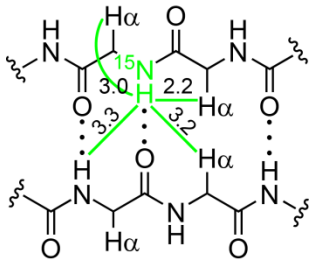

Figure 2.7. Four close contacts involving NH protons and Hα protons in antiparallel β-sheets. Typical distances are shown in angstroms.

The ^{15}N-edited NOESY spectrum of peptide [^{15}N]**1a** shows two sets of NOEs: one set is associated with the F_{20}NH proton from the monomer; the other set is associated with the F_{20}NH proton from the tetramer (Figure 2.8a). The monomer F_{20}NH proton gives only an intraresidue

NOE to the $F_{20}H\alpha$ proton. The tetramer $F_{20}NH$ proton gives two NOEs associated with β-sheet folding: a stronger interresidue NOE to the $F_{19}H\alpha$ proton and an intraresidue NOE to the $F_{20}H\alpha$ proton. The tetramer $F_{20}NH$ proton also gives an intermolecular NOE associated with interstrand interaction to the $A_{21}H\alpha$ proton diagonally across the peptide dimer. This NOE is significant, because it reflects the dimer within the tetramer (Figure 2.9a). The tetramer $F_{20}NH$ proton can not give an intermolecular NOE to the $F_{20}NH$ proton diagonally across the peptide dimer, because the tetramer is symmetrical (Figure S2.7). Figure 2.9 summarizes the observed NOEs involving the ^{15}NH protons between the dimers within the tetramer of peptide [^{15}N]**1a**.

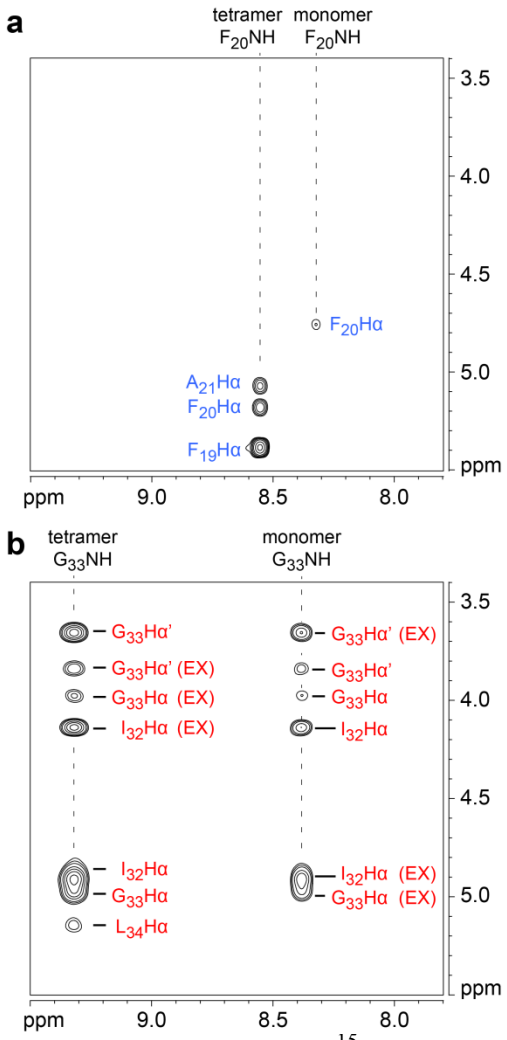

Figure 2.8. ^{15}N-Edited NOESY spectra of (a) peptide [^{15}N]**1a** and (b) peptide [^{15}N]**1b** at 8.0 mM in 9:1 H_2O/D_2O at 600 MHz and 293 K. The $G_{33}H\alpha$ corresponds to the *pro-R* α-proton and the $G_{33}H\alpha$' corresponds to the *pro-S* α-proton. Crosspeaks associated with chemical exchange between the monomer and tetramer are labeled EX.[20]

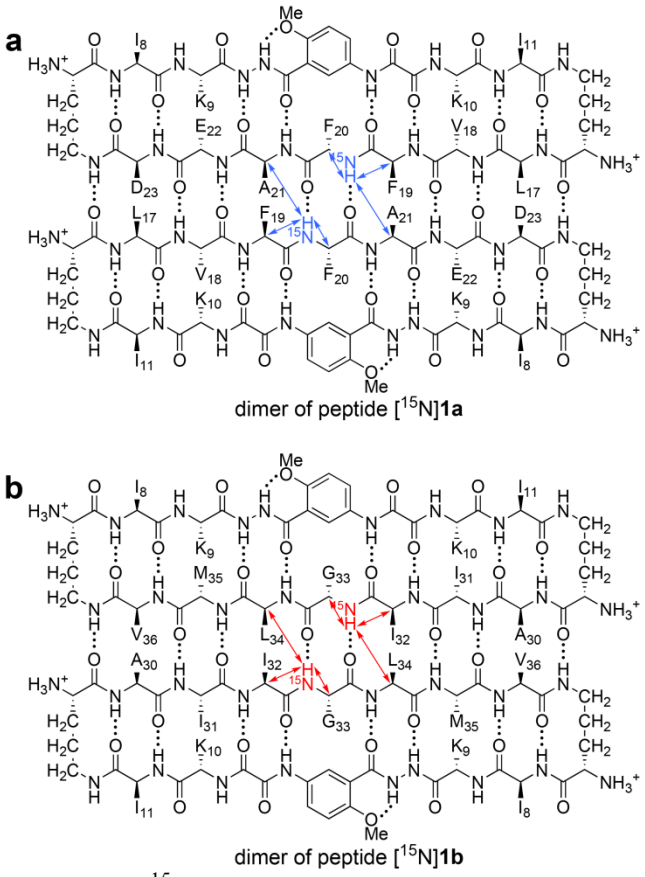

Figure 2.9. NOEs involving the ^{15}NH protons between the dimers of peptides [^{15}N]**1a** and [^{15}N]**1b** within the respective tetramers. Blue and red arrows illustrate observed NOEs.

The ^{15}N-edited NOESY spectrum of peptide [^{15}N]**1b** also shows two sets of NOEs: one set is associated with the G_{33}NH proton from the monomer; the other set is associated with the G_{33}NH proton from the tetramer (Figure 2.8b). The monomer G_{33}NH proton gives a pattern of NOEs associated with β-sheet folding: two intraresidue NOEs to the diastereotopic G_{33}Hα and G_{33}Hα' protons and one interresidue NOE to the I_{32}Hα proton. The tetramer G_{33}NH proton also gives a pattern of NOEs associated with β-sheet folding: two intraresidue NOEs to the G_{33}Hα and G_{33}Hα' protons and one interresidue NOE to the I_{32}Hα proton. The tetramer G_{33}NH proton also gives an intermolecular NOE associated with interstrand interaction to the L_{34}Hα proton diagonally across the peptide dimer. This NOE is significant, because it reflects the dimer within the tetramer. The tetramer G_{33}NH proton can not give an intermolecular NOE to the G_{33}NH

proton diagonally across the peptide dimer, because the tetramer is symmetrical (Figure S2.8). Figure 2.9 summarizes the observed NOEs involving the ^{15}NH protons between the dimers within the tetramer of peptide [^{15}N]**1b**.

Molecular Models of the Tetramers. I constructed energy-minimized models consistent with the observed NOEs to help understand the structures of the tetramers of peptides **1a** and **1b**. I began with the X-ray crystallographic coordinates of a tetramer formed by a homologous macrocyclic β-sheet peptide (PDB ID: 3T4G).[10a] I mutated the side chains to the residues of peptides **1a** and **1b**. I modified the alignment of the β-sheet dimers and oriented the dimers to reflect the observed NOEs. I then generated the minimum-energy models (local minima) of the tetramers. These models help illustrate the structures formed by the peptides derived from the central and C-terminal regions of Aβ. Figures 2.10 and 2.11 illustrate these models.

The energy-minimized model of the peptide **1a** tetramer consists of a β-sandwich of two four-stranded β-sheets that laminate together and form a hydrophobic core (Figure 2.10). The β-sheets exhibit a distinct twist that imparts a saddle shape. The side chains of L_{17}, F_{19}, and A_{21} form a hydrophobic surface that packs in the hydrophobic core, while the side chains of E_{22} and D_{23} are exposed to solvent. The β-sheet dimers do not completely overlap, but rather are rotated roughly 30 degrees about the normal axis. The rotation and twist of the β-sheets allow the corners to pack tightly against each other. The corners of the β-sheet layers are nearly in contact, which is consistent with the observed interlayer NOEs between the Hao protons and the I_{11} side-chain protons.

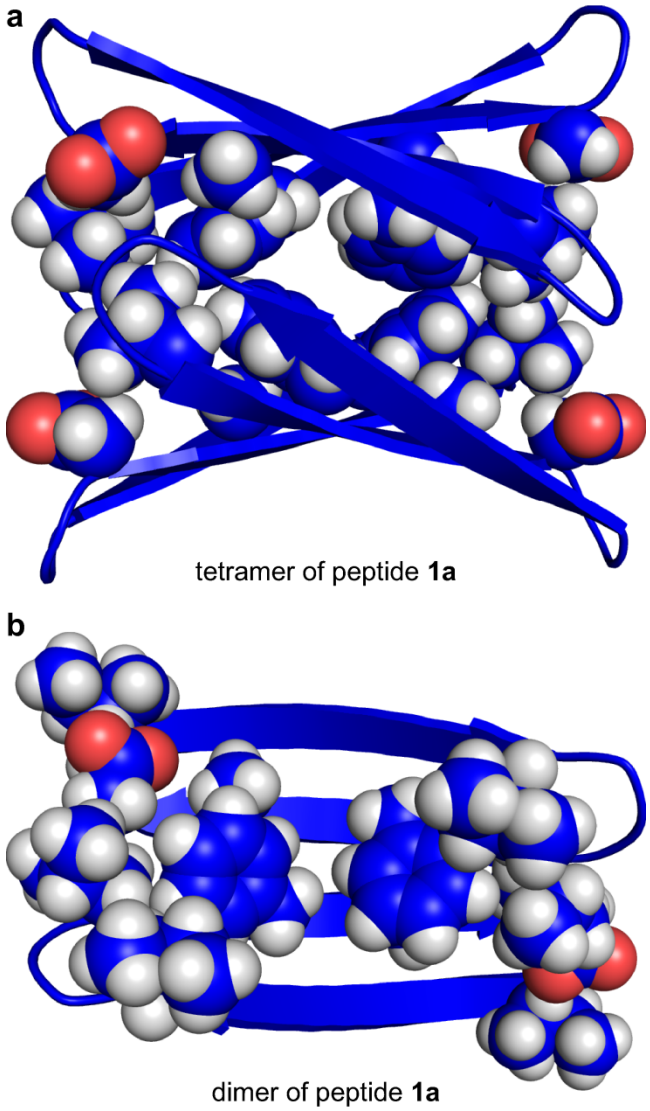

Figure 2.10. Molecular model of the tetramer formed by peptide **1a**. (a) The tetramer with the side chains of L_{17}, F_{19}, A_{21}, and D_{23} shown. (b) Dimer subunit of the tetramer with the side chains of L_{17}, F_{19}, A_{21}, D_{23}, I_{8}, and I_{11} shown.

The energy-minimized model of the peptide **1b** tetramer is similar to that of peptide **1a** in that it also consists two four-stranded β-sheets that laminate together (Figure 2.11). The β-sheets are slightly less twisted, and the side chains of A_{30}, I_{32}, L_{34}, and V_{36} form the hydrophobic surface that packs in the hydrophobic core. Like peptide **1a**, the β-sheets are rotated roughly 30 degrees about the normal axis, allowing the corners to pack tightly against each other.

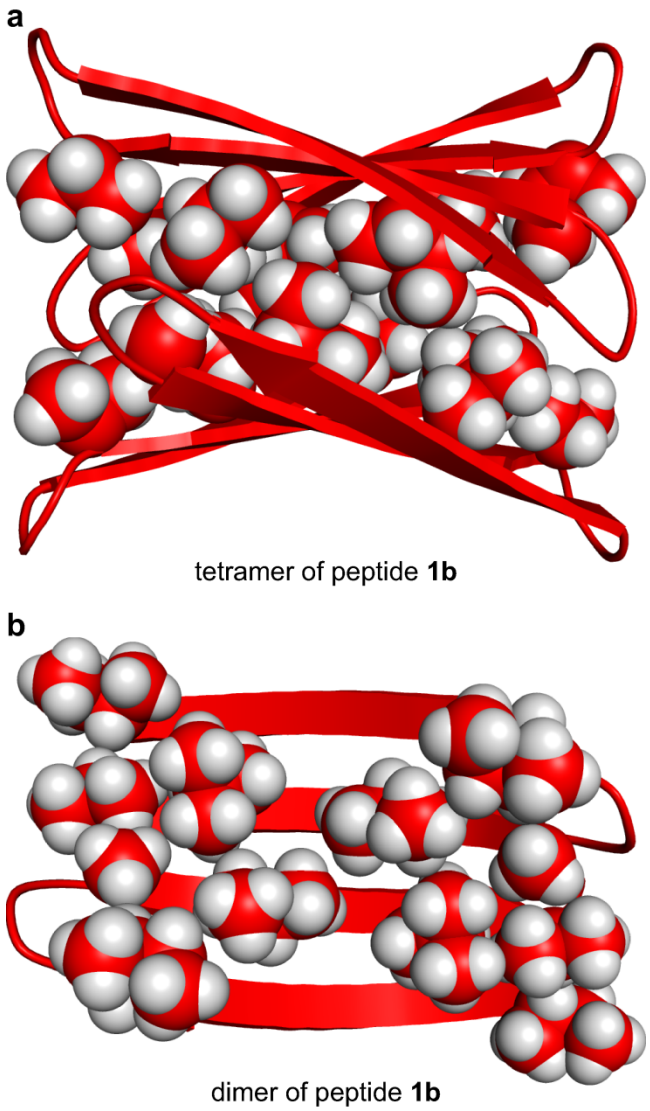

Figure 2.11. Molecular model of the tetramer formed by peptide **1b**. (a) The tetramer with the side chains of A_{30}, I_{32}, L_{34}, and V_{36} shown. (b) Dimer subunit of the tetramer with the side chains of A_{30}, I_{32}, L_{34}, V_{36}, I_8, and I_{11} shown.

CONCLUSION

Macrocyclic β-sheet peptides **1** provide a platform with which to study the self-assembly of amyloid-derived peptides. Essential to the design of these β-sheet-forming peptides is the use of an amphiphilic template strand containing the peptide sequence IKHaoKI to block uncontrolled aggregation. The unnatural amino acid Hao promotes β-sheet formation and blocks uncontrolled hydrogen-bonding interactions. The Ile residues in the template strand give a distinct hydrophobic surface that promotes peptide assembly, while the Lys residues give a distinct hydrophilic surface that disfavors aggregation.

Incorporation of the central and C-terminal regions of Aβ into peptides **1** allows the study of these regions. The peptides containing these regions assemble through hydrogen-bonding and hydrophobic interactions to form β-sheet dimers that further assemble to form tetramers. NOESY and other ^{1}H NMR studies show that the tetramers comprise a β-sandwich of two hydrogen-bonded dimers. Molecular modeling further elucidates the structures of the tetramers. The tetramers that form reflect the propensities of the central and C-terminal regions to assemble and adopt β-sheet structure.

Incorporation of a single ^{15}N isotopic label into peptides **1** provides a spectroscopic probe that simplifies the spectra of the monomers and tetramers. ^{1}H,^{15}N HSQC studies show that each peptide gives a single crosspeak associated with the monomer and a single crosspeak associated with the tetramer. ^{15}N-Edited NOESY studies corroborate the pairing of the dimers within the tetramers. The hydrophobic amino acids Gly, Ala, Val, Leu, Ile, and Phe are widespread in amyloidogenic peptides and proteins and are readily available with an ^{15}N isotopic label at reasonable cost. The incorporation of a single ^{15}N-labeled amino acid as a spectroscopic probe promises to be broadly useful in studying the assembly and coassembly of peptides. In the accompanying chapter, I apply this approach to study the coassembly of peptides derived from the central and C-terminal regions of Aβ.

REFERENCES AND NOTES

1. (a) Selkoe, D. J. *Nature* **2003**, *426*, 900-904; (b) Ross, C. A.; Poirier, M. A. *Nat. Med.* **2004**, *10*, S10-S17; (c) Chiti, F.; Dobson, C. M. *Annu. Rev. Biochem.* **2006**, *75*, 333–366; (d) Knowles, T. P.; Vendruscolo, M.; Dobson, C. M. *Nat. Rev. Mol. Cell Biol.* **2014**, *15*, 384–396.

2. (a) Näslund, J.; Haroutunian, V.; Mohs, R.; Davis, K. L.; Davies, P.; Greengard, P.; Buxbaum, J. D. *JAMA* **2000**, *283*, 1571–1577; (b) Haass, C.; Selkoe, D. J. *Nat. Rev. Mol. Cell Biol.* **2007**, *8*, 101–112; (c) Querfurth, H. W.; LaFerla, F. M. *N. Eng. J. Med.* **2010**, *362*, 329–344.

3. Kirkitadze, M. D.; Bitan, G.; Teplow, D. B. *J. Neurosci. Res.* **2002**, *69* (5), 567–77.

4. (a) Petkova, A. T.; Ishii, Y.; Balbach, J. J.; Antzutkin, O. N.; Leapman, R. D.; Delaglio, F.; Tycko, R. *Proc. Natl. Acad. Sci. U.S.A.* **2002**, *99*, 16742–16747; (b) Paravastu, A. K.; Leapman, R. D.; Yau, W.-M.; Tycko, R. *Proc. Natl. Acad. Sci. U.S.A.* **2008**, *105*, 18349–18354; (c) Tycko, R.; Wickner, R. B. *Acc. Chem. Res.* **2013**, *46*, 1487–1496; (d) Lu, J.-X.; Qiang, W.; Yau, W.-M.; Schwieters, C. D.; Meredith, S. C.; Tycko, R. *Cell* **2013**, *154*, 1257–1268.

5. The fibrils formed by $A\beta_{1-42}$ adopt a more compact structure: (a) Xiao, Y.; Ma, B.; McElheny, D.; Parthasarathy, S.; Long, F.; Hoshi, M.; Nussinov, R.; Ishii, Y. *Nat. Struct. Mol. Biol.* **2015**, *22*, 499–505. (b) Walti, M. A.; Ravotti, F.; Arai, H.; Glabe, C. G.; Wall, J. S.; Bockmann, A.; Guntert, P.; Meier, B. H.; Riek, R. *Proc. Natl. Acad. Sci. U.S.A.* **2016**, *113*, E4976–E4984. (c) Colvin, M. T.; Silvers, R.; Ni, Q. Z.; Can, T. V.; Sergeyev, I.; Rosay, M.; Donovan, K. J.; Michael, B.; Wall, J.; Linse, S.; Griffin, R. G. *J. Am. Chem. Soc.* **2016,** *138*, 9663–9674.

6. (a) Cleary, J. P.; Walsh, D. M.; Hofmeister, J. J.; Shankar, G. M.; Kuskowski, M. A.; Selkoe, D. J.; Ashe, K. H. *Nat. Neurosci.* **2005**, *8*, 79–84; (b) Benilova, I.; Karran, E.; De Strooper, B. *Nat. Neurosci.* **2012**, *15*, 349–357; (c) Teplow, D. B. *Alzheimer's Res. Ther.* **2013**, *5*, 39–51; (d) Walsh, D. M.; Selkoe, D. J. *J. Neurochem.* **2007**, *101*, 1172–1184.

7. Liu, R.; McAllister, C.; Lyubchenko, Y.; Sierks, M. R. *J. Neurosci. Res.* **2004**, *75*, 162–171.

8. (a) Esler, W. P.; Stimson, E. R.; Ghilardi, J. R.; Lu, Y. A.; Felix, A. M.; Vinters, H. V.; Mantyh, P. W.; Lee, J. P.; Maggio, J. E. *Biochemistry* **1996**, *35*, 13914–13921; (b) Cukalevski, R.; Boland, B.; Frohm, B.; Thulin, E.; Walsh, D.; Linse, S. *ACS Chem. Neurosci.* **2012**, *3*, 1008–1016; (c) Tjernberg, L. O.; Callaway, D. J. E.; Tjernberg, A.; Hahne, S.; Lilliehook, C.; Terenius, L.; Thyberg, J.; Nordstedt, C. *J. Biol. Chem.* **1999**, *274*, 12619–12625.

9. (a) Larini, L.; Shea, J. E. *Biophys. J.* **2012**, *103*, 576–586; (b) Ball, K. A.; Phillips, A. H.; Wemmer, D. E.; Head-Gordon, T. *Biophys. J.* **2013**, *104*, 2714–2724; (c) Do, T. D.; LaPointe, N. E.; Nelson, R.; Krotee, P.; Hayden, E. Y.; Ulrich, B.; Quan, S.; Feinstein, S. C.; Teplow, D. B.; Eisenberg, D.; Shea, J. E.; Bowers, M. T. *J. Am. Chem. Soc.* **2016**, *138*, 549–557.

10. (a) Hoyer, W.; Gronwall, C.; Jonsson, A.; Stahl, S.; Hard, T. *Proc. Natl. Acad. Sci. U.S.A.* **2008**, *105*, 5099–5104; (b) Cerf, E.; Sarroukh, R.; Tamamizu-Kato, S.; Breydo, L.; Derclaye, S.; Dufrene, Y. F.; Narayanaswami, V.; Goormaghtigh, E.; Ruysschaert, J. M.; Raussens, V. *Biochem. J.* **2009**, *421*, 415–423; (c) Yu, L.; Edalji, R.; Harlan, J. E.; Holzman, T. F.; Lopez, A. P.; Labkovsky, B.; Hillen, H.; Barghorn, S.; Ebert, U.; Richardson, P. L.; Miesbauer, L.; Solomon, L.; Bartley, D.; Walter, K.; Johnson, R. W.;

Hajduk, P. J.; Olejniczak, E. T. *Biochemistry* **2009**, *48*, 1870–1877; (d) Sandberg, A.; Luheshi, L. M.; Söllvander, S.; Pereira de Barros, T.; Macao, B.; Knowles, T. P. J.; Biverstål, H.; Lendel, C.; Ekholm-Petterson, F.; Dubnovitsky, A.; Lannfelt, L.; Dobson, C. M.; Härd, T. *Proc. Natl. Acad. Sci. U.S.A.* **2010**, *107*, 15595–15600; (e) Lendel, C.; Bjerring, M.; Dubnovitsky, A.; Kelly, R. T.; Filippov, A.; Antzutkin, O. N.; Nielsen, N. C.; Hard, T. *Angew. Chem. Int. Ed.* **2014**, *53*, 1–6; (f) Spencer, R. K.; Li, H.; Nowick, J. S. *J. Am. Chem. Soc.* **2014**, 5595–5598; (g) Kreutzer, A. G.; Hamza, I. L.; Spencer, R. K.; Nowick, J. S. *J. Am. Chem. Soc.* **2016**, *138*, 4634–4642.

11. (a) Cheng, P. N.; Liu, C.; Zhao, M.; Eisenberg, D.; Nowick, J. S. *Nat. Chem.* **2012**, *4*, 927–933; (b) Liu, C.; Zhao, M.; Jiang, L.; Cheng, P. N.; Park, J.; Sawaya, M. R.; Pensalfini, A.; Gou, D.; Berk, A. J.; Glabe, C. G.; Nowick, J.; Eisenberg, D. *Proc. Natl. Acad. Sci. U.S.A.* **2012**, *109*, 20913–20918; (c) Buchanan, L. E.; Dunkelberger, E. B.; Tran, H. Q.; Cheng, P. N.; Chiu, C. C.; Cao, P.; Raleigh, D. P.; de Pablo, J. J.; Nowick, J. S.; Zanni, M. T. *Proc. Natl. Acad. Sci. U.S.A.* **2013**, *110*, 19285–19290.

12. Nowick, J. S.; Chung, D. M.; Maitra, K.; Maitra, S.; Stigers, K. D.; Sun, Y. *J. Am. Chem. Soc.* **2000**, *122*, 7654–7661.

13. (a) Nowick, J. S.; Brower, J. O. *J. Am. Chem. Soc.* **2003**, *125*, 876–877; (b) Woods, R. J.; Brower, J. O.; Castellanos, E.; Hashemzadeh, M.; Khakshoor, O.; Russu, W. A.; Nowick, J. S. *J. Am. Chem. Soc.* **2007**, *129*, 2548–2558.

14. For some related studies of peptide and protein coassembly, see:(a) Hammarstrom, P.; Schneider, F.; Kelly, J. W. *Science* **2001**, *293*, 2459–246210. (b) Schnarr, N. A.; Kennan, A. J. *J. Am. Chem. Soc.* ***2002***, *124*, 9779–9783. (c) Hadley, E. B.; Testa, O. D.; Woolfson, D. N.; Gellman, S. H. *Proc. Natl. Acad. Sci. U.S.A.* **2008**, *105*, 530–535. (d)

Xu, F.; Zahid, S.; Silva, T.; Nanda, V. *J. Am. Chem. Soc.* **2011**, *133*, 15260–15263. (e) Fallas, J. A.; Hartgerink, J. D. *Nat. Commun.* **2012**, *3*, 1087. (f) Thomas, F.; Boyle, A. L.; Burton, A. J.; Woolfson, D. N. *J. Am. Chem. Soc.* **2013**, *135*, 5161–5166. (g) Negron, C.; Keating, A. E. *J. Am. Chem. Soc.* **2014**, *136*, 16544–16556.

15. Truex, N. L.; Nowick, J. S. *J. Am. Chem. Soc.* **2016**, *138*, 13891–13900.

16. ^{1}H NMR studies were performed without buffer at pH 2.5 ± 0.5 to keep peptides **1a** and **1b** in the fully protonated state.

17. (a) Khakshoor, O.; Demeler, B.; Nowick, J. S. *J. Am. Chem. Soc.* **2007**, *129*, 5558–5569; (b) Pham, J. D.; Demeler, B.; Nowick, J. S. *J. Am. Chem. Soc.* **2014**, *136*, 5432–5442; (c) Pham, J. D.; Spencer, R. K.; Chen, K. H.; Nowick, J. S. *J. Am. Chem. Soc.* **2014**, *136*, 12682–12690.

18. (a) Polson, A. *J. Phys. Colloid. Chem.* **1950**, *54*, 649–652; (b) Teller, D. C.; Swanson, E.; de Haën, C. *Methods Enzymol.* **1979**, *61*, 104–124; (c) Yao, S.; Howlett, G. J.; Norton, R. S. *J. Biol. NMR* **2000**, *16*, 109–119; (d) Cohen, Y.; Avram, L.; Frish, L. *Angew. Chem. Int. Ed.* **2005**, *44*, 520–554; (e) Cohen, Y.; Avram, L.; Evan-Salem, T.; Slovak, S.; Shemesh, N.; Frish, L. In *Analytical Methods in Supramolecular Chemistry*, 2nd ed.; Schalley, C. A., Ed. Wiley-VCH: Weinheim: 2012; pp 197–285.

19. The ratio of diffusion coefficients of an oligomer and monomer reflects the oligomerization state as well as the shapes of the molecules. A tetramer will have a diffusion coefficient of about 0.59 to 0.63 times that of the monomer, while a dimer will have a diffusion coefficient of about 0.75 to 0.79 times that of the monomer. A tetramer could not easily be distinguished from a pentamer and could only marginally be distinguished from a trimer on the basis of diffusion coefficients measured by DOSY.

The observation of well-defined dimer subunits by NOESY in conjunction with the observed ratios of diffusion coefficients by DOSY clearly establishes the tetrameric state of the oligomers.

20. Chemical exchange between the monomer and tetramer of peptide **1a** is slow on the hundred-millisecond time scale at 298 K, but exchange increases at higher temperatures. An EXSY experiment shows a set of EXSY crosspeaks that indicate chemical exchange on the hundred-millisecond time scale at 318 K. (See the Supporting Information.) In contrast, chemical exchange between the monomer and tetramer of peptide **1b** occurs on the hundred-millisecond time scale even at 293 K.

SUPPORTING INFORMATION FOR

Assembly of Peptides Derived from β-Sheet Regions of β-Amyloid

2.I. SUPPLEMENTAL FIGURES

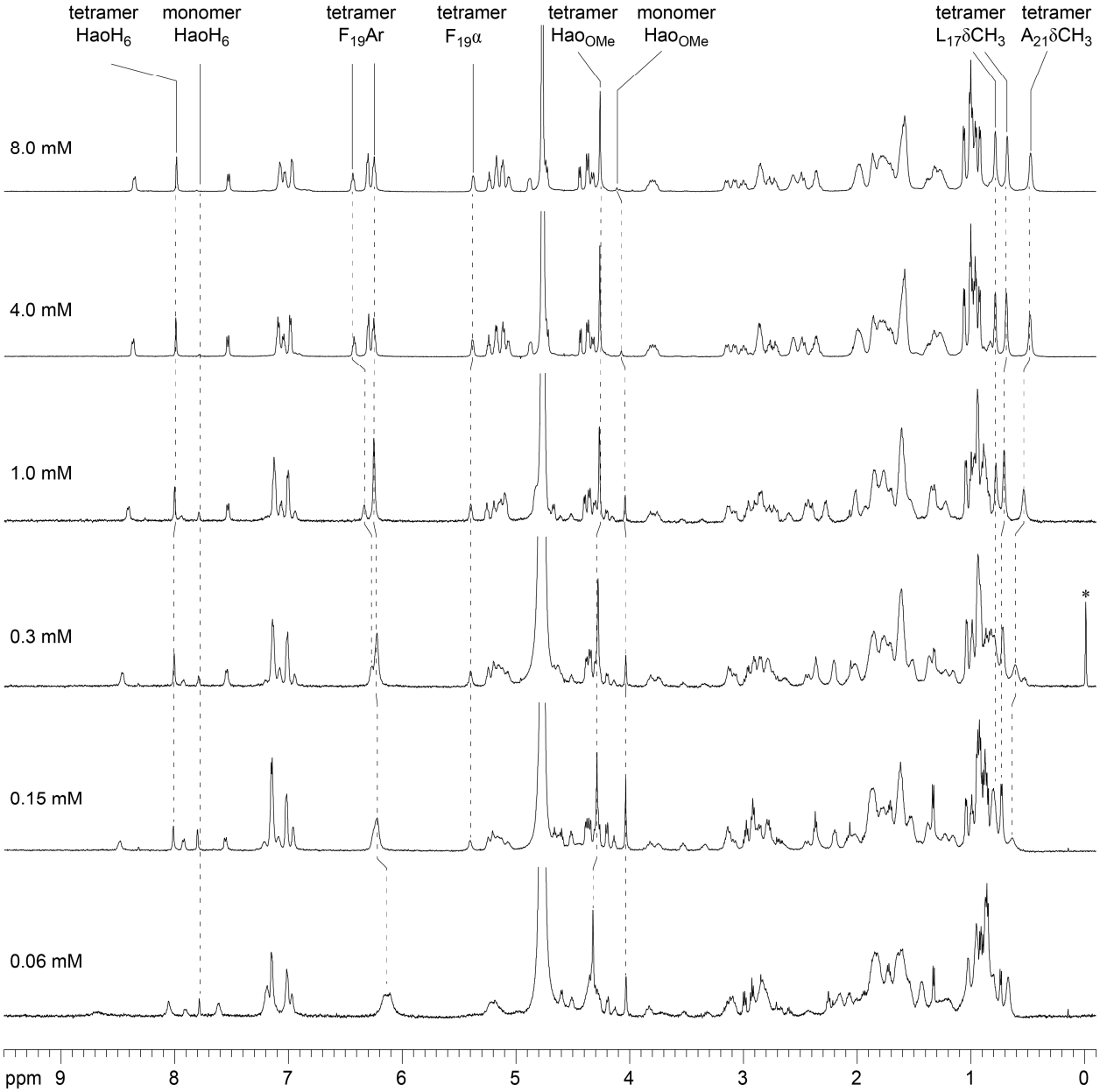

Figure S2.1. ^{1}H NMR spectra of peptide **1a** at various concentrations in D_2O at 600 MHz and 298 K. The 0.3 mM sample contains DSA as an internal standard, which is marked by an asterisk (*).

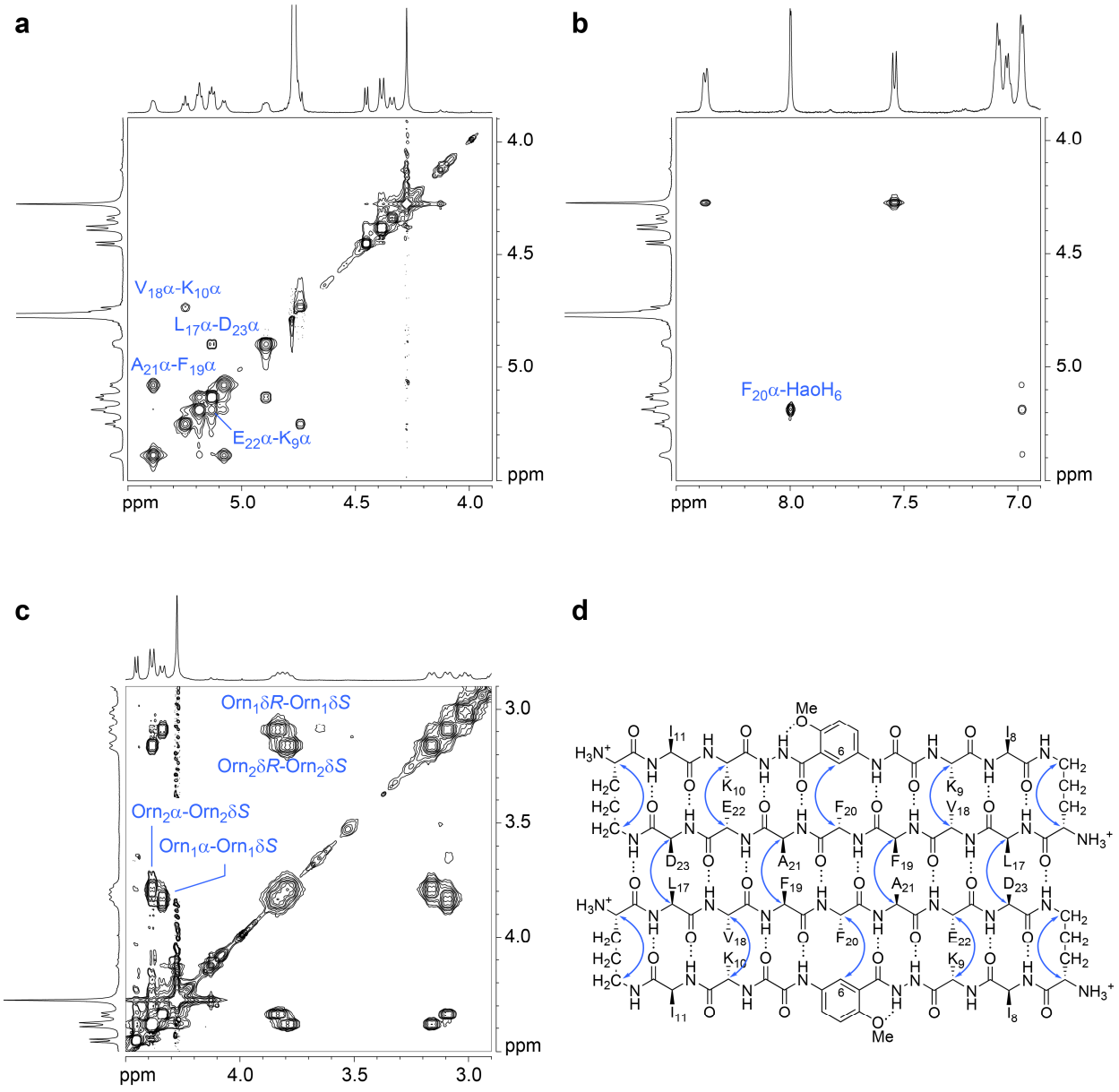

Figure S2.2. Expansions of the NOESY spectrum of peptide **1a** at 8.0 mM in D_2O at 600 MHz and 298 K. Key NOEs associated with β-sheet folding and dimerization are highlighed in blue. The $^{\delta}$Orn *pro-R* δ-protons are designated Ornδ*R*; The $^{\delta}$Orn *pro-R* δ-protons are designated Ornδ*R*.

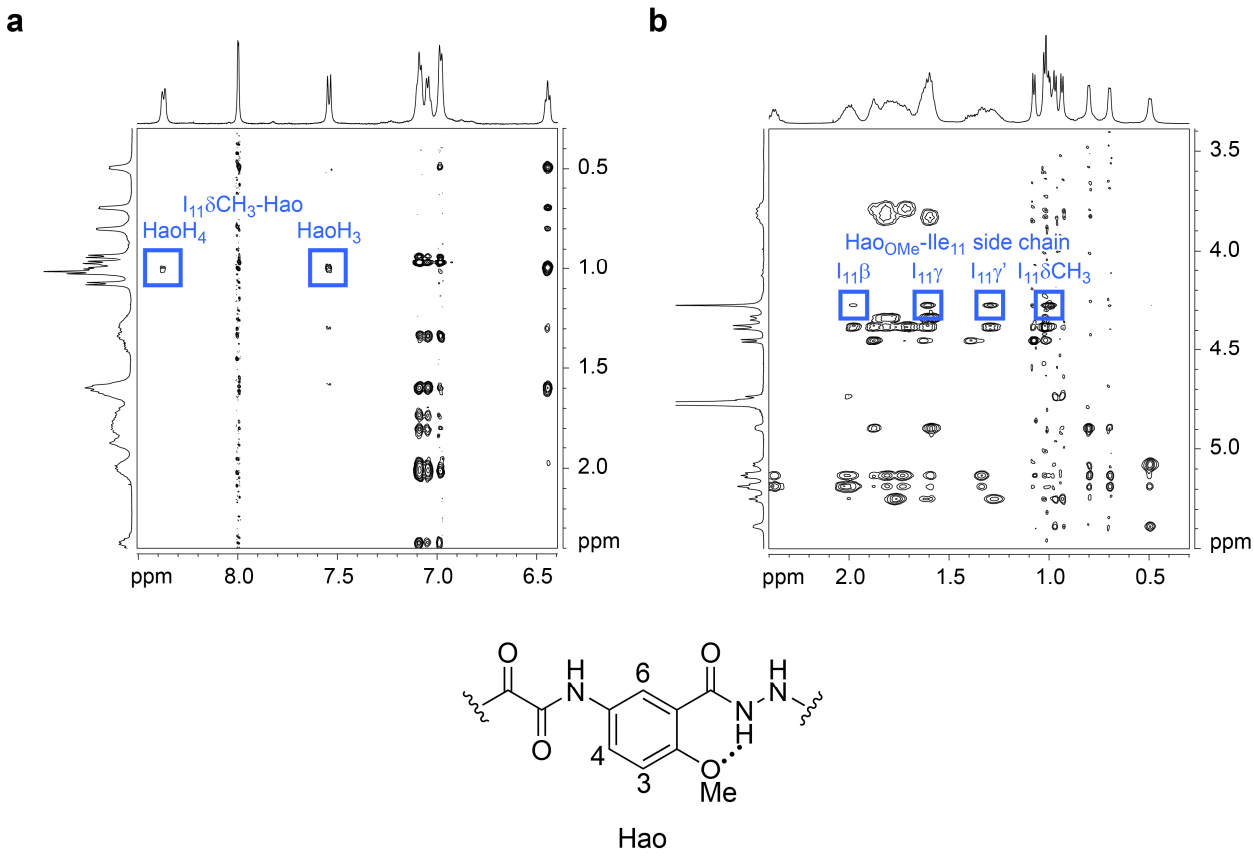

Figure S2.3. Expansions of the NOESY spectrum of peptide **1a** at 8.0 mM in D_2O at 600 MHz and 298 K. Key interlayer NOEs associated with tetramerization are highlighted in blue.

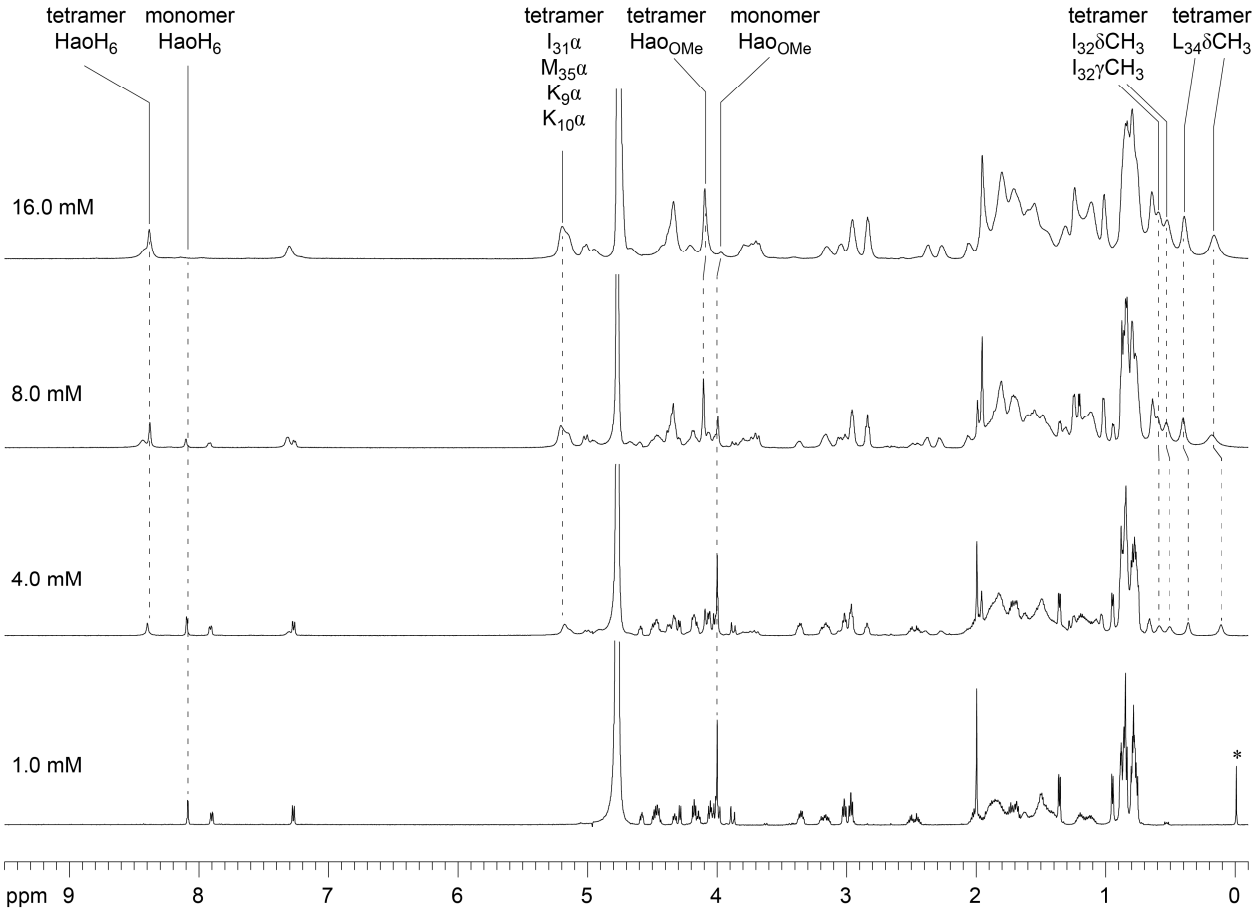

Figure S2.4. ^{1}H NMR spectra of peptide **1b** at various concentrations in D_2O at 600 MHz and 298 K. The 1.0 mM sample contains DSA as an internal standard, which is marked by an asterisk (*).

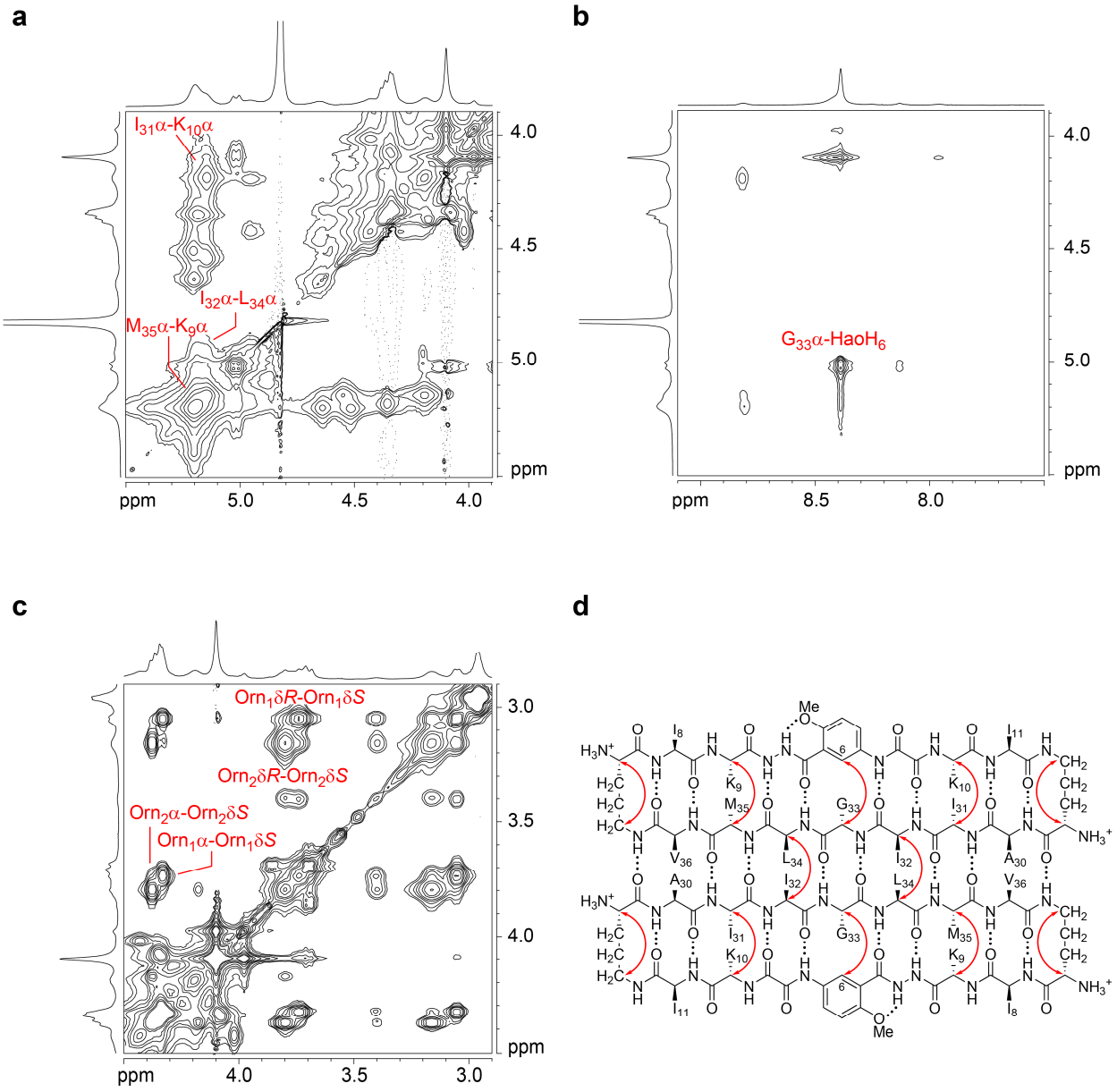

Figure S2.5. Expansions of the NOESY spectrum of peptide **1b** at 16.0 mM in D_2O at 600 MHz and 293 K. Key NOEs associated with β-sheet folding and dimerization are highlighed in red. The G_{33} *pro-S* α-proton is designated G_{33}α'; the $^{\delta}$Orn *pro-R* δ-protons are designated Ornδ*R*; The $^{\delta}$Orn *pro-R* δ-protons are designated Ornδ*R*.

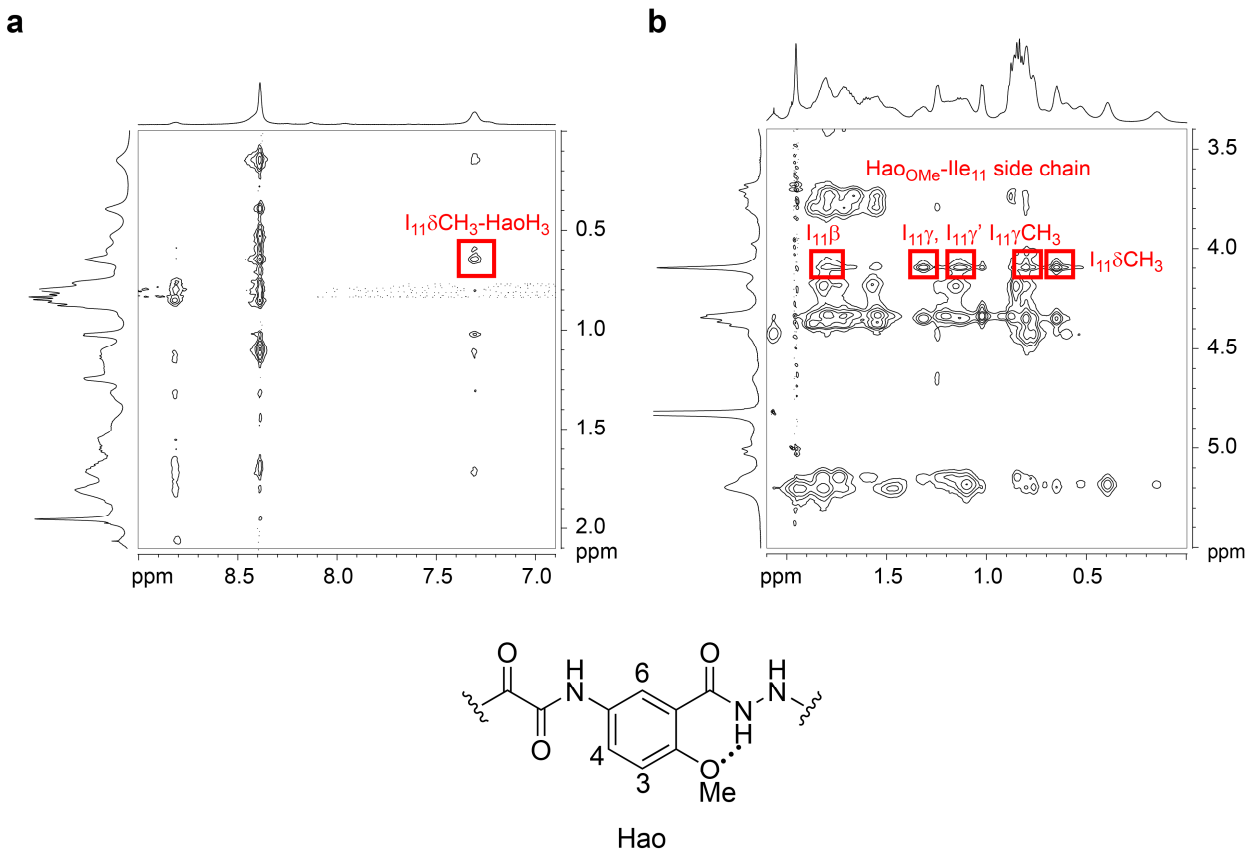

Figure S2.6. Expansions of the NOESY spectrum of peptide **1b** at 16.0 mM in D_2O at 600 MHz and 293 K. Key interlayer NOEs associated with tetramerization are highlighted in red.

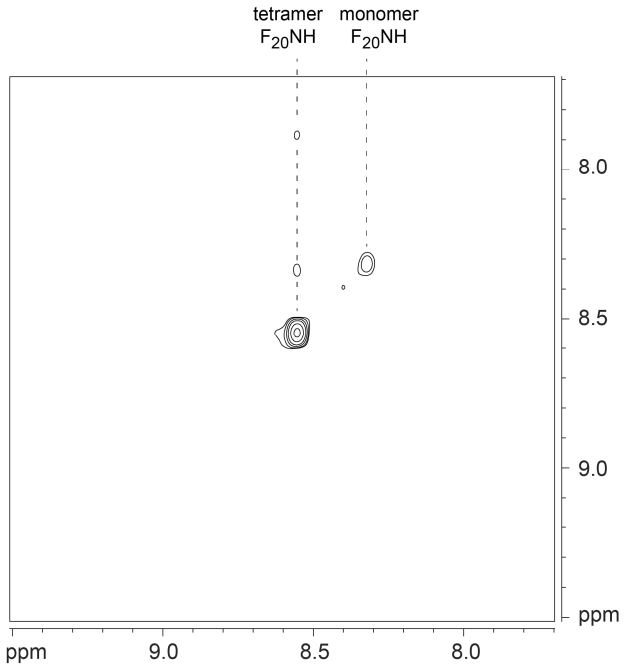

Figure S2.7. ^{15}N-Edited NOESY spectrum of peptide [^{15}N]**1a** at 8.0 mM in 9:1 H_2O/D_2O at 600 MHz and 293 K.

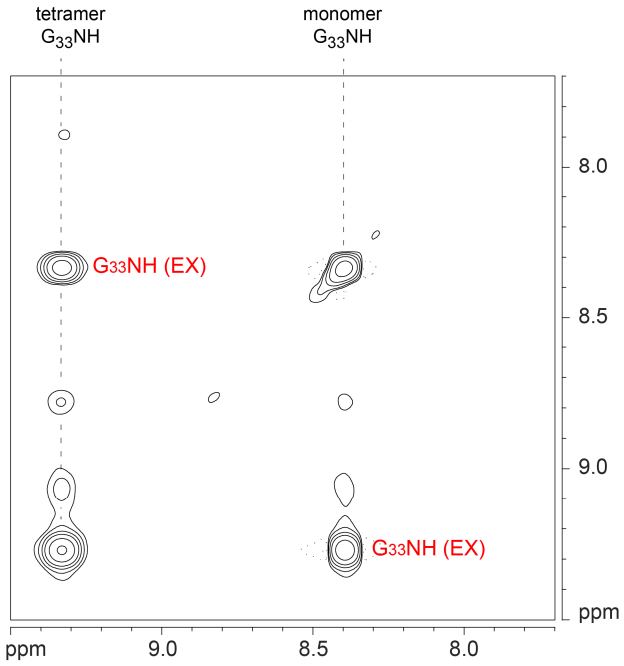

Figure S2.8. ^{15}N-Edited NOESY spectrum of peptide [^{15}N]**1b** at 8.0 mM in 9:1 H_2O/D_2O at 600 MHz and 293 K. Crosspeaks associated with chemical exchange between the monomers and tetramers are labeled EX.

2.II. MATERIALS AND METHODS

General

N,*N*-Dimethylformamide (DMF), 2,4,6-collidine, and piperidine were purchased from Alfa Aesar and used without further purification. HPLC grade acetonitrile (CH_3CN) was purchased from VWR International and used without further purification. Methylene chloride (CH_2Cl_2) was purchased from Fisher Scientific, stored under argon, and passed through a column of alumina before use.[1] Boc-Orn(Fmoc)-OH, HCTU, HBTU and HOBt were purchased from GL Biochem Ltd (Shanghai). 2-Chlorotrityl chloride resin and Fmoc protected amino acids were purchased from Chem-Impex International. *N*,*N*-Diisopropylethylamine (DIPEA), *N*-methylmorpholine (NMM), trifluoroacetic acid (TFA), and triisopropylsilane (TIPS) were purchased from Oakwood Chemical. Isotopically labeled glycine (^{15}N, 98%), phenylalanine (^{15}N, 98%), and deuterium oxide (D, 99.96%) were purchased from Cambridge Isotope Laboratories, Inc. Fmoc-Hao-OH was synthesized according to previously reported procedures.[2]

Synthesis of Peptides 1

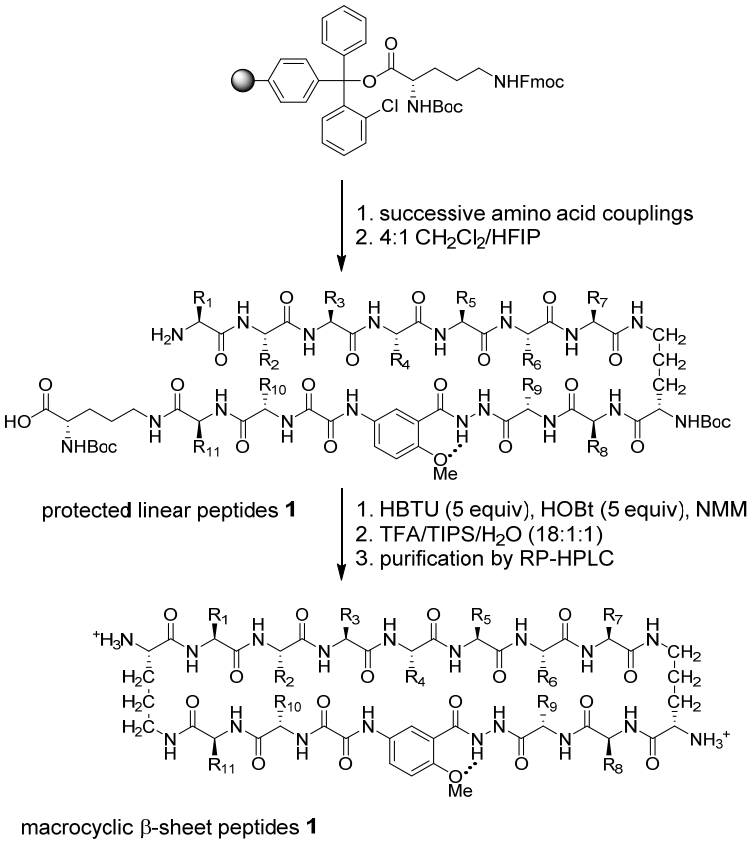

Resin Loading. 2-Chlorotrityl chloride resin (300 mg, 1.1 meq/g, 100–200 mesh) was suspended in ca. 8 mL of CH_2Cl_2 in a 10-mL Bio-Rad Poly-Prep column and allowed to swell (15 min). The CH_2Cl_2 was drained and a solution of Boc-Orn(Fmoc)-OH (0.22 mmol, 100.0 mg) in CH_2Cl_2 (7.6 mL) and 2,4,6-collidine (0.4 mL), was added. The suspension was agitated gently overnight (10–12 h) and the solution was drained. The capping solution 17:2:1 CH_2Cl_2/MeOH/DIPEA (8 mL) was added. The mixture was agitated gently (1 h), and then the solution was drained.

Solid-Phase Peptide Synthesis. The loaded resin was transferred to a solid-phase peptide synthesis vessel with DMF (3 × 2 mL). Successive rounds of solid-phase peptide synthesis were performed on a PS3^{TM} Peptide Synthesizer (Protein Technologies) using the following conditions: The Fmoc deprotection steps (2 × 5 min) were performed with a 20% piperidine in DMF solution. The coupling steps (1 × 20 min) were performed for the amino acids (4 equiv) with HCTU (4 equiv) and a 20% 2,4,6-collidine in DMF solution. The unnatural amino acid Fmoc-Hao-OH (2 equiv) was coupled twice with 2 equiv of HCTU per coupling (60 min) to achieve complete coupling. DMF was used to rinse the resin after each deprotection (6 × 3 mL) and after each amino acid coupling (6 × 3 mL).

Cleavage from Resin. After the synthesis of each peptide was complete, the resin was transferred into the Poly-Prep column with CH_2Cl_2 (ca. 2 mL) and the solution was drained. The solid-phase peptide synthesis vessel was rinsed with ca. two additional portions of CH_2Cl_2 to ensure the complete transfer of the resin and the removal of DMF. A 1:4 HFIP/CH_2Cl_2 solution (8 mL) was added to the resin and the mixture was agitated gently. After 1 h, the solution was drained into a 250-mL round-bottom flask and the treatment with HFIP/CH_2Cl_2 solution was repeated. The combined solutions were evaporated under vacuum to give the protected linear peptides **1**.

Cyclization. The protected linear peptides **1** were cyclized with HBTU (5 equiv), HOBt (5 equiv), and NMM (8 equiv) in a solution of DMF (125 mL). The solution was stirred under N_2 overnight (12–24 h), and then the DMF was evaporated under vacuum. The peptides were placed under vacuum (ca. 0.1 mmHg) overnight to ensure complete removal of any residual DMF.

Deprotection. The protected cyclic peptides **1** were deprotected under acidic conditions with a solution of 18:1:1 TFA/triisopropylsilane/H_2O (10 mL). The solution was stirred for 2 h, then evaporated under vacuum. For peptides containing a methionine (**1b** and [^{15}N]**1b**), 50 mg of dithiothreitol (DTT) was added to the solution to prevent sulfur oxidation.

RP-HPLC Purification. The peptides were suspended in a solution of 20% aqueous CH_3CN (ca. 8 mL) and the suspensions were filtered through a 0.2 μm filter. The purity of each peptide was analyzed by analytical RP-HPLC on a Phenomenex Aeris 2.6μ XB-C18 column (150 mm x 4.6 mm) with a 5–100% gradient over 20 min of CH_3CN in H_2O with 0.1% TFA at 1.0 mL/min. The purification of each peptides was performed by preparative RP-HPLC on an Agilent Zorbax 7 μM SB-C18 Prep HT column (21.2 mm x 250 mm) with a 15–30% gradient over 10 min and 30–60% gradient over 45 min of CH_3CN in H_2O with 0.1% TFA at 15.0 mL/min. The pure fractions were combined and concentrated under vacuum. The peptides were re-suspended in a solution of H_2O with 0.1% TFA (ca. 10–15 mL), then lyophilized to give peptides **1** as a white powder in 8–22% yield (30–80 mg) based on the resin loading of the first amino acid Boc-Orn(Fmoc)-OH).

Fmoc-Protection of ^{15}N-Labeled Amino Acids[3]

Fmoc-[^{15}N]Phe-OH: A 100-mL one-neck round-bottom flask equipped with a magnetic stirring bar was charged with ^{15}N-labeled phenylalanine (1.0 g, 6 mmol) and a solution of 1:1 CH_3CN/H_2O (50 mL). Et_3N (0.6 g, 6 mmol) and Fmoc-OSu (1.9 g, 5.7 mmol) were added, then the reaction mixture was stirred until the solution turned clear (ca. 15 min). Additional Et_3N was added until the pH was roughly 8.5, then the mixture was stirred for 1 h. The mixture was poured into a solution of 1.0 M HCl (250 mL) in a 400-mL beaker while stirring vigorously. The Fmoc-[^{15}N]Phe-OH precipitated from the solution and the solid was isolated by filtering the mixture through a sintered glass filter funnel with a medium frit. The funnel was covered with a piece of filter paper and the solid was dried by aspirating air through the funnel. The solid was suspended in ca. 200 mL of EtOAc to form a turbid solution. The solution was stirred vigorously for 10 min, dried over $MgSO_4$, filtered, and then concentrated under vacuum to give a white solid. The isolated solid was ground into a fine powder to give ca. 1.94 g (92%). ^{1}H NMR (500 MHz, $CDCl_3$): δ 7.77 (d, J = 7.5 Hz, 2H), 7.55 (t, J = 6.2 Hz, 2H), 7.40 (t, J = 7.4 Hz, 2H), 6.80 (m, 5H), 7.15 (d, J = 6.6 Hz, 2H), 5.19 (dd, J = 91.9, 8.2 Hz, 1H), 4.70 (m, 1H), 4.46 (dd, J = 10.4, 7.3 Hz, 1H), 4.37 (t, J = 8.7 Hz, 1H), 4.21 (t, J = 6.7 Hz, 1H), 3.18 (m, 2H); ^{13}C NMR (125 MHz, $CDCl_3$) δ 175.2, 156.0 (d, $^1J_{CN}$ = 25 Hz), 144.0, 141.6, 135.6, 129.6, 129.0, 128. 0, 127.6, 127.3, 125.3, 120.3, 67.3, 54.7 (d, $^1J_{CN}$ = 13.8 Hz), 47.4, 37.9, 30.0.

Fmoc-[^{15}N]Gly-OH: A 100-mL one-neck round-bottom flask equipped with a magnetic stirring bar was charged with ^{15}N-labeled glycine (1.0 g, 13 mmol) and a solution of 1:1 CH_3CN/H_2O (50 mL). Et_3N (1.3 g, 13 mmol) and Fmoc-OSu (4.2 g, 12.5 mmol) were added, then the reaction mixture was stirred until the solution turned clear (ca. 15 min). Additional Et_3N was added until the pH was roughly 8.5, then the mixture was stirred for 1 h. The mixture was poured into a solution of 1.0 M HCl (250 mL) in a 400-mL beaker while stirring vigorously. The Fmoc-[^{15}N]Gly-OH precipitated from the solution and the solid was isolated by filtering the mixture through a sintered glass filter funnel with a medium frit. The funnel was covered with a piece of filter paper and the solid was dried by aspirating air through the funnel. The solid was suspended in ca. 200 mL of EtOAc to form a turbid solution. The solution was stirred vigorously for 10 min, dried over $MgSO_4$, filtered, and then concentrated under vacuum to give a white solid. The isolated solid was ground into a fine powder to give ca. 3.48 g (92%) isolated yield. ^{1}H NMR (500 MHz, $CDCl_3$): δ 7.77 (d, J = 7.5 Hz, 2H), 7.60 (d, J = 7.4 Hz, 2H), 7.40 (t, J = 7.5 Hz, 2H), 7.32 (t, J = 7.5, 1 Hz, 2H), 5.28 (dt J = 92.6, 5.6 Hz), 4.43 (d, J = 7.0 Hz, 2H), 4.24 (t, J = 7.0 Hz, 1H), 4.04 (d, 5.5 Hz, 2H); ^{13}C NMR (125 MHz, $CDCl_3$): δ 173.6, 156.5, 144.0, 141.6, 128.0, 127.3, 125.3, 120.3, 67.6, 47.3, 42.6 (d, $^1J_{CN}$ = 13.8 Hz).

NMR Spectroscopy of Peptides 1

Sample Preparation. NMR spectroscopy of peptides **1a** and **1b** was performed in D_2O. The solutions were prepared by dissolving a weighed portion of the peptide in the appropriate volume of solvent. The molecular weights of the peptides were calculated as the TFA salts with all amino groups assumed to be protonated (**1a**, M.W. 2223.85 g/mol and **1b**, M.W. 2099.91 g/mol). The solutions were allowed to stand for 24 h to allow complete hydrogen to deuterium exchange of the amide NH protons.

^{1}H NMR, TOCSY, ROESY, and NOESY Data Collection. NMR spectra were recorded on a Bruker 600 MHz spectrometer with a TBI probe. Presaturation water suppression was applied as needed. TOCSY spectra were recorded with 2048 points in the f_2 dimension and 512 increments in the f_1 dimension with a 150-ms spin-lock mixing time. ROESY spectra were recorded with 2048 points in the f_2 dimension and 512 increments in the f_1 dimension with a 200-ms spin-lock mixing time. NOESY spectra were recorded with 2048 points in the f_2 dimension and 512 increments in the f_1 dimension with a 150-ms mixing time.

^{1}H NMR, TOCSY, ROESY, and NOESY Data Processing. NMR spectra were processed with Bruker XwinNMR software. Automatic baseline correction was applied in both dimensions after phasing the spectra. TOCSY and ROESY spectra were Fourier transformed to a final matrix size of 2048 x 1024 real points using a Qsine weighting function and forward linear prediction. NOESY spectra were Fourier transformed to a final matrix size of 2048 x 2048 real points using a Qsine weighting function and forward linear prediction.

Diffusion-Ordered Spectroscopy (DOSY) Experiments. DOSY experiments were performed on a Bruker 500 MHz spectrometer equipped with a TCI cryoprobe, with a diffusion delay (Δ) of 75-ms and a diffusion gradient length (δ) of 2.5-ms. Sixteen sets of FIDs were recorded with the gradient strength incremented from 5%–95% using a linear ramp. The combined FIDs were Fourier transformed in Bruker's TopSpin^{TM} software to give a pseudo-2D spectrum. After phasing and performing baseline correction, each pseudo-2D spectrum was processed with logarithmic scaling on the Y-axis. The Y-axis was calibrated to the diffusion coefficient of the residual HOD peak in D_2O (1.9×10^{-9} m^2/s at 298 K).[4] The diffusion coefficients of the peptides were read and converted from logarithmic values to linear values.

NMR Spectroscopy of Peptides [^{15}N]1

Sample Preparation. NMR spectroscopy of peptides [^{15}N]**1a** and [^{15}N]**1b** was performed in 9:1 H_2O/D_2O. The solutions were prepared by dissolving a weighed portion of the peptide in the appropriate volume of solvent. The molecular weights of the peptides were calculated as the TFA salts with all amino groups assumed to be protonated ([^{15}N]**1a**, M.W. 2224.85 g/mol and [^{15}N]**1b**, M.W. 2100.91 g/mol). 4,4-Dimethyl-4-silapentane-1-ammonium trifluoroacetate (DSA) was added as an internal standard for referencing chemical shifts.[5]

^{1}H NMR, ^{1}H,^{15}N HSQC, and ^{1}H,^{15}N NOESY-HSQC (^{15}N-edited NOESY) Data Collection. NMR spectra were recorded on a Bruker 600 MHz spectrometer with either a TBI probe or a BBFO cryoprobe. Gradient water suppression was applied as needed. ^{1}H,^{15}N HSQC spectra were recorded with 1024 points in the f_2 dimension and 512 increments in the f_1 dimension. ^{1}H,^{15}N NOESY-HSQC spectra were recorded with a 150-ms mixing time, and with 2048 points in the f_3 dimension (^{1}H), 1 increment in the f_2 dimension (^{15}N), and 1024 increments in the f_1 dimension (^{1}H).

^{1}H NMR, ^{1}H,^{15}N HSQC, and ^{1}H,^{15}N NOESY-HSQC (^{15}N-edited NOESY) Data Processing. NMR spectra were Fourier transformed in Bruker XwinNMR software with forward linear prediction and a Qsinc weighting function. Automatic baseline correction was applied in both dimensions after phasing the spectra. The ^{1}H,^{15}N HSQC spectra were processed to a final matrix size of 2048 x 1024 real points and with GB = 0.1 in the f_2 dimension. The ^{1}H,^{15}N NOESY-HSQC spectra were processed to a final 2D matrix size of 4096 x 2048 real points (f_3, f_1) and with GB = 0.05 in both dimensions.

Molecular Modeling of Peptides 1a and 1b.

Molecular models of the tetramers of peptides **1a** and **1b** were generated from the X-ray crystallographic structure of a similar macrocyclic β-sheet peptide (PDB 3T4G). This peptide contains AIIGLMV ($A\beta_{30–36}$) in the heptapeptide strand and $KFF^{Br}K$ in positions R_8-R_{11} in the template strand. The PDB coordinates were imported into PyMOL. Symmetry mates were generated to create two hydrogen-bonded dimers sandwiched on the surface displaying the side chains of A_{30}, I_{32}, L_{34}, and V_{36}. The alignment of each dimer was shifted by two residues to match the alignment of the dimers of peptides **1a** and **1b**. The residues of the dimers were mutated to match peptide **1a** or peptide **1b**, and the side chain torsion angles of χ_1 and χ_2 were adjusted for Ile (180^o and 60^o) and Phe (180^o). The dimers were then rotated manually to reflect the observed interlayer NOEs between Ile_{11} and the methoxy group of Hao.

The coordinates were exported from PyMOL as a .pdb file. The file was imported into MacroModel with the Maestro user interface. Atom types and bond orders were edited as needed to correct errors in bond type and charge. Distance constraints were applied to reflect the folding and dimerization of the macrocycles. Four interlayer distance constraints between the δ-methyl group of Ile_{11} and the methoxy group of Hao were applied to reflect the observed interlayer contacts. Minimization was performed with the MMFFs force field and GB/SA water solvation. All constraints were removed and minimization was repeated to generate a minimum-energy conformation (local minimum). The coordinates were exported in .pdb file format and imported into PyMOL.

2.III. REFERENCES

1. Pangborn, A. B.; Giardello, M. A.; Grubbs, R. H.; Rosen, R. K.; Timmers, F. J. *Organometallics* **1996**, *15*, 1518–1520.

2. (a) Nowick, J. S.; Chung, D. M.; Maitra, K.; Maitra, S.; Stigers, K. D.; Sun, Y. *J. Am. Chem. Soc.* **2000**, *122*, 7654–7661; (b) Cheng, P.-N.; Nowick, J. S. *J. Org. Chem.* **2011**, *76*, 3166–3173.

3. Podlech, J.; Gurrath, M.; Müller, G. 9-Fluorenylmethoxycarbonyl Group. In *Houben-Weyl Methods of Organic Chemistry*, Goodman, M., Ed. Thieme: Stuttgart, 2003; Vol. E22a, p 61.

4. Longsworth, L. G. *J. Phys. Chem.* **1960**, *64*, 1914–1917.

5. Nowick, J. S.; Khakshoor, O.; Hashemzadeh, M.; Brower, J. O. *Org. Lett.* **2003**, *5*, 3511–3513.

2.IV. Characterization Data

RP-HPLC of peptide **1a**

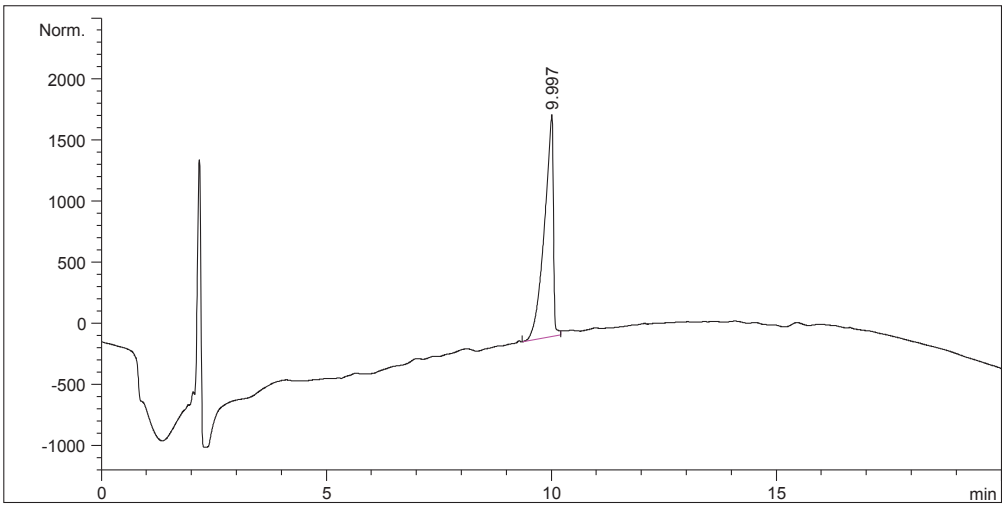

Peak #	RetTime [min]	Type	Width [min]	Area mAU *s	Height [mAU]	Area %
1	9.997	BV	0.1928	2.50833e4	1820.18323	100.0000
Totals :				2.50833e4	1820.18323	

column:	Aeris XB-C18 2.6µ
dimensions:	150 mm x 4.6 mm
mobile phase:	A: H_2O, 0.1% TFA B: CH_3CN, 0.1% TFA
gradient:	A/B (95:5) to (0:100) in 20 min
flow rate:	1.0 mL/min
detection:	VWD, wavelength = 214 nm
temperature:	298 K

MS (ESI) of peptide **1a**

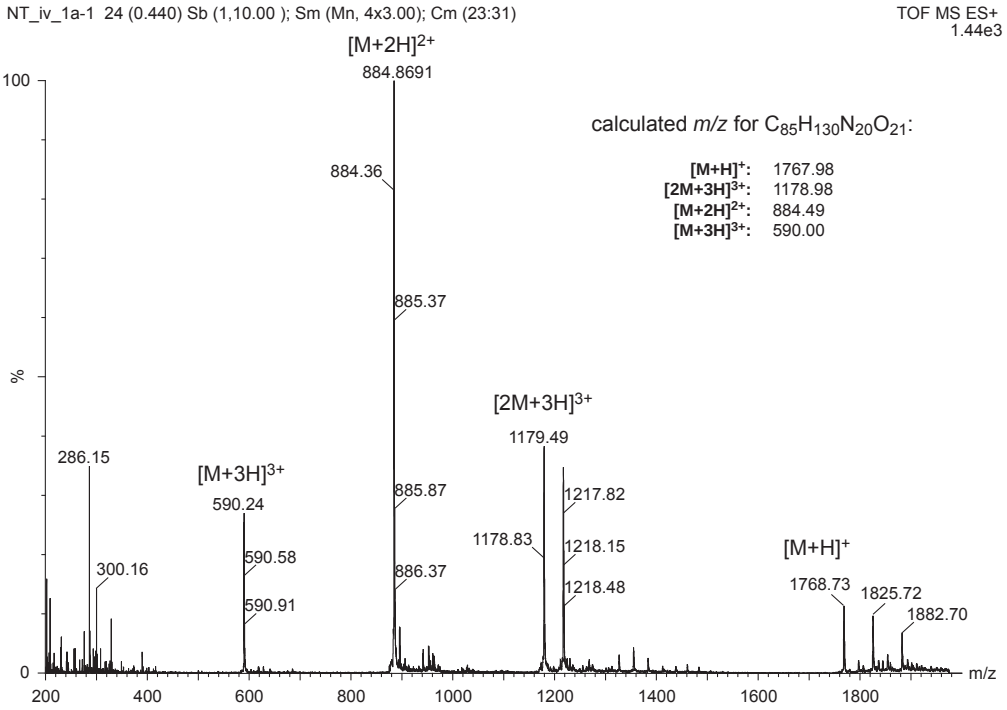

calculated *m/z* for $C_{85}H_{130}N_{20}O_{21}$:

$[M+H]^+$:	1767.98
$[2M+3H]^{3+}$:	1178.98
$[M+2H]^{2+}$:	884.49
$[M+3H]^{3+}$:	590.00

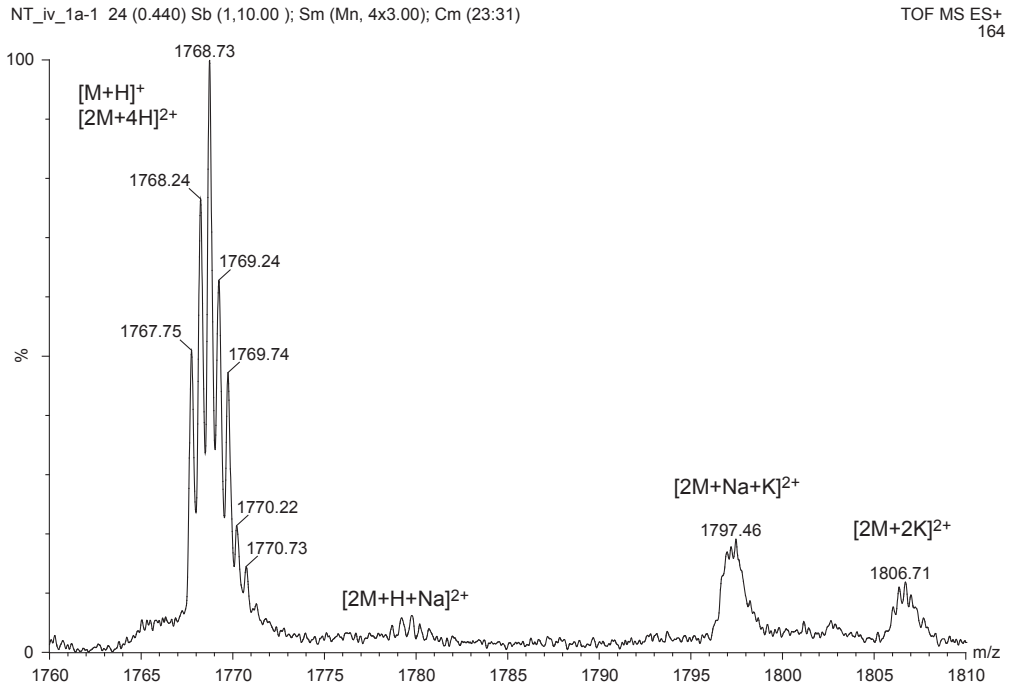
NT_iv_1a-1 24 (0.440) Sb (1,10.00); Sm (Mn, 4x3.00); Cm (23:31)
TOF MS ES+
164
100
%
0
1768.73
[M+H]+
[2M+4H]2+
1768.24
1769.24
1767.75
1769.74
1770.22
1770.73
[2M+H+Na]2+
[2M+Na+K]2+
1797.46
[2M+2K]2+
1806.71
m/z
1760
1765
1770
1775
1780
1785
1790
1795
1800
1805
1810

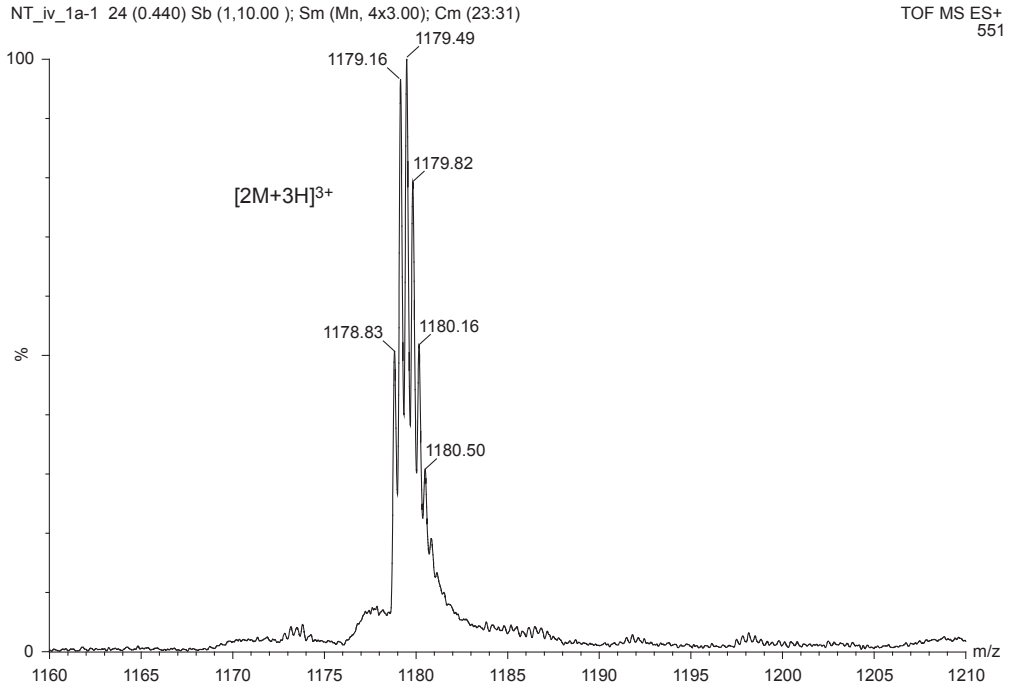
NT_iv_1a-1 24 (0.440) Sb (1,10.00); Sm (Mn, 4x3.00); Cm (23:31)
TOF MS ES+
551
100
%
0
1179.49
1179.16
1179.82
[2M+3H]3+
1178.83
1180.16
1180.50
m/z
1160
1165
1170
1175
1180
1185
1190
1195
1200
1205
1210

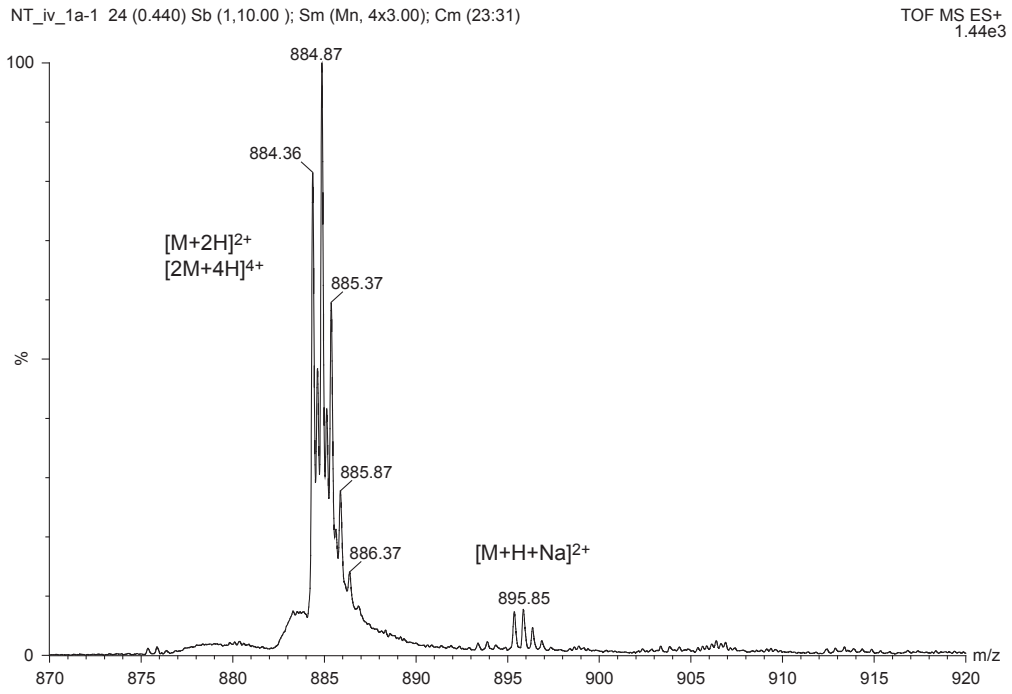
NT_iv_1a-1 24 (0.440) Sb (1,10.00); Sm (Mn, 4x3.00); Cm (23:31)
TOF MS ES+
1.44e3
100
%
0
884.87
884.36
[M+2H]2+
[2M+4H]4+
885.37
885.87
886.37
[M+H+Na]2+
895.85
m/z
870
875
880
885
890
895
900
905
910
915
920

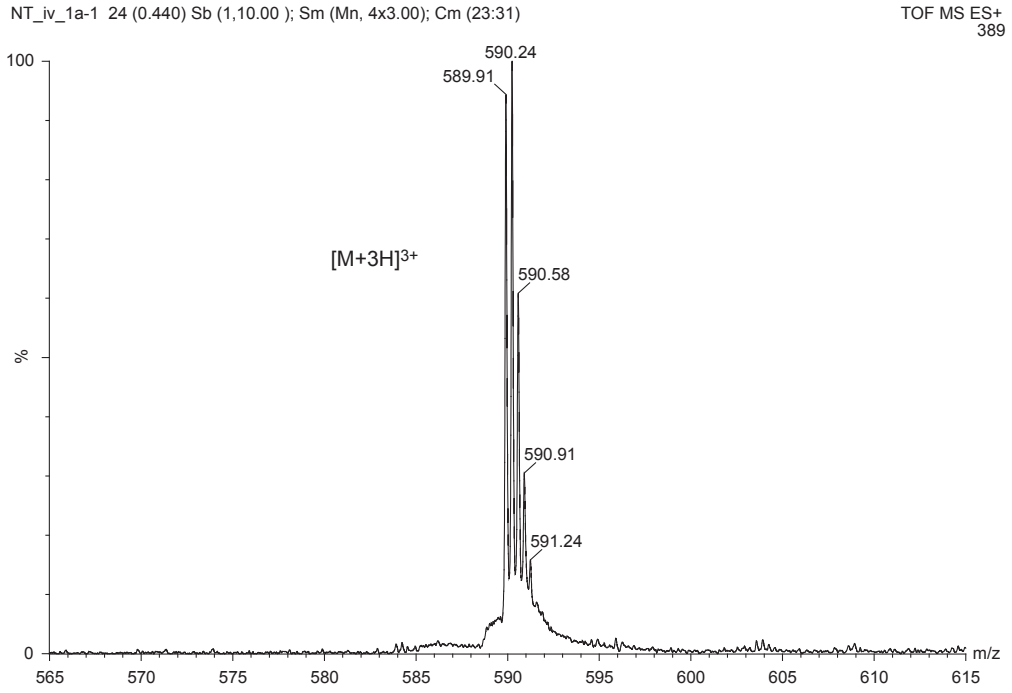
NT_iv_1a-1 24 (0.440) Sb (1,10.00); Sm (Mn, 4x3.00); Cm (23:31)
TOF MS ES+
389
100
%
0
590.24
589.91
[M+3H]3+
590.58
590.91
591.24
m/z
565
570
575
580
585
590
595
600
605
610
615

^{1}H NMR of peptide **1a**, 0.15 mM in D_2O at 600 MHz and 293 K

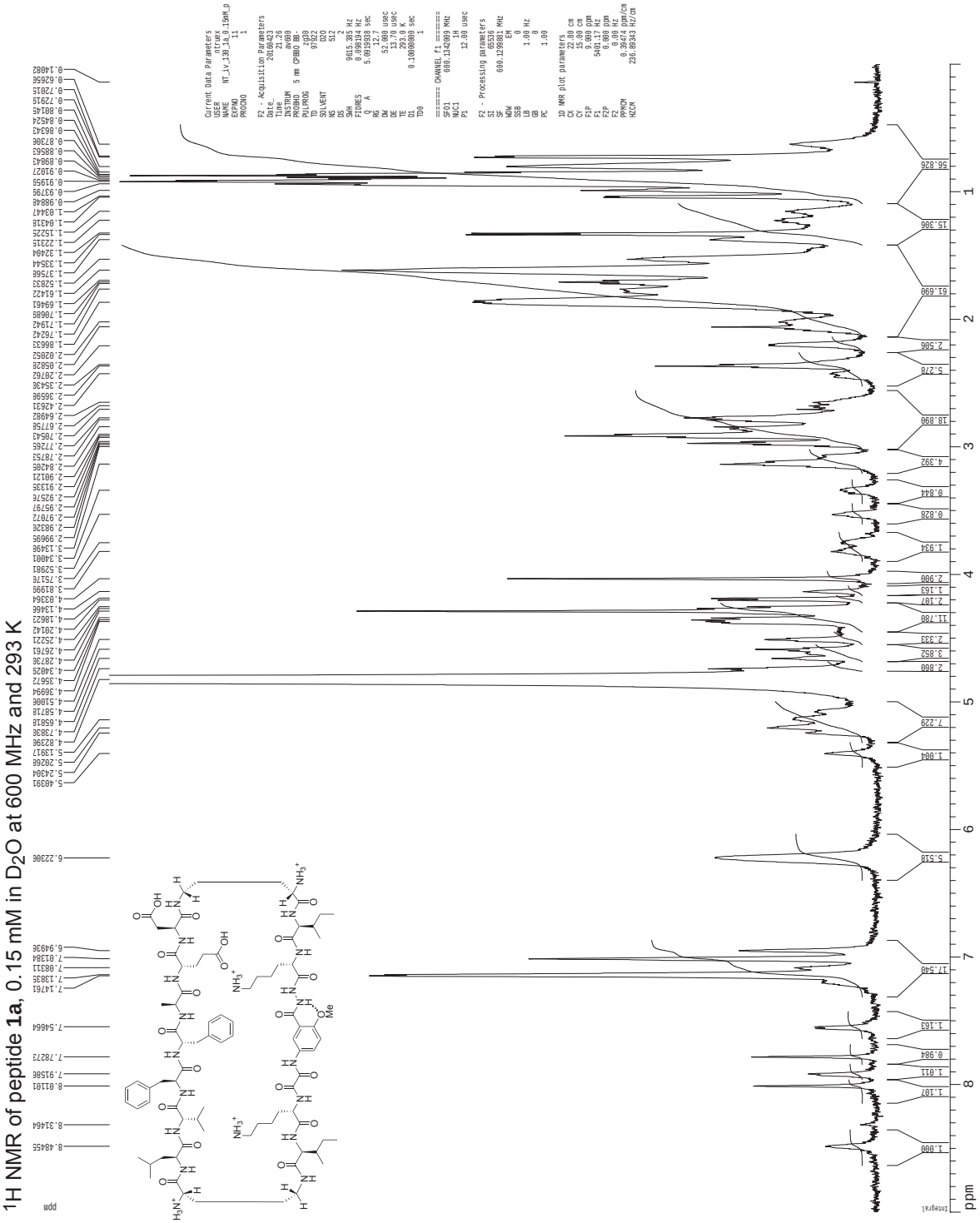

^{1}H NMR of peptide **1a**, 0.15 mM in D_2O at 600 MHz and 293 K

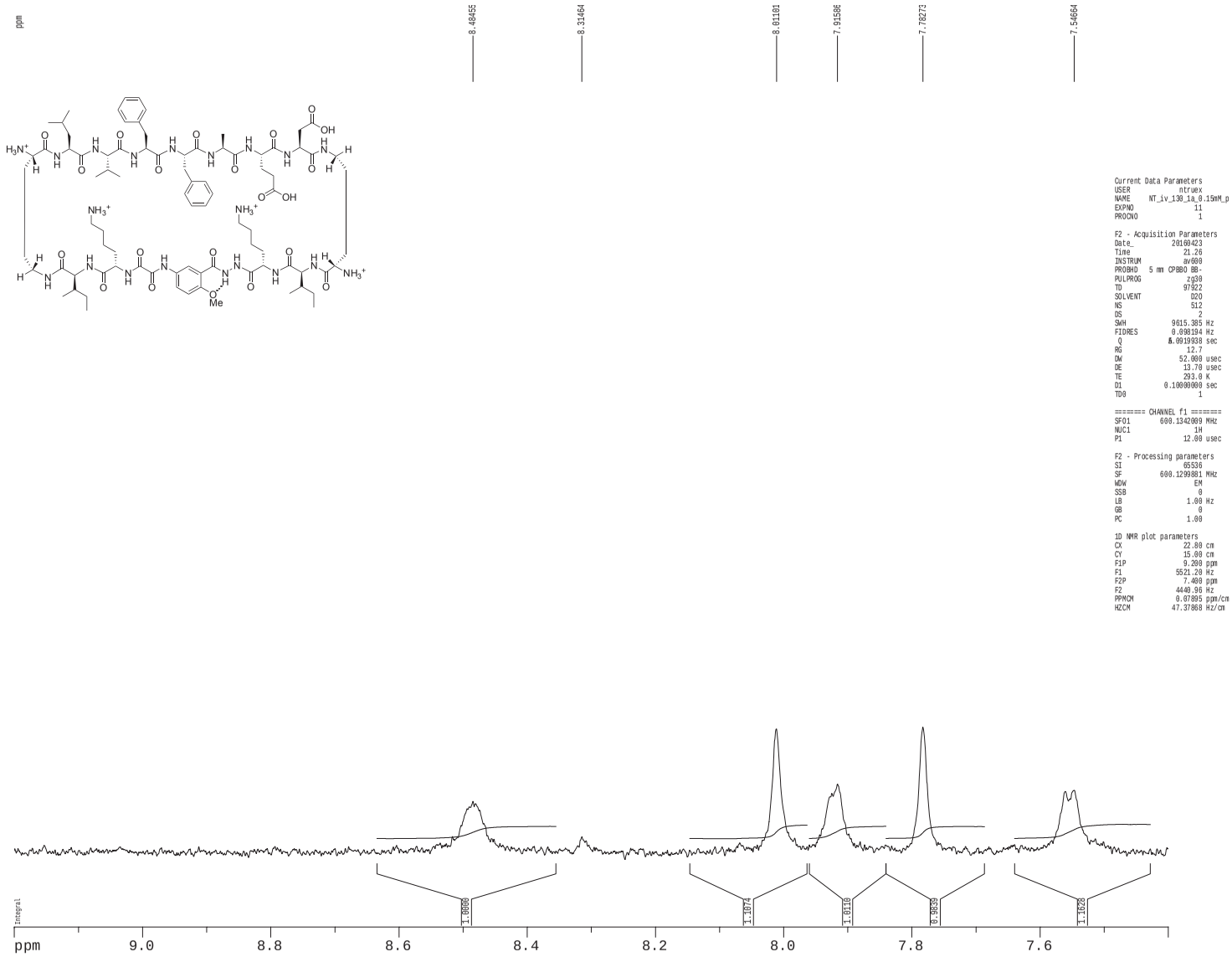

^{1}H NMR of peptide **1a**, 0.15 mM in D_2O at 600 MHz and 293 K

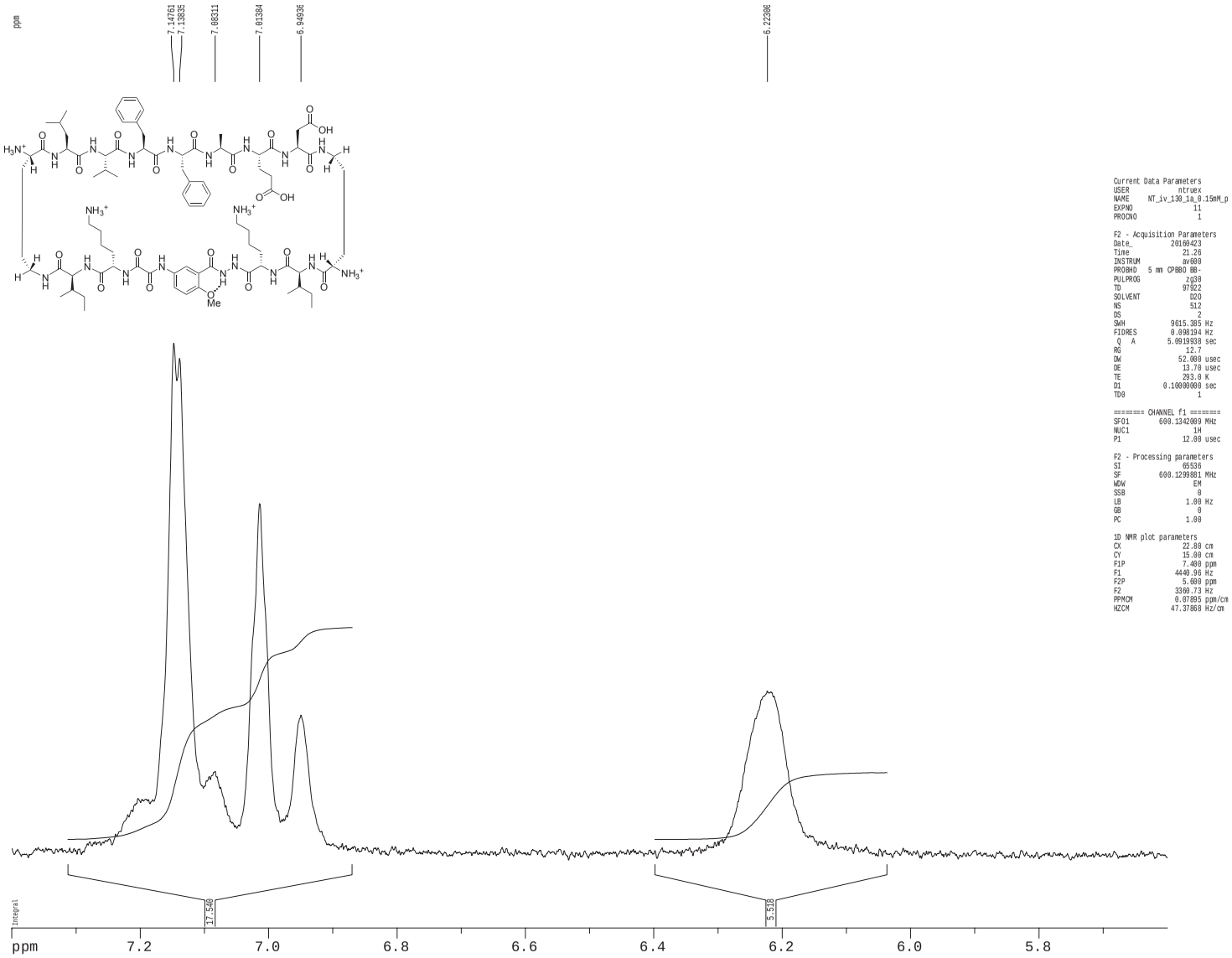


```
Current Data Parameters
USER              ntruex
NAME      NT_iv_130_1a_0.15mM_p
EXPNO                 11
PROCNO                 1

F2 - Acquisition Parameters
Date_          20160423
Time              21.26
INSTRUM           av600
PROBHD   5 mm CPBBO BB-
PULPROG           zg30
TD                97922
SOLVENT             D2O
NS                  512
DS                    2
SWH            9615.385 Hz
FIDRES         0.098194 Hz
 Q  A          5.0919938 sec
RG                 12.7
DW               52.000 usec
DE               13.70 usec
TE                293.0 K
D1           0.10000000 sec
TD0                    1

======= CHANNEL f1 =======
SFO1         600.1342009 MHz
NUC1                1H
P1                12.00 usec

F2 - Processing parameters
SI                 65536
SF           600.1299801 MHz
WDW                  EM
SSB                   0
LB                 1.00 Hz
GB                    0
PC                 1.00

1D NMR plot parameters
CX                22.00 cm
CY                15.00 cm
F1P               7.400 ppm
F1               4440.96 Hz
F2P               5.600 ppm
F2               3360.73 Hz
PPMCM          0.07895 ppm/cm
HZCM          47.37868 Hz/cm
```

^{1}H NMR of peptide **1a**, 0.15 mM in D_2O at 600 MHz and 293 K

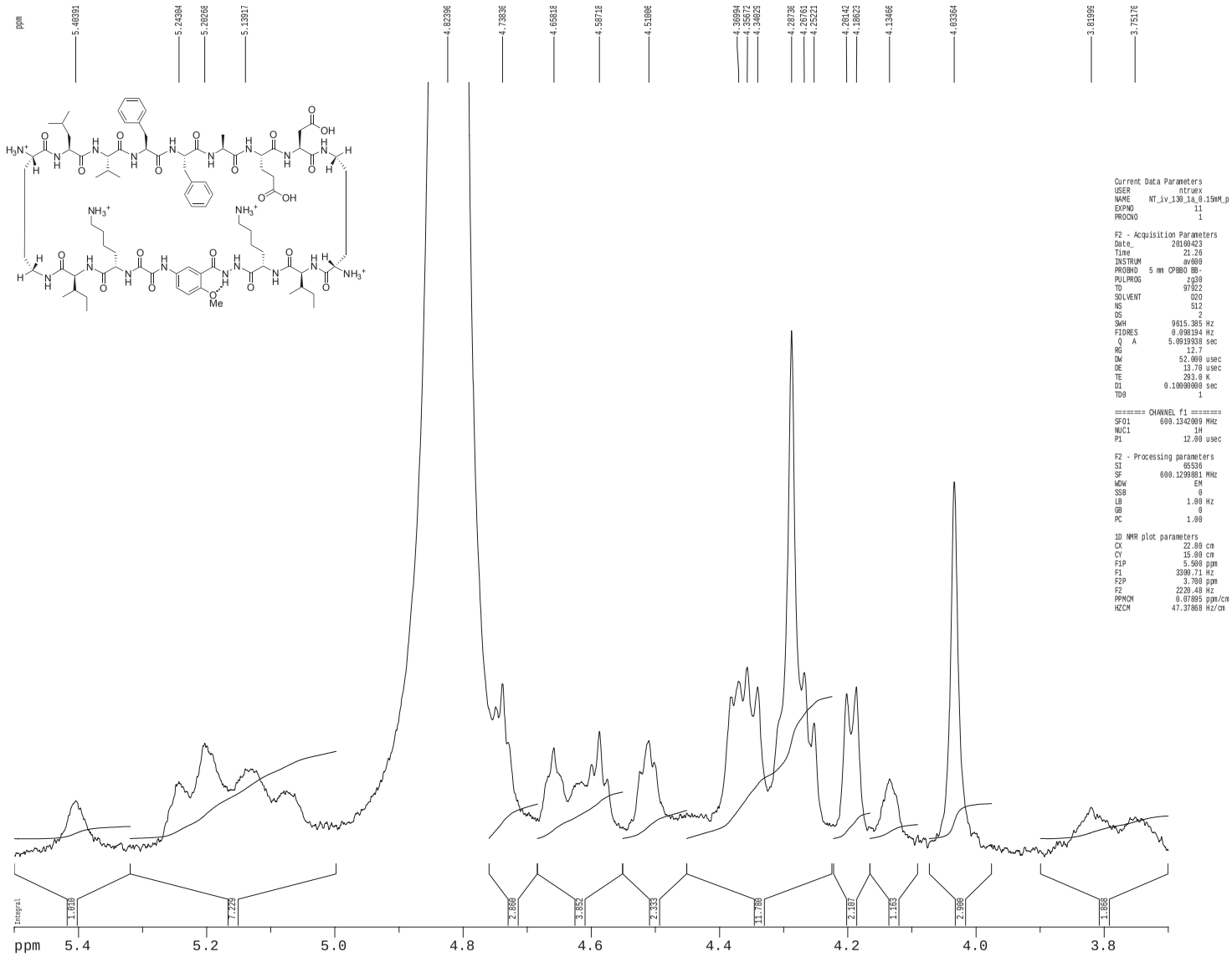


```
Current Data Parameters
USER              ntruex
NAME      NT_iv_130_1a_0.15mM_p
EXPNO                 11
PROCNO                 1

F2 - Acquisition Parameters
Date_          20160423
Time              21.26
INSTRUM           av600
PROBHD   5 mm CPBBO BB-
PULPROG           zg30
TD                97922
SOLVENT             D2O
NS                  512
DS                    2
SWH            9615.385 Hz
FIDRES         0.098194 Hz
 Q  A          5.0919938 sec
RG                 12.7
DW               52.000 usec
DE               13.70 usec
TE                293.0 K
D1           0.10000000 sec
TD0                   1

======= CHANNEL f1 =======
SFO1         600.1342009 MHz
NUC1                 1H
P1                12.00 usec

F2 - Processing parameters
SI                65536
SF           600.1299801 MHz
WDW                  EM
SSB                   0
LB                 1.00 Hz
GB                    0
PC                 1.00

1D NMR plot parameters
CX                22.00 cm
CY                15.00 cm
F1P               5.500 ppm
F1              3300.71 Hz
F2P               3.700 ppm
F2              2220.48 Hz
PPMCM          0.07895 ppm/cm
HZCM          47.37868 Hz/cm
```

^{1}H NMR of peptide **1a**, 0.15 mM in D_2O at 600 MHz and 293 K

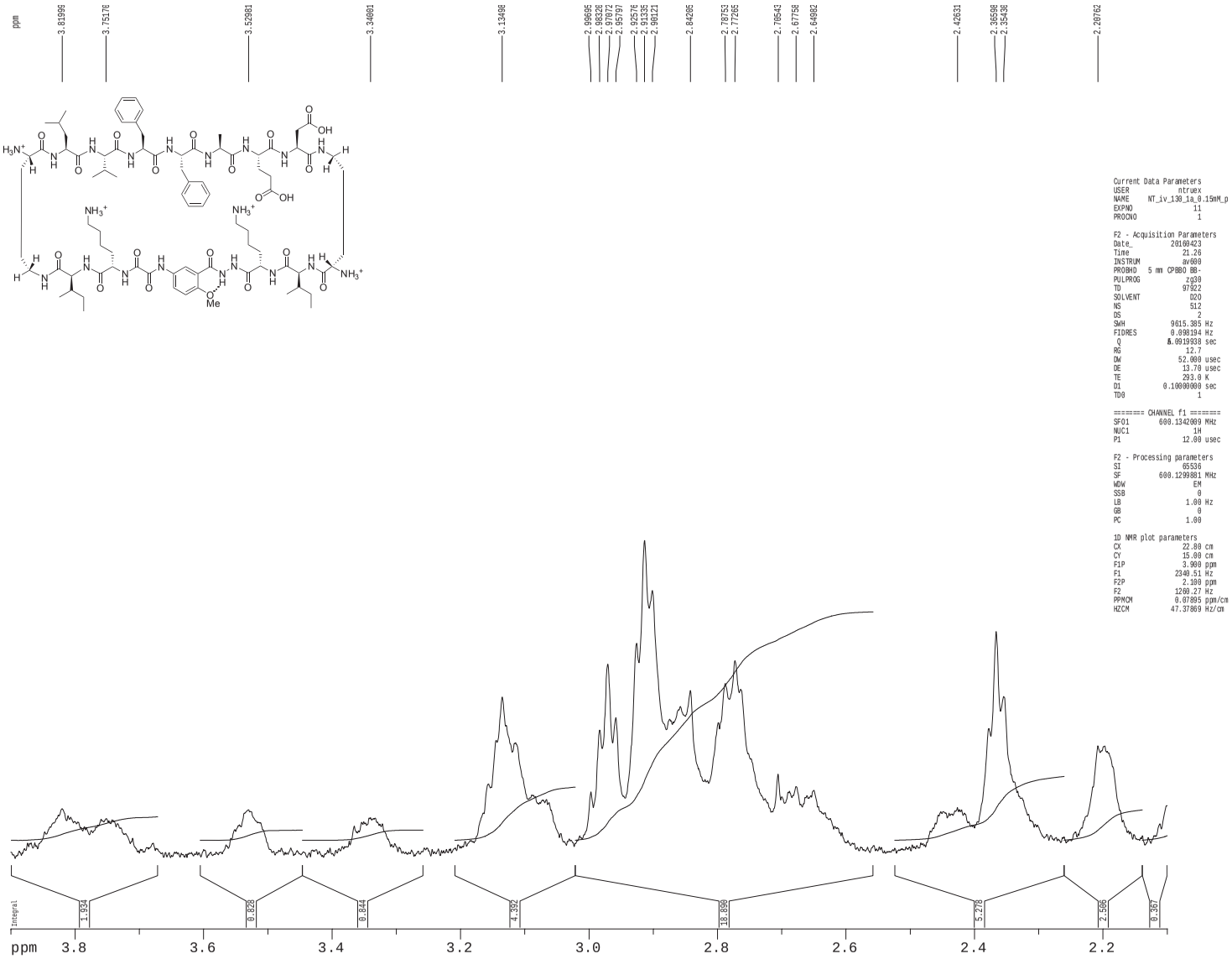

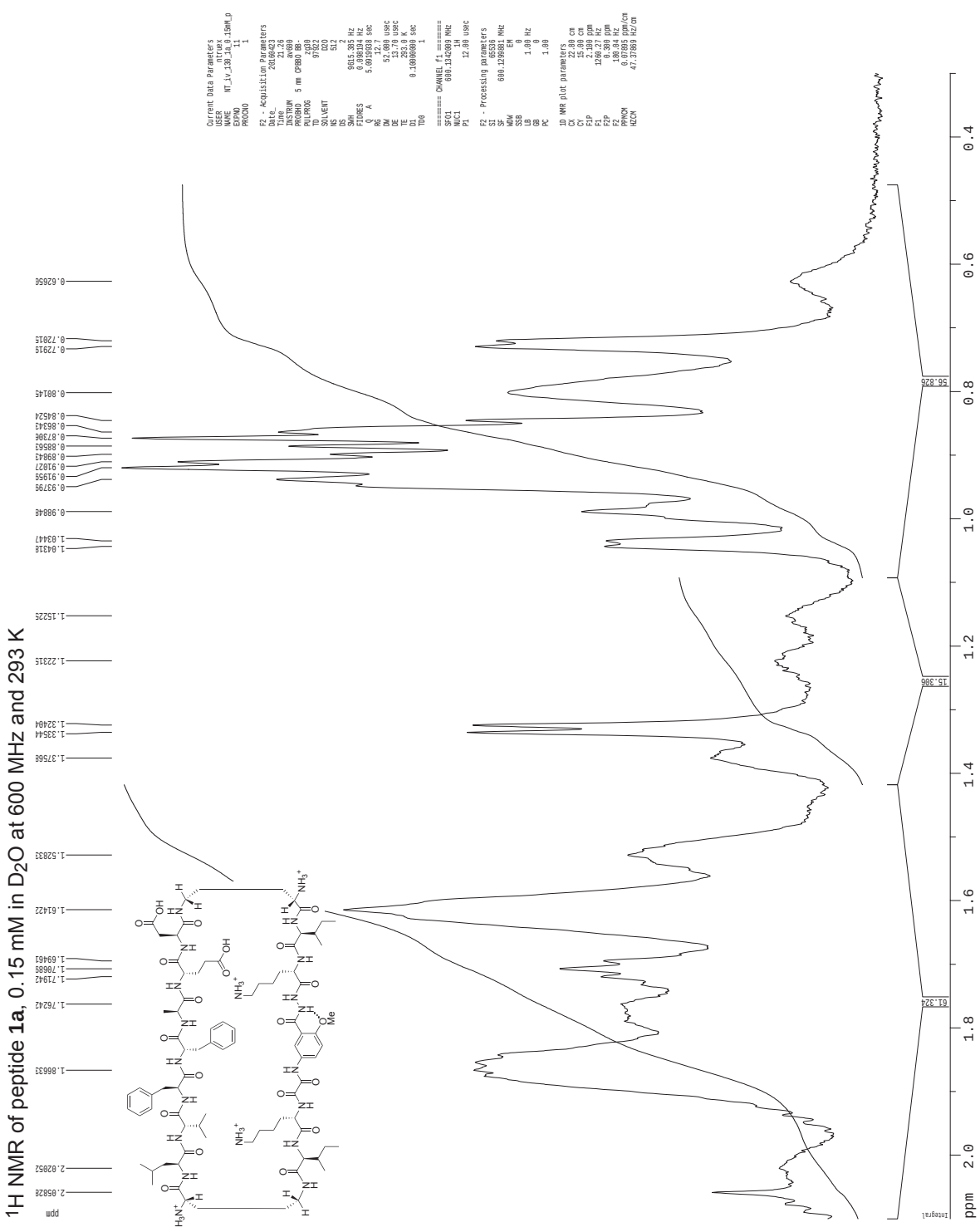
1H NMR of peptide 1a, 0.15 mM in D2O at 600 MHz and 293 K
Current Data Parameters
USER ntruex
NAME NT_1v_130_1a_0.15mM_p
EXPNO 11
PROCNO 1
F2 - Acquisition Parameters
Date_ 20180423
Time 21.26
INSTRUM av600
PROBHD 5 mm CPBBO BB-
PULPROG zgpr
TD 98304
SOLVENT D2O
NS 512
DS 16
SWH 9615.385 Hz
FIDRES 0.098194 Hz
AQ 5.6919308 sec
RG 228
DW 52.000 usec
DE 13.70 usec
TE 293.0 K
D1 0.10000000 sec
TD0 1
====== CHANNEL f1 ======
SFO1 600.1342009 MHz
NUC1 1H
P1 12.00 usec
F2 - Processing parameters
SI 65536
SF 600.1296881 MHz
WDW EM
SSB 0
LB 1.00 Hz
GB 0
PC 1.00
1D NMR plot parameters
CX 22.00 cm
CY 15.00 cm
F1P 2.100 ppm
F2P 1260.27 Hz
F1 0.000 ppm
F2 -180.04 Hz
PPMCM 0.07895 ppm/cm
HZCM 47.37869 Hz/cm
0.62656
0.72914
0.72915
0.80145
0.84524
0.86343
0.87296
0.88562
0.89843
0.90327
0.91956
0.93796
0.98848
1.03447
1.04318
1.15225
1.22315
1.32404
1.33544
1.37566
1.52833
1.61422
1.69461
1.70868
1.71942
1.76242
1.86653
2.02052
2.05828
56.826
15.386
61.324
ppm
2.0
1.8
1.6
1.4
1.2
1.0
0.8
0.6
0.4
Integral

^{1}H NMR 2D TOCSY of peptide **1a** with presaturation suppression of the HOD peak
0.15 mM in D_2O at 600 MHz and 293 K with 150-ms spin-lock mixing time

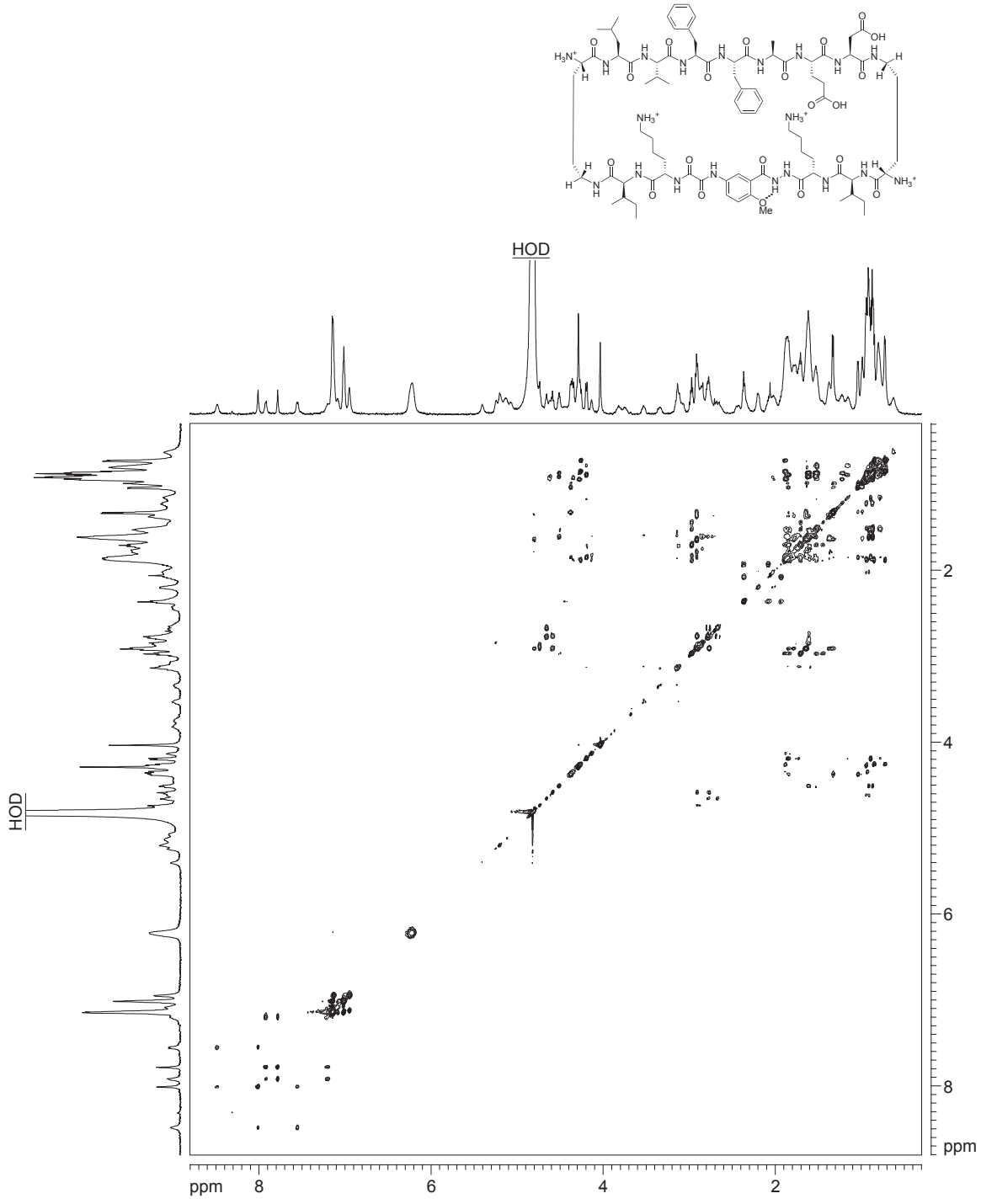

^{1}H NMR 2D TOCSY of peptide **1a** with presaturation suppression of the HOD peak
0.15 mM in D_2O at 600 MHz and 293 K with 150-ms spin-lock mixing time

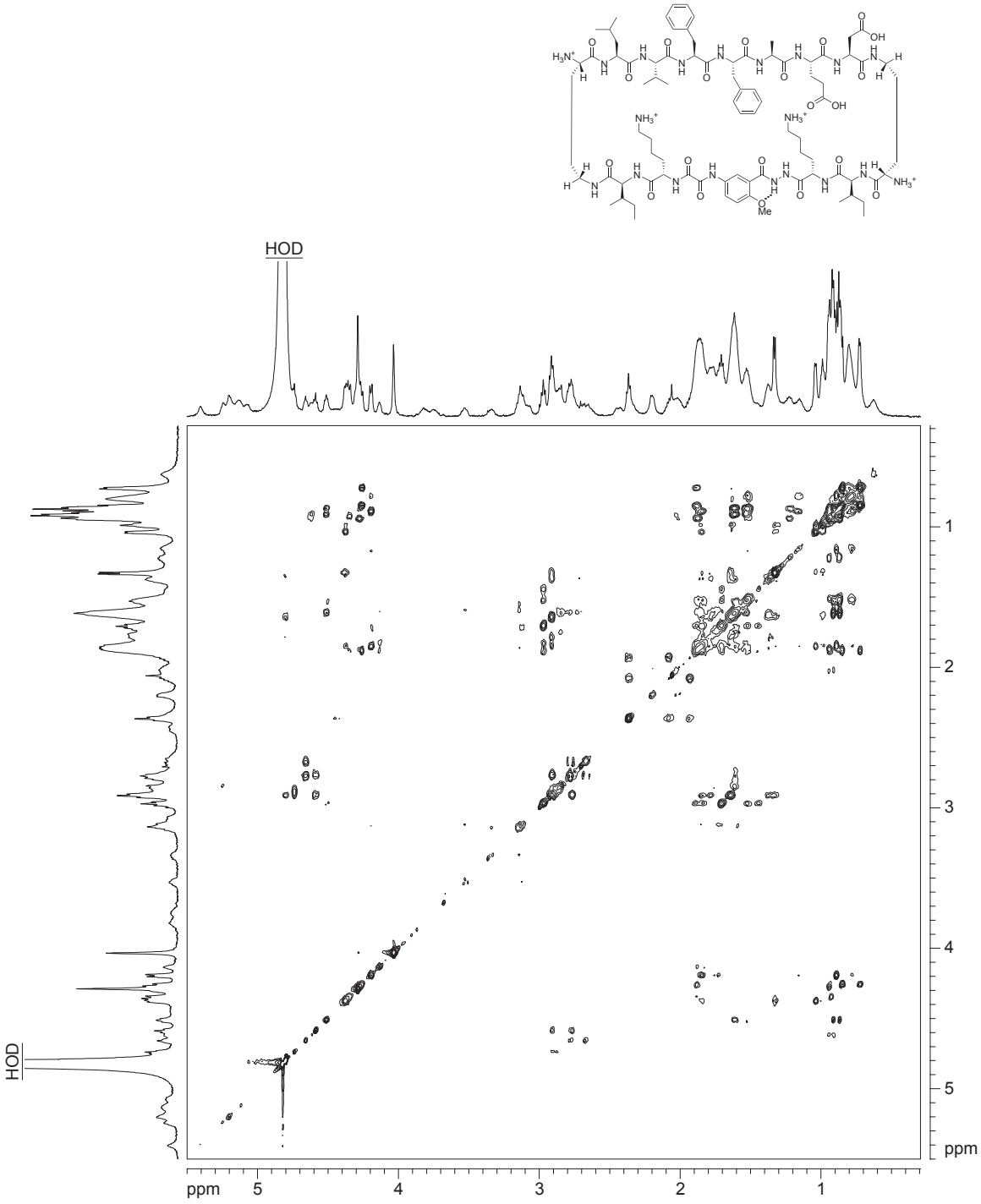

^{1}H NMR 2D ROESY of peptide **1a** with presaturation suppression of the HOD peak
0.15 mM in D_2O at 600 MHz and 293 K with 200-ms spin-lock mixing time

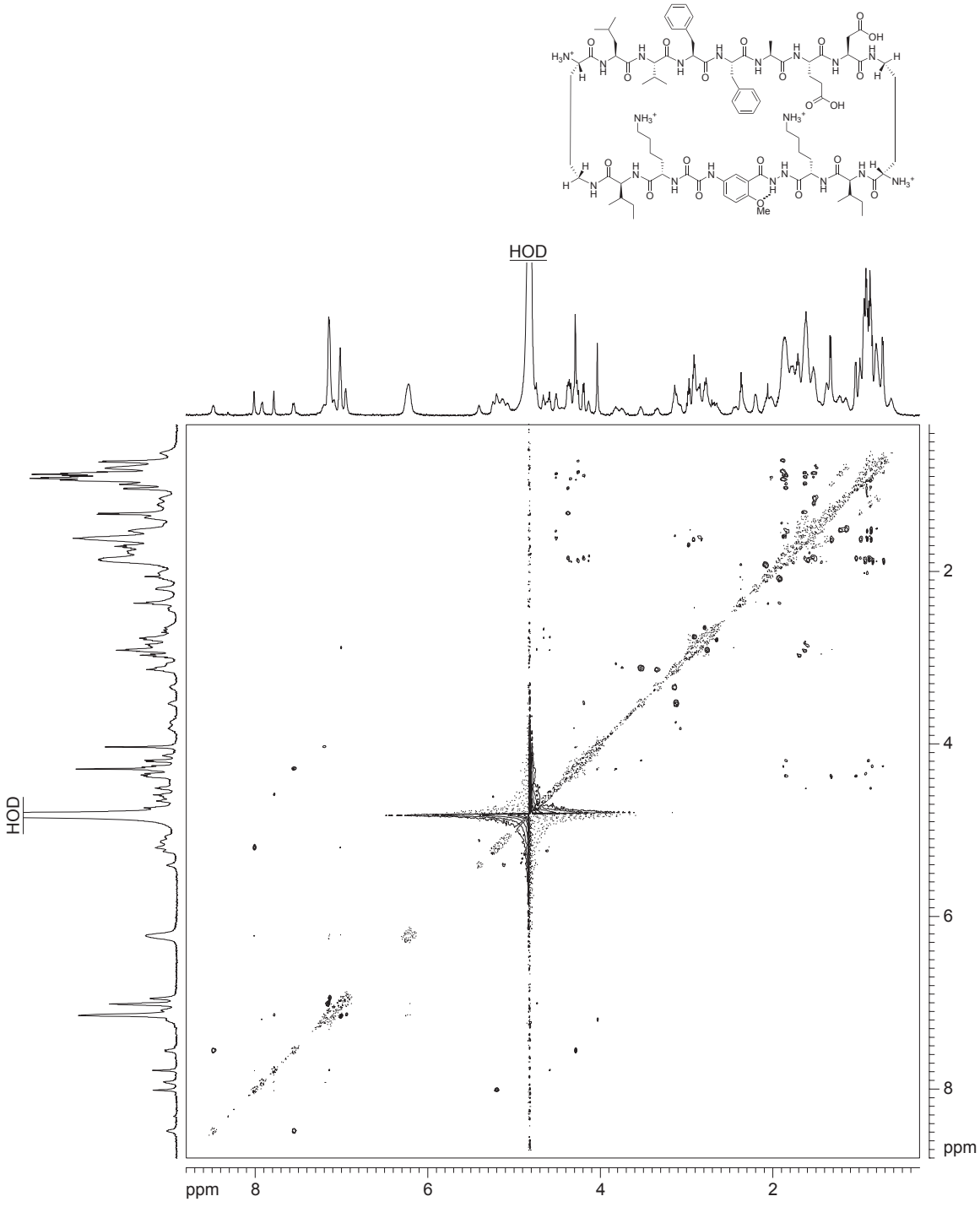

^{1}H NMR 2D ROESY of peptide **1a** with presaturation suppression of the HOD peak
0.15 mM in D_2O at 600 MHz and 293 K with 200-ms spin-lock mixing time

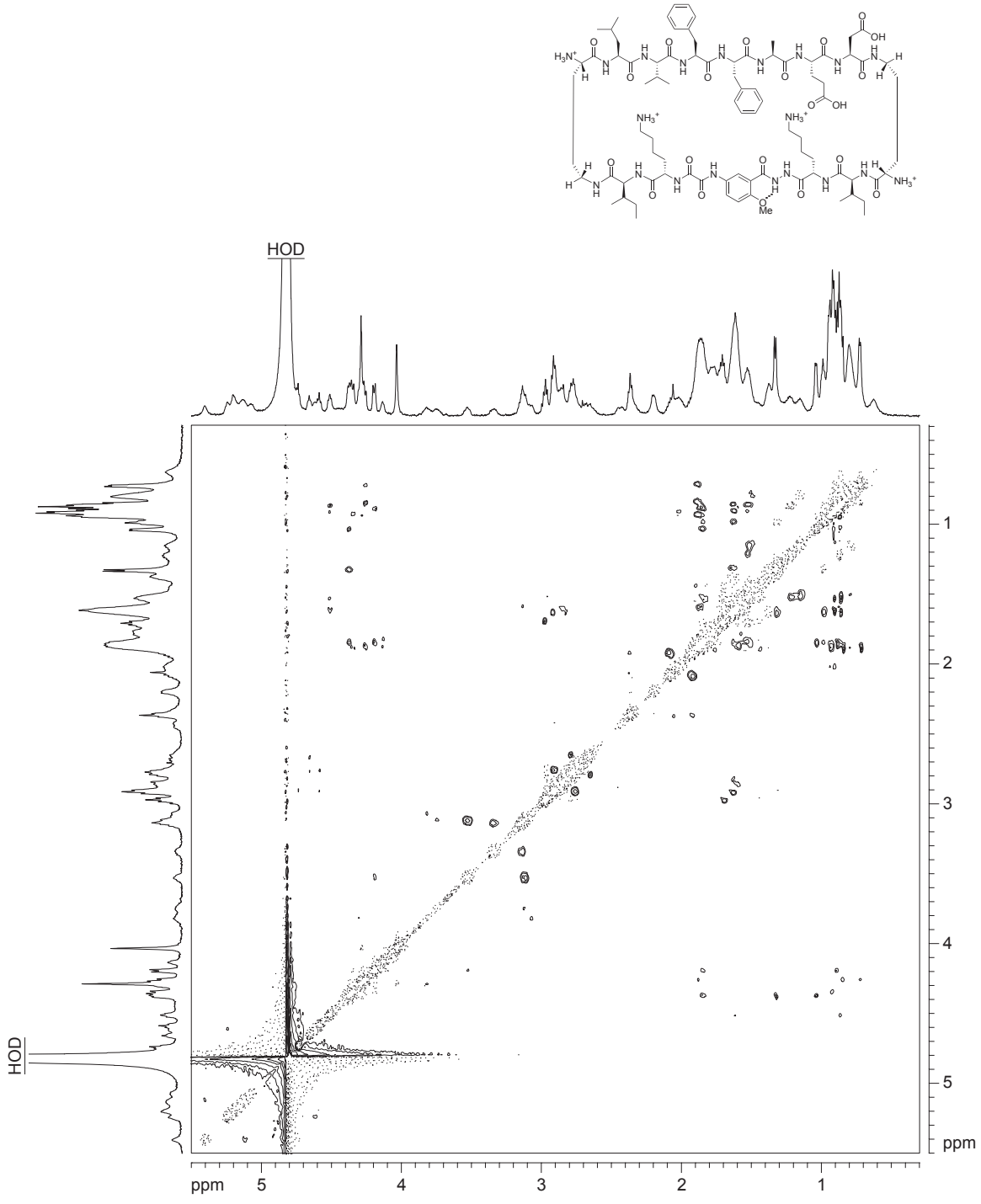

^{1}H NMR DOSY of peptide **1a**, 0.15 mM in D_2O at 500 MHz and 298 K

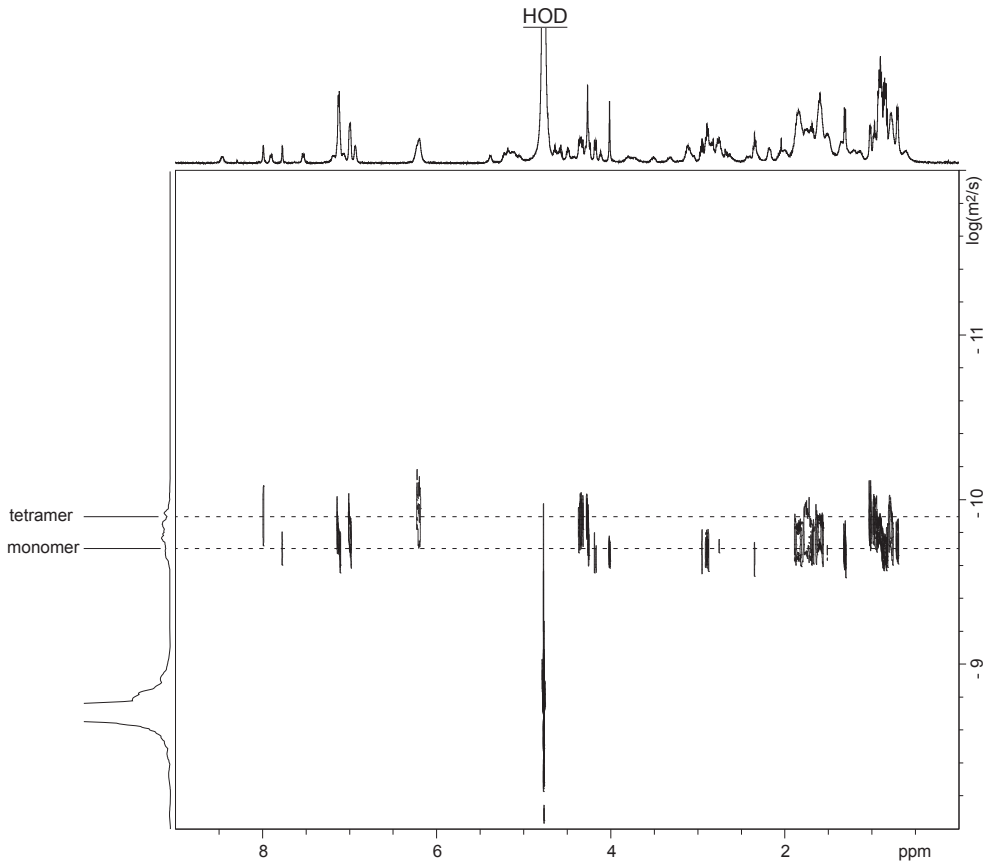

Calculations for peptide **1a** at 0.15 mM

D_{HOD} = 19.0 x 10^{-10} m^2/s [a]
log (D_{HOD}) = -8.721

$D_{monomer}$: log(D) = -9.69; D = $10^{-9.69}$ = 20.4 ± 1.7 x 10^{-11} m^2/s

$D_{tetramer}$: log(D) = -9.90; D = $10^{-9.90}$ = 12.6 ± 1.6 x 10^{-11} m^2/s

[a]Longsworth, L. G. *J. Phys. Chem.* **1960**, *64*, 1914−1917.

^{1}H NMR of peptide **1a**, 8 mM in D_2O at 600 MHz and 298 K

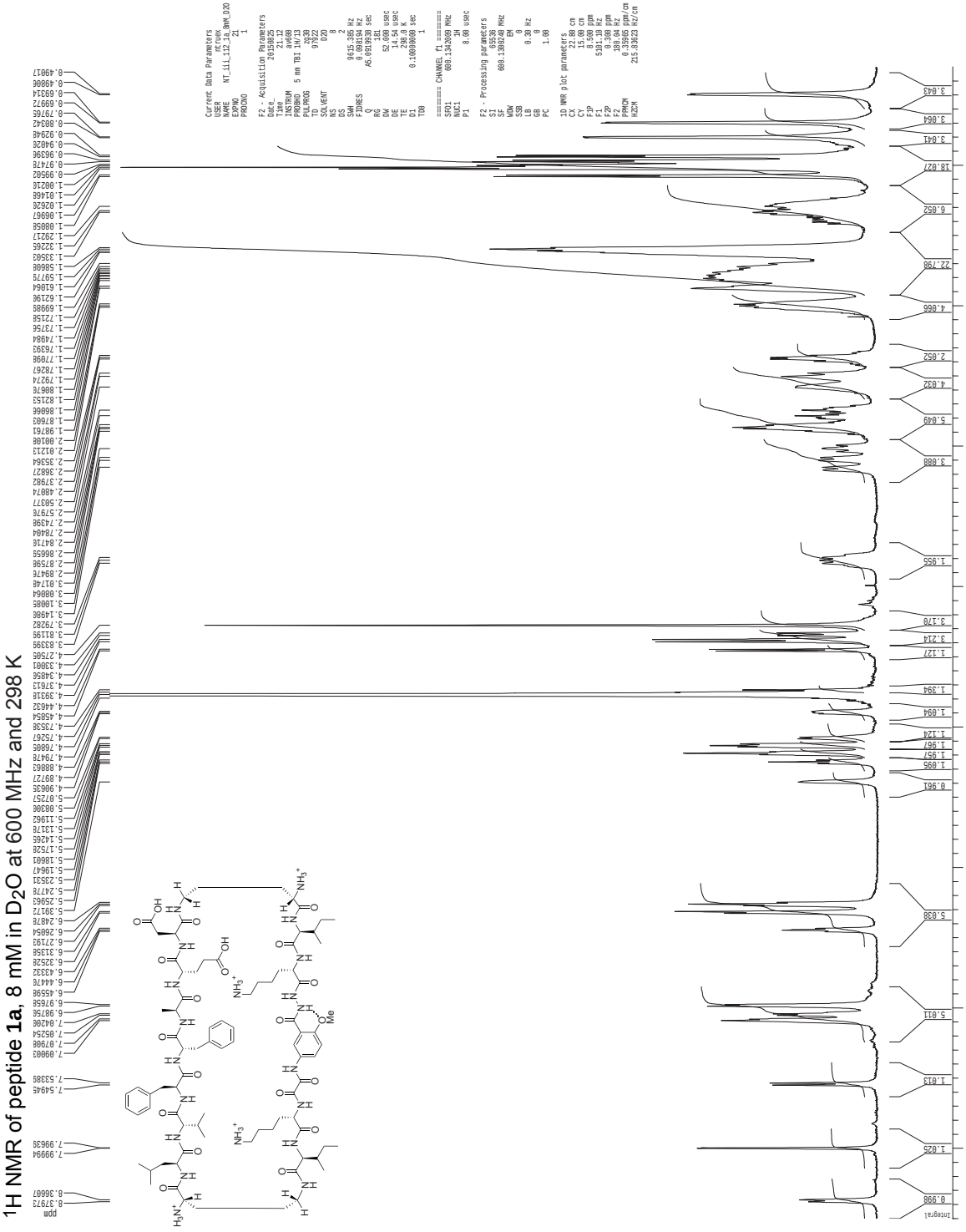

^{1}H NMR of peptide **1a**, 8 mM in D_2O at 600 MHz and 298 K

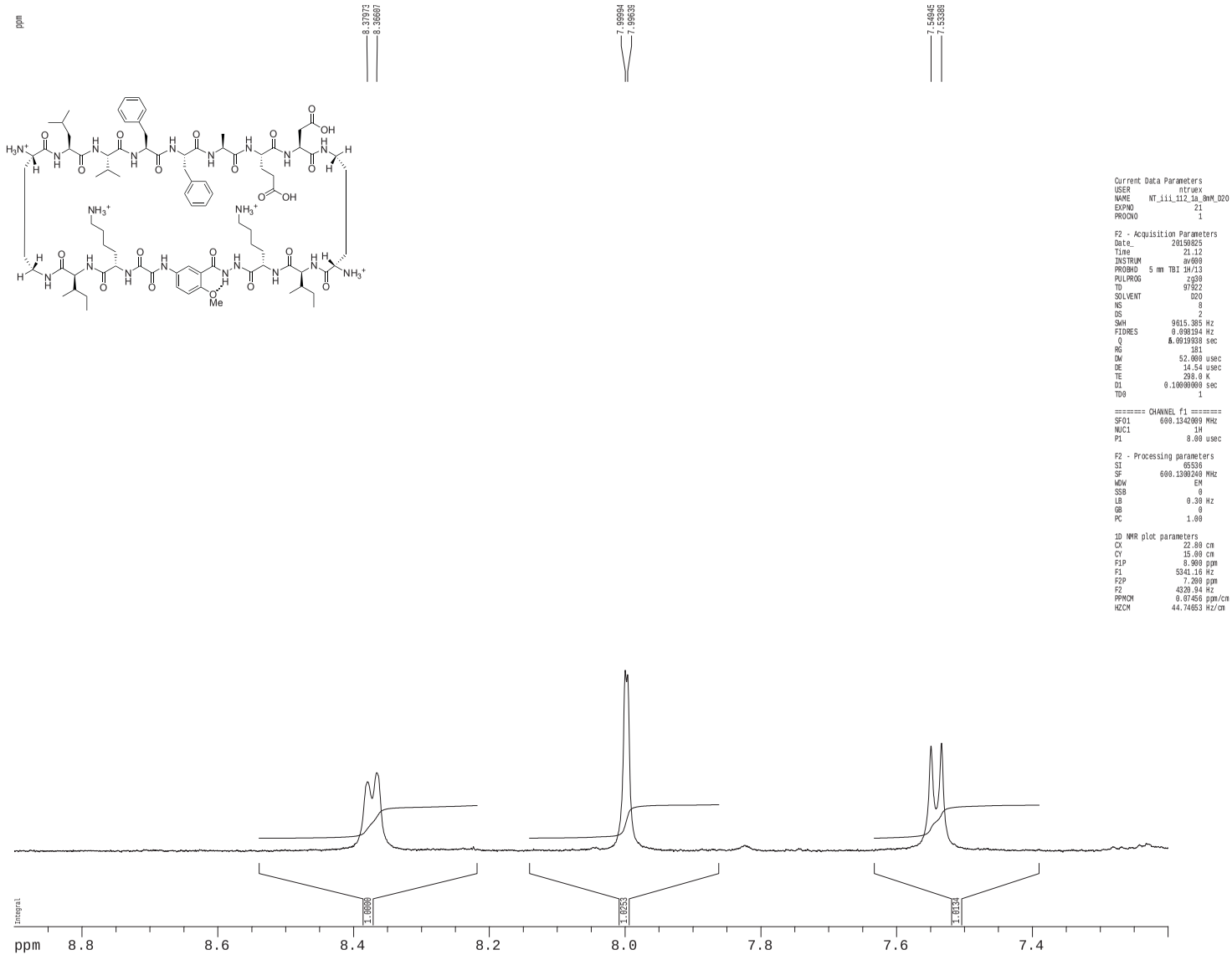

^{1}H NMR of peptide **1a**, 8 mM in D_2O at 600 MHz and 298 K

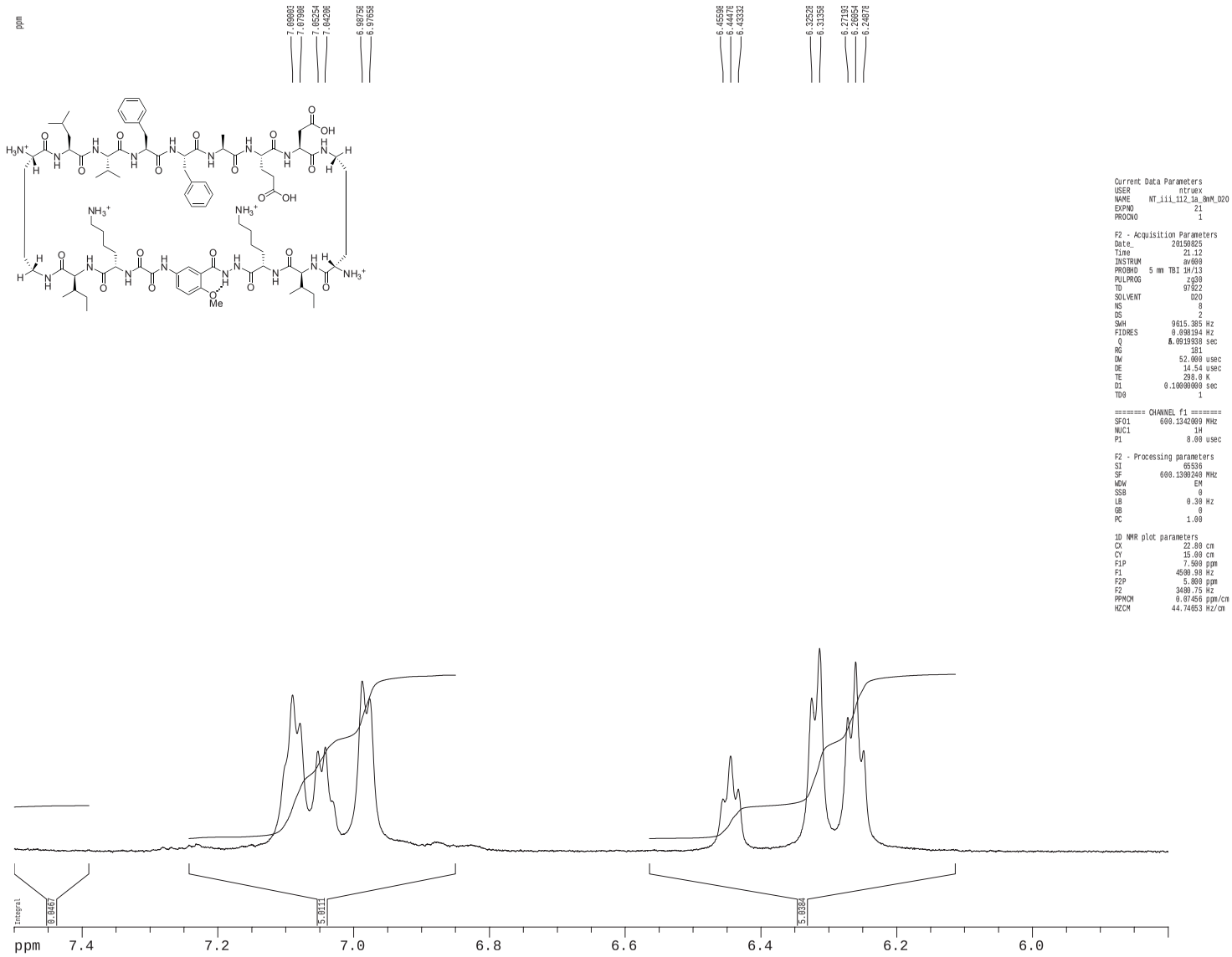

^{1}H NMR of peptide **1a**, 8 mM in D_2O at 600 MHz and 298 K

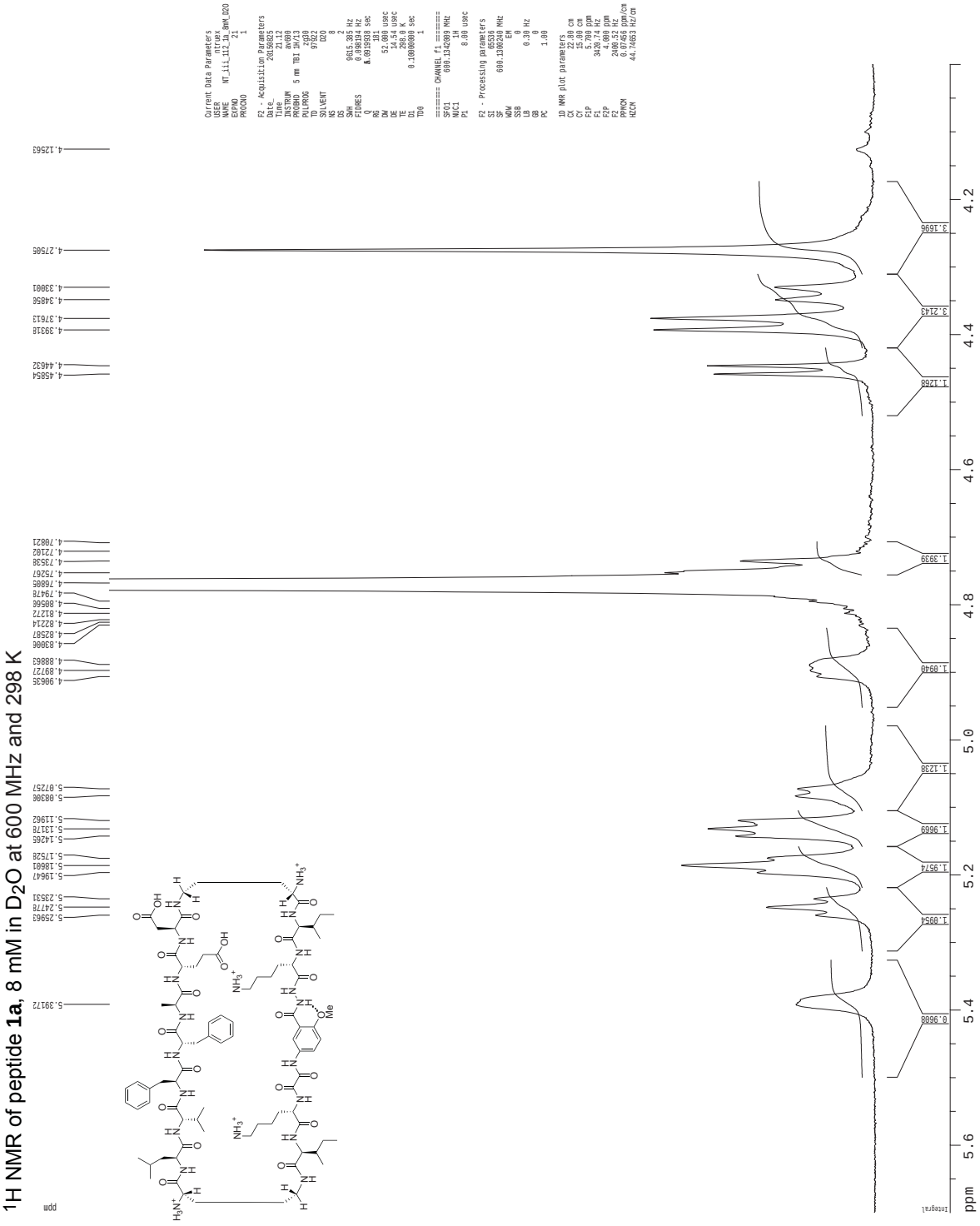

^{1}H NMR of peptide **1a**, 8 mM in D_2O at 600 MHz and 298 K

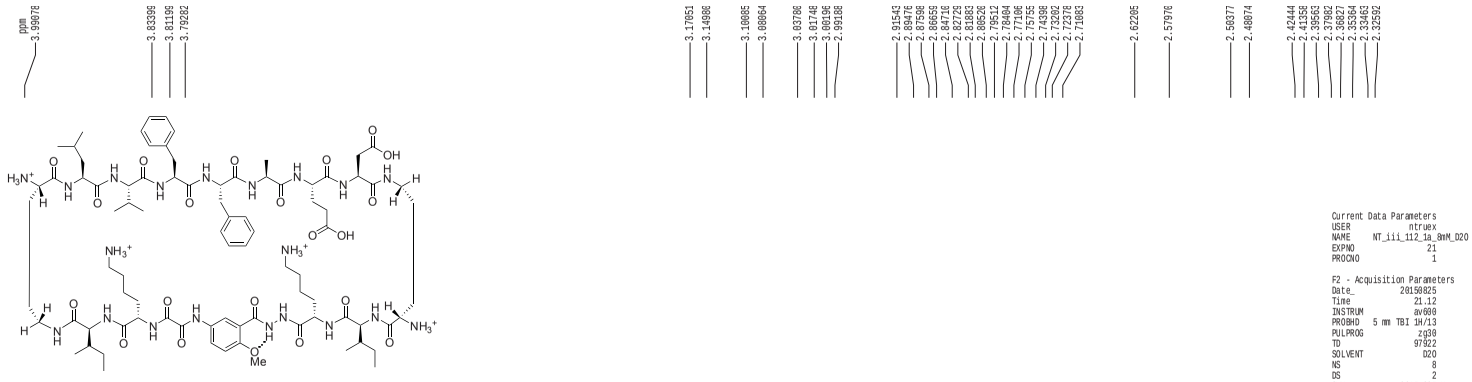

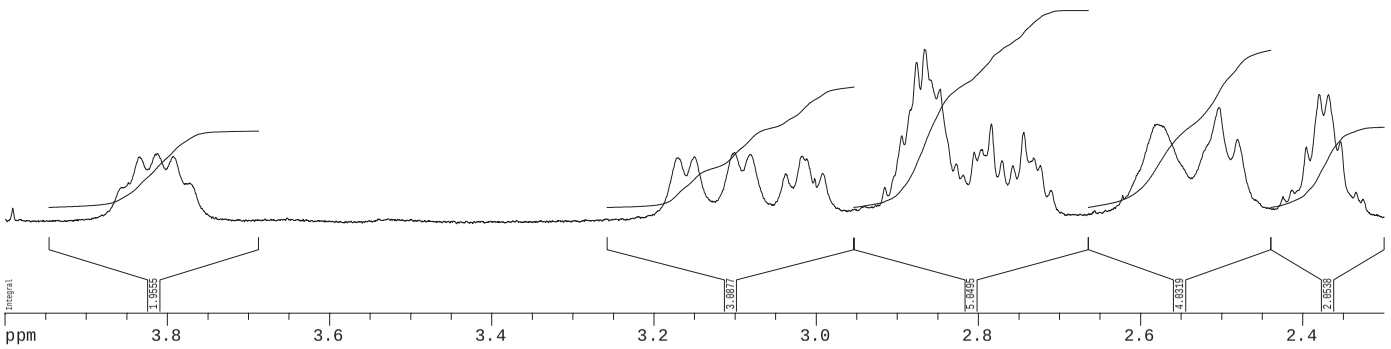


```
Current Data Parameters
USER              ntruex
NAME      NT_iii_112_1a_8mM_D2O
EXPNO                 21
PROCNO                1

F2 - Acquisition Parameters
Date_          20150825
Time              21.12
INSTRUM           av600
PROBHD   5 mm TBI 1H/13
PULPROG           zg30
TD                97922
SOLVENT             D2O
NS                    8
DS                    2
SWH            9615.385 Hz
FIDRES         0.098194 Hz
AQ             5.0919938 sec
RG                  181
DW               52.000 usec
DE               14.54 usec
TE                298.0 K
D1           0.10000000 sec
TD0                   1

======= CHANNEL f1 =======
SFO1        600.1342009 MHz
NUC1                1H
P1                8.00 usec

F2 - Processing parameters
SI                65536
SF          600.1300240 MHz
WDW                  EM
SSB                   0
LB                 0.30 Hz
GB                    0
PC                 1.00

1D NMR plot parameters
CX                22.00 cm
CY                15.00 cm
F1P               4.000 ppm
F1              2400.52 Hz
F2P               2.300 ppm
F2              1380.30 Hz
PPMCM          0.07456 ppm/cm
HZCM          44.74654 Hz/cm
```

^{1}H NMR of peptide **1a**, 8 mM in D_2O at 600 MHz and 298 K

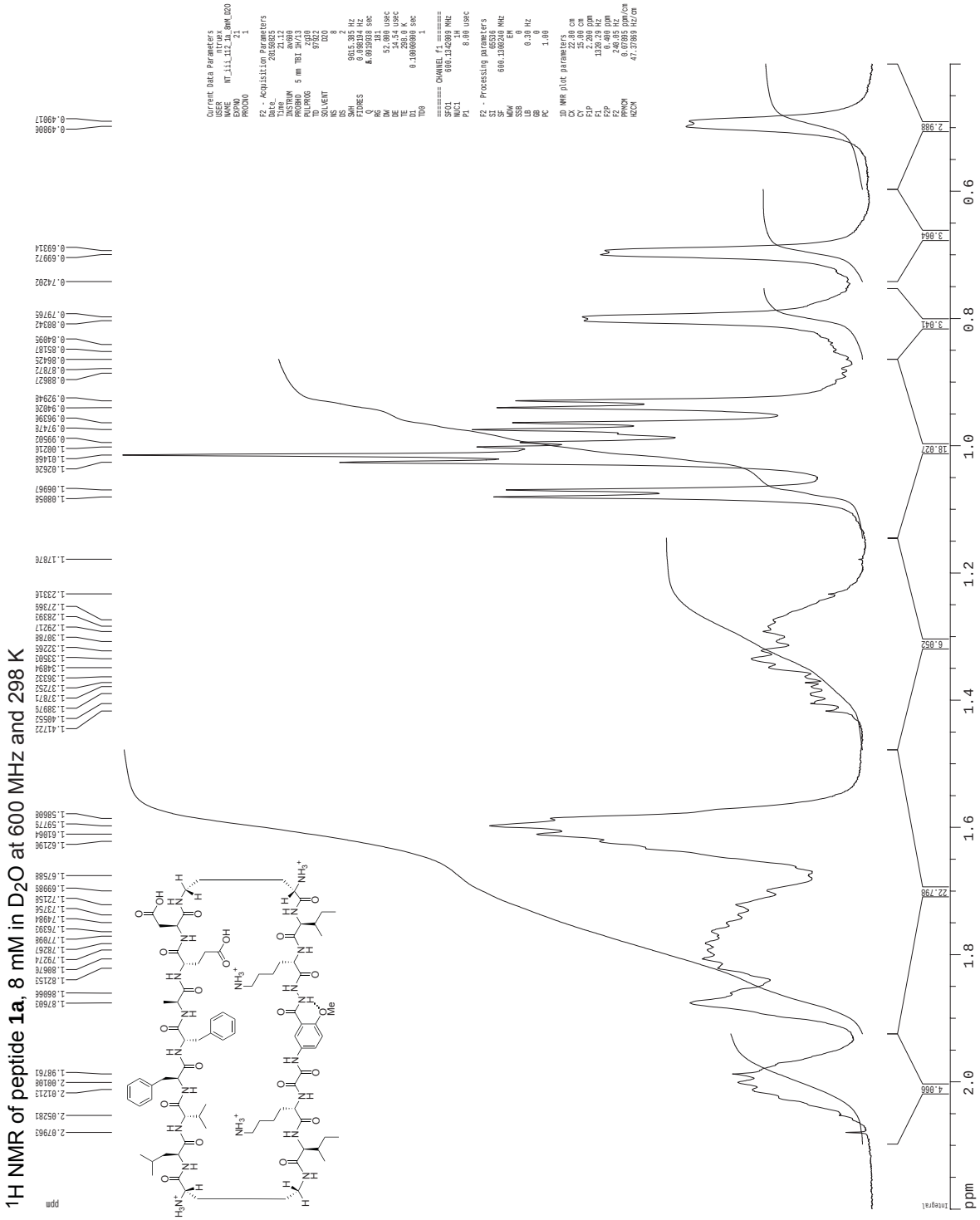

^{1}H NMR 2D TOCSY of peptide **1a** with presaturation suppression of the HOD peak
8 mM in D_2O at 600 MHz and 298 K with 150-ms spin-lock mixing time

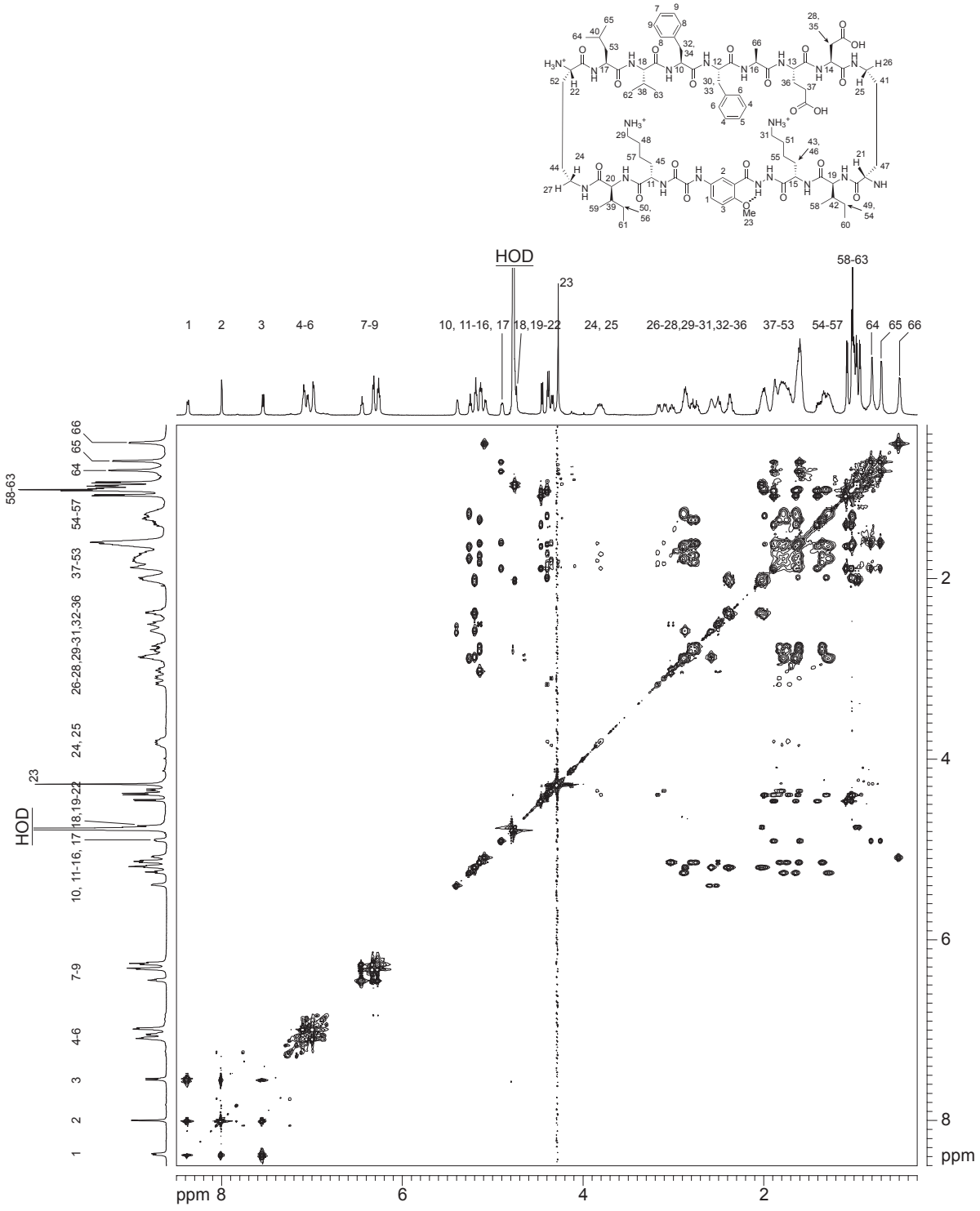

^{1}H NMR 2D TOCSY of peptide **1a** with presaturation suppression of the HOD peak
8 mM in D_2O at 600 MHz and 298 K with 150-ms spin-lock mixing time

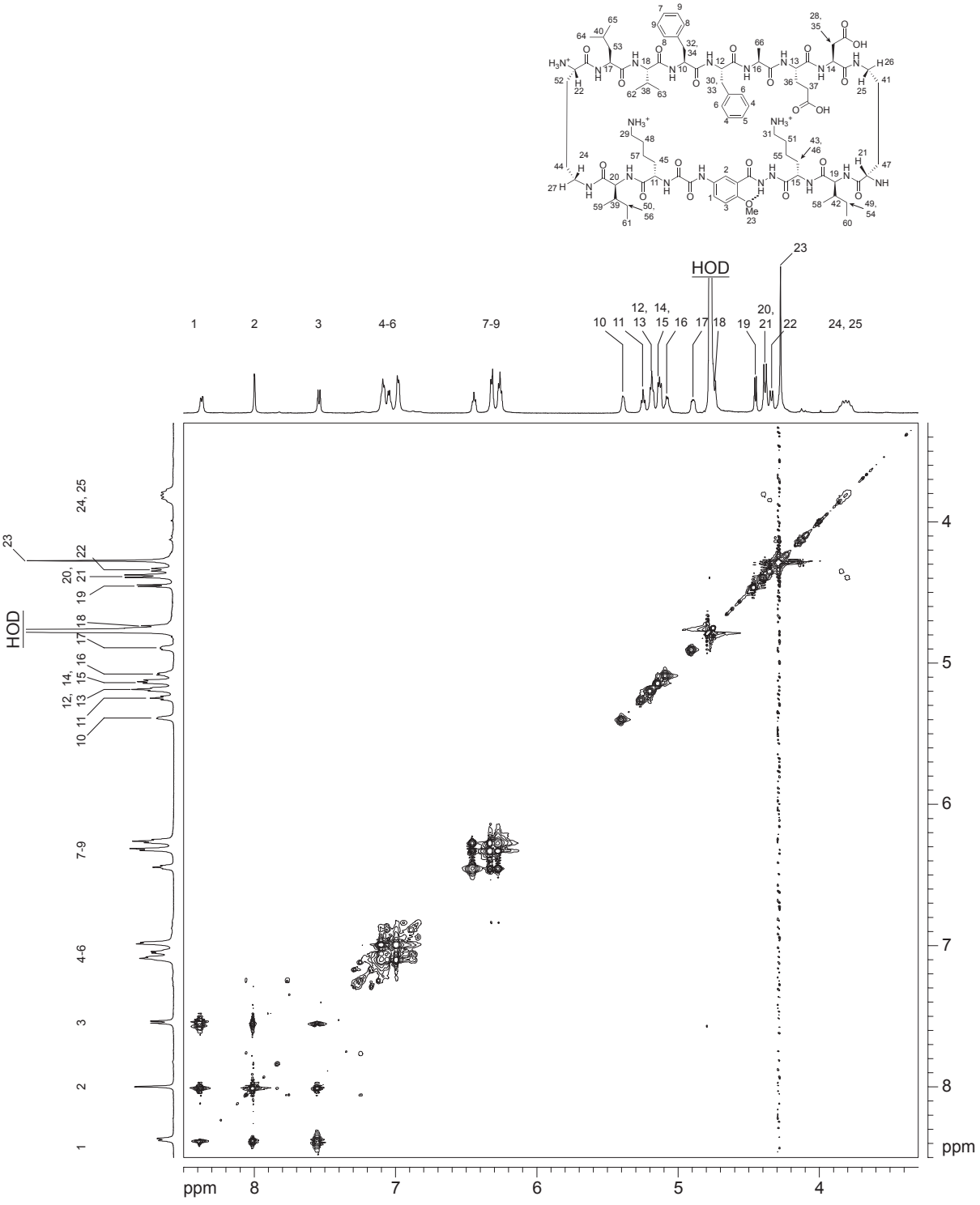

^{1}H NMR 2D TOCSY of peptide **1a** with presaturation suppression of the HOD peak
8 mM in D_2O at 600 MHz and 298 K with 150-ms spin-lock mixing time

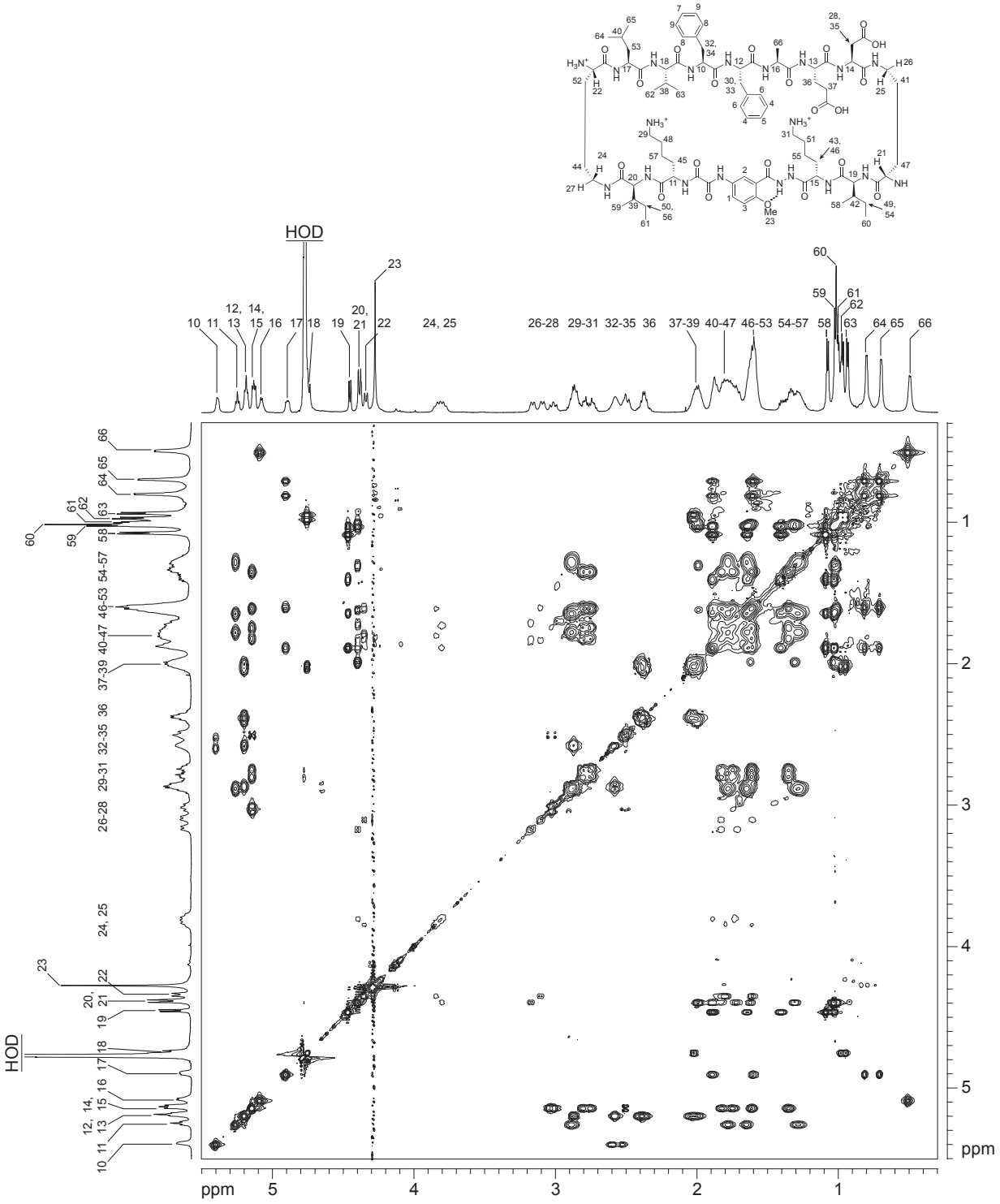

^{1}H NMR 2D NOESY of peptide **1a** with presaturation suppression of the HOD peak
8 mM in D_2O at 600 MHz and 298 K with 150-ms mixing time

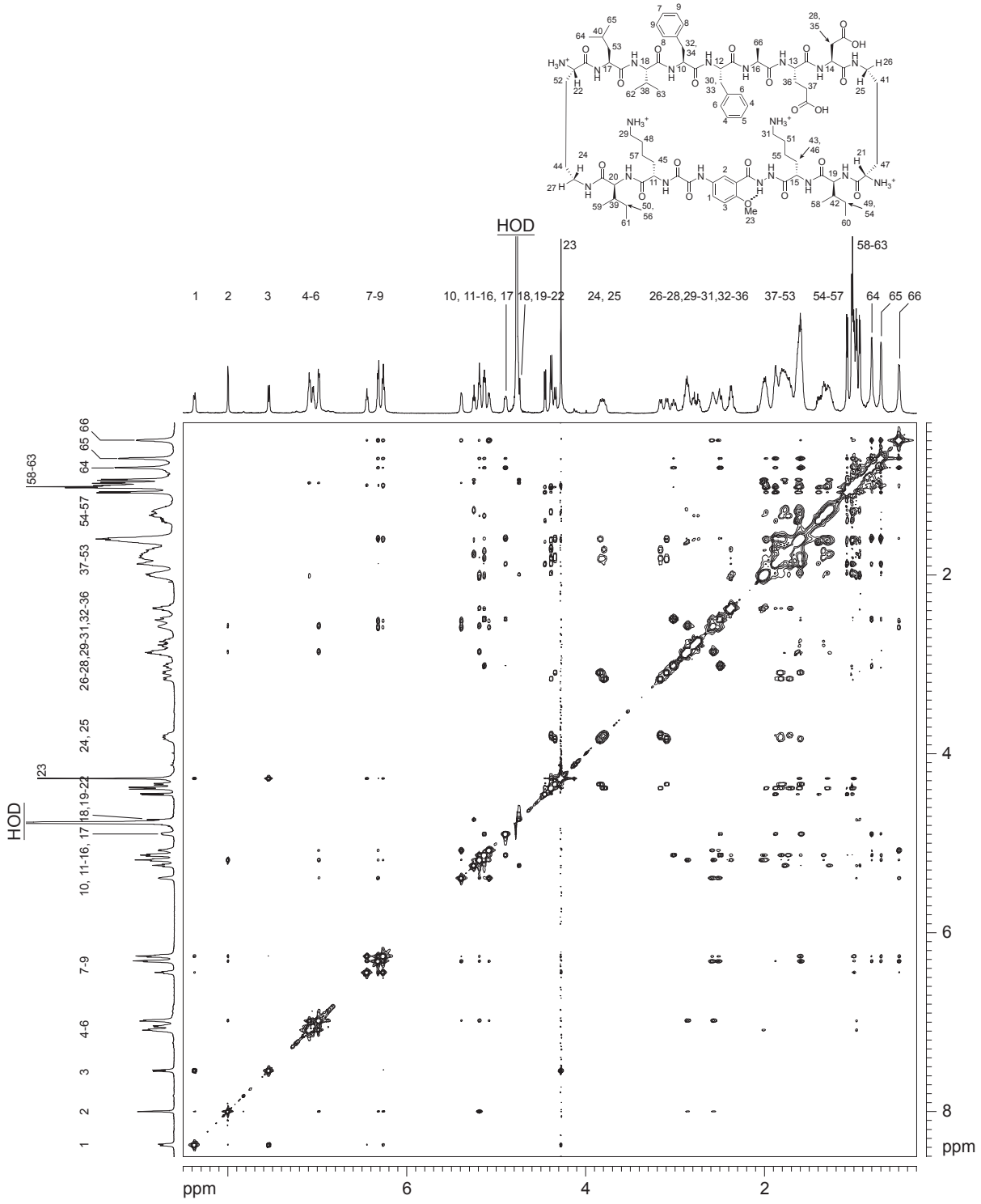

^{1}H NMR 2D NOESY of peptide **1a** with presaturation suppression of the HOD peak
8 mM in D_2O at 600 MHz and 298 K with 150-ms mixing time

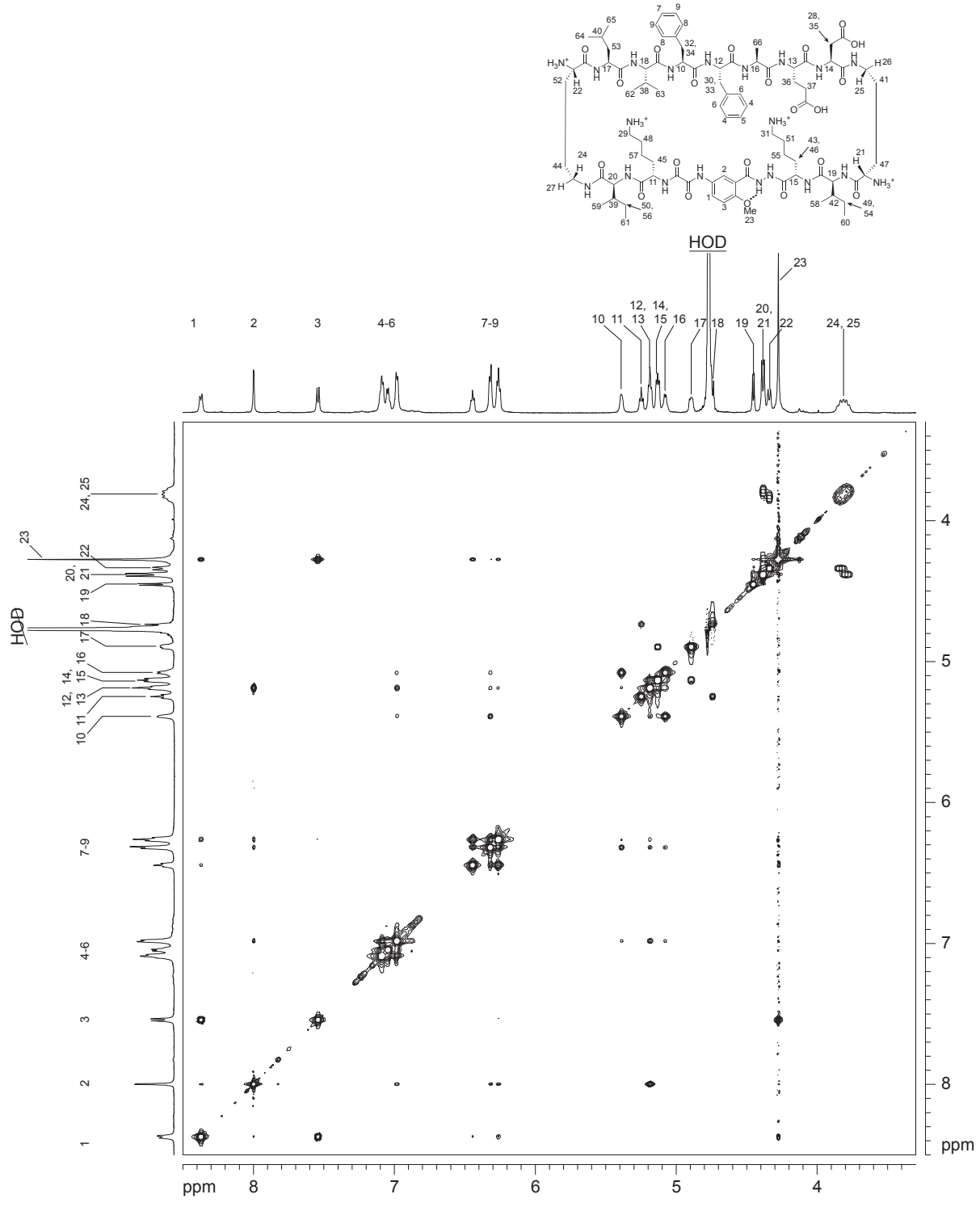

^{1}H NMR 2D NOESY of peptide **1a** with presaturation suppression of the HOD peak
8 mM in D_2O at 600 MHz and 298 K with 150-ms mixing time

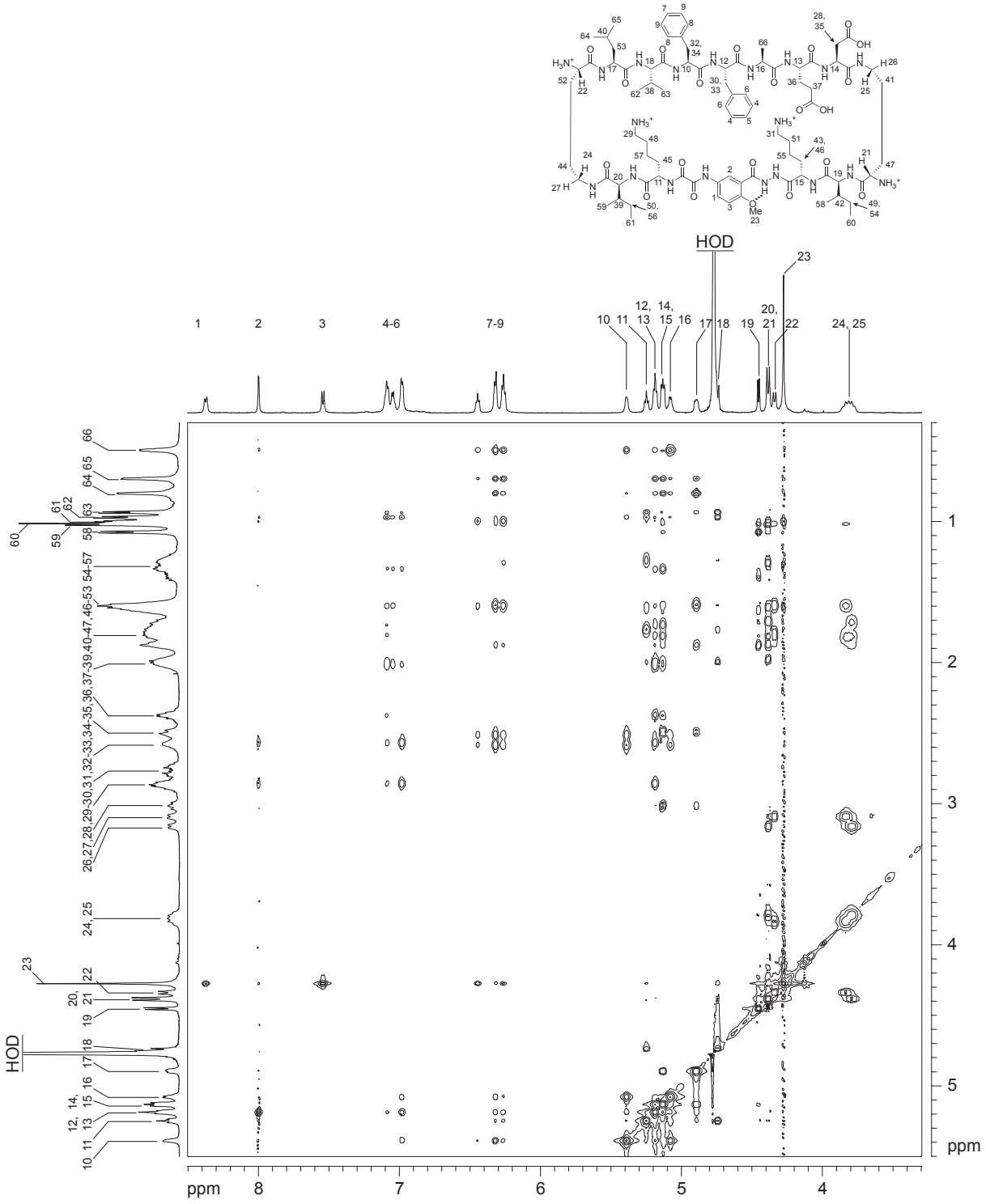

^{1}H NMR 2D NOESY of peptide **1a** with presaturation suppression of the HOD peak
8 mM in D_2O at 600 MHz and 298 K with 150-ms mixing time

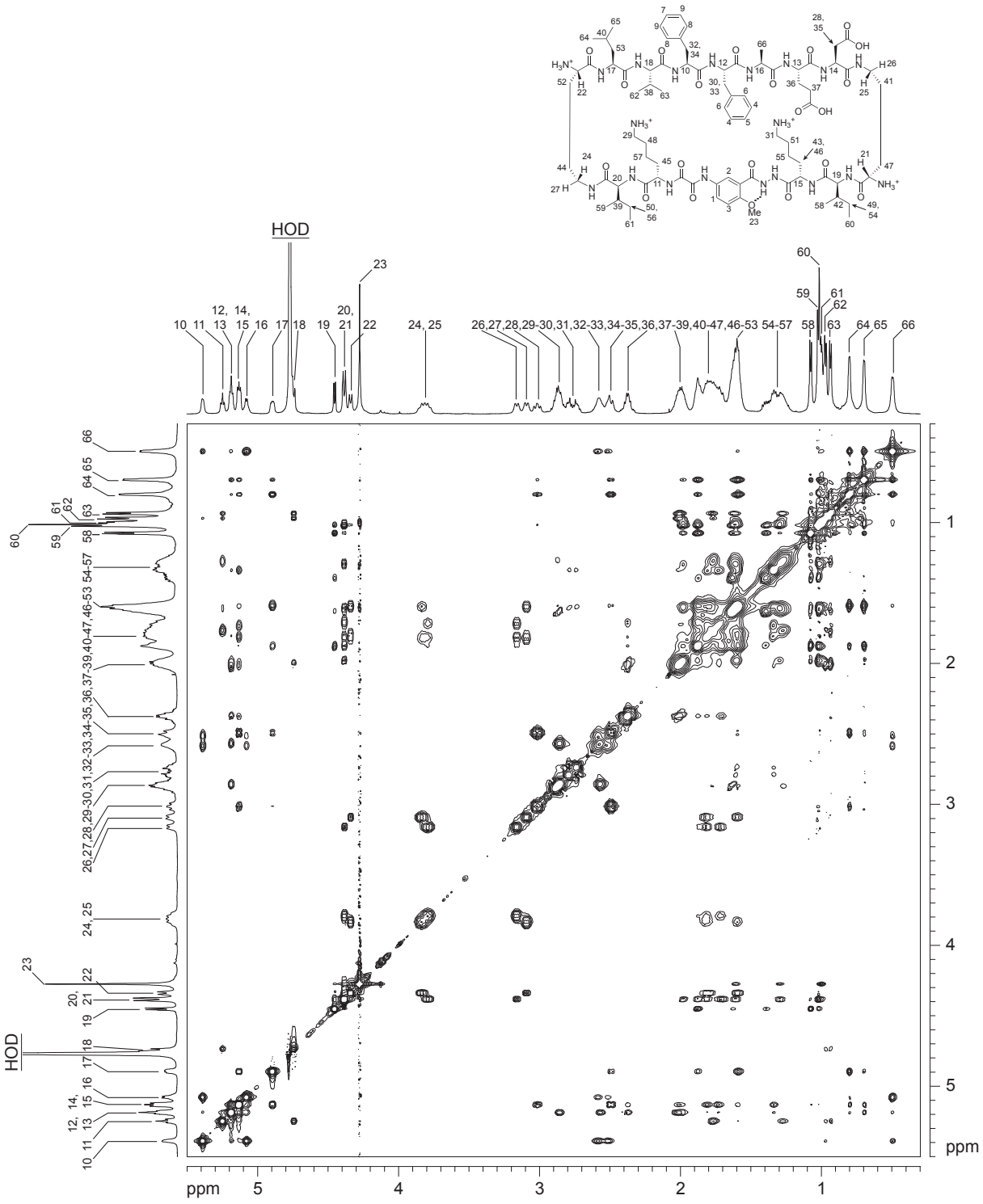

^{1}H NMR 2D EXSY of peptide **1a** with presaturation suppression of the HOD peak
8 mM in D_2O at 600 MHz and 318 K with 200-ms spin-lock mixing time
Exchange crosspeaks are shown in red;
ROE crosspeaks are shown in black.

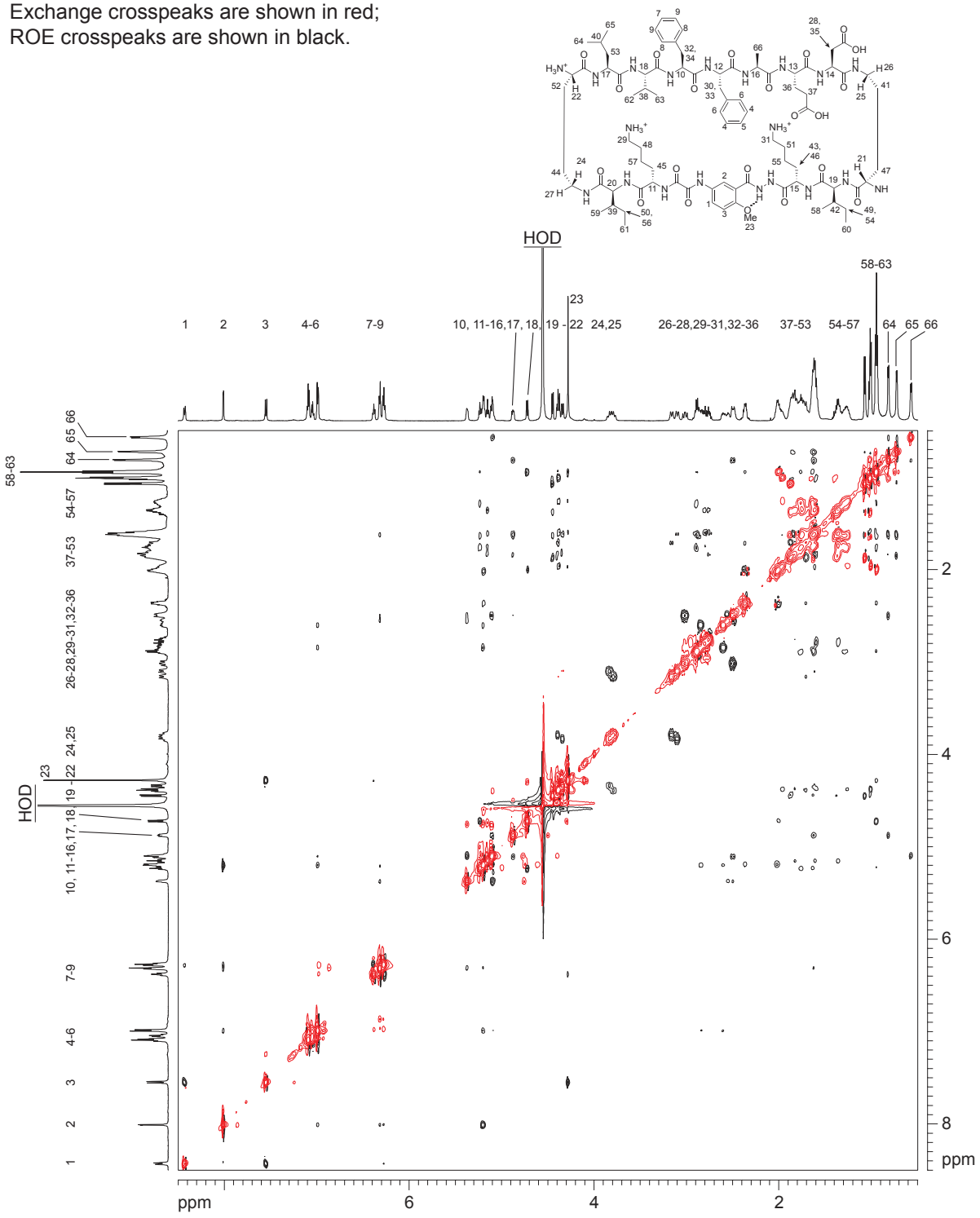

^{1}H NMR 2D EXSY of peptide **1a** with presaturation suppression of the HOD peak
8 mM in D_2O at 600 MHz and 318 K with 200-ms spin-lock mixing time
Exchange crosspeaks are shown in red;
ROE crosspeaks are shown in black.

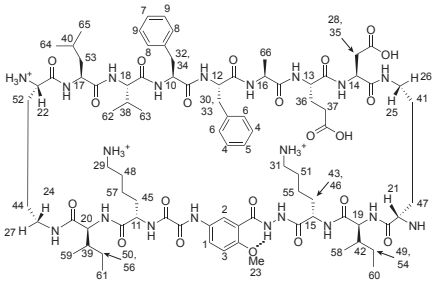

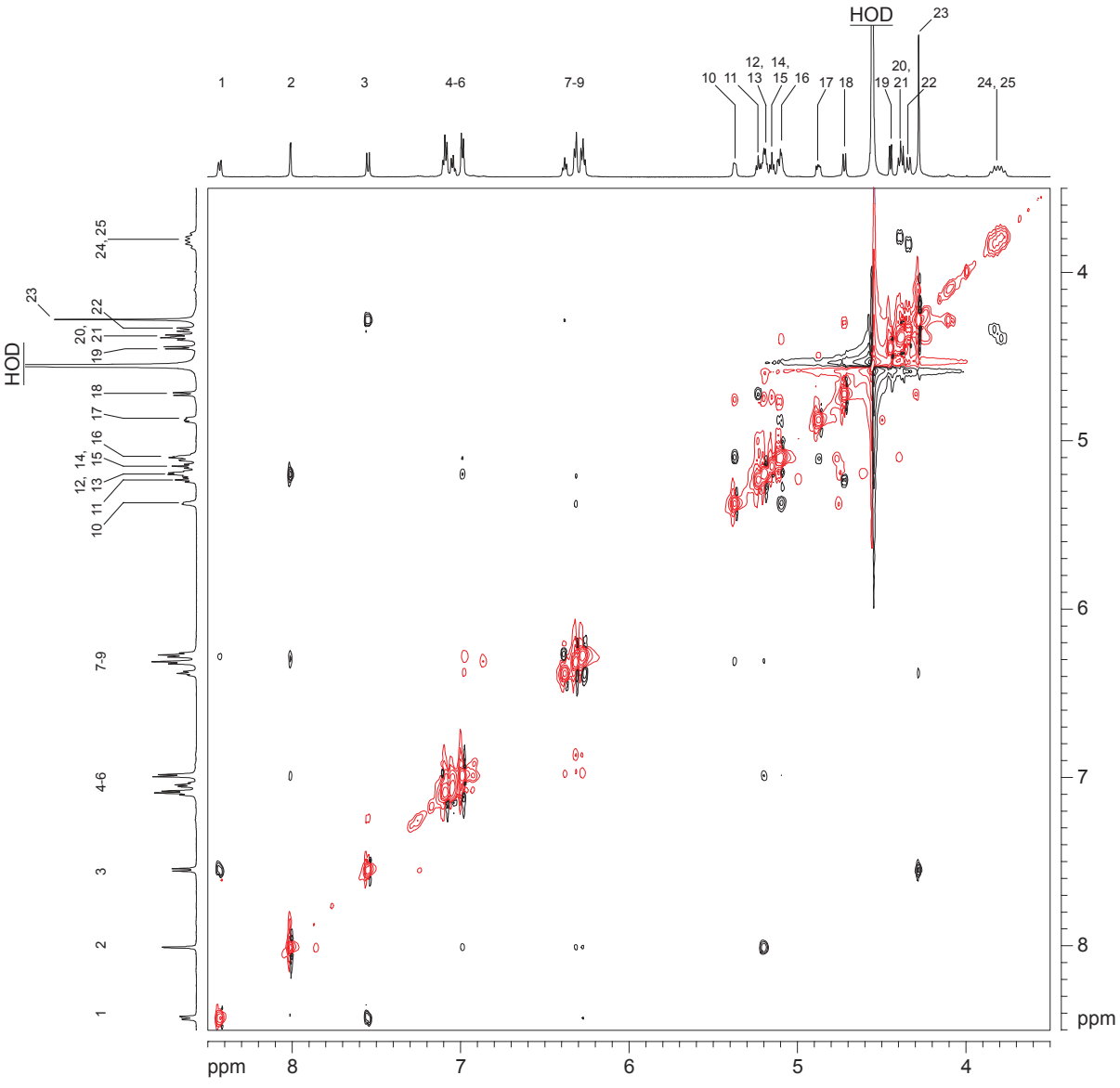

^{1}H NMR 2D EXSY of peptide **1a** with presaturation suppression of the HOD peak
8 mM in D_2O at 600 MHz and 318 K with 200-ms spin-lock mixing time
Exchange crosspeaks are shown in red;
ROE crosspeaks are shown in black.

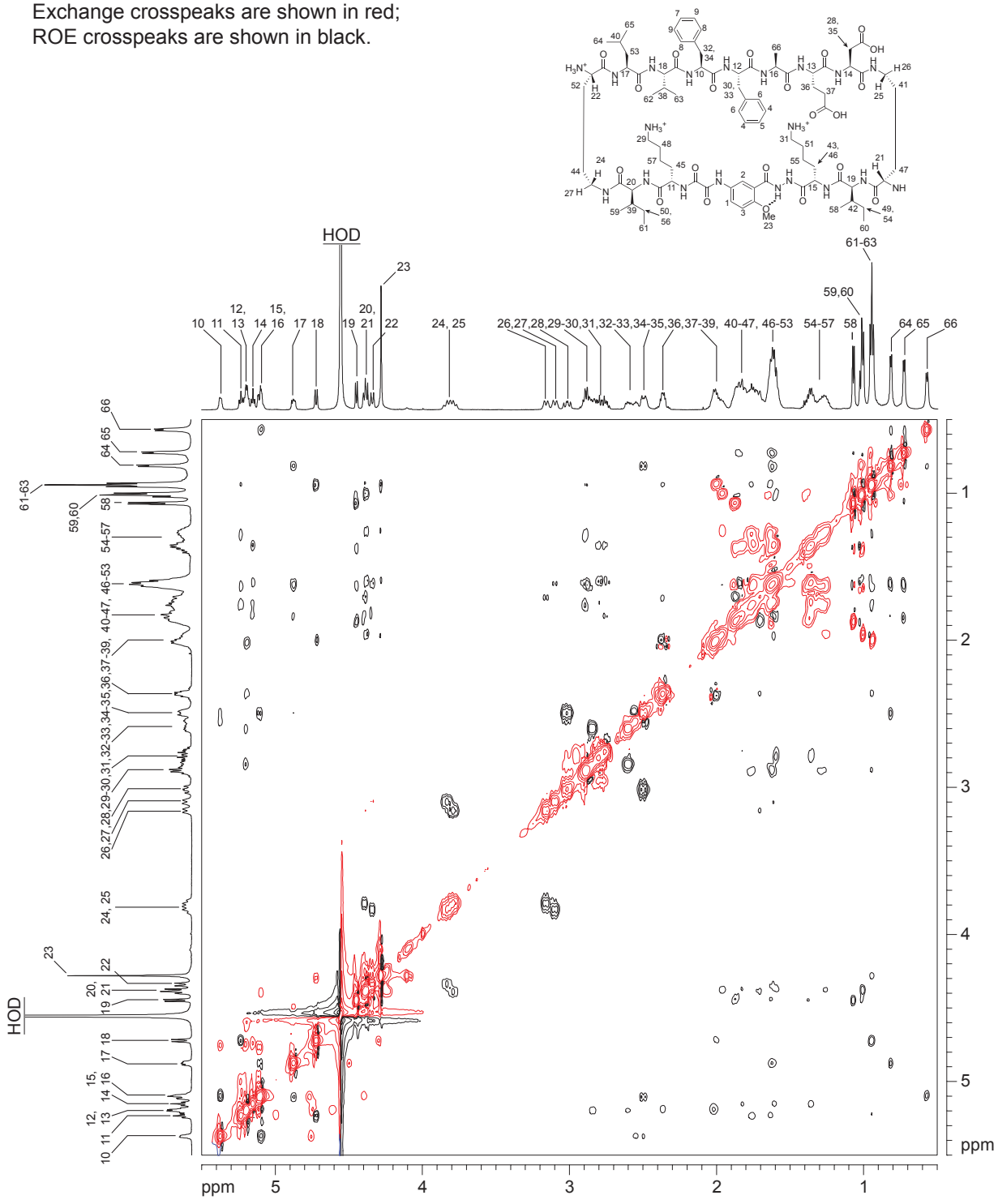

^{1}H NMR DOSY of peptide **1a**, 8 mM in D_2O at 500 MHz and 298 K
tetramer predominates

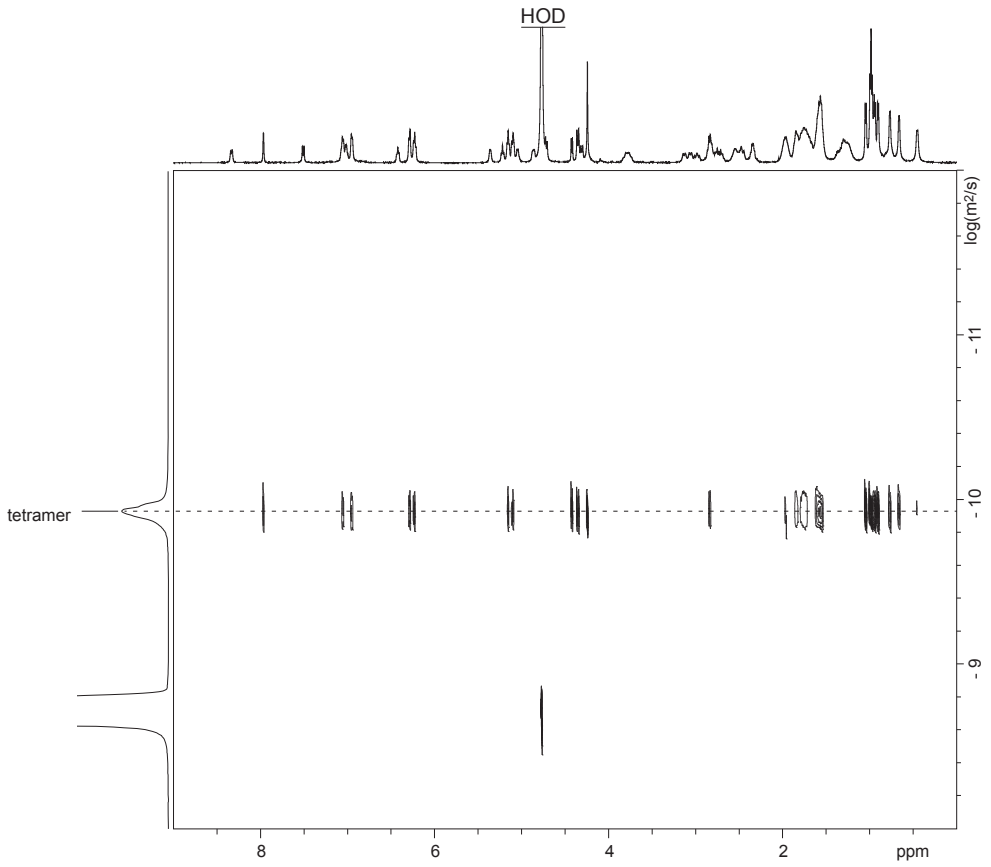

Calculations for peptide **1a** at 8.0 mM

D_{HOD} = 19.0 x 10^{-10} m^2/s [a]
log (D_{HOD}) = -8.721

$D_{tetramer}$: log(D) = -9.928; D = $10^{-9.928}$ = 11.8 ± 1.0 x 10^{-11} m^2/s

[a]Longsworth, L. G. *J. Phys. Chem.* **1960**, *64*, 1914−1917.

RP-HPLC of peptide **1b**

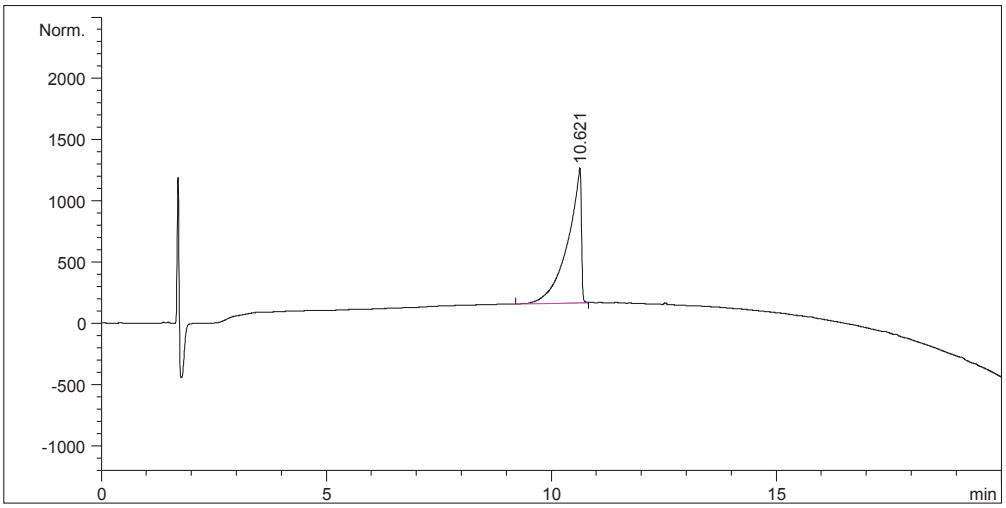

Peak #	RetTime [min]	Type	Width [min]	Area mAU *s	Height [mAU]	Area %
1	10.621	BV	0.2642	2.29549e4	1098.58997	100.0000
Totals :				2.29549e4	1098.58997	

column:	Aeris XB-C18 2.6µ
dimensions:	150 mm x 4.6 mm
mobile phase:	A: H_2O, 0.1% TFA B: CH_3CN, 0.1% TFA
gradient:	A/B (95:5) to (0:100) in 20 min
flow rate:	1.0 mL/min
detection:	VWD, wavelength = 214 nm
temperature:	298 K

MS (ESI) of peptide **1b**

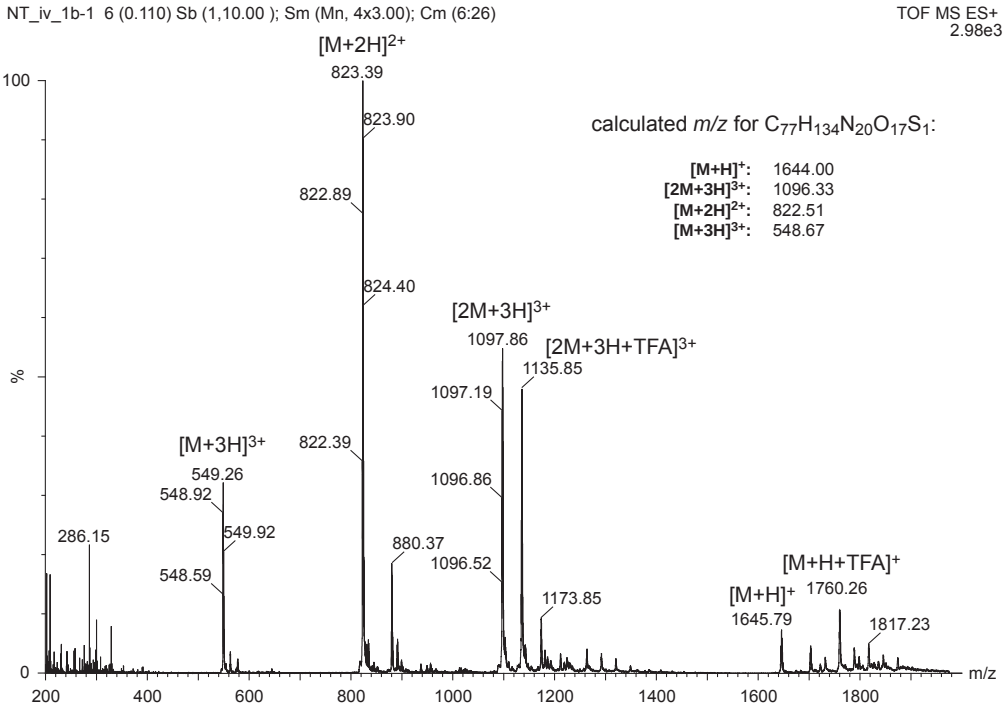

calculated *m/z* for $C_{77}H_{134}N_{20}O_{17}S_1$:

$[M+H]^+$:	1644.00
$[2M+3H]^{3+}$:	1096.33
$[M+2H]^{2+}$:	822.51
$[M+3H]^{3+}$:	548.67

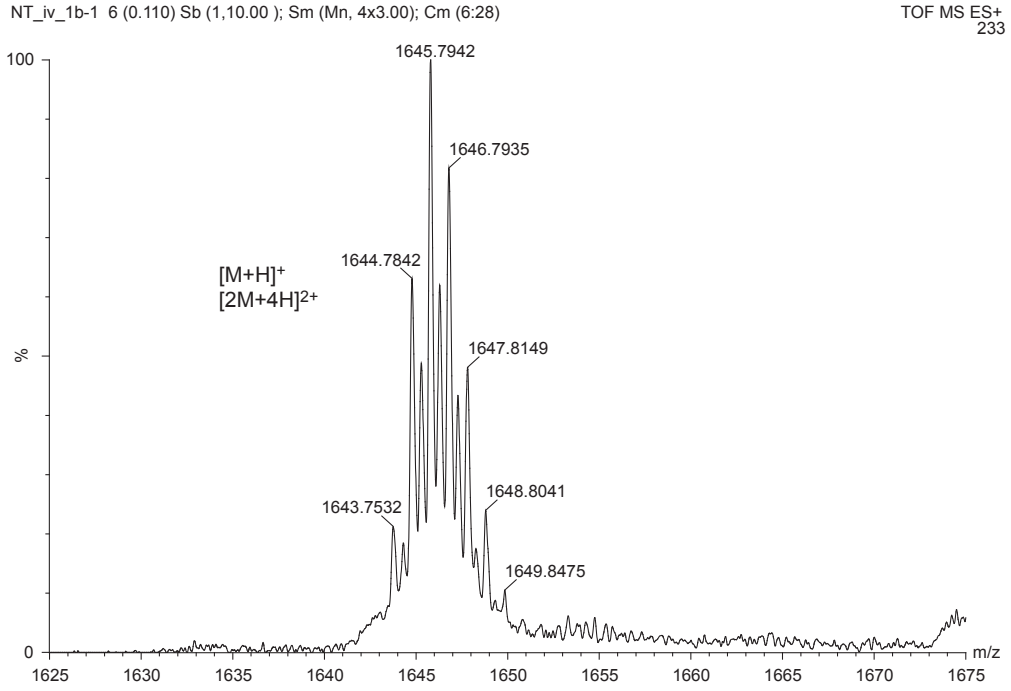
NT_iv_1b-1 6 (0.110) Sb (1,10.00); Sm (Mn, 4x3.00); Cm (6:28)
TOF MS ES+
233
100
%
0
1645.7942
1646.7935
1644.7842
[M+H]+
[2M+4H]2+
1647.8149
1648.8041
1643.7532
1649.8475
m/z
1625
1630
1635
1640
1645
1650
1655
1660
1665
1670
1675

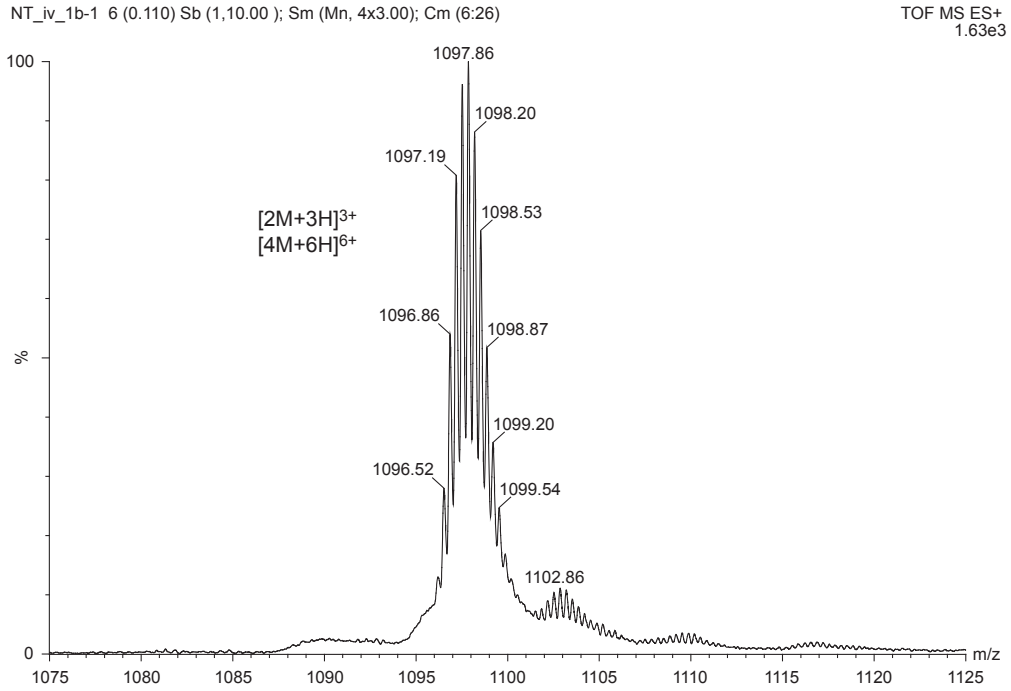
NT_iv_1b-1 6 (0.110) Sb (1,10.00); Sm (Mn, 4x3.00); Cm (6:26)
TOF MS ES+
1.63e3
100
%
0
1097.86
1098.20
1097.19
[2M+3H]3+
[4M+6H]6+
1098.53
1096.86
1098.87
1099.20
1096.52
1099.54
1102.86
m/z
1075
1080
1085
1090
1095
1100
1105
1110
1115
1120
1125

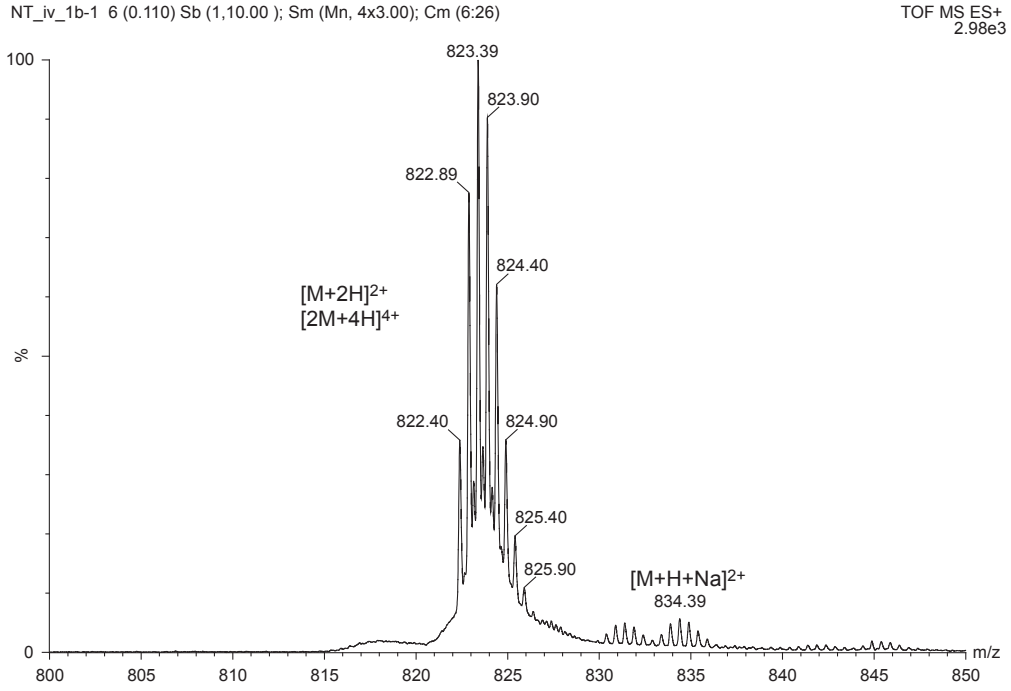
NT_iv_1b-1 6 (0.110) Sb (1,10.00); Sm (Mn, 4x3.00); Cm (6:26)
TOF MS ES+
2.98e3
100
%
0
823.39
823.90
822.89
824.40
[M+2H]2+
[2M+4H]4+
822.40
824.90
825.40
825.90
[M+H+Na]2+
834.39
m/z
800
805
810
815
820
825
830
835
840
845
850

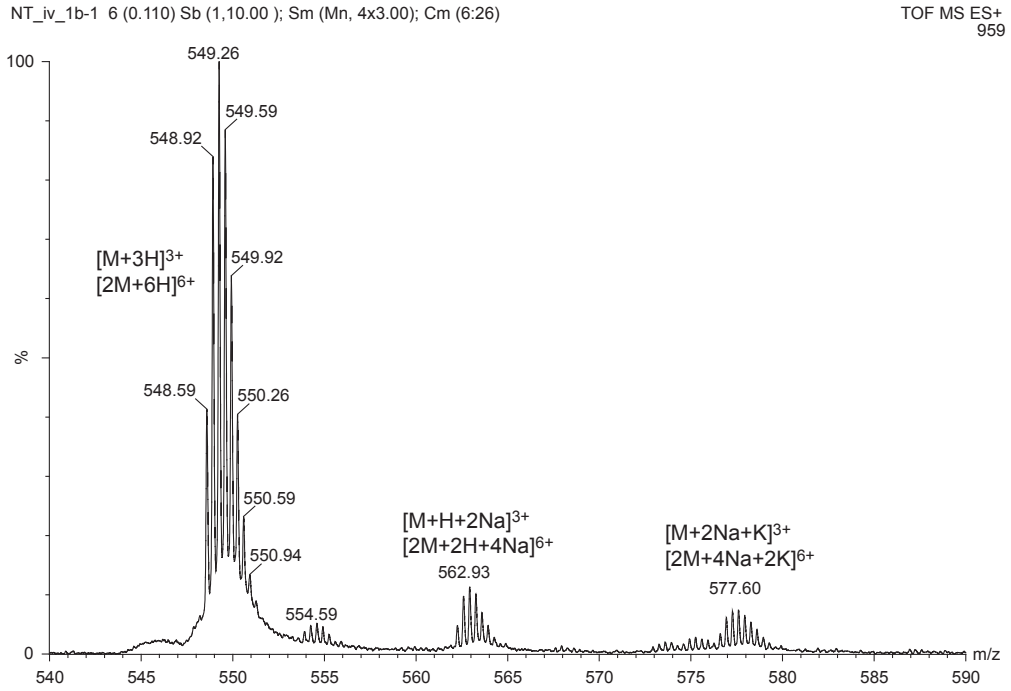
NT_iv_1b-1 6 (0.110) Sb (1,10.00); Sm (Mn, 4x3.00); Cm (6:26)
TOF MS ES+
959
100
%
0
549.26
549.59
548.92
[M+3H]3+
[2M+6H]6+
549.92
548.59
550.26
550.59
550.94
554.59
[M+H+2Na]3+
[2M+2H+4Na]6+
562.93
[M+2Na+K]3+
[2M+4Na+2K]6+
577.60
m/z
540
545
550
555
560
565
570
575
580
585
590

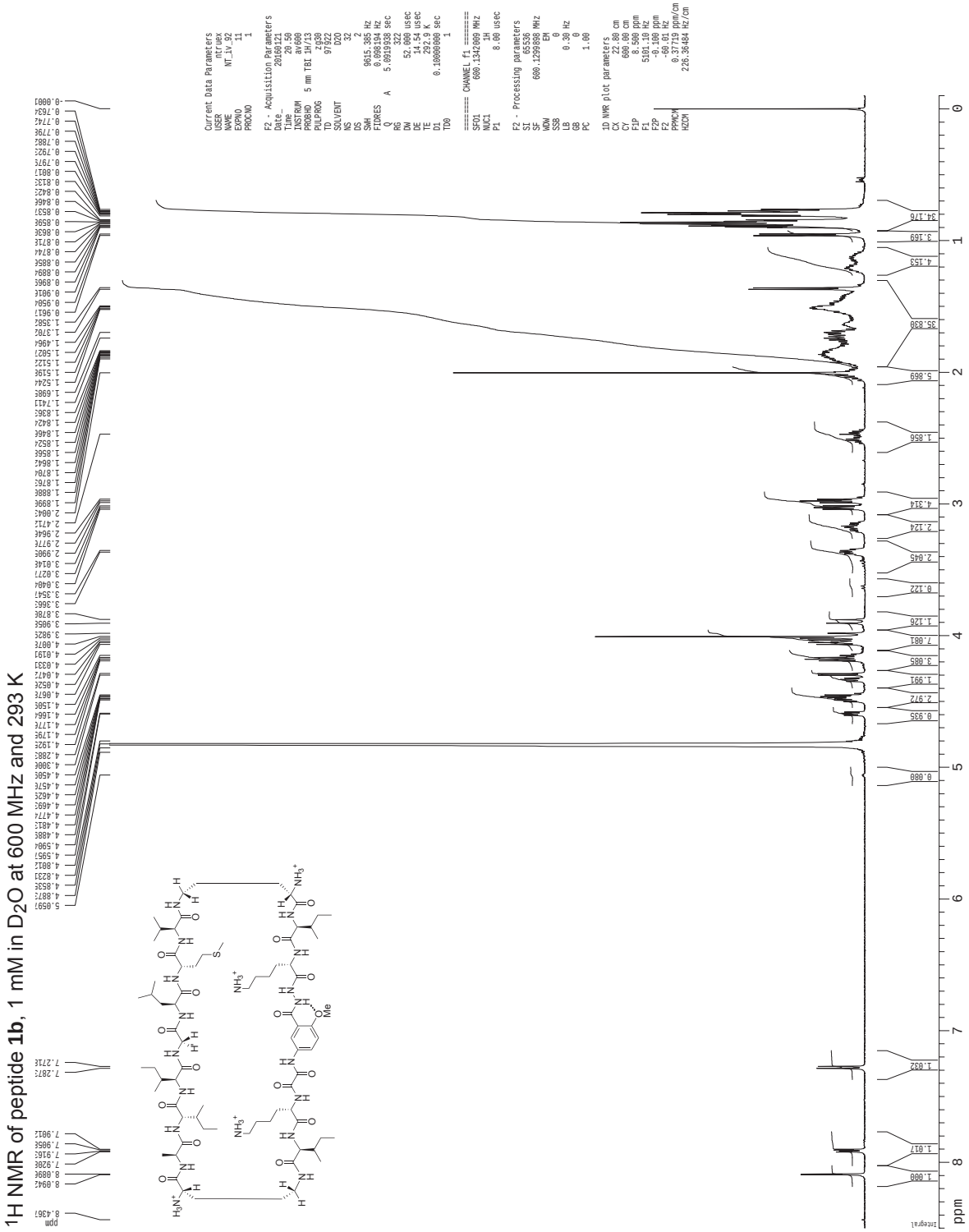
1H NMR of peptide 1b, 1 mM in D2O at 600 MHz and 293 K
Current Data Parameters
USER ntriwex
NAME NT_iv_92
EXPNO 11
PROCNO 1
F2 - Acquisition Parameters
Date_ 20160121
Time 20.50
INSTRUM av600
PROBHD 5 mm TBI 1H/13
PULPROG zg30
TD 97922
SOLVENT D2O
NS 32
DS 2
SWH 9615.385 Hz
FIDRES 0.098194 Hz
Q 5.09919938 sec
A
RG 322
DW 52.000 usec
DE 14.54 usec
TE 292.0 K
D1 0.10000000 sec
TD0 1
======== CHANNEL f1 ========
SFO1 600.1342009 MHz
NUC1 1H
P1 8.00 usec
F2 - Processing parameters
SI 65536
SF 600.1299898 MHz
WDW EM
SSB 0
LB 0.30 Hz
GB 0
PC 1.00
1D NMR plot parameters
CX 22.80 cm
CY 600.00 cm
F1P 9.500 ppm
F1 5701.19 Hz
F2P -0.100 ppm
F2 -60.01 Hz
PPMCM 0.37719 ppm/cm
HZCM 226.36484 Hz/cm
integral
ppm
34.176
3.169
4.153
35.836
5.869
1.856
4.314
2.124
2.045
0.122
1.126
7.081
3.085
1.991
2.972
0.935
0.000
1.032
1.017
1.000

^{1}H NMR of peptide **1b**, 1 mM in D_2O at 600 MHz and 293 K

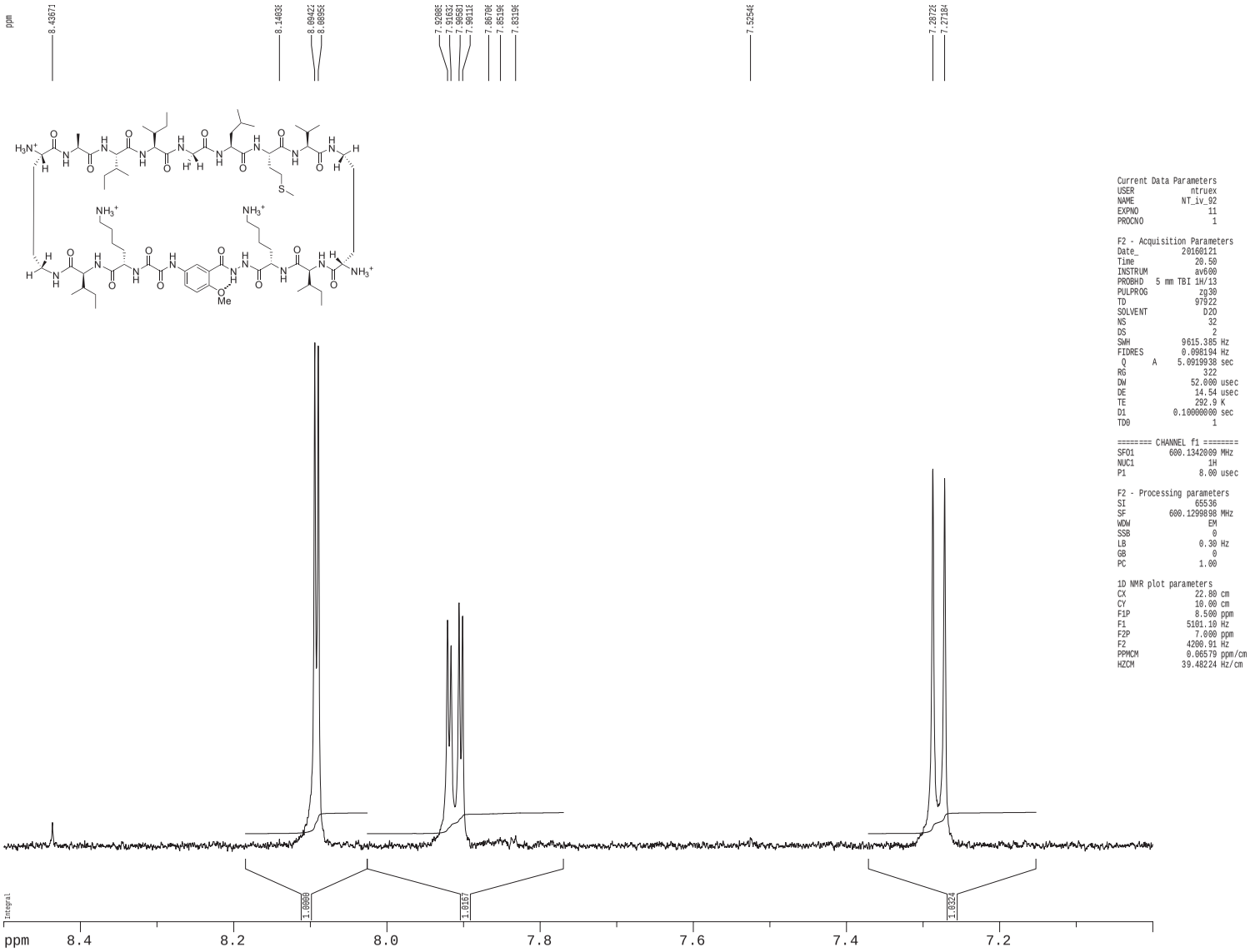


```
Current Data Parameters
USER                ntruex
NAME             NT_iv_92
EXPNO                  11
PROCNO                  1

F2 - Acquisition Parameters
Date_            20160121
Time                20.50
INSTRUM             av600
PROBHD   5 mm TBI 1H/13
PULPROG              zg30
TD                  97922
SOLVENT               D2O
NS                     32
DS                      2
SWH              9615.385 Hz
FIDRES           0.098194 Hz
 Q      A      5.0919938 sec
RG                    322
DW                 52.000 usec
DE                 14.54 usec
TE                 292.9 K
D1            0.10000000 sec
TD0                     1

======== CHANNEL f1 =======
SFO1          600.1342009 MHz
NUC1                   1H
P1                  8.00 usec

F2 - Processing parameters
SI                  65536
SF            600.1299898 MHz
WDW                    EM
SSB                     0
LB                   0.30 Hz
GB                      0
PC                   1.00

1D NMR plot parameters
CX                  22.80 cm
CY                  10.00 cm
F1P                 8.500 ppm
F1                5101.10 Hz
F2P                 7.000 ppm
F2                4200.91 Hz
PPMCM             0.06579 ppm/cm
HZCM             39.48224 Hz/cm
```

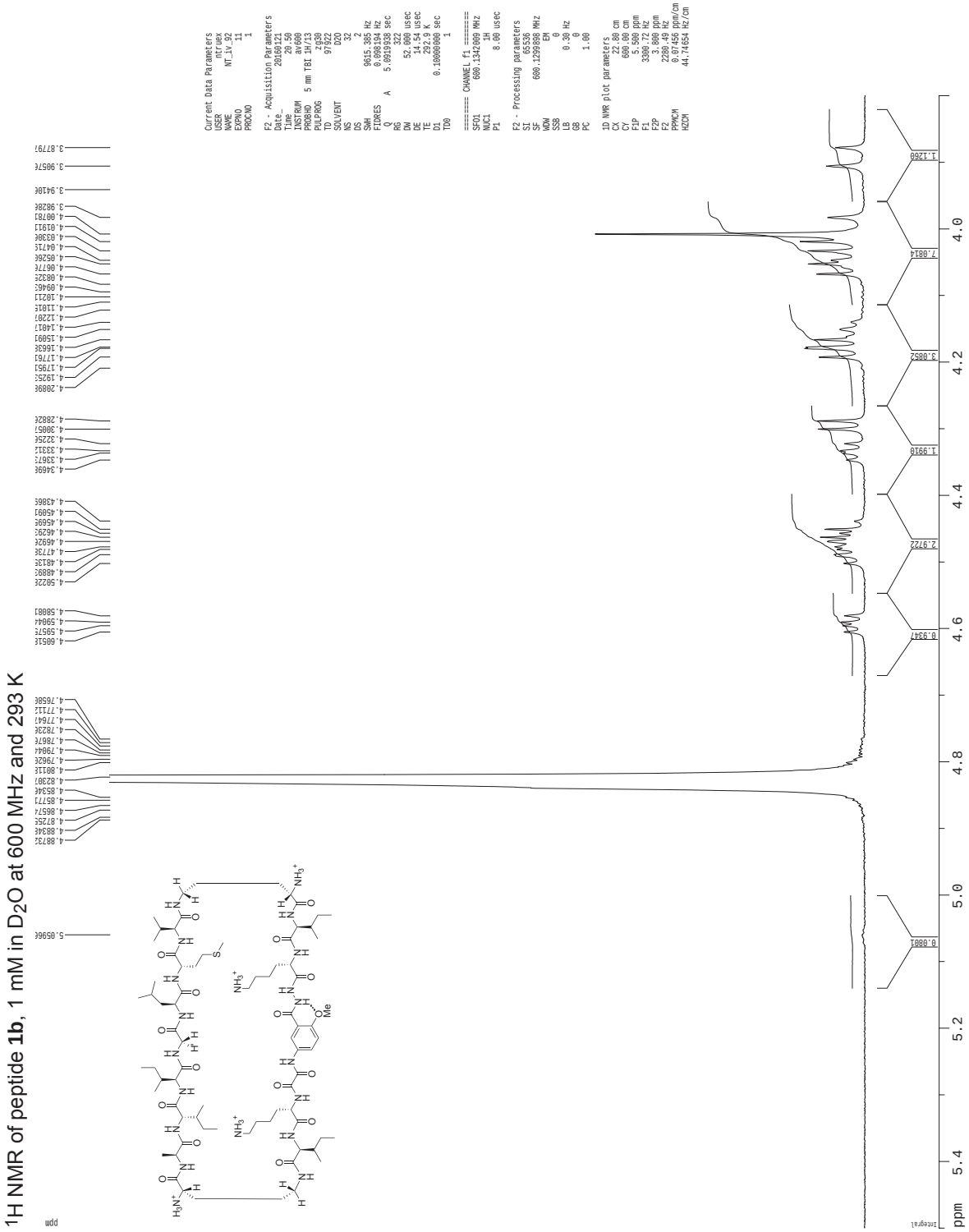
1H NMR of peptide 1b, 1 mM in D2O at 600 MHz and 293 K
Current Data Parameters
USER ntriex
NAME NT_iv_92
EXPNO 11
PROCNO 1
F2 - Acquisition Parameters
Date_ 20160121
Time 20.59
INSTRUM av600
PROBHD 5 mm TBI 1H/13
PULPROG zg30
TD 97922
SOLVENT D2O
NS 32
DS 2
SWH 9615.385 Hz
FIDRES 0.098194 Hz
Q 5.09919938 sec
A
RG 322
DW 52.000 usec
DE 14.14 usec
TE 292.3 K
D1 0.10000000 sec
TD0 1
======== CHANNEL f1 ========
SFO1 600.1342009 MHz
NUC1 1H
P1 8.00 usec
F2 - Processing parameters
SI 65536
SF 600.1299898 MHz
WDW EM
SSB 0
LB 0.30 Hz
GB 0
PC 1.00
1D NMR plot parameters
CX 22.00 cm
CY 600.00 cm
F1P 5.500 ppm
F1 3300.72 Hz
F2P 3.800 ppm
F2 2280.49 Hz
PPMCM 0.07456 ppm/cm
HZCM 44.74654 Hz/cm
integral
ppm
5.4
5.2
5.0
4.8
4.6
4.4
4.2
4.0
0.9341
2.9722
1.9910
3.0852
7.0814
1.1260
0.8801
Me

^{1}H NMR of peptide **1b**, 1 mM in D_2O at 600 MHz and 293 K

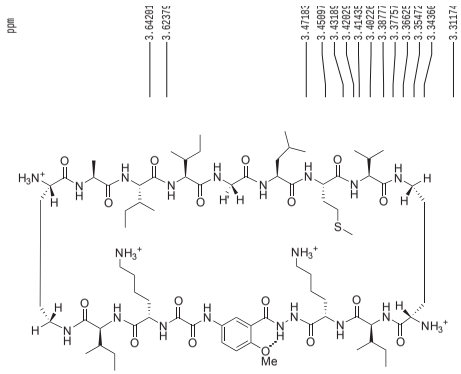


```
Current Data Parameters
USER                ntruex
NAME             NT_iv_92
EXPNO                  11
PROCNO                  1

F2 - Acquisition Parameters
Date_            20160121
Time                20.50
INSTRUM             av600
PROBHD   5 mm TBI 1H/13
PULPROG              zg30
TD                  97922
SOLVENT               D2O
NS                     32
DS                      2
SWH              9615.385 Hz
FIDRES           0.098194 Hz
 Q       A     5.0919938 sec
RG                    322
DW                52.000 usec
DE                 14.54 usec
TE                 292.9 K
D1            0.10000000 sec
TD0                     1

======== CHANNEL f1 =======
SFO1          600.1342009 MHz
NUC1                   1H
P1                  8.00 usec

F2 - Processing parameters
SI                  65536
SF            600.1299898 MHz
WDW                    EM
SSB                     0
LB                   0.30 Hz
GB                      0
PC                   1.00

1D NMR plot parameters
CX                  22.80 cm
CY                  10.00 cm
F1P                  3.800 ppm
F1                2280.49 Hz
F2P                  2.300 ppm
F2                1380.30 Hz
PPMCM             0.06579 ppm/cm
HZCM             39.48224 Hz/cm
```

^{1}H NMR of peptide **1b**, 1 mM in D_2O at 600 MHz and 293 K

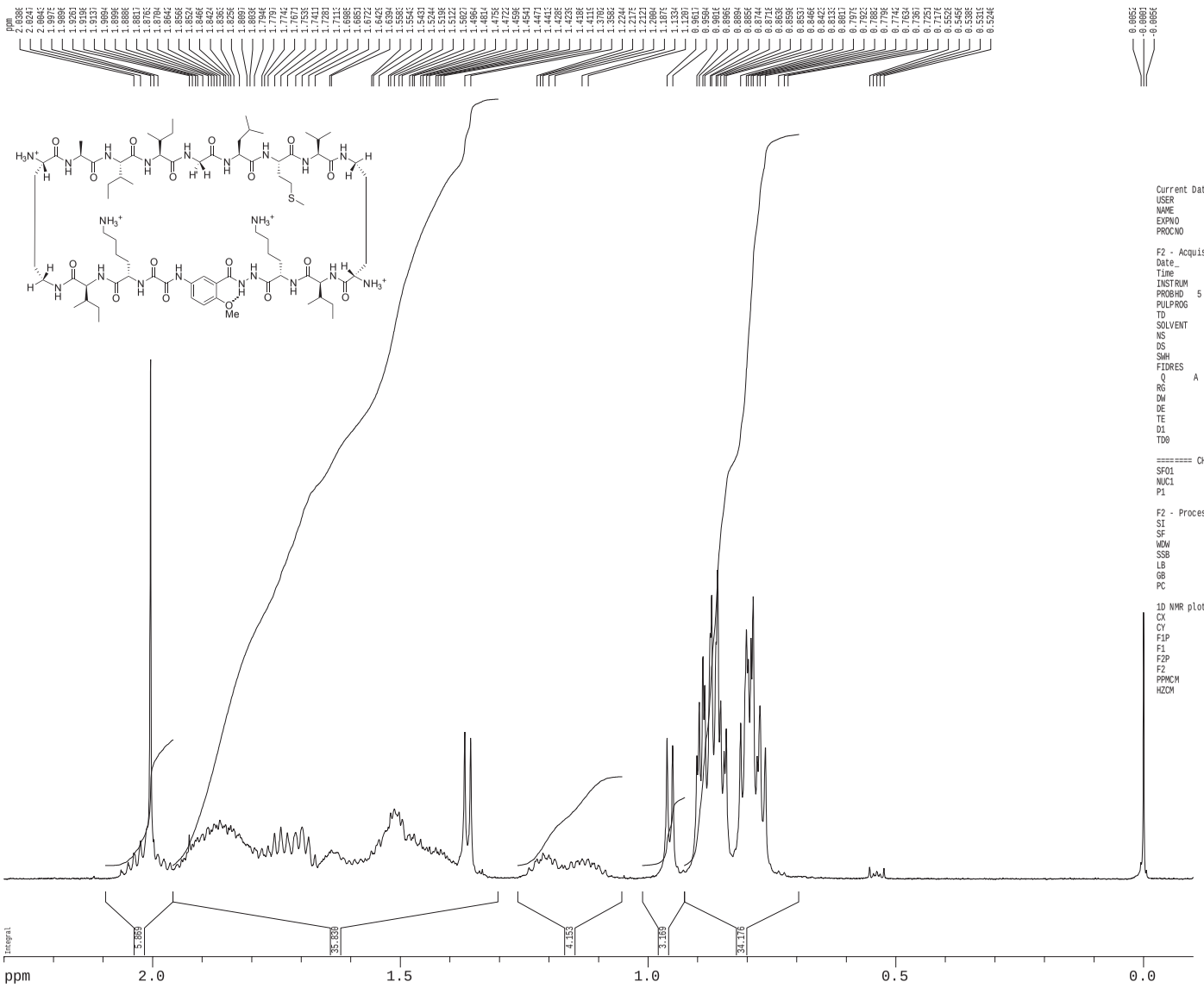


```
Current Data Parameters
USER                ntruex
NAME             NT_iv_92
EXPNO                  11
PROCNO                  1

F2 - Acquisition Parameters
Date_            20160121
Time                20.50
INSTRUM             av600
PROBHD   5 mm TBI 1H/13
PULPROG             zg30
TD                 97922
SOLVENT              D2O
NS                    32
DS                     2
SWH              9615.385 Hz
FIDRES           0.098194 Hz
 Q       A     5.0919938 sec
RG                   322
DW                52.000 usec
DE                14.54 usec
TE                292.9 K
D1            0.10000000 sec
TD0                    1

======== CHANNEL f1 =======
SFO1          600.1342009 MHz
NUC1                   1H
P1                  8.00 usec

F2 - Processing parameters
SI                  65536
SF            600.1299898 MHz
WDW                    EM
SSB                     0
LB                   0.30 Hz
GB                      0
PC                   1.00

1D NMR plot parameters
CX                  22.80 cm
CY                  10.00 cm
F1P                 2.300 ppm
F1                1380.30 Hz
F2P                -0.100 ppm
F2                 -60.01 Hz
PPMCM             0.10526 ppm/cm
HZCM             63.17158 Hz/cm
```

^{1}H NMR 2D TOCSY of macrocycle **1b** with presaturation suppression of the HOD peak
1 mM in D_2O at 600 MHz and 293 K with 150-ms spin-lock mixing time

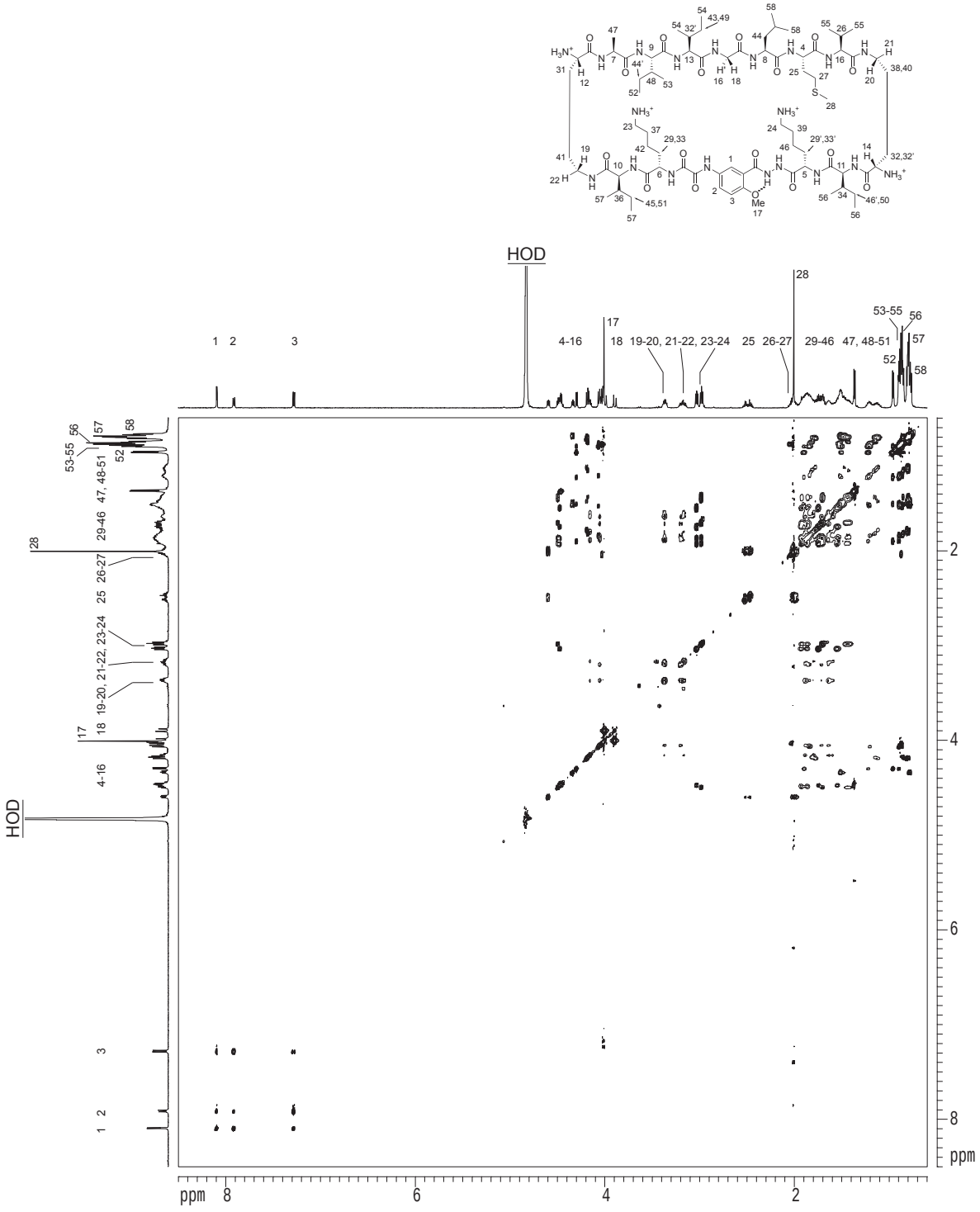

^{1}H NMR 2D TOCSY of macrocycle **1b** with presaturation suppression of the HOD peak
1 mM in D_2O at 600 MHz and 293 K with 150-ms spin-lock mixing time

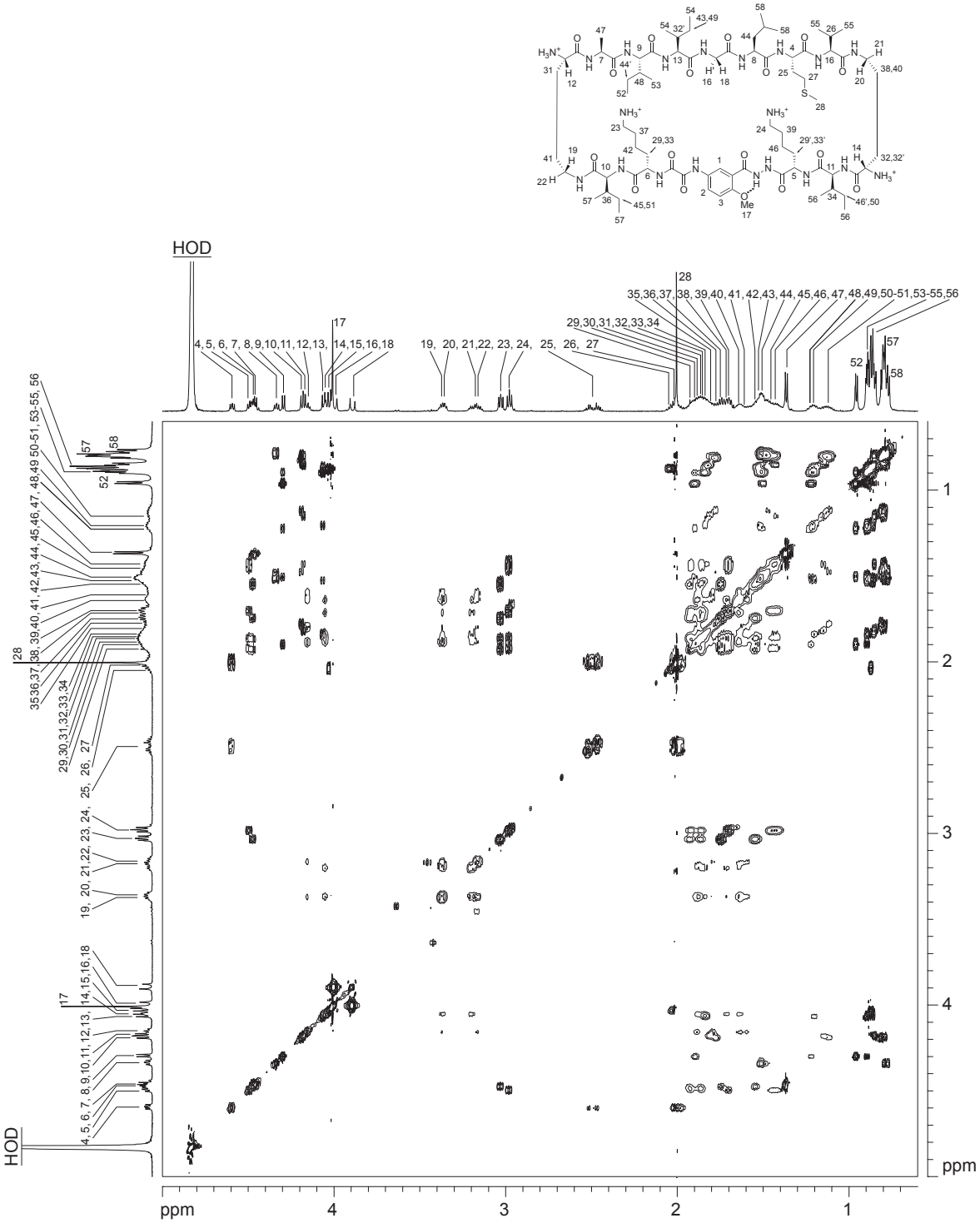

^{1}H NMR 2D ROESY of macrocycle **1b** with presaturation suppression of the HOD peak
1 mM in D_2O at 600 MHz and 293 K with 200-ms spin-lock mixing time

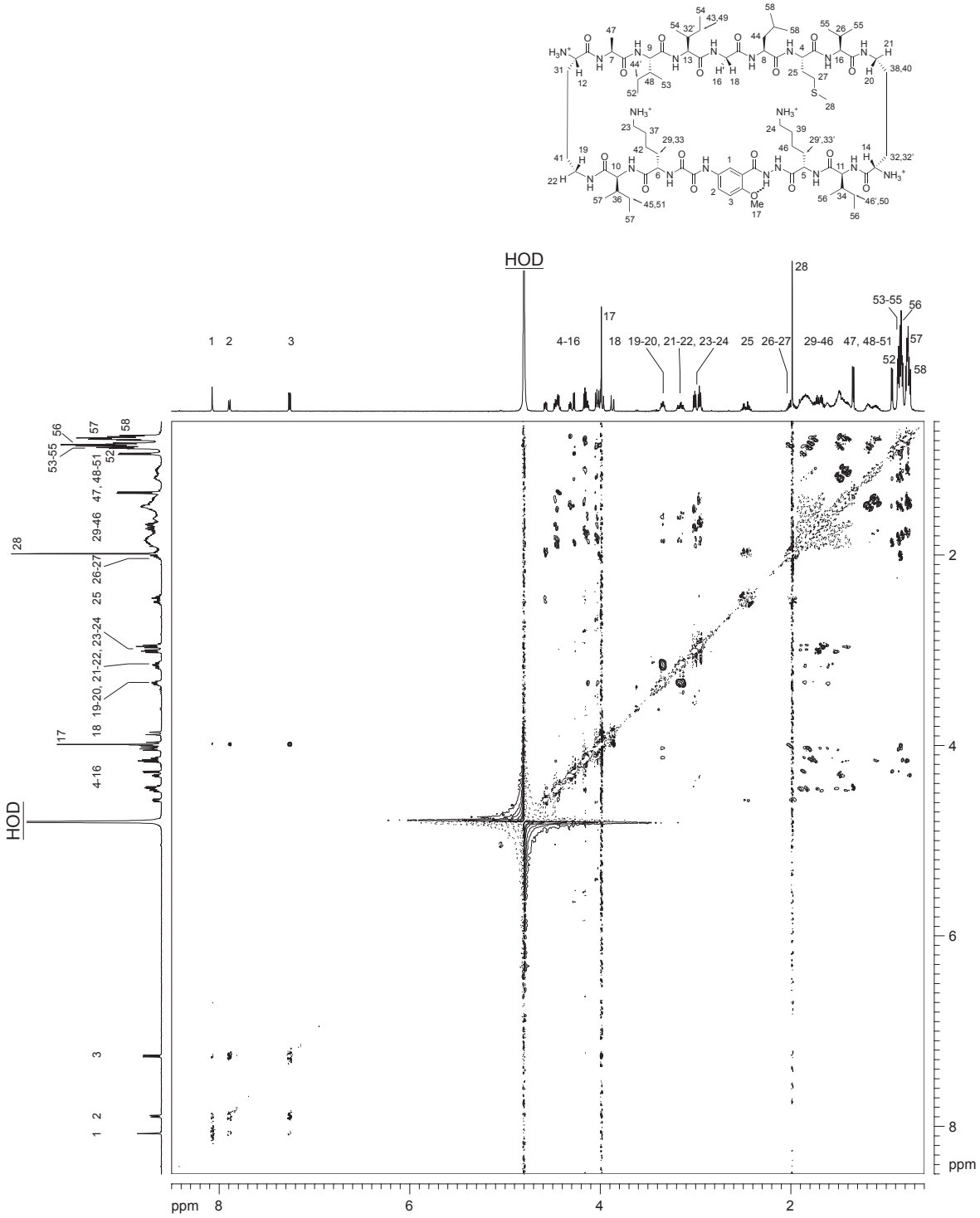

^{1}H NMR 2D ROESY of macrocycle **1b** with presaturation suppression of the HOD peak
1 mM in D_2O at 600 MHz and 293 K with 200-ms spin-lock mixing time

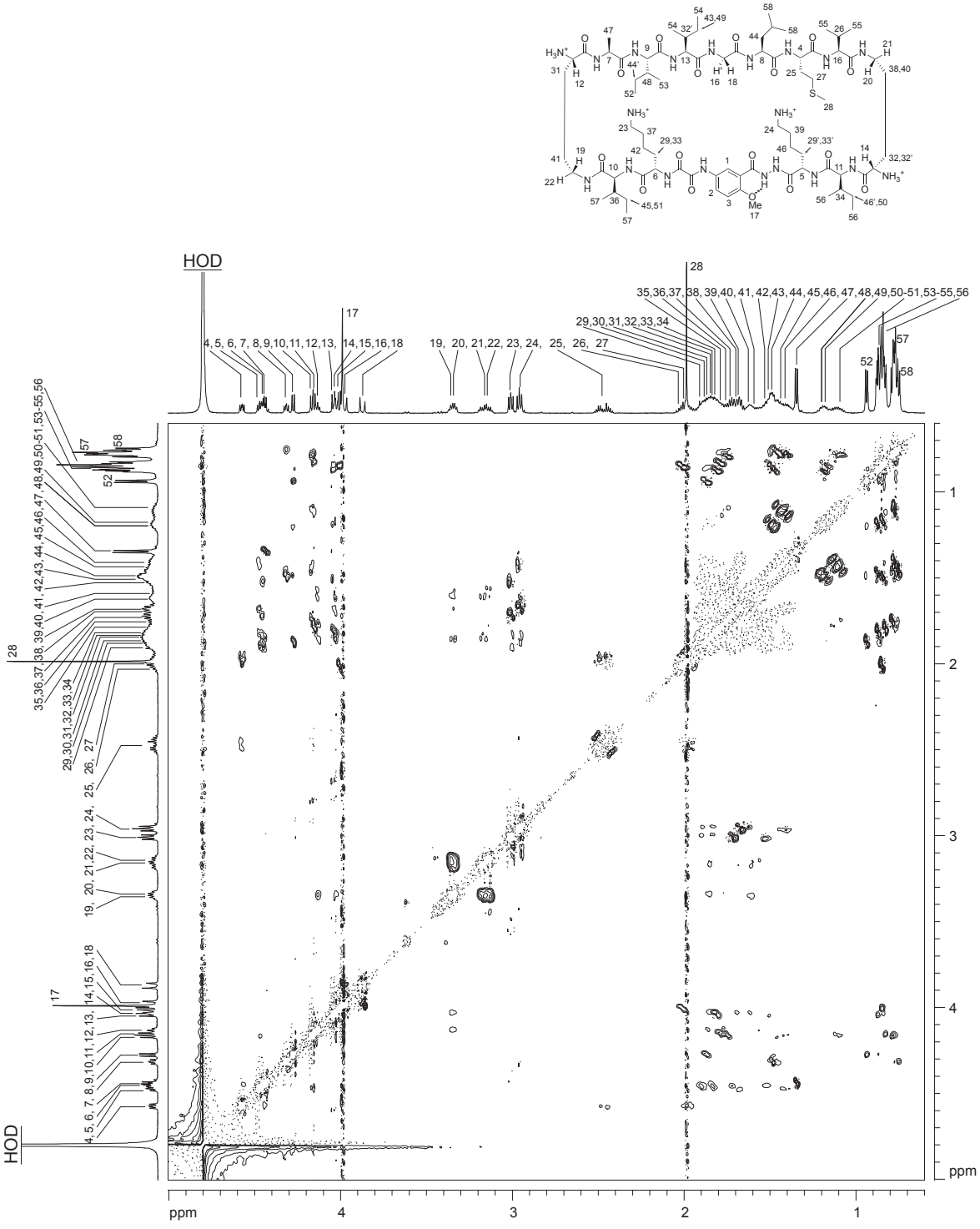

^{1}H NMR DOSY of peptide **1b**, 1 mM in D_2O at 500 MHz and 298 K
monomer predominates

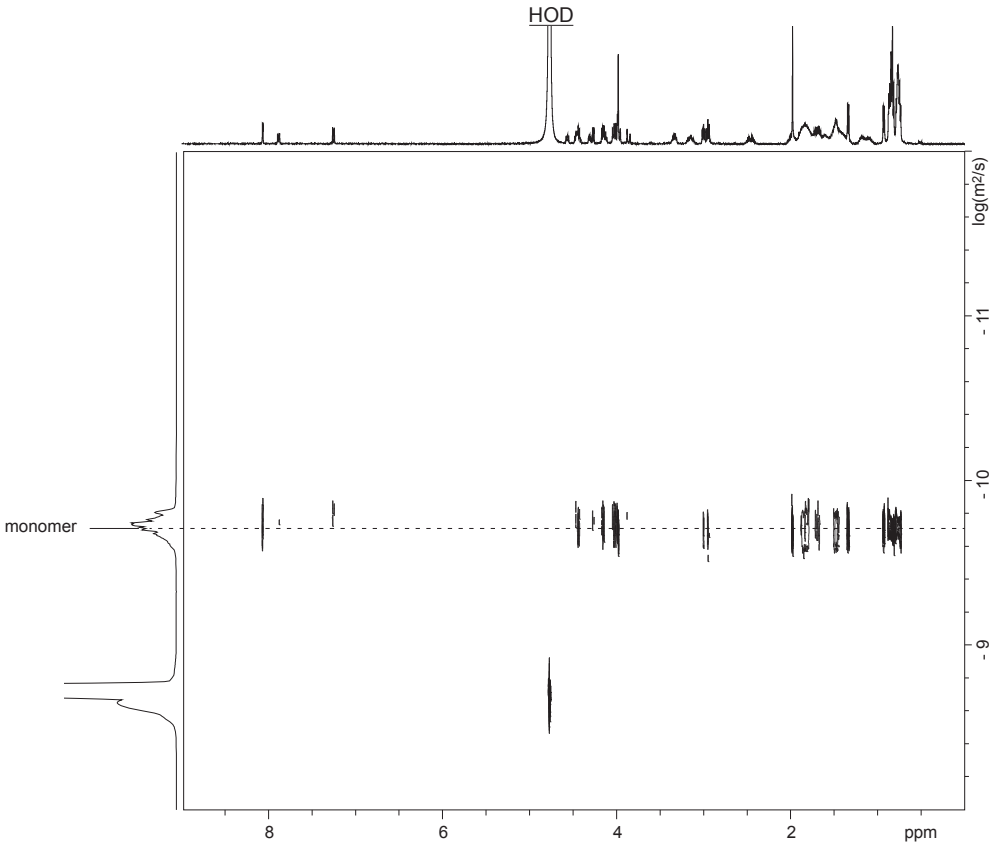

Calculations for peptide **1b** at 1.0 mM

D_{HOD} = 19.0 x 10^{-10} m^2/s [a]
log (D_{HOD}) = -8.721

$D_{monomer}$: log(D) = -9.712; D = $10^{-9.712}$ = 19.4 ± 1.7 x 10^{-11} m^2/s

[a]Longsworth, L. G. *J. Phys. Chem.* **1960**, *64*, 1914−1917.

^{1}H NMR of peptide **1b**, 16 mM in D_2O at 600 MHz and 293 K

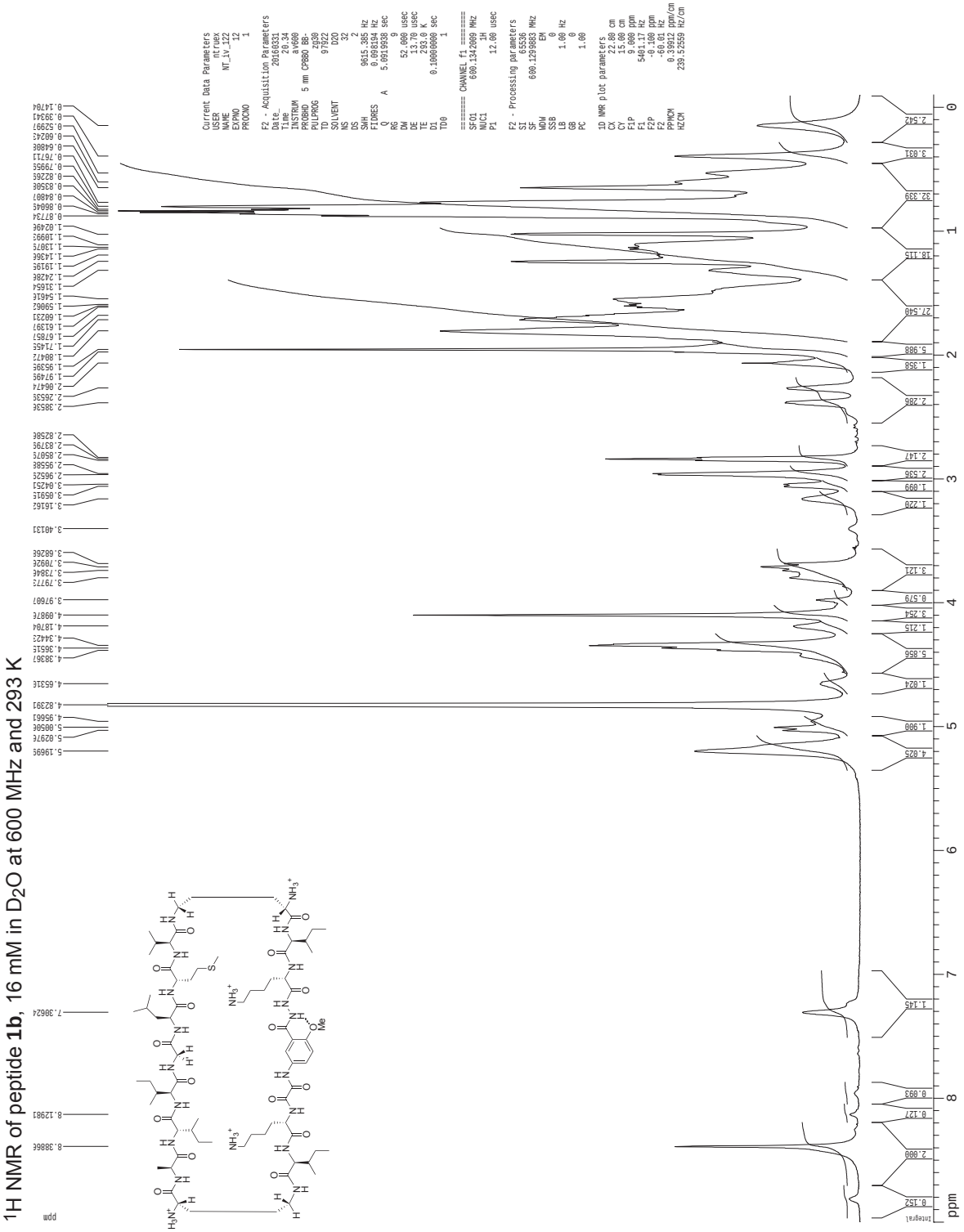

^{1}H NMR of peptide **1b**, 16 mM in D_2O at 600 MHz and 293 K

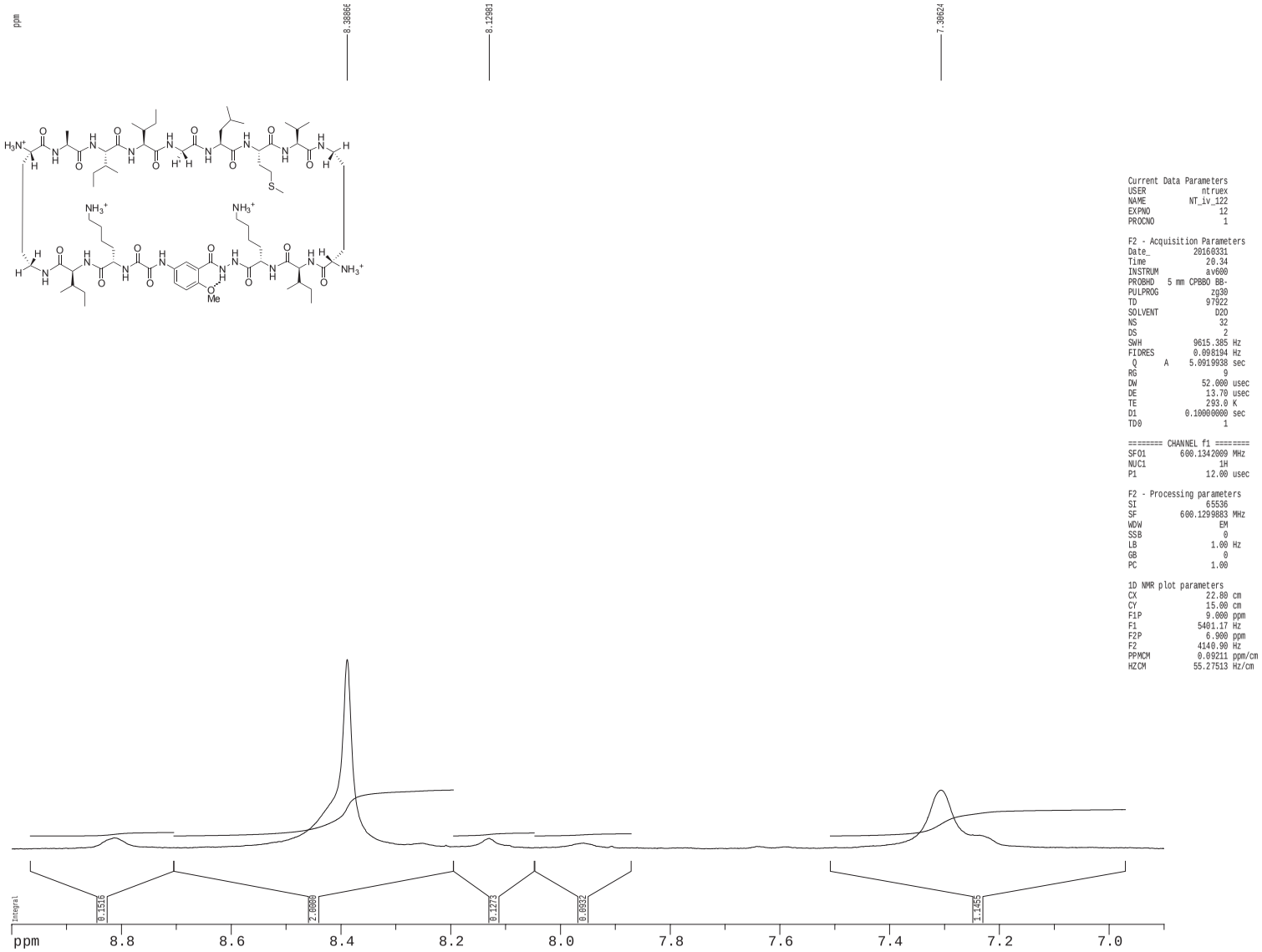


```
Current Data Parameters
USER                ntruex
NAME             NT_iv_122
EXPNO                   12
PROCNO                   1

F2 - Acquisition Parameters
Date_            20160331
Time                 20.34
INSTRUM              av600
PROBHD    5 mm CPBBO BB-
PULPROG                zg30
TD                    97922
SOLVENT                 D2O
NS                       32
DS                        2
SWH               9615.385 Hz
FIDRES               0.098194 Hz
 Q         A      5.0919938 sec
RG                       9
DW                  52.000 usec
DE                  13.70 usec
TE                  293.0 K
D1                0.10000000 sec
TD0                      1

======== CHANNEL f1 ========
SFO1            600.1342009 MHz
NUC1                     1H
P1                  12.00 usec

F2 - Processing parameters
SI                    65536
SF              600.1299883 MHz
WDW                      EM
SSB                       0
LB                    1.00 Hz
GB                        0
PC                    1.00

1D NMR plot parameters
CX                   22.80 cm
CY                   15.00 cm
F1P                   9.000 ppm
F1                 5401.17 Hz
F2P                   6.900 ppm
F2                 4140.90 Hz
PPMCM              0.09211 ppm/cm
HZCM              55.27513 Hz/cm
```

^{1}H NMR of peptide **1b**, 16 mM in D_2O at 600 MHz and 293 K

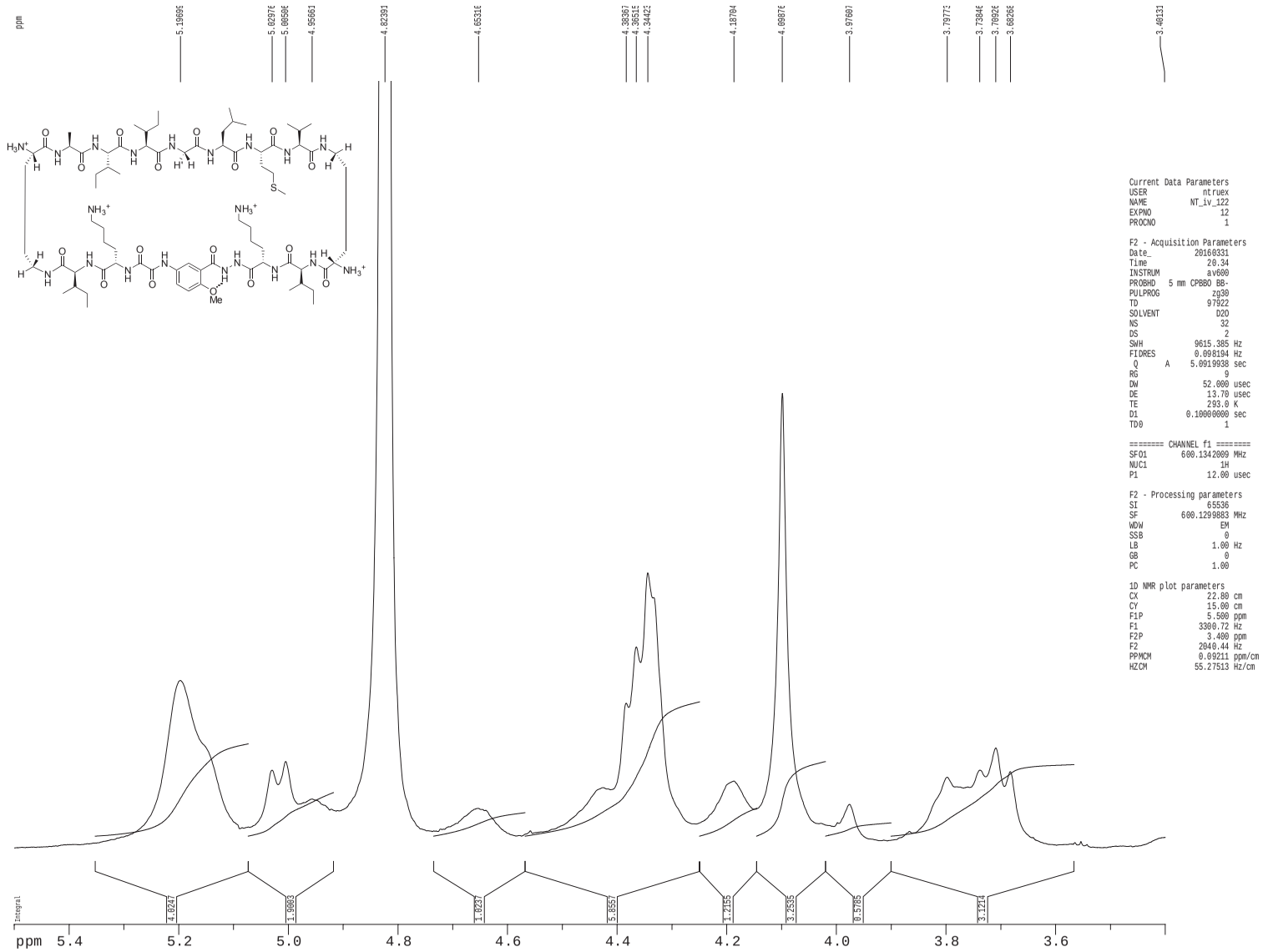


```
Current Data Parameters
USER                ntruex
NAME             NT_iv_122
EXPNO                   12
PROCNO                   1

F2 - Acquisition Parameters
Date_             20160331
Time                 20.34
INSTRUM              av600
PROBHD   5 mm CPBBO BB-
PULPROG                zg30
TD                    97922
SOLVENT                 D2O
NS                       32
DS                        2
SWH                9615.385 Hz
FIDRES             0.098194 Hz
 Q         A     5.0919938 sec
RG                       9
DW                  52.000 usec
DE                  13.70 usec
TE                  293.0 K
D1               0.10000000 sec
TD0                      1

======== CHANNEL f1 ========
SFO1            600.1342009 MHz
NUC1                    1H
P1                  12.00 usec

F2 - Processing parameters
SI                    65536
SF              600.1299883 MHz
WDW                     EM
SSB                      0
LB                    1.00 Hz
GB                       0
PC                    1.00

1D NMR plot parameters
CX                   22.80 cm
CY                   15.00 cm
F1P                   5.500 ppm
F1                  3300.72 Hz
F2P                   3.400 ppm
F2                  2040.44 Hz
PPMCM              0.09211 ppm/cm
HZCM              55.27513 Hz/cm
```

^{1}H NMR of peptide **1b**, 16 mM in D_2O at 600 MHz and 293 K

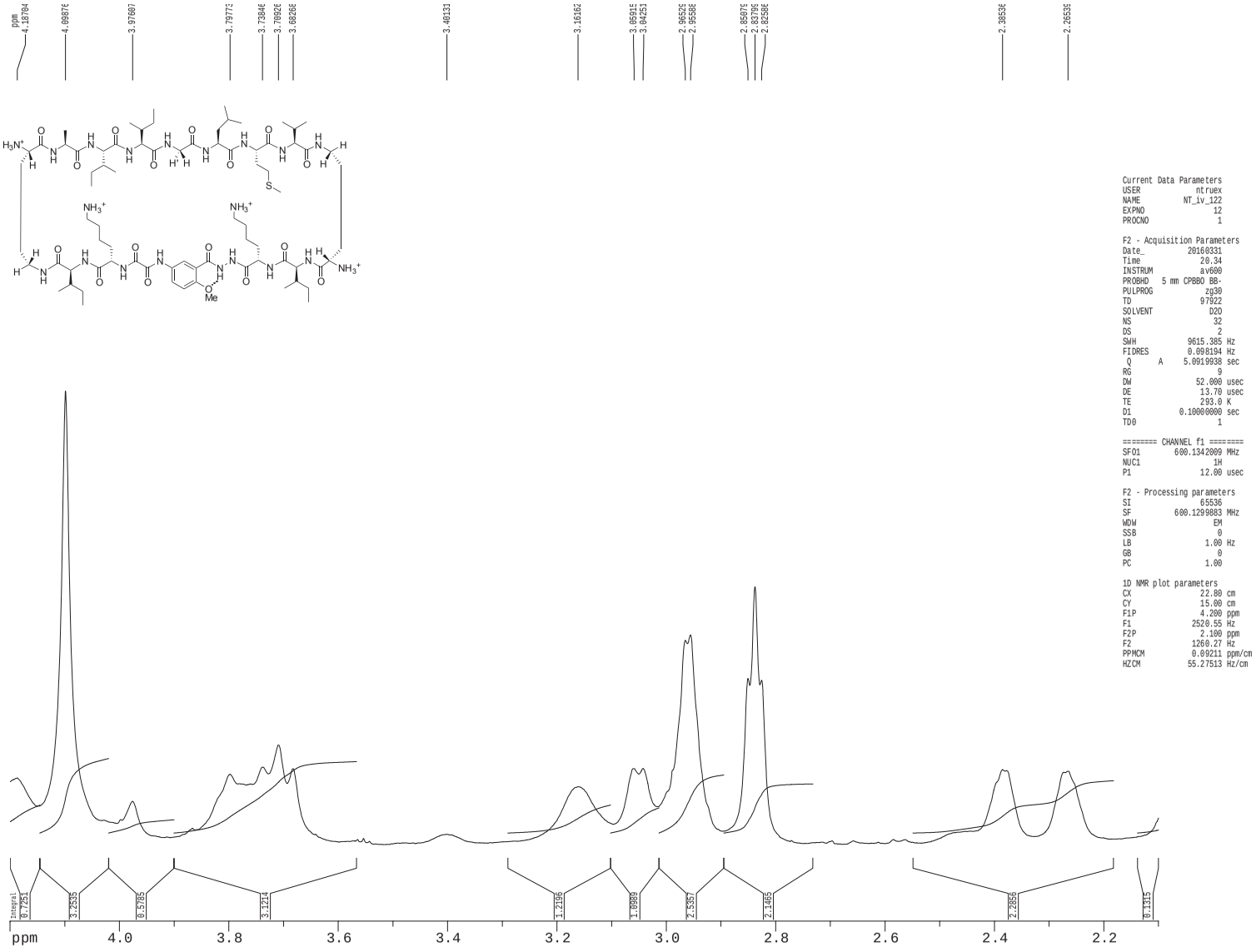


```
Current Data Parameters
USER                ntruex
NAME             NT_iv_122
EXPNO                   12
PROCNO                   1

F2 - Acquisition Parameters
Date_             20160331
Time                 20.34
INSTRUM              av600
PROBHD    5 mm CPBBO BB-
PULPROG                zg30
TD                    97922
SOLVENT                 D2O
NS                       32
DS                        2
SWH                9615.385 Hz
FIDRES             0.098194 Hz
 Q         A     5.0919938 sec
RG                       9
DW                  52.000 usec
DE                  13.70 usec
TE                  293.0 K
D1               0.10000000 sec
TD0                      1

======== CHANNEL f1 ========
SFO1            600.1342009 MHz
NUC1                    1H
P1                  12.00 usec

F2 - Processing parameters
SI                    65536
SF              600.1299883 MHz
WDW                     EM
SSB                      0
LB                    1.00 Hz
GB                       0
PC                    1.00

1D NMR plot parameters
CX                   22.80 cm
CY                   15.00 cm
F1P                   4.200 ppm
F1                 2520.55 Hz
F2P                   2.100 ppm
F2                 1260.27 Hz
PPMCM              0.09211 ppm/cm
HZCM              55.27513 Hz/cm
```

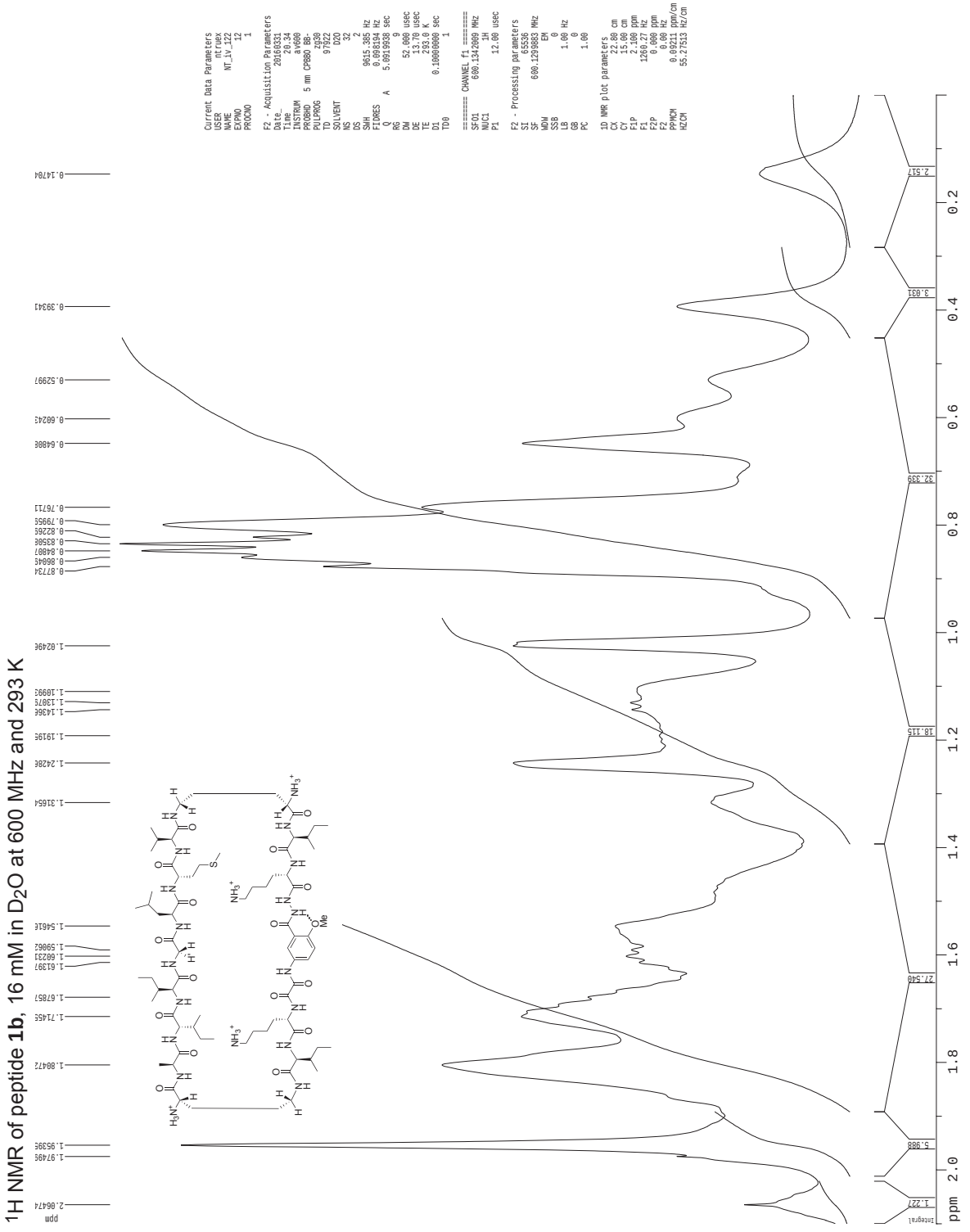
^{1}H NMR of peptide **1b**, 16 mM in D_2O at 600 MHz and 293 K
Current Data Parameters
USER
NAME NT_lv_122
EXPNO 12
PROCNO 1
F2 - Acquisition Parameters
Date_ 20160331
Time 23.34
INSTRUM av600
PROBHD 5 mm CPBBO BB-
PULPROG zg30
TD 97922
SOLVENT D2O
NS 32
DS 2
SWH 9615.385 Hz
FIDRES 0.098194 Hz
AQ 5.0891998 sec
RG 9
DW 52.000 usec
DE 13.70 usec
TE 293.0 K
D1 0.10000000 sec
TD0 1
======== CHANNEL f1 ========
SFO1 600.1342009 MHz
NUC1 1H
P1 12.00 usec
F2 - Processing parameters
SI 65536
SF 600.1299883 MHz
WDW EM
SSB 0
LB 1.00 Hz
GB 0
PC 1.00
1D NMR plot parameters
CX 22.80 cm
CY 15.00 cm
F1P 2.100 ppm
F1 1260.27 Hz
F2P 0.000 ppm
F2 0.00 Hz
PPMCM 0.09211 ppm/cm
HZCM 55.27513 Hz/cm
0.14704
0.39341
0.52997
0.60242
0.64808
0.76711
0.79956
0.82266
0.83506
0.84807
0.86046
0.87734
1.02496
1.10992
1.13075
1.14366
1.19196
1.24286
1.31654
1.54616
1.59062
1.60231
1.61391
1.67857
1.74456
1.80472
1.95396
1.97496
2.06474
ppm
integral
1.227
5.988
27.548
18.115
32.339
3.031
2.517
2.0
1.8
1.6
1.4
1.2
1.0
0.8
0.6
0.4
0.2

^{1}H NMR 2D TOCSY of macrocycle **1b** with presaturation suppression of the HOD peak
16 mM in D_2O at 600 MHz and 293 K with 150-ms spin-lock mixing time

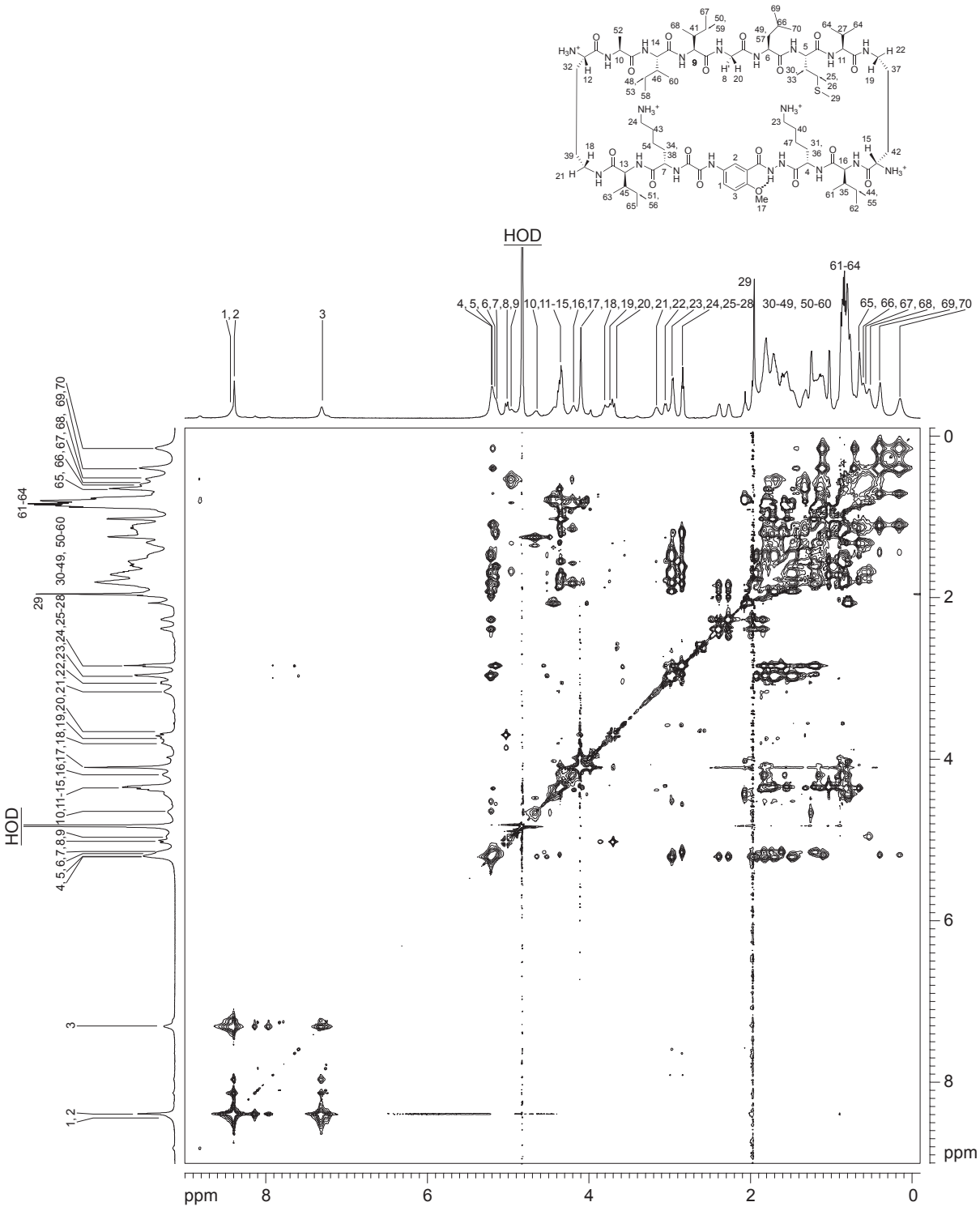

^{1}H NMR 2D TOCSY of macrocycle **1b** with presaturation suppression of the HOD peak
16 mM in D_2O at 600 MHz and 293 K with 150-ms spin-lock mixing time

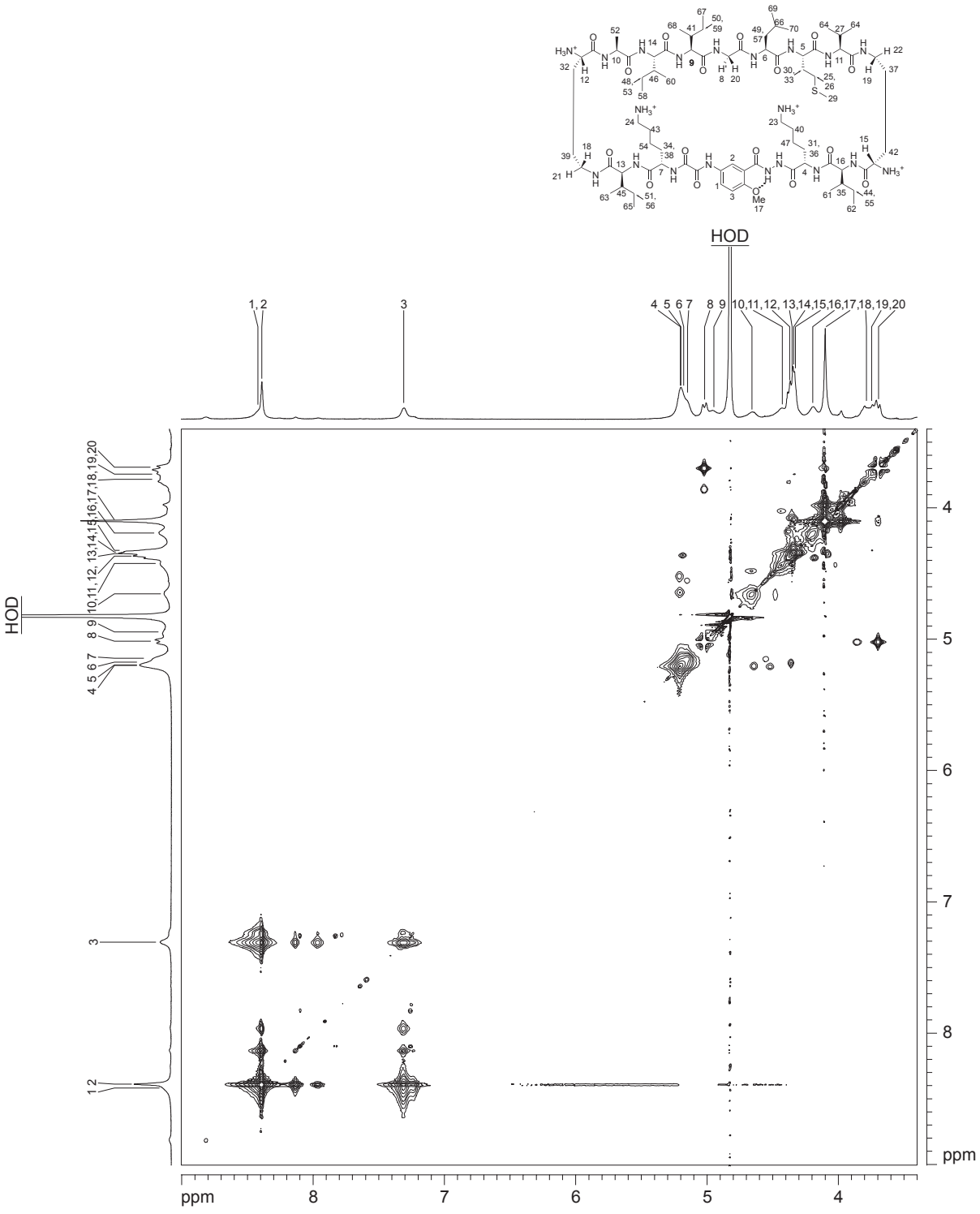

^{1}H NMR 2D TOCSY of macrocycle **1b** with presaturation suppression of the HOD peak
16 mM in D_2O at 600 MHz and 293 K with 150-ms spin-lock mixing time

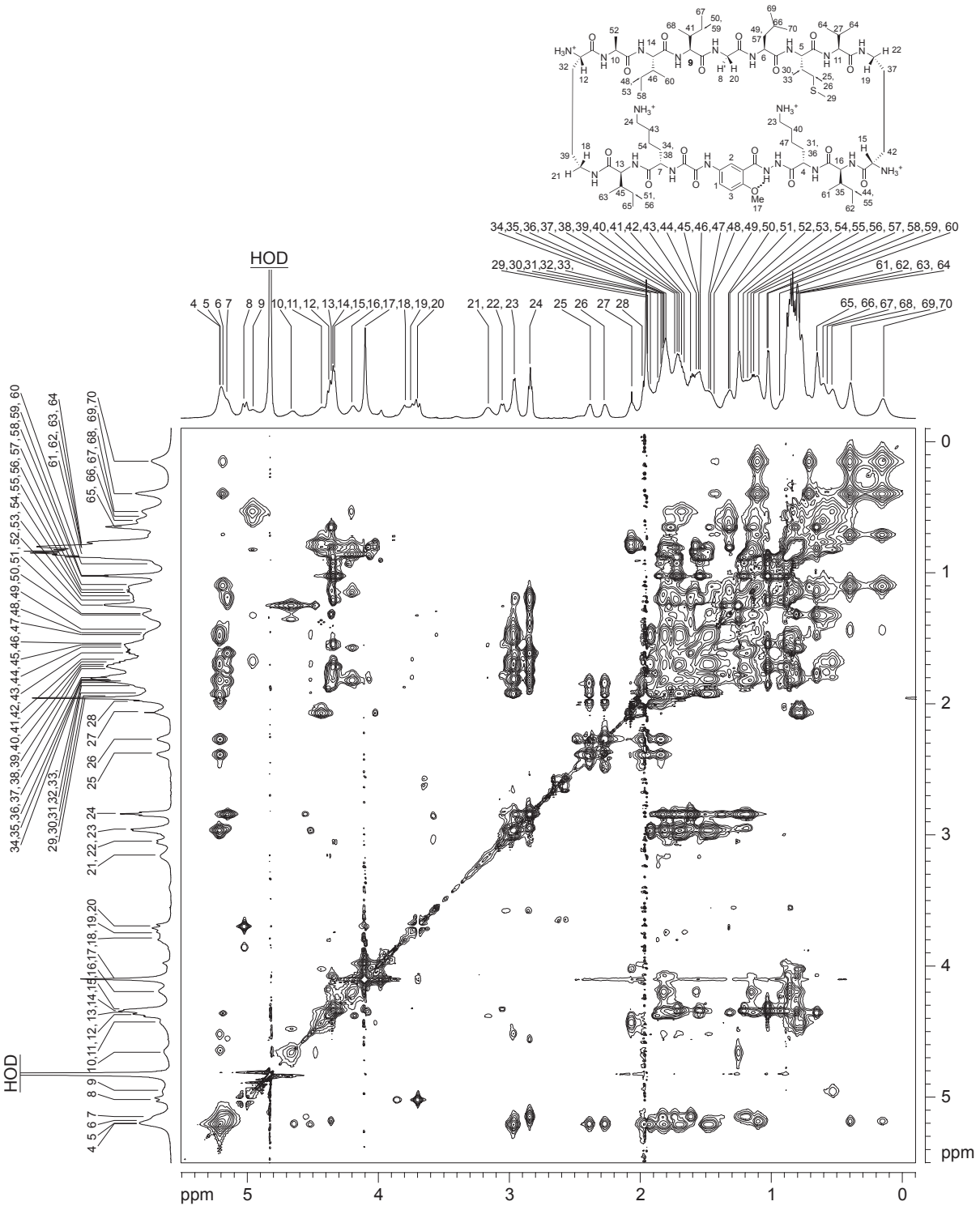

^{1}H NMR 2D NOESY of macrocycle **1b** with presaturation suppression of the HOD peak
16 mM in D_2O at 600 MHz and 293 K with 150-ms mixing time

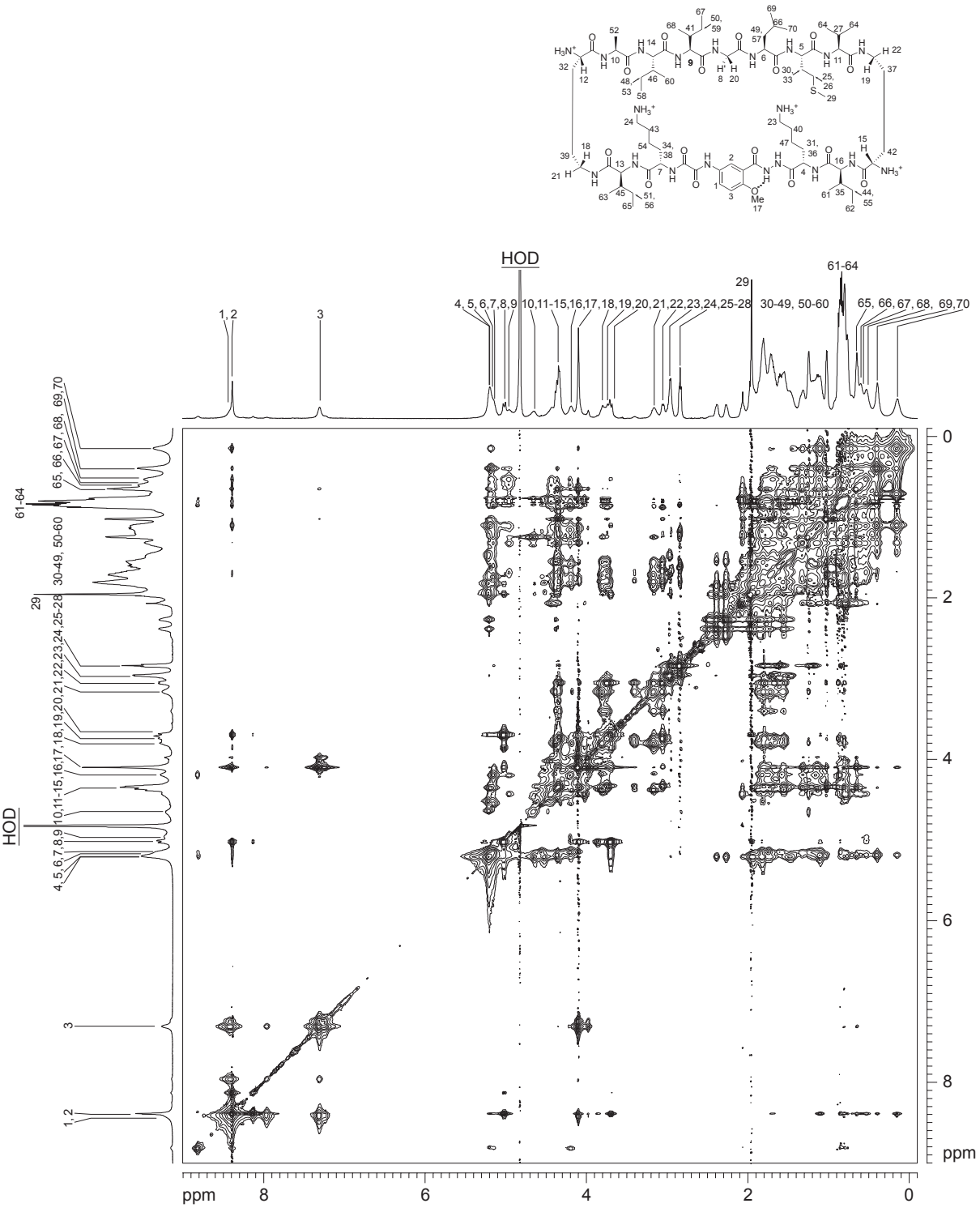

^{1}H NMR 2D NOESY of macrocycle **1b** with presaturation suppression of the HOD peak
16 mM in D_2O at 600 MHz and 293 K with 150-ms mixing time

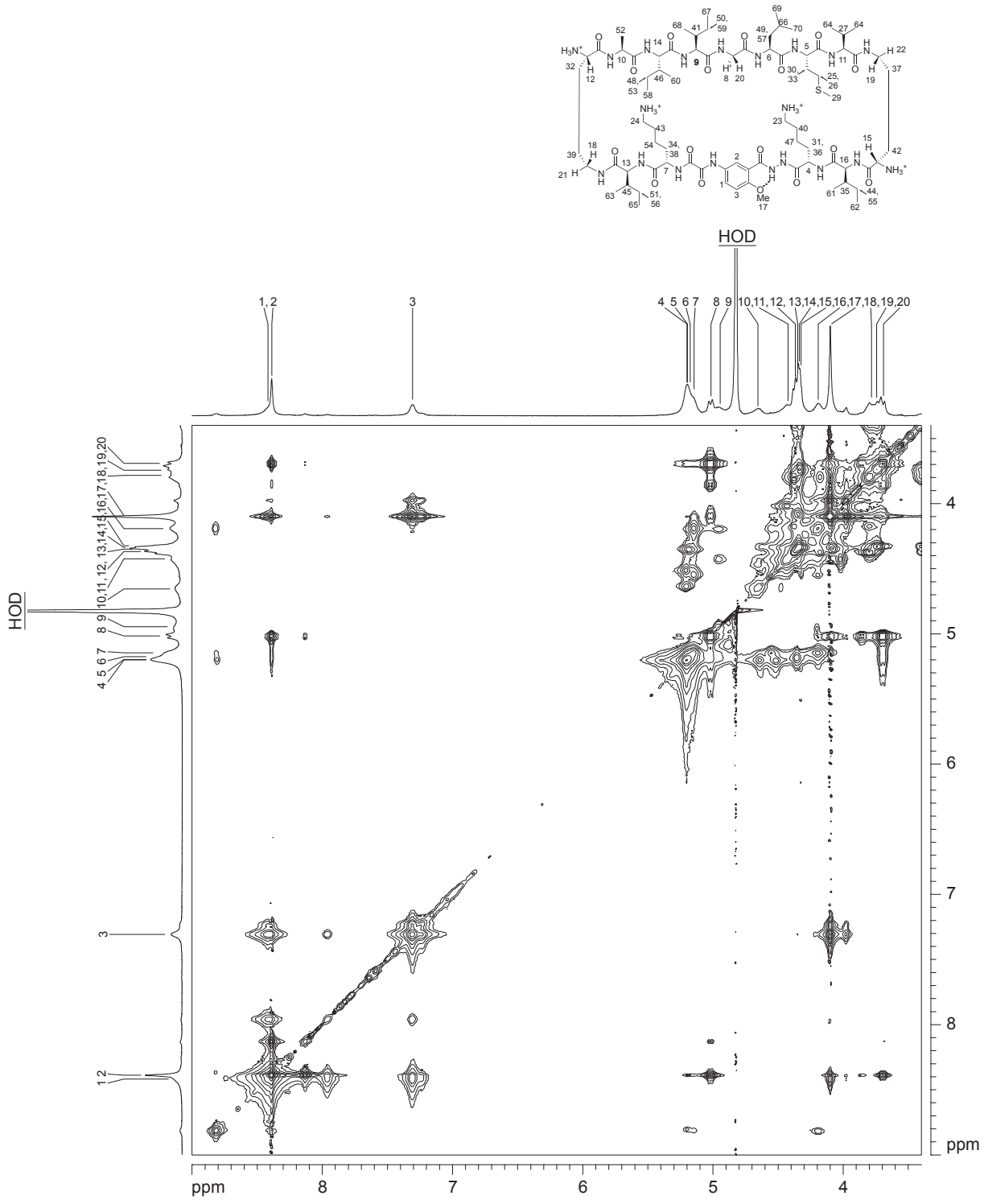

^{1}H NMR 2D NOESY of macrocycle **1b** with presaturation suppression of the HOD peak
16 mM in D_2O at 600 MHz and 293 K with 150-ms mixing time

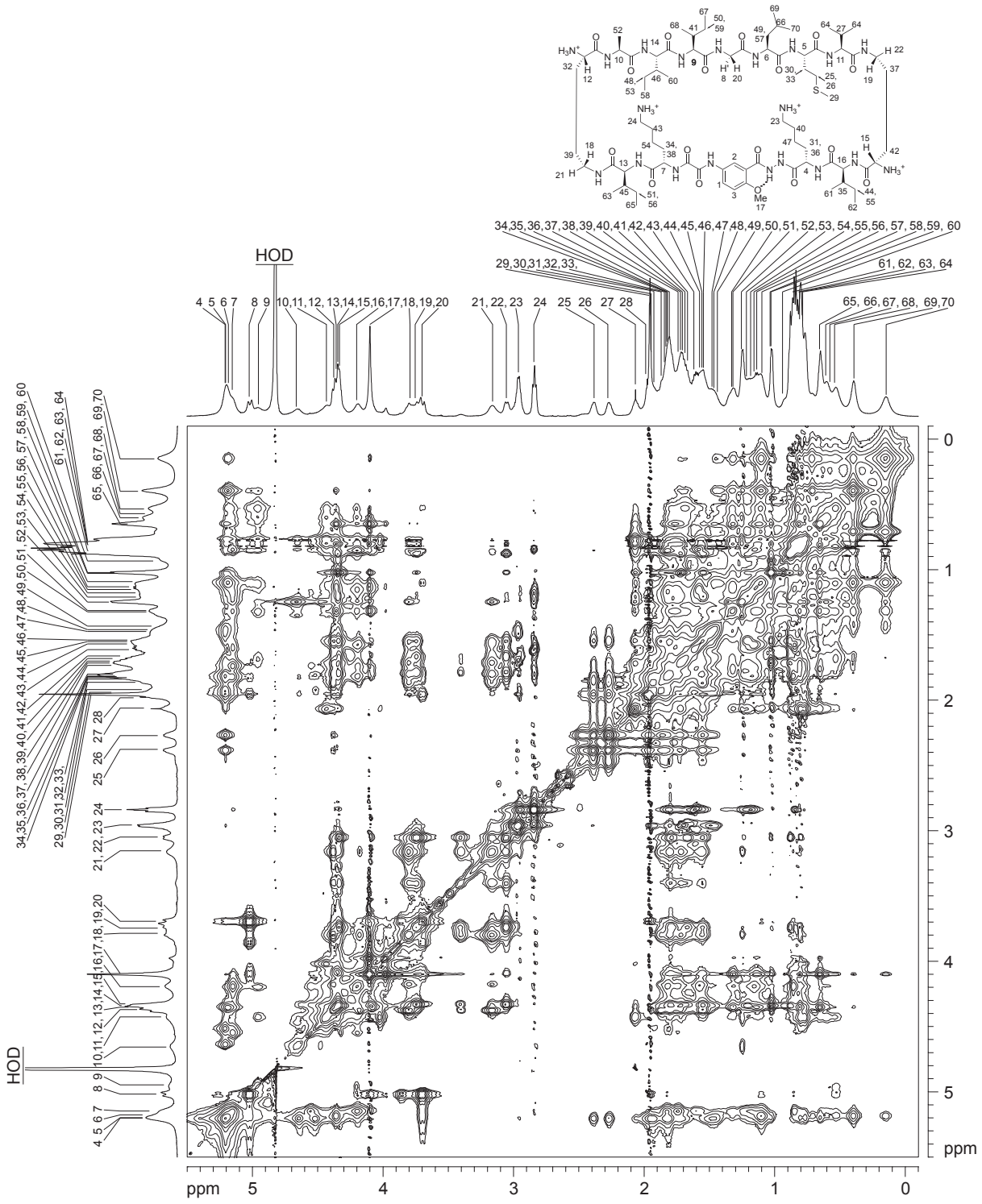

^{1}H NMR DOSY of peptide **1b**, 16 mM in D_2O at 500 MHz and 298 K
tetramer predominates

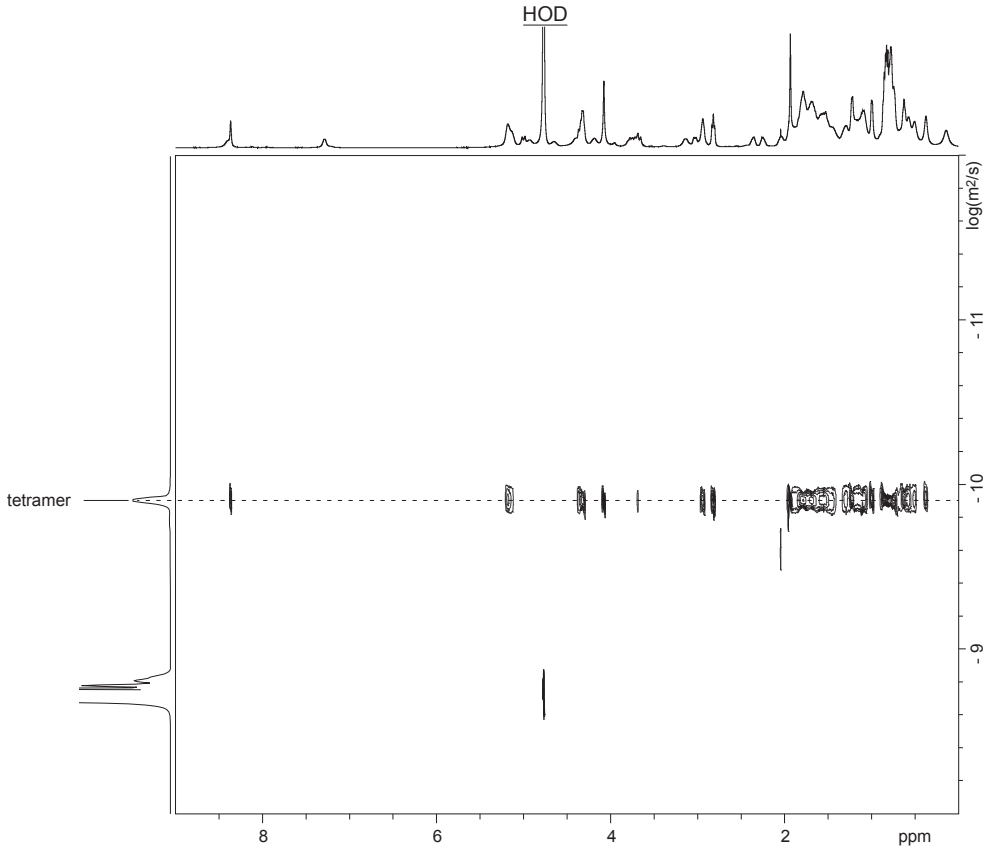

Calculations for peptide **1b** at 16.0 mM

D_{HOD} = 19.0 x 10^{-10} m^2/s [a]
log (D_{HOD}) = -8.721

$D_{tetramer}$: log(D) = -9.924; D = $10^{-9.924}$ = 11.9 ± 1.1 x 10^{-11} m^2/s

[a]Longsworth, L. G. *J. Phys. Chem.* **1960**, *64*, 1914−1917.

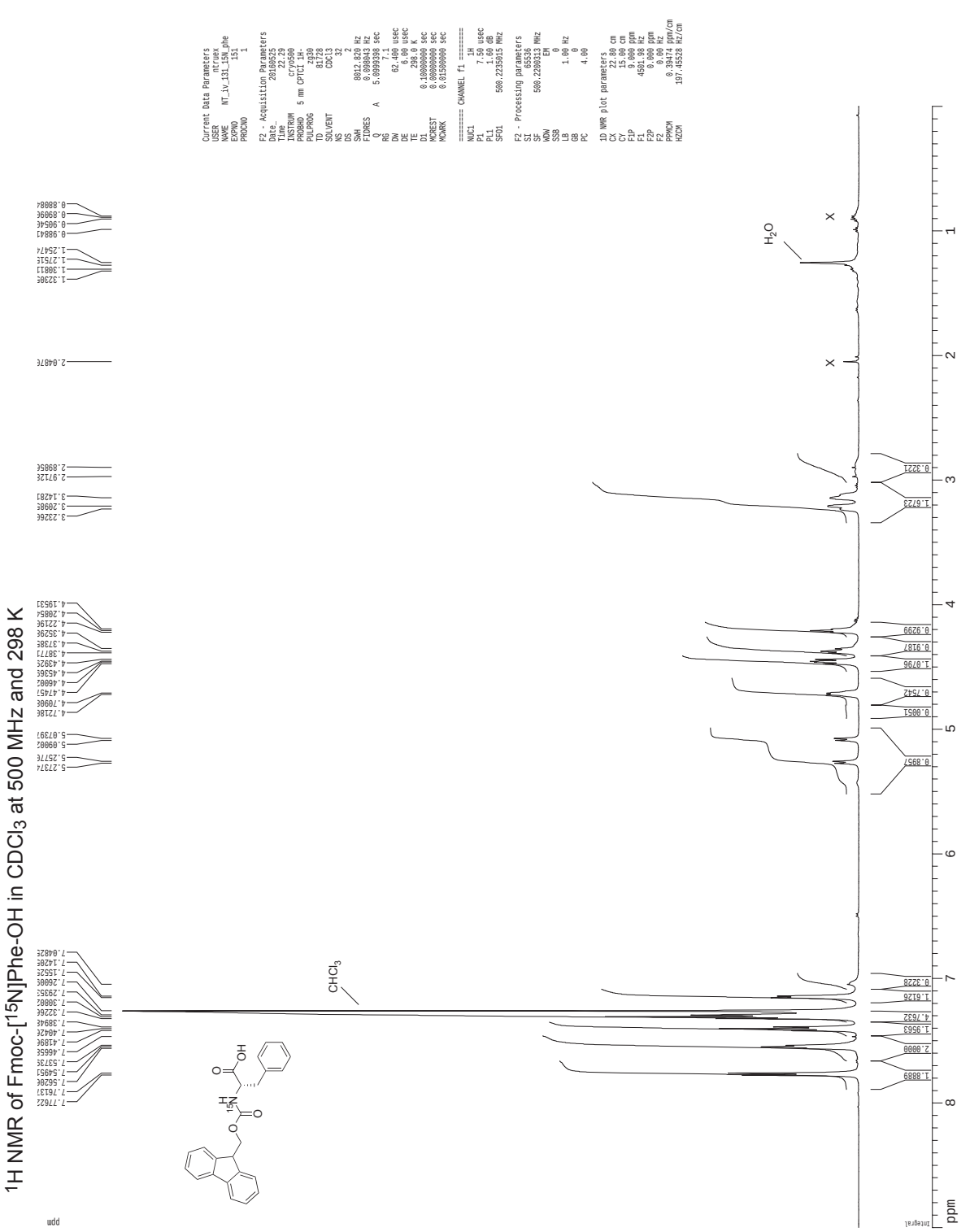
1H NMR of Fmoc-[15N]Phe-OH in CDCl3 at 500 MHz and 298 K
CHCl3
H2O
X
X
ppm
Integral

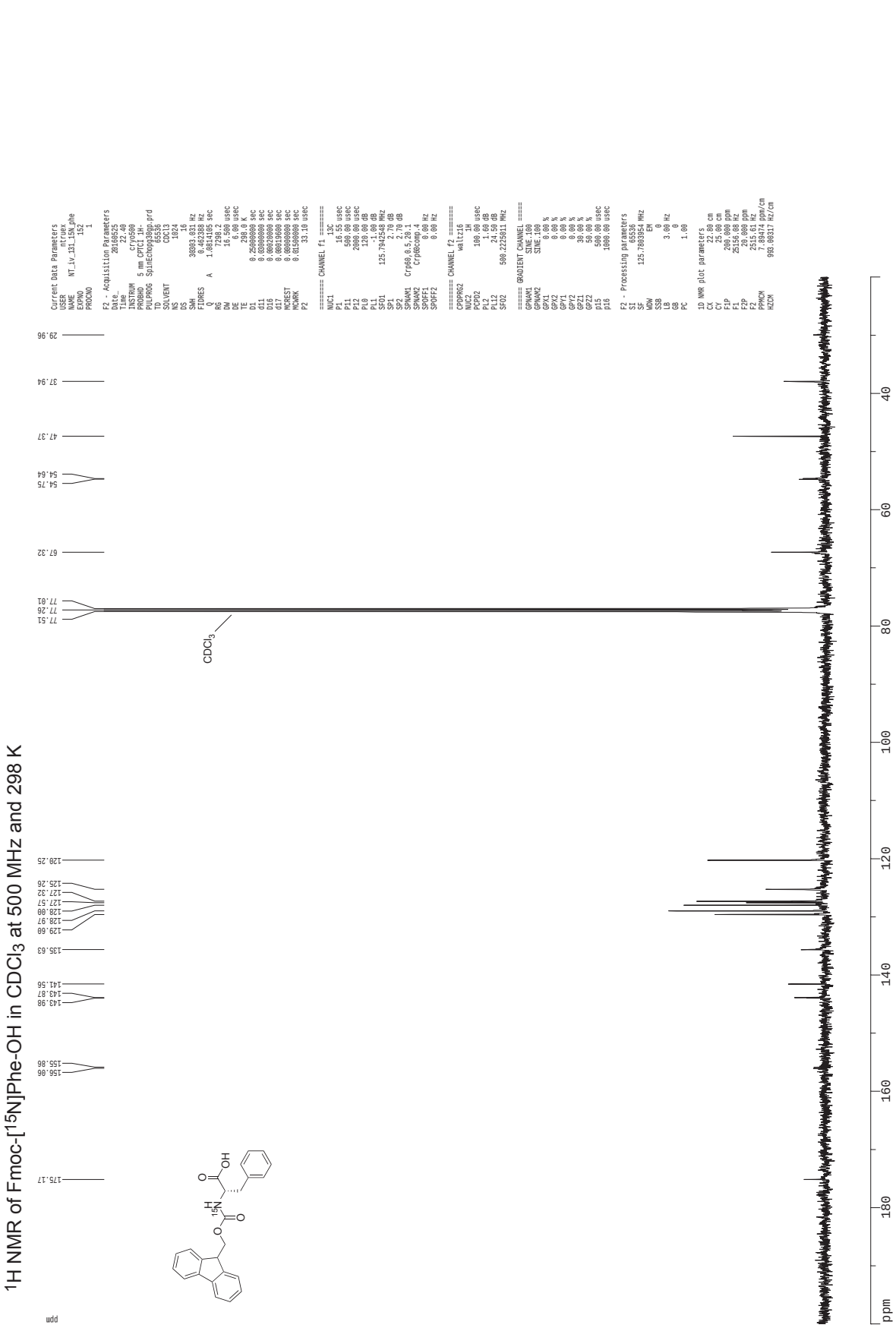
1H NMR of Fmoc-[15N]Phe-OH in CDCl3 at 500 MHz and 298 K
Current Data Parameters
USER ntruex
NAME NT_lv_131_15N_phe
EXPNO 152
PROCNO 1
F2 - Acquisition Parameters
Date_ 20160525
Time 22.40
INSTRUM cryo500
PROBHD 5 mm CPTCI 1H-
PULPROG SpinEchopg30pp.prd
TD 65536
SOLVENT CDCl3
NS 1024
DS 16
SWH 30303.031 Hz
FIDRES 0.462388 Hz
A 1.08141405 sec
RG 7280.2
DW 16.500 usec
DE 6.00 usec
TE 298.0 K
D1 0.25000000 sec
d11 0.03000000 sec
d16 0.00020000 sec
d17 0.00001000 sec
MCREST 0.00000000 sec
MCWRK 0.01500000 sec
P2 33.10 usec
======== CHANNEL f1 ========
NUC1 13C
P1 16.55 usec
P11 500.00 usec
P12 2000.00 usec
PL10 120.00 dB
PL11 120.00 dB
SFO1 125.7942548 MHz
SP1 2.70 dB
SP2 2.70 dB
SPNAM1 Crp60,0.5,20.1
SPNAM2 Crp60comp.4
SPOFF1 0.00 Hz
SPOFF2 0.00 Hz
======== CHANNEL f2 ========
CPDPRG2 waltz16
NUC2 1H
PCPD2 100.00 usec
PL2 1.60 dB
PL12 24.50 dB
SFO2 500.2225011 MHz
====== GRADIENT CHANNEL ====
GPNAM1 SINE.100
GPNAM2 SINE.100
GPX1 0.00 %
GPY1 0.00 %
GPZ1 0.00 %
GPX2 30.00 %
GPY2 50.00 %
GPZ2 80.00 %
GPZ3 100.00 %
p16 1000.00 usec
F2 - Processing parameters
SI 65536
SF 125.7800354 MHz
WDW EM
SSB 0
LB 3.00 Hz
GB 0
PC 1.00
1D NMR plot parameters
CX 22.00 cm
CY 25.00 cm
F1P 2500.000 ppm
F1 1257.951 Hz
F2P 20.000 ppm
F2 2515.61 Hz
PPMCM 7.89474 ppm/cm
HZCM 993.00317 Hz/cm
175.17
155.86
156.06
143.98
143.87
141.56
135.63
129.60
128.97
128.00
127.57
127.32
125.26
120.25
77.51
77.26
77.01
67.32
54.75
54.64
47.37
37.94
29.96
CDCl3
ppm
180
160
140
120
100
80
60
40

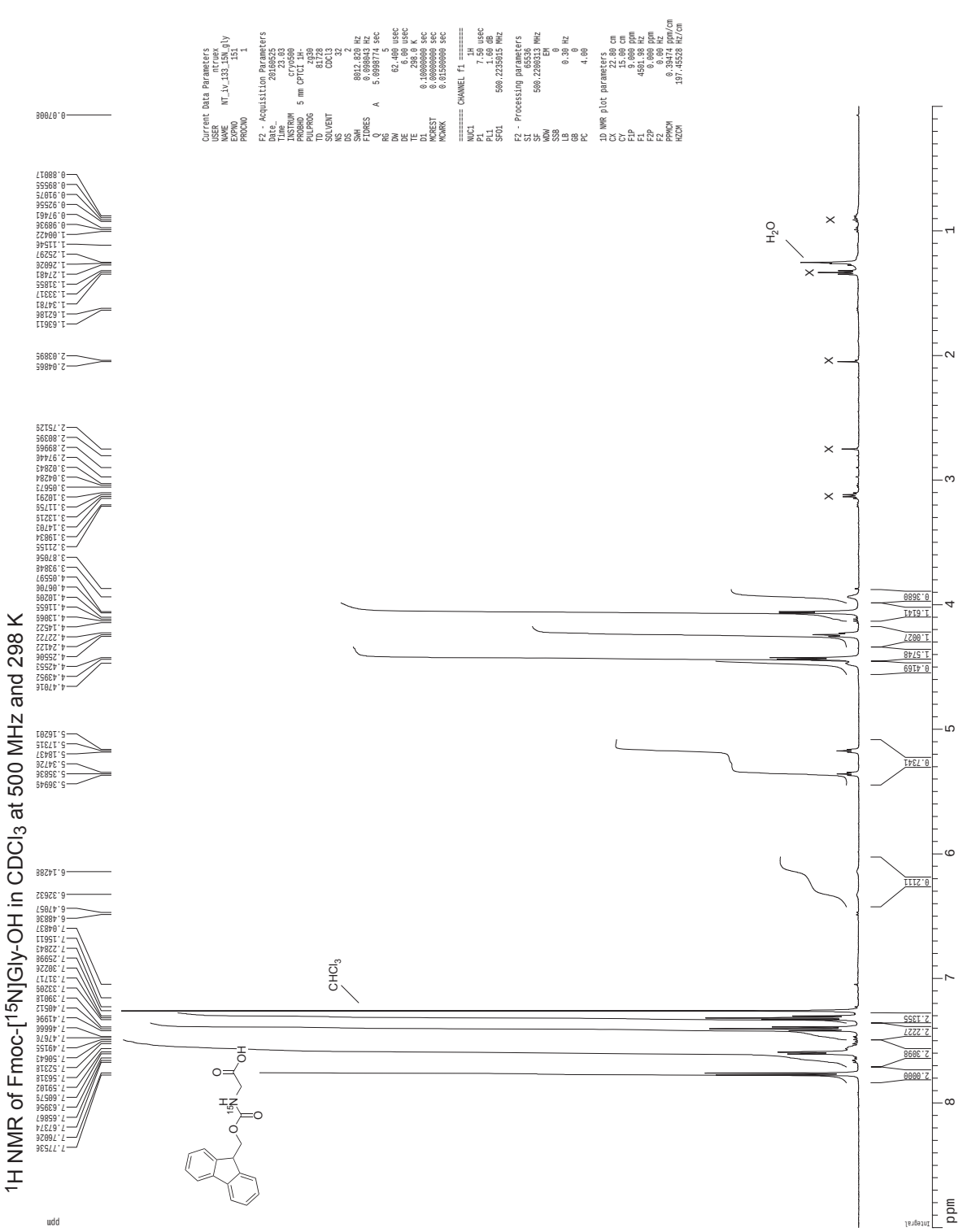
1H NMR of Fmoc-[15N]Gly-OH in CDCl3 at 500 MHz and 298 K
Current Data Parameters
NAME NT_iv_133_15N_gly
EXPNO 151
PROCNO 1
F2 - Acquisition Parameters
Date_ 20160525
Time 23.03
INSTRUM cryo500
PROBHD 5 mm CPTCI 1H-
PULPROG zg30
TD 81728
SOLVENT CDCl3
NS 32
DS 2
SWH 8012.820 Hz
FIDRES 0.098044 Hz
AQ 5.0998774 sec
RG 5
DW 62.400 usec
DE 6.00 usec
TE 298.0 K
D1 0.10000000 sec
MCREST 0.00000000 sec
MCWORK 0.01500000 sec
======== CHANNEL f1 ========
NUC1 1H
P1 7.50 usec
PL1 1.00 dB
SFO1 500.2235015 MHz
F2 - Processing parameters
SI 65536
SF 500.2200313 MHz
WDW EM
SSB 0
LB 0.30 Hz
GB 0
PC 4.00
1D NMR plot parameters
CX 22.80 cm
CY 15.00 cm
F1P 9.000 ppm
F2P -0.800 ppm
PPMCM 0.39474 ppm/cm
HZCM 197.45528 Hz/cm
CHCl3
H2O
ppm
Integral

^{13}C NMR of Fmoc-[^{15}N]Gly-OH in $CDCl_3$ at 500 MHz and 298 K

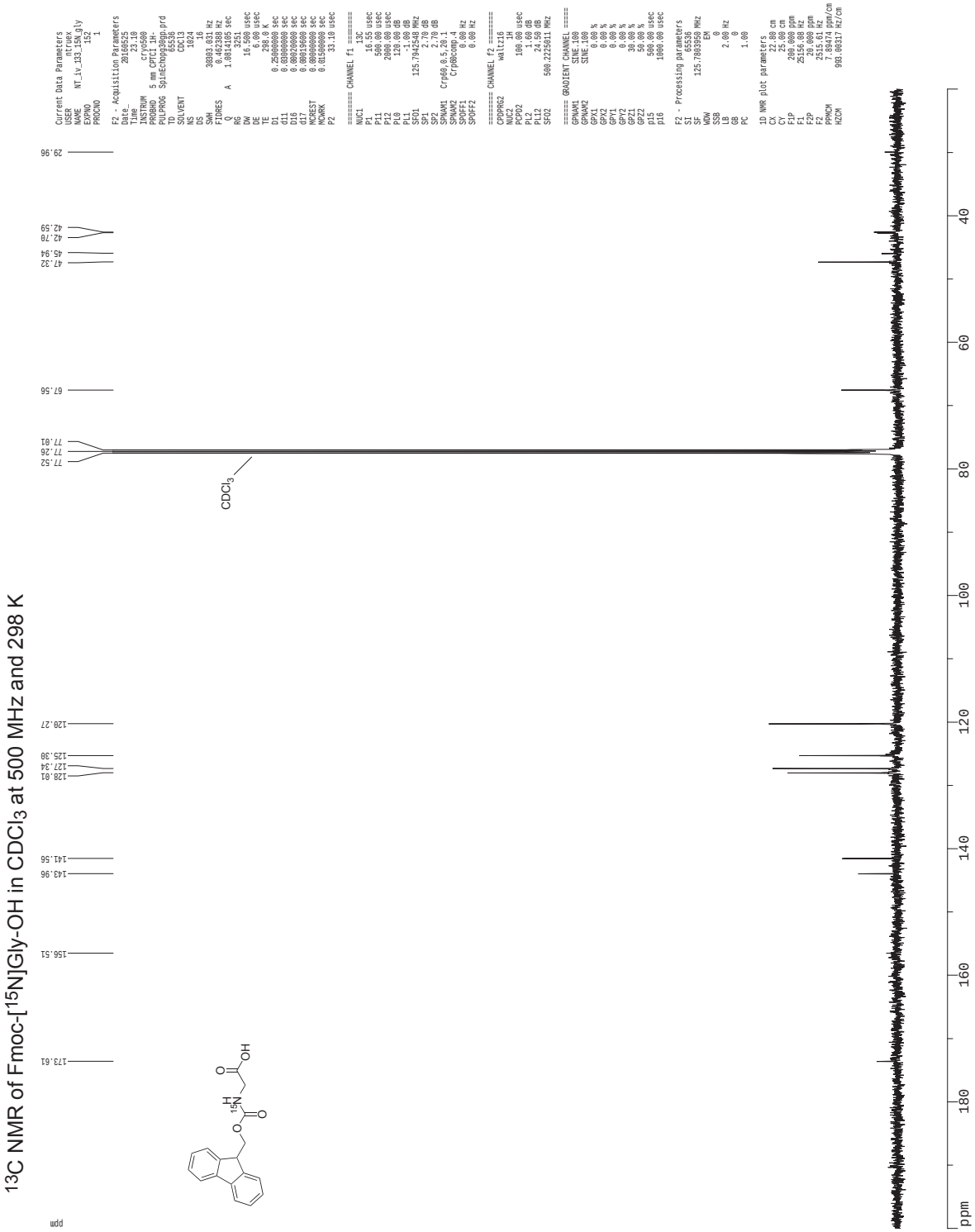

$^{1}H,^{15}N$ HSQC of peptide [^{15}N]**1a** in 9:1 H_2O/D_2O at 600 MHz and 293 K
8.0 mM total concentration

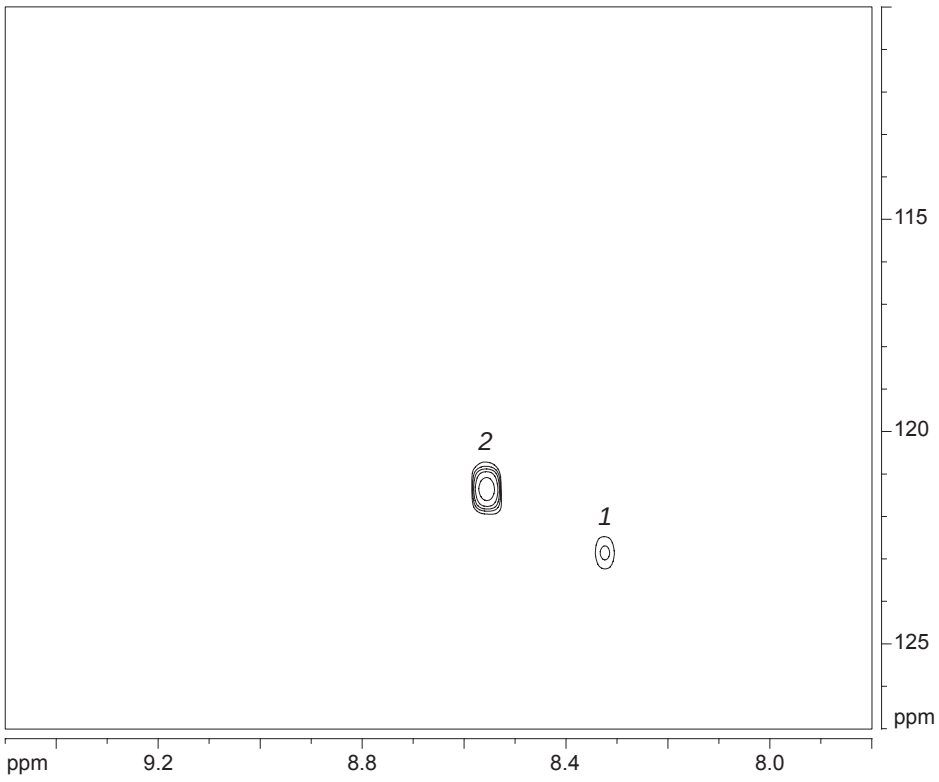

$^{1}H,^{15}N$ HSQC of peptide [^{15}N]**1b** in 9:1 H_2O/D_2O at 600 MHz and 293 K
8.0 mM total concentration

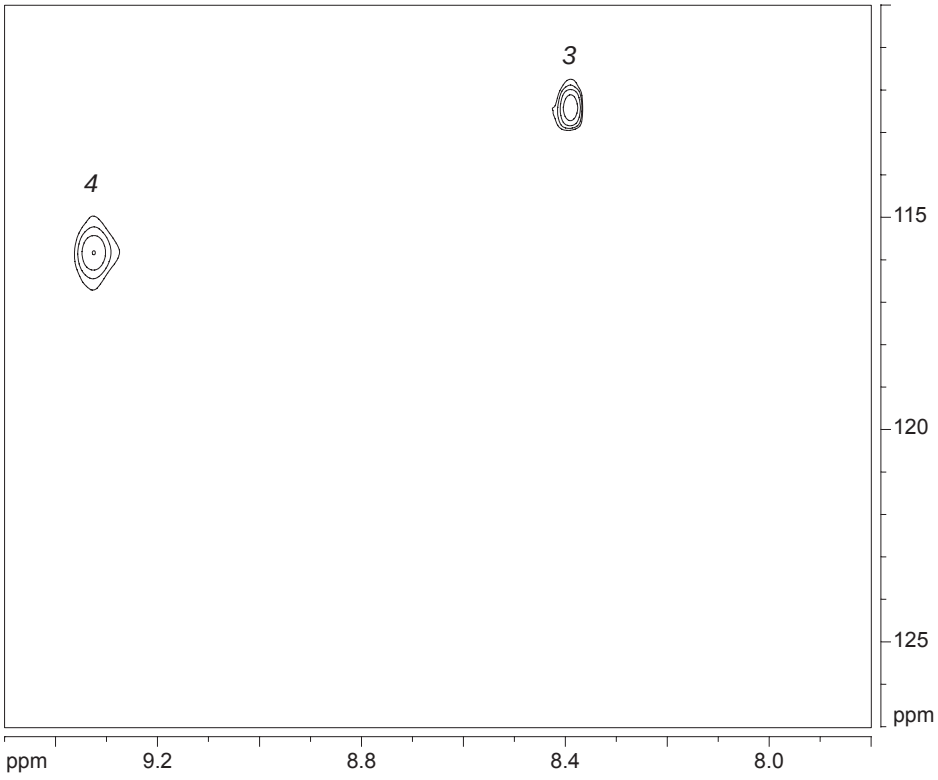

CHAPTER 3

Coassembly of Peptides Derived from β-Sheet Regions of β-Amyloid

INTRODUCTION

Interactions among β-sheets are critical in the aggregation of the β-amyloid peptide (Aβ) to form oligomers and fibrils in Alzheimer's disease.[1] Two regions of the 40- or 42-residue peptide adopt β-sheet structure and promote aggregation: the central region and the C-terminal region.[2] The central region comprises the hydrophobic pentapeptide LVFFA ($A\beta_{17–23}$), and the C-terminal region comprises the hydrophobic undecapeptide AIIGLMVGGVV ($A\beta_{30–40}$) or the hydrophobic tridecapeptide AIIGLMVGGVVIA ($A\beta_{30–42}$).

Elucidating the roles of the central and C-terminal regions of Aβ is critical to understanding Aβ aggregation. These two regions assemble differently in the fibrils and in the toxic oligomers that cause synaptic dysfunction and cell death. In $A\beta_{1–40}$ fibrils, the peptide forms parallel β-sheets, with the central and C-terminal regions laminated together.[3,4] In the oligomers, the peptide is thought to form β-hairpins comprising antiparallel β-sheets.[5]

In the preceding chapter, I incorporated residues from the central and C-terminal regions into macrocyclic β-sheet peptides **1**, and I determined how the peptides assembled in aqueous solution.[6] Peptides **1** consist of a heptapeptide strand, a template strand containing the unnatural amino acid Hao, and two δ-linked ornithine turn units.[7,8,9] I incorporated residues LVFFAED ($A\beta_{17–23}$) and residues AIIGLMV ($A\beta_{30–36}$) into the heptapeptide strands of peptides **1a** and **1b**, respectively. I incorporated isoleucine residues (I_8 and I_{11}) into the template strand to promote assembly and lysine residues (K_9 and K_{10}) to maintain solubility. ^{1}H NMR studies of peptides **1a** and **1b** show that the peptides assemble to form sandwich-like homotetramers, consisting of two hydrogen-bonded dimers.

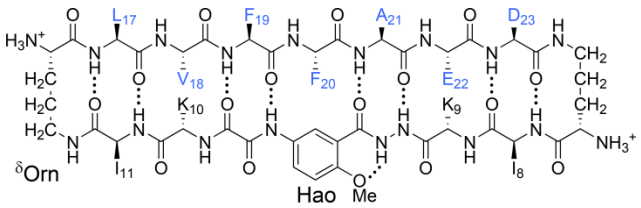

macrocyclic β-sheet peptide **1a**

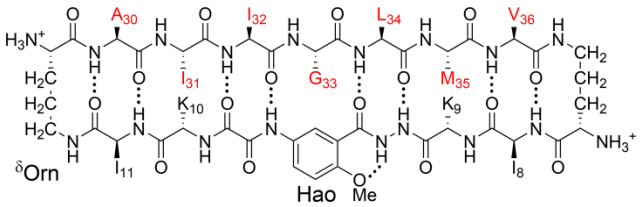

macrocyclic β-sheet peptide **1b**

Incorporation of a single isotopic label into peptides **1** facilitated the identification and quantification of the tetramers. The peptides [^{15}N]**1a** and [^{15}N]**1b** each contain a single ^{15}N-labeled amino acid in the center of the heptapeptide strand. Peptide [^{15}N]**1a** contains an ^{15}N label in the F_{20} residue; peptide [^{15}N]**1b** contains an ^{15}N label in the G_{33} residue. ^{1}H,^{15}N HSQC studies show only the resonances associated with the ^{15}N label, reducing each spectrum to two crosspeaks: The ^{1}H,^{15}N HSQC spectrum of peptide [^{15}N]**1a** shows one crosspeak associated with the monomer and another associated with the homotetramer. The ^{1}H,^{15}N HSQC spectrum of peptide [^{15}N]**1b** also shows one crosspeak associated with the monomer and another associated with the homotetramer.

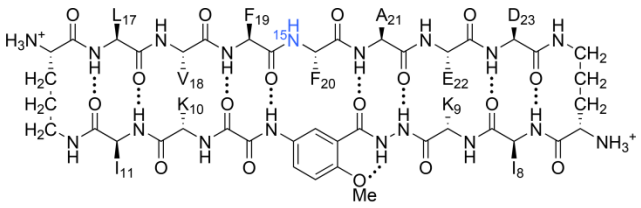

macrocyclic β-sheet peptide [^{15}N]**1a**

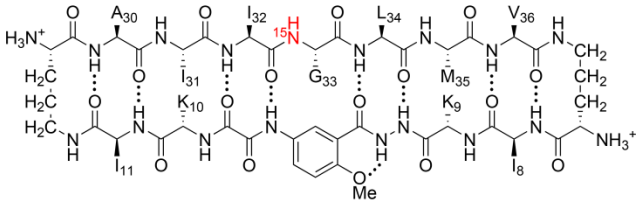

macrocyclic β-sheet peptide [^{15}N]**1b**

In this chapter, I ask whether these peptides prefer to coassemble or to segregate.[10] To address this question, I mix peptides **1a** and **1b** and characterize the oligomers that form. ^{1}H NMR studies show that peptides **1a** and **1b** form a mixture of homotetramers and heterotetramers, but the ^{1}H NMR spectrum of the mixture is largely indecipherable. To characterize the complex mixture of homotetramers and heterotetramers, I use the ^{15}N-labeled peptides [^{15}N]**1a** and [^{15}N]**1b** and ^{1}H,^{15}N NMR spectroscopy. ^{1}H,^{15}N HSQC, in conjunction with Job's method of continuous variation, reveals that the peptides form three heterotetramers in 3:1, 2:2, and 1:3 stoichiometries, in addition to the two homotetramers. The following describes the characterization of these five tetramers and the equilibria among them.

RESULTS AND DISCUSSION

Peptides 1a and 1b Coassemble upon Mixing. The ^{1}H NMR spectrum of pure peptide **1a** at 8.0 mM predominately shows the homotetramer; the ^{1}H NMR spectrum of pure peptide **1b** at 8.0 mM shows the monomer and the homotetramer. In a 1:1 mixture of peptides **1a** and **1b** at 8.0 mM total concentration, the ^{1}H NMR spectrum shows many new resonances: The resonances from the homotetramer of peptide **1a** diminish greatly and the resonances from the homotetramer of peptide **1b** nearly disappear. New resonances appear in the spectrum in the aromatic region

between 6 and 9 ppm and also in the methyl region below 1 ppm. Several new Hao methoxy (Hao_{OMe}) resonances appear between 4 and 4.5 ppm. The Hao_{OMe} resonance from the homotetramer of peptide **1a** diminishes greatly and the Hao_{OMe} resonance from the homotetramer of peptide **1b** almost completely disappears. The multitude of new resonances in the spectrum of the 1:1 mixture suggests that several new oligomers form, rather than just one. Figure 3.1 shows the ^{1}H NMR spectra of pure **1a**, pure **1b**, and the 1:1 mixture.

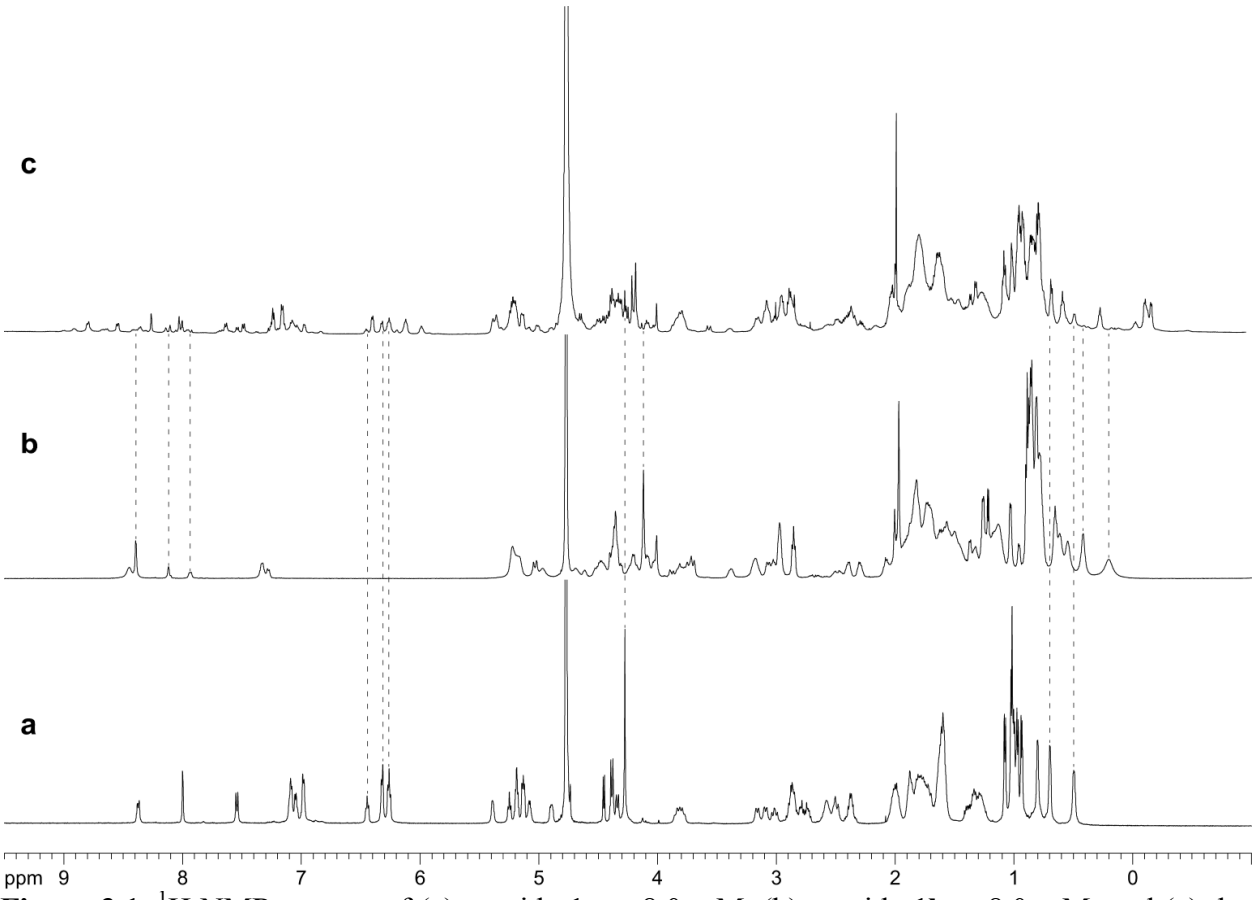

Figure 3.1. ^{1}H NMR spectra of (a) peptide **1a** at 8.0 mM, (b) peptide **1b** at 8.0 mM, and (c) the 1:1 mixture of peptides **1a** and **1b** at 8.0 mM total concentration in D_2O at 600 MHz and 298 K. Dotted lines illustrate how the resonances from the 1:1 mixture compare with the resonances of pure **1a** and pure **1b**.

Peptides 1a and 1b Form Heterotetramers. Our laboratory has previously shown that related macrocyclic β-sheets can assemble to form tetramers.[11] In the preceding chapter, I established that both peptide **1a** and peptide **1b** form tetramers by measuring the diffusion coefficients (*D*) with DOSY NMR.[6] Here, I use DOSY NMR to determine whether the species that form upon mixing peptides **1a** and **1b** are also tetramers. The homotetramers of peptides **1a** and **1b** have diffusion coefficients of about 12 x 10^{-11} m^2/s in D_2O at 298 K. The diffusion coefficients of the species that predominate in the 1:1 mixture are comparable, 11.4 x 10^{-11} m^2/s (Table 3.1), indicating that these species are also tetramers.

Table 3.1. Diffusion coefficients (*D*) of peptides 1a and 1b in D_2O at 298 K

	$MW_{tetramer}$[a] (Da)	conc. (mM)	*D* (10^{-11} m^2/s)	oligomer state
1a	7068	8.0	11.8 ± 1.0	A_4 homotetramer
1b	6572	16.0	11.9 ± 1.1	B_4 homotetramer
1a + **1b**		8.0[b]	11.4 ± 1.1	heterotetramers

[a]Molecular weight calculated for the neutral (uncharged) peptide.
[b]Total concentration of the 1:1 mixture of peptides **1a** and **1b**.

In this chapter, I describe the homotetramers and heterotetramers formed by peptides **1a** and **1b** using the letters A and B. The homotetramers are designated A_4 and B_4, and the 3:1, 2:2, and 1:3 heterotetramers are designated A_3B_1, A_2B_2, and A_1B_3. Two topological isomers of the A_2B_2 heterotetramer could form: one consisting of two homodimers (A•A and B•B); the other consisting of two heterodimers (A•B and A•B). Figure 3.2 illustrates the homotetramers and heterotetramers, where a single β-strand represents either peptide **1a** or **1b**.

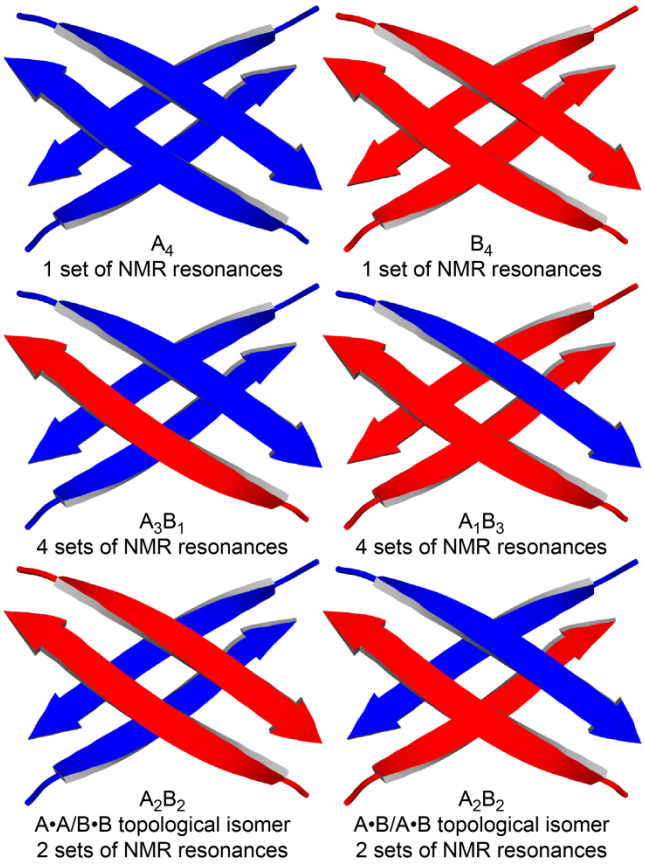

Figure 3.2. Cartoons illustrating homotetramers and heterotetramers, in which peptide **1a** is represented by a blue arrow and peptide **1b** is represented by a red arrow.

The complex mixture of monomers, homotetramers, and heterotetramers can give as many as 16 resonances in the ^{1}H NMR spectrum: two from the A monomer and A_4 homotetramer; two from the B monomer and B_4 homotetramer, four from the A_3B_1 heterotetramer, four from the A_1B_3 heterotetramer, and either two or four from the A_2B_2 heterotetramer. The A_2B_2 heterotetramer would give four resonances if both the A•A/B•B and A•B/A•B topological isomers formed, but only two resonances if just one of the two isomers formed.

Elucidation of the A_2B_2 Topological Isomer. I used peptides [^{15}N]**1a** and [^{15}N]**1b** to elucidate the dimers within the A_2B_2 heterotetramer. In the preceding chapter, I used these peptides and ^{15}N-edited NOESY to help establish the pairing of the dimers within the A_4 and B_4

homotetramers.[6] Here, I compare the ^{15}N-edited NOESY spectra of pure [^{15}N]**1a** and pure [^{15}N]**1b** to that of the 1:1 mixture to determine which A_2B_2 topological isomer forms (Figure 3.3). The spectra show that the A_2B_2 heterotetramer consists of an A•A and a B•B homodimer, and not of two A•B heterodimers (Figure 3.4).

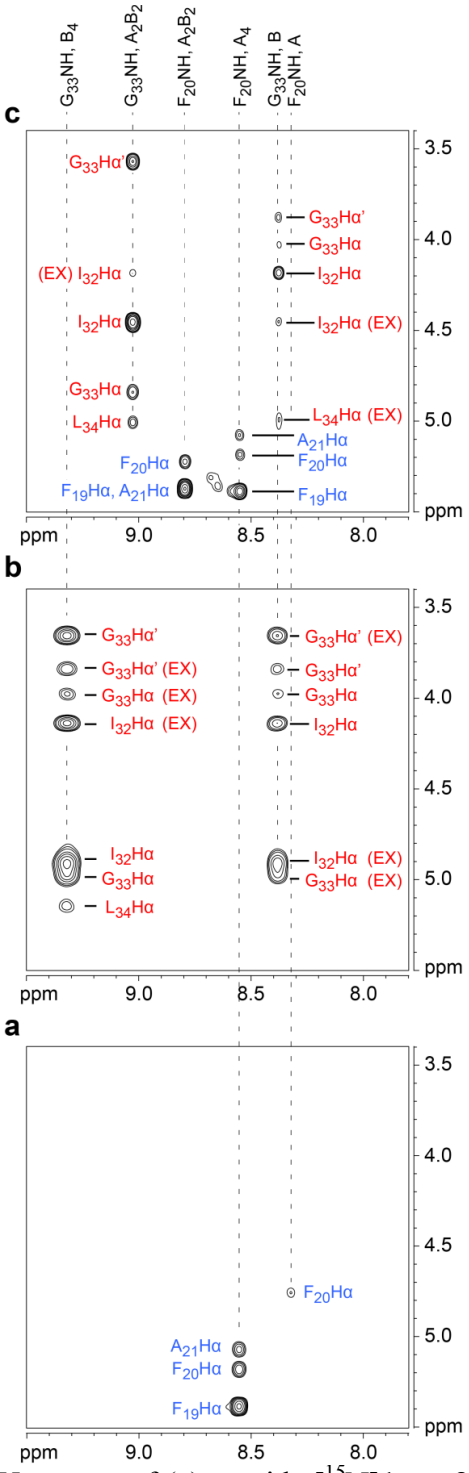

Figure 3.3. ^{15}N-Edited NOESY spectra of (a) peptide [^{15}N]**1a** at 8.0 mM, (b) peptide [^{15}N]**1b** at 8.0 mM, and (c) the 1:1 mixture of peptides [^{15}N]**1a** and [^{15}N]**1b** at 8.0 mM total concentration in 9:1 H_2O/D_2O at 600 MHz and 293 K. The G_{33}Hα corresponds to the *pro-R* α-proton and the G_{33}Hα' corresponds to the *pro-S* α-proton. Crosspeaks associated with chemical exchange of peptide **1b** between the monomer and the B_4 and A_2B_2 tetramers are labeled EX. Dotted lines illustrate how the crosspeaks from the 1:1 mixture compare with the crosspeaks of pure [^{15}N]**1a** and pure [^{15}N]**1b**.

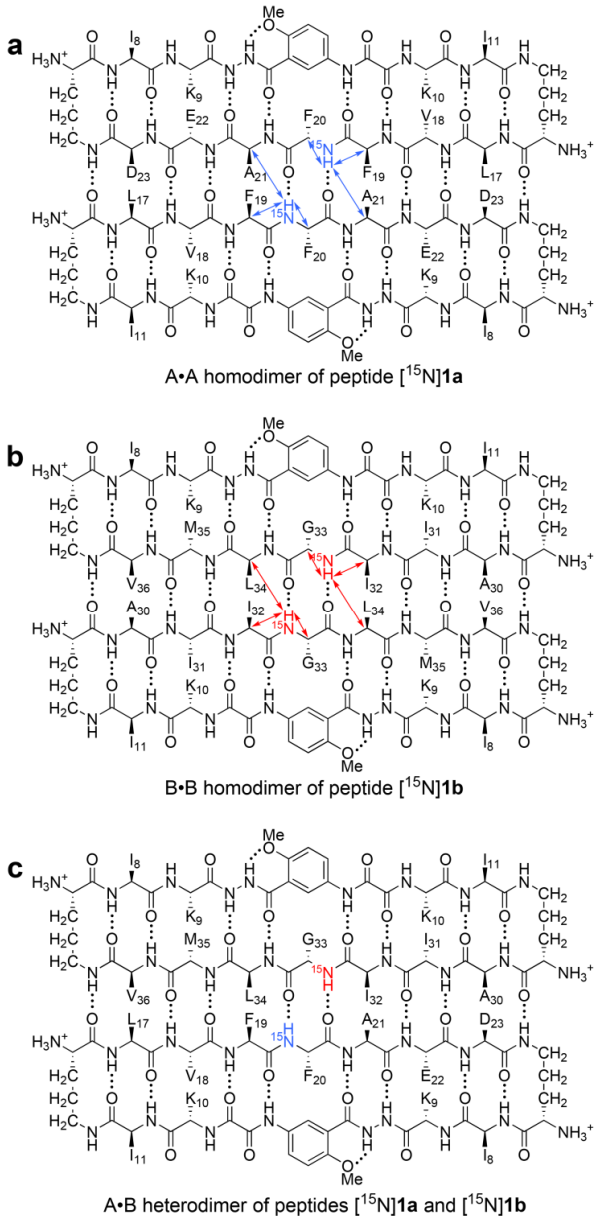

Figure 3.4. NOEs involving the ^{15}NH protons within the A_2B_2 heterotetramer. (a) The A•A homodimer with blue arrows illustrating the NOEs observed within the dimers. (b) The B•B homodimer with red arrows illustrating the NOEs observed within the dimers. (c) The A•B heterodimer (not formed).

The ^{15}N-edited NOESY spectrum of the 1:1 mixture of peptides [^{15}N]**1a** and [^{15}N]**1b** shows four distinct sets of resonances: two sets associated with the A_2B_2 heterotetramer; one set associated with the A_4 homotetramer; and one set associated with the B monomer (Figure 3.3c). In addition to the NOEs, the spectrum also shows crosspeaks associated with chemical exchange between the monomer of peptide [^{15}N]**1b** and the A_2B_2 heterotetramer.

The A_2B_2 heterotetramer gives two sets of resonances: one set from the F_{20}NH proton of peptide [^{15}N]**1a** and the other set from the G_{33}NH proton of peptide [^{15}N]**1b**. The F_{20}NH proton of peptide [^{15}N]**1a** gives a strong interresidue NOE to the F_{19}Hα proton and a weaker intraresidue NOE to the F_{20}Hα proton. Figure 3.4a summarizes these NOEs. An intermolecular NOE between the F_{20}NH and the A_{21}Hα protons is not observed as a separate crosspeak because the F_{20}Hα and the A_{21}Hα resonances overlap.[12] The F_{20}NH proton gives an additional NOE to the A_{21}Hβ protons, which corroborates the proximity of these residues (Figure S3.2). An intermolecular NOE is not observed between the F_{20}NH proton of peptide [^{15}N]**1a** and the L_{34}Hα proton of peptide [^{15}N]**1b** (Figure 3.3c); an intermolecular NOE is also not observed between the F_{20}NH proton of peptide [^{15}N]**1a** and the G_{33}NH proton of peptide [^{15}N]**1b** (Figure S3.3). The absence of these two NOEs indicates that peptide [^{15}N]**1a** is not part of an A•B heterodimer (Figure 3.4c).

The G_{33}NH proton of peptide [^{15}N]**1b** gives an interresidue NOE to the I_{32}Hα proton and intraresidue NOEs to the G_{33}Hα and G_{33}Hα' protons (Figure 3.3c). The G_{33}NH proton also gives an intermolecular NOE to the L_{34}Hα proton.[12] This NOE confirms that the B•B homodimer forms within the A_2B_2 heterotetramer and rules out the A•B heterodimer. Figure 3.4b summarizes these NOEs.[13] Collectively, the ^{15}N-edited NOESY studies establish that the A•A/B•B topological isomer that forms exclusively is the A_2B_2 heterotetramer.

^{1}H,^{15}N HSQC Reveals That Peptides [^{15}N]1a and [^{15}N]1b Form Three Heterotetramers: A_3B_1, A_2B_2, and A_1B_3. I compared the ^{1}H,^{15}N HSQC spectra of pure [^{15}N]**1a** and pure [^{15}N]**1b** to that of the 1:1 mixture to show which crosspeaks are associated with heterotetramers.[6] The ^{1}H,^{15}N HSQC spectrum of the 1:1 mixture of peptides [^{15}N]**1a** and [^{15}N]**1b** at 8.0 mM total concentration shows 10 new crosspeaks (14 crosspeaks in total). The crosspeaks are sharp and distinct, indicating that the tetramers exchange slowly on the NMR time scale. The two crosspeaks designated *1* and *2* come from the monomer and homotetramer of peptide [^{15}N]**1a**; the two crosspeaks designated *3* and *4* come from the monomer and homotetramer of peptide [^{15}N]**1b**. The 10 remaining crosspeaks designated *5–14* come from the heterotetramers. Figure 3.5a shows the ^{1}H,^{15}N HSQC spectrum of the 1:1 mixture of peptides [^{15}N]**1a** and [^{15}N]**1b**. Table 3.2 summarizes the chemical shifts of crosspeaks *1–14*.

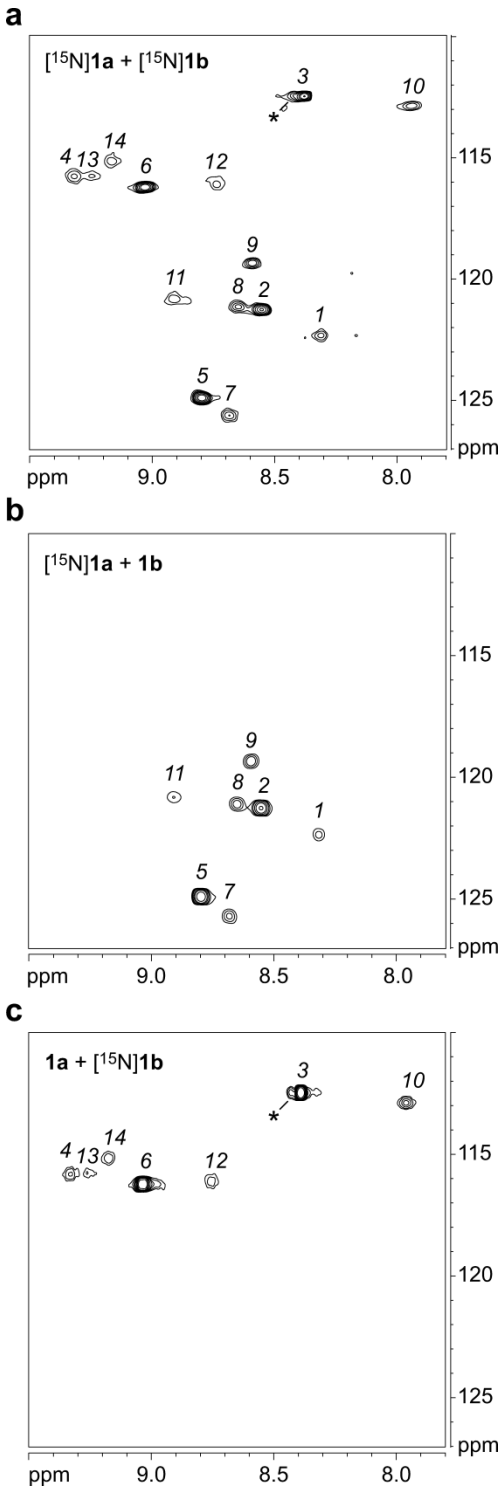

Figure 3.5. $^{1}H,^{15}N$ HSQC spectra of 8.0 mM mixtures in 9:1 H_2O/D_2O at 600 MHz and 293 K of peptides: (a) [^{15}N]**1a** and [^{15}N]**1b**; (b) [^{15}N]**1a** and **1b**; (c) **1a** and [^{15}N]**1b**. The asterisk (*) indicates a crosspeak from a minor unidentified species associated with peptide [^{15}N]**1b**.

Table 3.2. Chemical shifts of peptides [^{15}N]1a and [^{15}N]1b[a]

crosspeak	δ F_{20}		δ G_{33}		species
	^{1}H	^{15}N	^{1}H	^{15}N	
1	8.32	122.3	–	–	A monomer
2	8.56	121.3	–	–	A_4 homotetramer
3	–	–	8.39	112.5	B monomer
4	–	–	9.33	115.8	B_4 homotetramer
5	8.81	124.9	–	–	A_2B_2 heterotetramer
6	–	–	9.03	116.2	A_2B_2 heterotetramer
7	8.69	125.7	–	–	A_3B_1 heterotetramer
8	8.66	121.1	–	–	A_3B_1 heterotetramer
9	8.60	119.3	–	–	A_3B_1 heterotetramer
10	–	–	7.94	112.8	A_3B_1 heterotetramer
11	8.92	120.9	–	–	A_1B_3 heterotetramer
12	–	–	8.74	116.1	A_1B_3 heterotetramer
13	–	–	9.25	115.8	A_1B_3 heterotetramer
14	–	–	9.17	115.1	A_1B_3 heterotetramer

[a] ^{1}H,^{15}N HSQC spectrum was recorded for the 1:1 mixture at 8.0 mM in 9:1 H_2O/D_2O at 293 K.

The remaining crosspeaks *5–14* come from the A_3B_1, A_2B_2, and A_1B_3 heterotetramers. Crosspeaks *5* and *6* are prominent and strikingly similar in intensity to each other. These two crosspeaks come from the A_2B_2 heterotetramer. Crosspeaks *7–14* are weaker and are also similar in intensity to each other. These eight crosspeaks are associated with the A_3B_1 and A_1B_3 heterotetramers.

I mixed peptides [^{15}N]**1a** and **1b** and also mixed peptides **1a** and [^{15}N]**1b** to assign crosspeaks *7–14* to the respective peptides. Figures 3.5b and 3.5c show the ^{1}H,^{15}N HSQC spectra of these mixtures of labeled and unlabeled peptides. The ^{1}H,^{15}N HSQC spectrum of peptides [^{15}N]**1a** and **1b** shows that crosspeaks *1*, *2*, *5*, *7*, *8*, *9*, and *11* come from peptide [^{15}N]**1a**; the ^{1}H,^{15}N HSQC spectrum of peptides **1a** and [^{15}N]**1b** shows that crosspeaks *3*, *4*, *6*, *10*, *12*, *13*, and *14* come from peptide [^{15}N]**1b**. These spectra confirm that half of the crosspeaks come from peptide **1a** and that half of the crosspeaks come from peptide **1b**.

Assigning the ^{1}H,^{15}N HSQC Crosspeaks of the A_3B_1 and A_1B_3 Heterotetramers. To assign which of the crosspeaks *7–14* come from the A_3B_1 heterotetramer and which come from the A_1B_3 heterotetramer, I compared ^{1}H,^{15}N HSQC spectra of 3:1 and 1:3 mixtures of peptides [^{15}N]**1a** and [^{15}N]**1b** to that of the 1:1 mixture. In the spectra of the 3:1, 1:1, and 1:3 mixtures,

the relative intensities of crosspeaks *1–14* vary, but the chemical shifts do not. The f_1 projections of the $^1H,^{15}N$ HSQC spectra conveniently illustrate the relative intensities of the crosspeaks as one-dimensional ^{15}N spectra. Figure 3.6 shows the f_1 projections of pure [^{15}N]**1a**, the 3:1, 1:1, and 1:3 mixtures, and pure [^{15}N]**1b**.

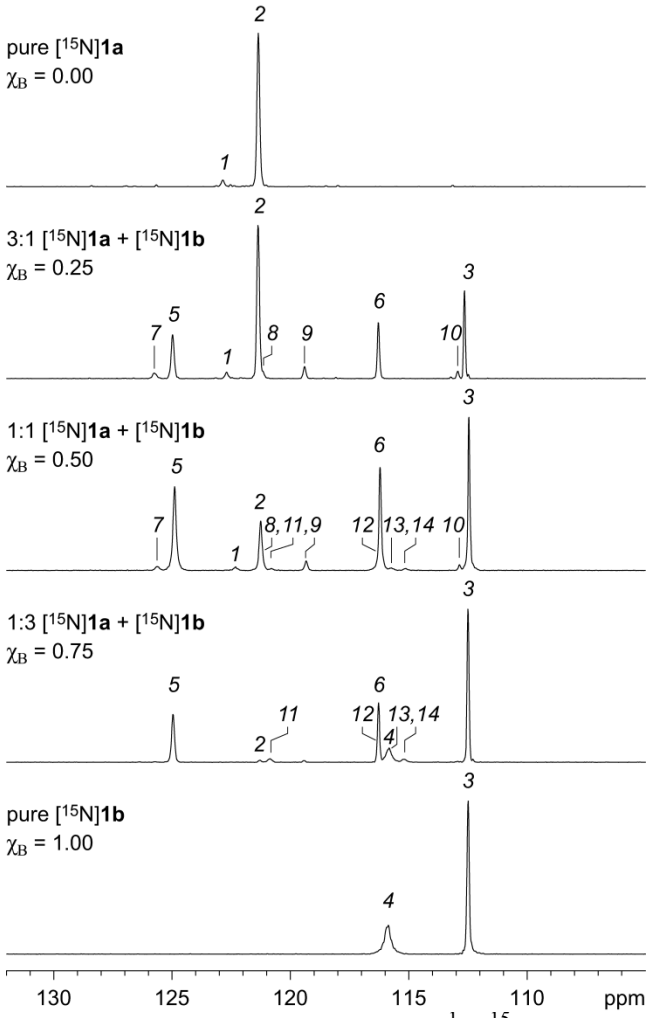

Figure 3.6. ^{15}N spectra from the f_1 projections of the $^1H,^{15}N$ HSQC spectra of mixtures of peptides [^{15}N]**1a** and [^{15}N]**1b**. Spectra were recorded at 8.0 mM total concentration and varying mole fractions of peptide in 9:1 H_2O/D_2O at 600 MHz and 293 K. The mole fraction of peptide [^{15}N]**1b** is designated χ_B.

The systematic variation of the crosspeaks as a function of the mole fraction χ_B clearly establishes which crosspeaks are associated with the A_3B_1 heterotetramer and which are associated with the A_1B_3 heterotetramer. Crosspeaks *7–10* have maximum relative intensities at

χ_B = 0.25 and come from the A_3B_1 heterotetramer. Crosspeaks *11–14* have maximum relative intensities at χ_B = 0.75 and come from the A_1B_3 heterotetramer. Figure 3.7 illustrates relative integrations of the crosspeaks versus the mole fraction of peptide [^{15}N]**1b**, χ_B.

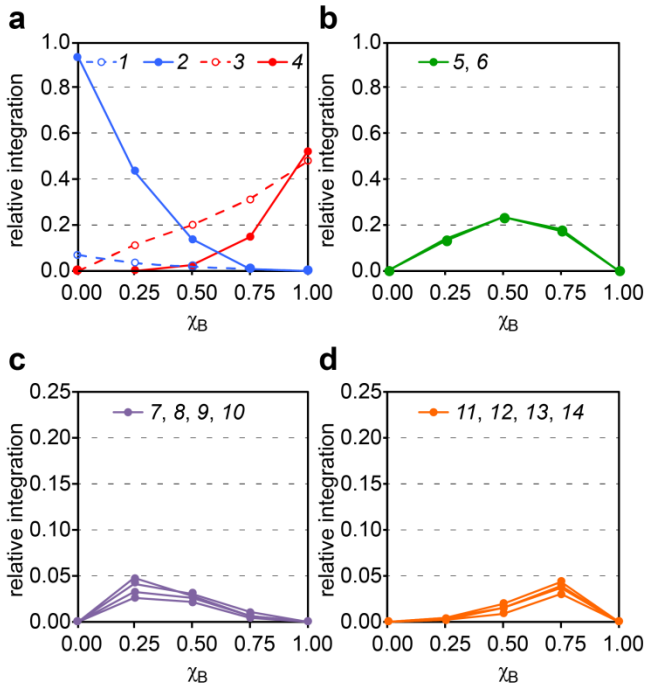

Figure 3.7. Plot of the relative integrations of crosspeaks *1–14* versus the mole fraction of peptide [^{15}N]**1b**, χ_B. The intensities were measured by integrating the crosspeaks in the ^{1}H,^{15}N HSQC spectra of the mixtures of peptides [^{15}N]**1a** and [^{15}N]**1b**.

Job's Method of Continuous Variation. I used Job's method to determine the relative stabilities of the homotetramers and the heterotetramers of peptides [^{15}N]**1a** and [^{15}N]**1b**. Although this method was first introduced to study inorganic complexes, it is useful in all areas of chemistry for studying molecular association.[14,15] Job's method is performed by mixing two compounds "A" and "B" in varying ratios while keeping the total concentration constant. The amount of a complex that forms is then plotted versus the mole fraction to give a plot known as a "Job plot". The appearance of the Job plot reflects the stoichiometry and relative stability of each complex. The mole fraction at which the maximum amount of the complex forms corresponds

with its stoichiometry. For example, an A_1B_2 heterotrimer would give a maximum in a 1:2 mixture ($\chi_B = 0.67$).

I applied Job's method to peptides [^{15}N]**1a** and [^{15}N]**1b**, recording ^{1}H,^{15}N HSQC spectra for nine samples at 8.0 mM total concentration.[16] I plotted the sum of the relative integrals of the ^{1}H,^{15}N HSQC crosspeaks for each species versus the mole fraction of peptide [^{15}N]**1b**, χ_B. For example, I plotted the curve for the A_3B_1 heterotetramer species using the sum of the relative integrals of crosspeaks *7–10*. Figure 3.8 illustrates the resulting Job plot.

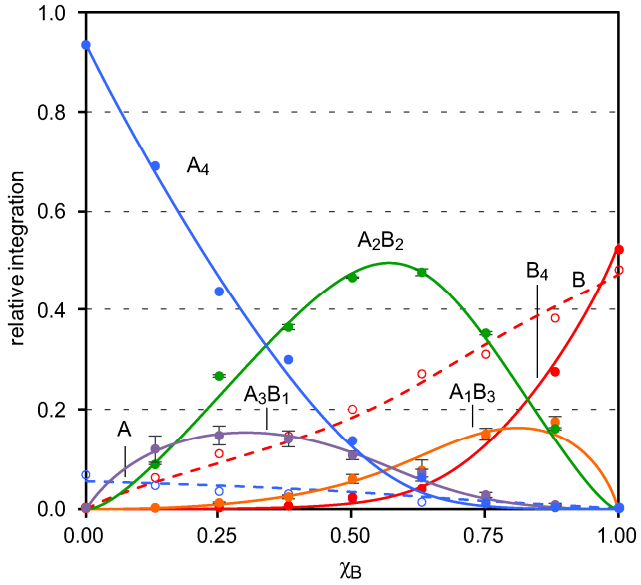

Figure 3.8. Job plot for peptides [^{15}N]**1a** and [^{15}N]**1b** showing the relative integrations of the monomers, homotetramers, and heterotetramers versus the mole fraction of peptide [^{15}N]**1b**, χ_B. The curves reflect a monomer-tetramer equilibrium model fitted to the data. The error bars reflect the standard deviations among the individual measurements used to determine the relative integrations of A_3B_1, A_2B_2, and A_1B_3. The relative stabilities determined for each species are $\phi_{4_4} = 1.00$, $\phi_{4_3} = 0.22$, $\phi_{4_2} = 0.67$, $\phi_{4_1} = 0.12$, $\phi_{4_0} = 0.12$, $\phi_{1_1} = 0.36$, and $\phi_{1_0} = 2.20$.

The Job plot shows that the A_2B_2 heterotetramer predominates over a wide range of mole fractions. At low mole fractions, $\chi_B \leq 0.25$, the A_4 homotetramer predominates. At high mole fractions, $\chi_B \geq 0.75$, the B monomer and B_4 heterotetramer predominate. The A_2B_2 heterotetramer reaches a maximum concentration at a mole fraction χ_B slightly greater than 0.50.

The A_3B_1 heterotetramer and the A_1B_3 heterotetramer form to a lesser extent, reaching a maximum concentration at low and high mole fractions χ_B, respectively.

Simulated Job Plots of Homotetramers and Heterotetramers. I generated simulated Job plots reflecting different homotetramer and heterotetramer stabilities to help interpret the data in Figure 3.8. I used an implementation developed by Collum and coworkers that readily accommodates homotetramer and heterotetramer equilibria.[17,18,19] I simulated a Job plot for a statistical distribution of homotetramers and heterotetramers and Job plots in which one of the heterotetramers is favored. These plots demonstrate how the relative stabilities of the tetramers affect the shapes of the curves. Figure 3.9 illustrates the resulting Job plots; the relative integrations of the species are plotted versus the mole fraction χ_B.

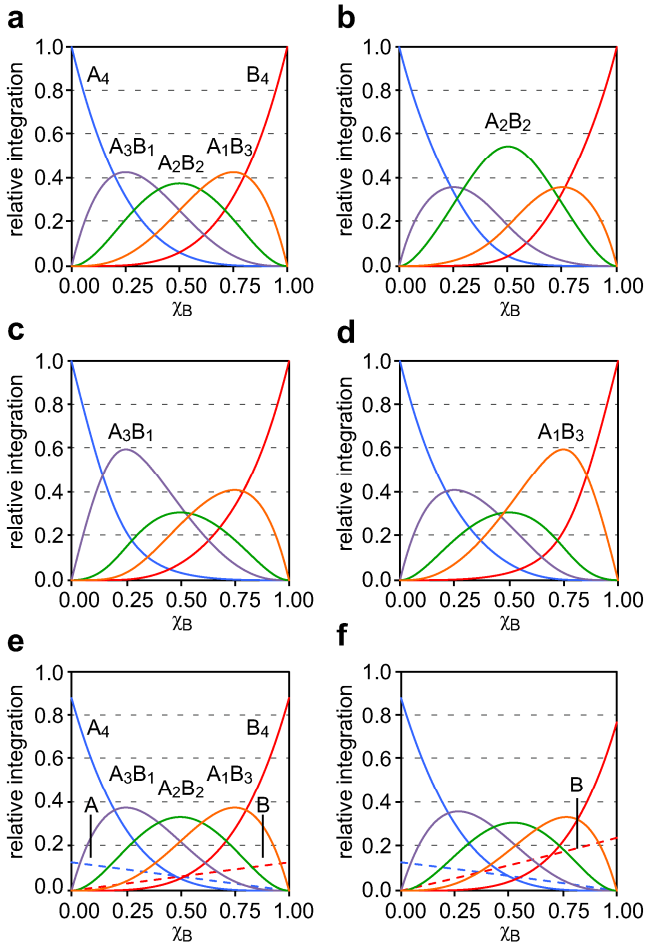

Figure 3.9. Simulated Job plots that show the relative integrations of the monomers, homotetramers, and heterotetramers versus the mole fraction of B, χ_B. (a) A statistical distribution of homotetramers and heterotetramers; $\phi_{4_4} = \phi_{4_3} = \phi_{4_2} = \phi_{4_1} = \phi_{4_0} = 1$. (b) A_2B_2 heterotetramer is favored; $\phi_{4_2} = 2$ and $\phi_{4_4} = \phi_{4_3} = \phi_{4_1} = \phi_{4_0} = 1$. (c) A_3B_1 heterotetramer is favored; $\phi_{4_3} = 2$ and $\phi_{4_4} = \phi_{4_2} = \phi_{4_1} = \phi_{4_0} = 1$. (d) A_1B_3 heterotetramer is favored; $\phi_{4_1} = 2$ and $\phi_{4_4} = \phi_{4_3} = \phi_{4_2} = \phi_{4_0} = 1$. (e) A statistical distribution of homotetramers and heterotetramers that also includes monomers; $\phi_{4_4} = \phi_{4_3} = \phi_{4_2} = \phi_{4_1} = \phi_{4_0} = 1$ and $\phi_{1_1} = \phi_{1_0} = 1$. (f) A statistical distribution of homotetramers and heterotetramers that also includes monomers, where the B monomer is favored $\phi_{4_4} = \phi_{4_3} = \phi_{4_2} = \phi_{4_1} = \phi_{4_0} = 1$, $\phi_{1_1} = 1$, and $\phi_{1_0} = 2$.

In the implementation by Collum and coworkers, the relative concentrations of the homotetramers and heterotetramers are calculated from equations based on a homotetramer-heterotetramer equilibrium model. The parameters ϕ_{N_n} are ascribed to each of the homotetramers and heterotetramers in the equations, where the subscripts N and n are integers in which the value of N describes the oligomer size and the value of n describes the number of "A" subunits. The value of each ϕ_{N_n} reflects the relative stability of each homotetramer or heterotetramer. The

parameters ϕ_{4_4}, ϕ_{4_3}, ϕ_{4_2}, ϕ_{4_1}, and ϕ_{4_0} describe the relative stabilities of A_4, A_3B_1, A_2B_2, A_1B_3, and B_4, respectively. When each tetramer is equally stable, all parameters are equal (e.g., $\phi_{4_4} = \phi_{4_3} = \phi_{4_2} = \phi_{4_1} = \phi_{4_0} = 1$) and a statistical distribution of homotetramers and heterotetramers forms.

The Job plot of a statistical distribution of homotetramers and heterotetramers is symmetrical, where the maximum of each curve reflects the tetramer stoichiometry. In the 1:1 mixture, the A_2B_2 heterotetramer predominates, with smaller fractions of the A_3B_1 and A_1B_3 heterotetramers in equal amounts, and with traces of the A_4 and B_4 homotetramers in equal amounts. In the 3:1 mixture, the A_3B_1 heterotetramer predominates, with smaller fractions of the A_4 homotetramer and A_2B_2 heterotetramer, and with traces of the A_1B_3 heterotetramer. Similarly, in the 1:3 mixture, the A_1B_3 heterotetramer predominates, with smaller fractions of the B_4 homotetramer and A_2B_2 heterotetramer, and with traces of the A_3B_1 heterotetramer. Figure 3.9a illustrates the Job plot for a statistical distribution of homotetramers and heterotetramers.

The appearance of the Job plot changes if any of the tetramers are favored or disfavored. If the A_2B_2 tetramer is favored, the A_2B_2 curve shows a pronounced increase and the A_3B_1 and A_1B_3 curves diminish slightly (Figure 3.9b). If the A_3B_1 tetramer is favored, the A_3B_1 curve shows a pronounced increase and the A_2B_2 curve diminishes slightly (Figure 3.9c). If the A_1B_3 tetramer is favored, the A_1B_3 curve shows a pronounced increase and the A_2B_2 curve diminishes slightly (Figure 3.9d).

Analysis of the Job Plot. I modified the implementation by Collum and coworkers to accommodate the equilibrium of the monomers with the homotetramers and heterotetramers. In our implementation, the relative concentrations of the monomers, homotetramers, and heterotetramers are calculated from equations based on a monomer-homotetramer-heterotetramer equilibrium model. The parameters ϕ_{1_1} and ϕ_{1_0} reflect the relative stabilities of the monomers A

and B. The Job plot of a statistical distribution of homotetramers and heterotetramers that also includes the monomers is similar to the Job plot without monomers, except that the fraction of each tetramer is slightly diminished (Figure 3.9e). If the equilibrium favors one of the two monomers, a greater fraction of that monomer forms (Figure 3.9f).

I analyzed the data from our Job's method experiment by nonlinear least-squares fitting of the model to the data. During the fit, the parameters ϕ_{43}, ϕ_{42}, ϕ_{41}, ϕ_{40}, ϕ_{11}, and ϕ_{10} were allowed to vary, while the parameter ϕ_{44} remained fixed at 1. Figure 3.8 illustrates the Job plot with the fitted curves ($\phi_{44} = 1.00$, $\phi_{43} = 0.22$, $\phi_{42} = 0.67$, $\phi_{41} = 0.12$, $\phi_{40} = 0.12$, $\phi_{11} = 0.36$, $\phi_{10} = 2.20$).

The model fits the data well. The quality of the fit corroborates that peptides [^{15}N]**1a** and [^{15}N]**1b** form a mixture of homotetramers and heterotetramers. The appearance of the resulting plot does not resemble the statistical distribution shown in Figure 3.9e. The Job plot shows little or no preference for the A_2B_2 heterotetramer, but it does show suppression of the A_3B_1 and A_1B_3 heterotetramers.

The Job's method of continuous variation study and nonlinear least-squares fitting of the data establish that peptides **1a** and **1b** prefer to segregate within the heterotetramers. The suppression of the A_3B_1 and A_1B_3 heterotetramers shows that the A•B heterodimer subunit is disfavored and that heterotetramers containing an A•B heterodimer subunit are less stable. This finding explains why the A_2B_2 heterotetramer contains two homodimers rather than two heterodimers. Peptide **1a**, which contains $A\beta_{17–23}$, prefers to pair with itself to form a hydrogen-bonded homodimer; peptide **1b**, which contains $A\beta_{30–36}$, prefers to pair with itself to form a hydrogen-bonded homodimer.

Molecular Models of A_2B_2 Heterotetramers. I constructed energy-minimized models of A_2B_2 heterotetramers to help understand the preferential pairing of peptides **1a** and **1b** to form

homodimers. By combining the monomer subunits of the models of the A_4 and B_4 homotetramers developed in the preceding chapter[6] and re-minimizing, I generated two models of the A_2B_2 heterotetramers: the A•A/B•B topological isomer that was observed, and the A•B/A•B topological isomer that was not. Figure 3.10 illustrates the resulting models of these two topological isomers.

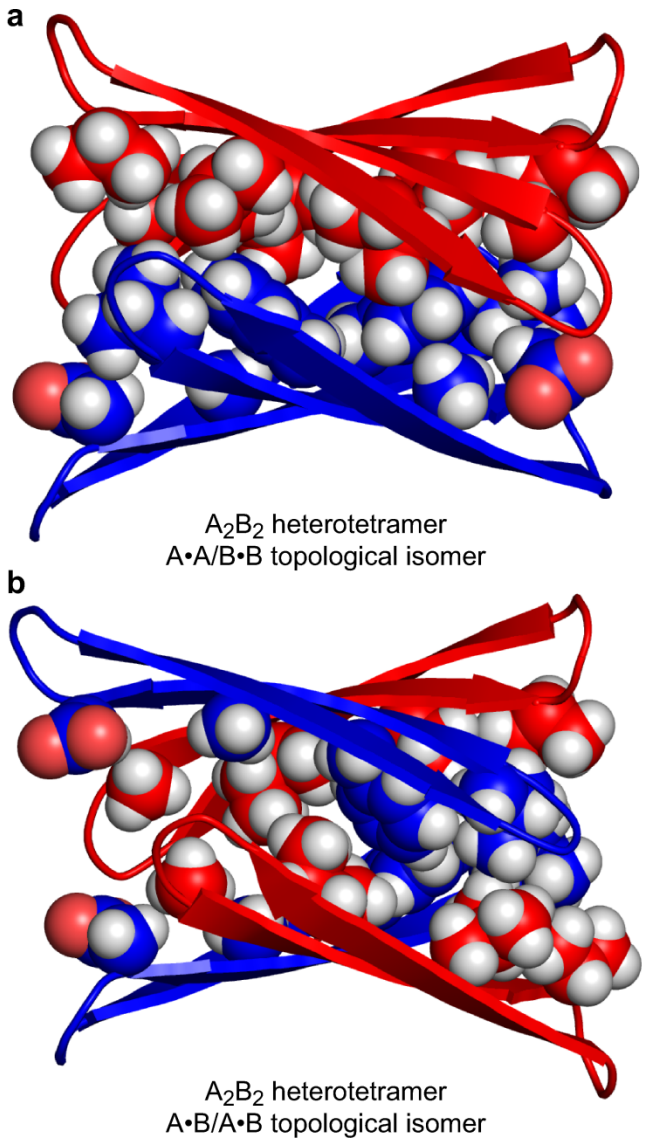

Figure 3.10. Molecular models of the topological isomers of the A_2B_2 heterotetramer of peptides **1a** and **1b**. (a) The A•A/B•B topological isomer. (b) The A•B/A•B topological isomer. Each model is a minimum-energy structure (local minimum) generated with MacroModel using the MMFFs force field with GB/SA water solvation.

The models show that the A_2B_2 heterotetramers can form sandwich-like structures that are similar to the homotetramers. Both topological isomers consist of two, four-stranded β-sheets that laminate together through hydrophobic packing. The side chains of L_{17}, F_{19}, and A_{21} from peptide **1a** and of A_{30}, I_{32}, L_{34}, and V_{36} from peptide **1b** form hydrophobic surfaces that pack in the hydrophobic core of each heterotetramer. The interface between the A•A and B•B homodimers in the A•A/B•B topological isomer is uniformly packed. In contrast, the interface between the two A•B heterodimers in the A•B/A•B topological isomer is densely packed at one end and lightly packed at the other (Figure 3.10b).

The A•A homodimer of peptide **1a** exhibits a large hydrophobic surface, with intimate contacts between the side chains of L_{17}, F_{19}, and A_{21}. The large F_{19} and small A_{21} residues fit together well to help provide a uniformly packed surface (Figure 3.11a). The B•B homodimer of peptide **1b** also exhibits a large hydrophobic surface, with intimate contacts between the side chains of A_{30}, I_{32}, L_{34}, and V_{36}. These residues also provide a uniformly packed surface (Figure 3.11b). The A•B heterodimer exhibits a hydrophobic surface with intimate contacts between the side chains of L_{17}, F_{19}, and A_{21} from peptide **1a** and the side chains of I_{32}, L_{34}, and V_{36} from peptide **1b**. The side chains do not pack uniformly, but rather the side chains pack densely at one end of the dimer and pack lightly at the other (Figure 3.11c).

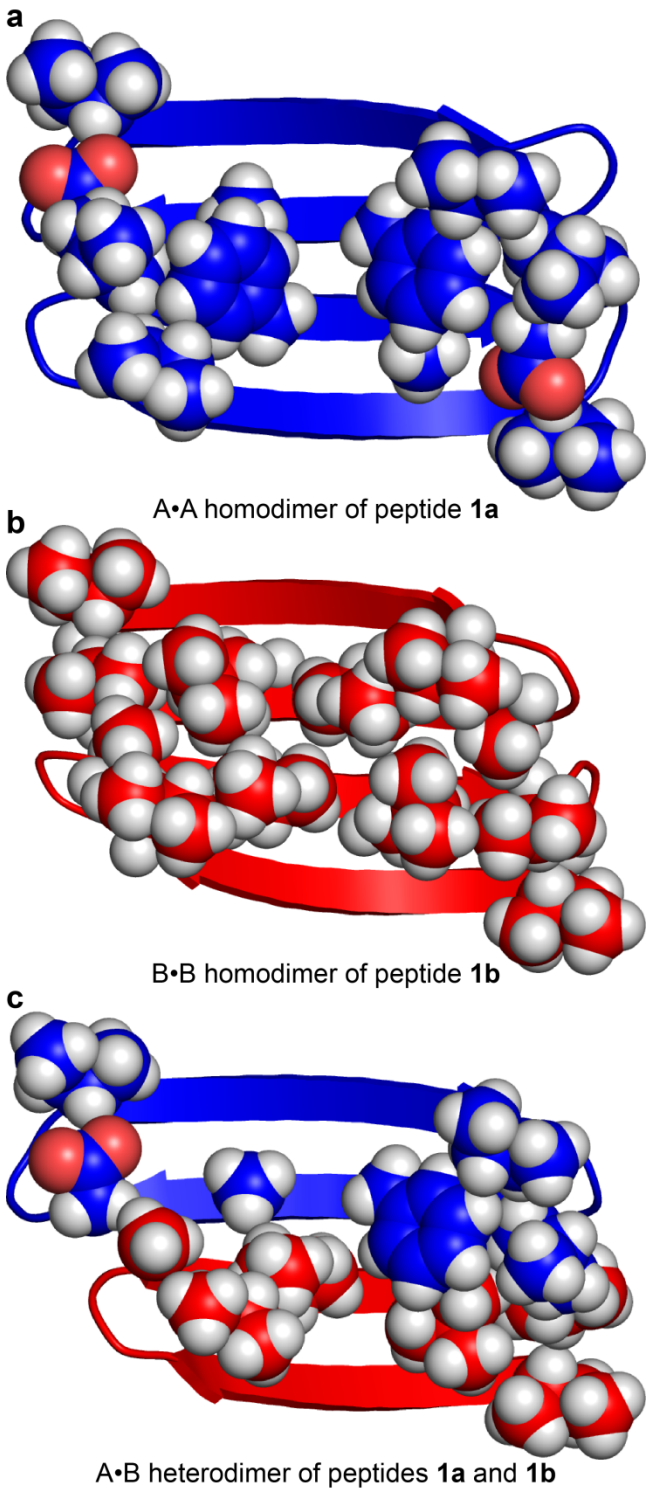

Figure 3.11. Molecular models of the homodimer and heterodimer subunits of the A_2B_2 heterotetramers of peptides **1a** and **1b**.

These molecular models suggest that differences between the homodimers and heterodimers formed by peptides **1a** and **1b** dictate the observed differences in the A_2B_2

heterotetramer stability. The uniform packing of the A•A and B•B homodimers appears to drive the formation of the observed A_2B_2 heterotetramer. The non-uniform packing of the A•B heterodimer appears to suppress the formation of the A_3B_1 and A_1B_3 heterotetramers, and also the alternative topological isomer of the A_2B_2 heterotetramer.

CONCLUSION

In framing the question behind these studies, I set out to determine whether peptides derived from the central and C-terminal regions of Aβ prefer to coassemble or to segregate. I found that the answer is more nuanced, at least in the context of the model system provided by peptides **1**. Peptides **1a** and **1b** can coassemble, but the resulting heterotetramers reflect a preference to segregate within the dimer subunits. The heterotetramers comprising heterodimers are disfavored, while the heterotetramers comprising homodimers are not. These findings recapitulate the segregation within $A\beta_{1–40}$ fibrils, in which the central region assembles to form a hydrogen-bonded β-sheet and the C-terminal region assembles to form a hydrogen-bonded β-sheet.[3] The two β-sheets coassemble through hydrophobic contacts.

^{15}N-Isotopic labeling, ^{1}H,^{15}N NMR spectroscopy, and Job's method of continuous variation proved essential in these studies. Incorporation of a single ^{15}N-isotopic label provided a sensitive and non-perturbing spectroscopic probe. ^{15}N-Labeled peptides are readily prepared from commercially available ^{15}N-labeled amino acids using solid-phase peptide synthesis. ^{1}H,^{15}N HSQC facilitated identification of the monomers, homotetramers, and heterotetramers. Job's method of continuous variation assigned the resonances of each monomer and tetramer and established the relative stability of the tetramers. ^{15}N-Edited NOESY established the identity of the topological isomer of the A_2B_2 heterotetramer.

These techniques, which proved useful for elucidating the assembly and coassembly of β-sheet peptides, should also be valuable in broader contexts. Peptide and protein assemblies occur widely in coiled coils, helix bundles, and collagen helices, as well as in amyloid oligomers and other β-sheet supramolecular assemblies. I envision that ^{15}N-isotopic labeling in conjunction with ^{1}H,^{15}N NMR spectroscopy and Job's method will also be valuable for studying these assemblies.

REFERENCES AND NOTES

1. (a) Näslund, J.; Haroutunian, V.; Mohs, R.; Davis, K. L.; Davies, P.; Greengard, P.; Buxbaum, J. D. *JAMA* **2000**, *283*, 1571–1577; (b) Haass, C.; Selkoe, D. J. *Nat. Rev. Mol. Cell Biol.* **2007**, *8*, 101–112; (c) Querfurth, H. W.; LaFerla, F. M. *N. Eng. J. Med.* **2010**, *362*, 329–344; (d) Knowles, T. P.; Vendruscolo, M.; Dobson, C. M. *Nat. Rev. Mol. Cell Biol.* **2014**, *15*, 384–396.

2. Liu, R.; McAllister, C.; Lyubchenko, Y.; Sierks, M. R. *J. Neurosci. Res.* **2004**, *75*, 162–171.

3. (a) Petkova, A. T.; Ishii, Y.; Balbach, J. J.; Antzutkin, O. N.; Leapman, R. D.; Delaglio, F.; Tycko, R. *Proc. Natl. Acad. Sci. U.S.A.* **2002**, *99*, 16742–16747; (b) Paravastu, A. K.; Leapman, R. D.; Yau, W.-M.; Tycko, R. *Proc. Natl. Acad. Sci. U.S.A.* **2008**, *105*, 18349–18354; (c) Tycko, R.; Wickner, R. B. *Acc. Chem. Res.* **2013**, *46*, 1487–1496; (d) Lu, J.-X.; Qiang, W.; Yau, W.-M.; Schwieters, C. D.; Meredith, S. C.; Tycko, R. *Cell* **2013**, *154*, 1257–1268.

4. The fibrils formed by $A\beta_{1-42}$ adopt a more compact structure: (a) Xiao, Y.; Ma, B.; McElheny, D.; Parthasarathy, S.; Long, F.; Hoshi, M.; Nussinov, R.; Ishii, Y. *Nat. Struct. Mol. Biol.* **2015**, *22*, 499–505. (b) Walti, M. A.; Ravotti, F.; Arai, H.; Glabe, C. G.; Wall, J. S.; Bockmann, A.; Guntert, P.; Meier, B. H.; Riek, R. *Proc. Natl. Acad. Sci. U.S.A.* **2016**, *113*, E4976–E4984. (c) Colvin, M. T.; Silvers, R.; Ni, Q. Z.; Can, T. V.; Sergeyev, I.; Rosay, M.; Donovan, K. J.; Michael, B.; Wall, J.; Linse, S.; Griffin, R. G. *J. Am. Chem. Soc.* **2016,** *138*, 9663–9674.

5. (a) Hoyer, W.; Gronwall, C.; Jonsson, A.; Stahl, S.; Hard, T. *Proc. Natl. Acad. Sci. U.S.A.* **2008**, *105*, 5099–5104; (b) Cerf, E.; Sarroukh, R.; Tamamizu-Kato, S.; Breydo, L.; Derclaye, S.; Dufrene, Y. F.; Narayanaswami, V.; Goormaghtigh, E.; Ruysschaert, J. M.; Raussens, V.

Biochem. J. **2009**, *421*, 415–423; (c) Yu, L.; Edalji, R.; Harlan, J. E.; Holzman, T. F.; Lopez, A. P.; Labkovsky, B.; Hillen, H.; Barghorn, S.; Ebert, U.; Richardson, P. L.; Miesbauer, L.; Solomon, L.; Bartley, D.; Walter, K.; Johnson, R. W.; Hajduk, P. J.; Olejniczak, E. T. *Biochemistry* **2009**, *48*, 1870–1877; (d) Sandberg, A.; Luheshi, L. M.; Söllvander, S.; Pereira de Barros, T.; Macao, B.; Knowles, T. P. J.; Biverstål, H.; Lendel, C.; Ekholm-Petterson, F.; Dubnovitsky, A.; Lannfelt, L.; Dobson, C. M.; Härd, T. *Proc. Natl. Acad. Sci. U.S.A.* **2010**, *107*, 15595–15600; (e) Lendel, C.; Bjerring, M.; Dubnovitsky, A.; Kelly, R. T.; Filippov, A.; Antzutkin, O. N.; Nielsen, N. C.; Hard, T. *Angew. Chem. Int. Ed.* **2014**, *53*, 1–6; (f) Spencer, R. K.; Li, H.; Nowick, J. S. *J. Am. Chem. Soc.* **2014**, 5595–5598; (g) Kreutzer, A. G.; Hamza, I. L.; Spencer, R. K.; Nowick, J. S. *J. Am. Chem. Soc.* **2016**, *138*, 4634–4642.

6. Truex, N. L.; Wang, Y.; Nowick, J. S. *J. Am. Chem. Soc.* **2016**. *138*, 13882–13890.

7. (a) Cheng, P. N.; Liu, C.; Zhao, M.; Eisenberg, D.; Nowick, J. S. *Nat. Chem.* **2012**, *4*, 927–933; (b) Liu, C.; Zhao, M.; Jiang, L.; Cheng, P. N.; Park, J.; Sawaya, M. R.; Pensalfini, A.; Gou, D.; Berk, A. J.; Glabe, C. G.; Nowick, J.; Eisenberg, D. *Proc. Natl. Acad. Sci. U.S.A.* **2012**, *109*, 20913–20918; (c) Buchanan, L. E.; Dunkelberger, E. B.; Tran, H. Q.; Cheng, P. N.; Chiu, C. C.; Cao, P.; Raleigh, D. P.; de Pablo, J. J.; Nowick, J. S.; Zanni, M. T. *Proc. Natl. Acad. Sci. U.S.A.* **2013**, *110*, 19285–19290.

8. Nowick, J. S.; Chung, D. M.; Maitra, K.; Maitra, S.; Stigers, K. D.; Sun, Y. *J. Am. Chem. Soc.* **2000**, *122*, 7654–7661.

9. (a) Nowick, J. S.; Brower, J. O. *J. Am. Chem. Soc.* **2003**, *125*, 876–877; (b) Woods, R. J.; Brower, J. O.; Castellanos, E.; Hashemzadeh, M.; Khakshoor, O.; Russu, W. A.; Nowick, J. S. *J. Am. Chem. Soc.* **2007**, *129*, 2548–2558.

10. For some related studies of peptide and protein coassembly, see:(a) Hammarstrom, P.; Schneider, F.; Kelly, J. W. *Science* **2001**, *293*, 2459–246210. (b) Schnarr, N. A.; Kennan, A. J. *J. Am. Chem. Soc.* ***2002***, *124*, 9779–9783. (c) Hadley, E. B.; Testa, O. D.; Woolfson, D. N.; Gellman, S. H. *Proc. Natl. Acad. Sci. U.S.A.* **2008**, *105*, 530–535. (d) Xu, F.; Zahid, S.; Silva, T.; Nanda, V. *J. Am. Chem. Soc.* **2011**, *133*, 15260–15263. (e) Fallas, J. A.; Hartgerink, J. D. *Nat. Commun.* **2012**, *3*, 1087. (f) Thomas, F.; Boyle, A. L.; Burton, A. J.; Woolfson, D. N. *J. Am. Chem. Soc.* **2013**, *135*, 5161–5166. (g) Negron, C.; Keating, A. E. *J. Am. Chem. Soc.* **2014**, *136*, 16544–16556.

11. (a) Khakshoor, O.; Demeler, B.; Nowick, J. S. *J. Am. Chem. Soc.* **2007**, *129*, 5558–5569; (b) Pham, J. D.; Demeler, B.; Nowick, J. S. *J. Am. Chem. Soc.* **2014**, *136*, 5432–5442; (c) Pham, J. D.; Spencer, R. K.; Chen, K. H.; Nowick, J. S. *J. Am. Chem. Soc.* **2014**, *136*, 12682–12690.

12. I used ^{1}H NMR TOCSY to assign residues associated with these NOEs (Figures 3.S1 and 3.S2).

13. The ^{1}H NMR NOESY spectrum of the 1:1 mixture of peptides **1a** and **1b** shows additional NOEs associated with the stacking of the two homodimers to form a sandwich-like tetramer. The spectrum shows NOEs between the F_{19} aromatic protons of peptide **1a** and the I_{32} and L_{34} side-chain protons of peptide **1b** (Figure S3.4a). The spectrum also shows NOEs between the A_{21} side-chain protons of peptide **1a** and the I_{32} side-chain protons of peptide **1b** (Figure S3.4b). Figure S3.5 illustrates the stacking of the A•A and B•B homodimers of peptides **1a** and **1b** consistent with these NOEs.

14. Job, P. *Ann. Chim. Fr.* **1928**, *9*, 113–203.

15. (a) Ramanathan, P. S. *J. Inorg. Nucl. Chem.* **1972**, *35*, 3358–3360; (b) Ingham, K. C. *Anal. Biochem.* **1975**, *68*, 660–663; (c) Huang, C. Y. *Meth. Enzym.* **1982**, *87*, 509; (d) Gil, V. M.

S.; Oliveira, N. C. *J. Chem. Ed.* **1990**, *67*, 473–478; (e) Facchiano, A.; Ragone, R. *Anal. Biochem.* **2003**, *313*, 170–172; (f) Renny, J. S.; Tomasevich, L. L.; Tallmadge, E. H.; Collum, D. B. *Angew. Chem. Int. Ed.* **2013**, *52*, 11998–12013.

16. The 8.0 mM total concentration was chosen to favor tetramers in the mixtures of peptides [^{15}N]**1a** and [^{15}N]**1b**.

17. (a) McNeil, A. J.; Toombes, G. E.; Chandramouli, S. V.; Vanasse, B. J.; Ayers, T. A.; O'Brien, M. K.; Lobkovsky, E.; Gruner, S. M.; Marohn, J. A.; Collum, D. B. *J. Am. Chem. Soc.* **2004**, *126*, 5938–5939; (b) McNeil, A. J.; Toombes, G. E.; Gruner, S. M.; Lobkovsky, E.; Collum, D. B.; Chandramouli, S. V.; Vanasse, B. J.; Ayers, T. A. *J. Am. Chem. Soc.* **2004**, *126*, 16559–16568; (c) Liou, L. R.; McNeil, A. J.; Ramirez, A.; Toombes, G. E.; Gruver, J. M.; Collum, D. B. *J. Am. Chem. Soc.* **2008**, *130*, 4859–4868.

18. Widom, B. *Statistical Mechanics: A Concise Introduction for Chemists*. Cambridge University Press: New York, 2002.

19. Additional references on quantitative treatment of data from Job's method of continuous variation: (a) Likussar, W.; Boltz, D. F. *Anal. Chem.* **1971**, *43*, 1265–1272; (b) Bruneau, E.; Lavabre, D.; Levy, G.; Micheau, J. C. *J. Chem. Ed.* **1992**, *69*, 833–837; (c) Hirose, K. *J. Inclusion Phenom. Macrocyclic Chem.* **2001**, *39*, 193–209; (d) Olson, E. J.; Bühlmann, P. *J. Org. Chem.* **2011**, *76*, 8406–8412; (e) Olson, E. J.; Bühlmann, P. *J. Org. Chem.* **2014**, *79*, 830–830; (f) Hirose, K. In *Analytical Methods in Supramolecular Chemistry*, 2nd ed.; Schalley, C. A., Ed. Wiley-VCH: Weinheim: 2012; pp 27–66.

SUPPORTING INFORMATION FOR

Coassembly of Peptides Derived from β-Sheet Regions of β-Amyloid

3.I. SUPPLEMENTAL FIGURES

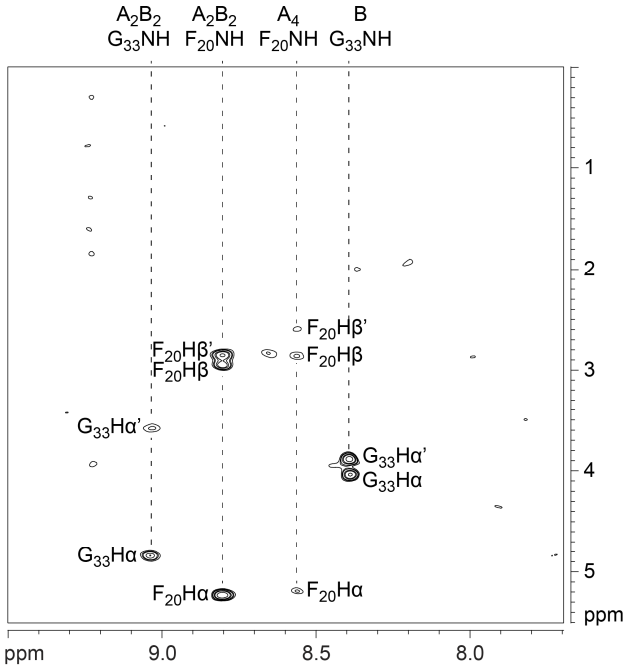

Figure S3.1. ^{15}N-Edited TOCSY spectrum of the 1:1 mixture of peptides [^{15}N]**1a** and [^{15}N]**1b** at 8.0 mM total concentration in 9:1 H_2O/D_2O at 600 MHz and 293 K.

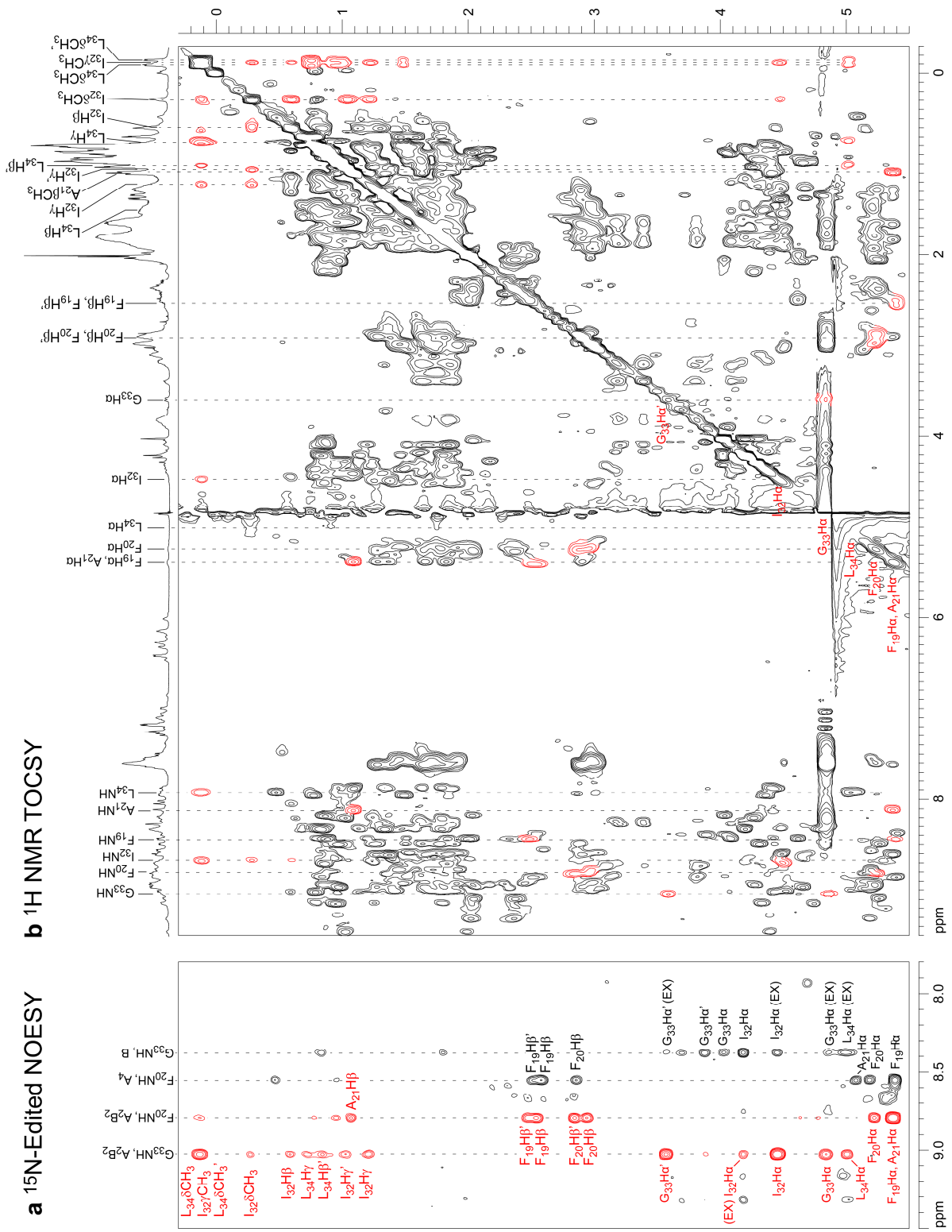

Figure S3.2. Comparison of the (a) ^{15}N-Edited NOESY spectrum of the 1:1 mixture of peptides [^{15}N]**1a** and [^{15}N]**1b** with the (b) ^{1}H NMR TOCSY spectrum of the 1:1 mixture of peptides **1a** and **1b** in 9:1 H_2O/D_2O at 600 MHz and 293 K. Key crosspeaks associated with the A_2B_2 heterotetramer are highlighted in red from F_{19}, F_{20}, and A_{21} of peptides [^{15}N]**1a** and **1a**, and also from I_{32}, G_{33}, L_{34} of peptides [^{15}N]**1b** and **1b**.

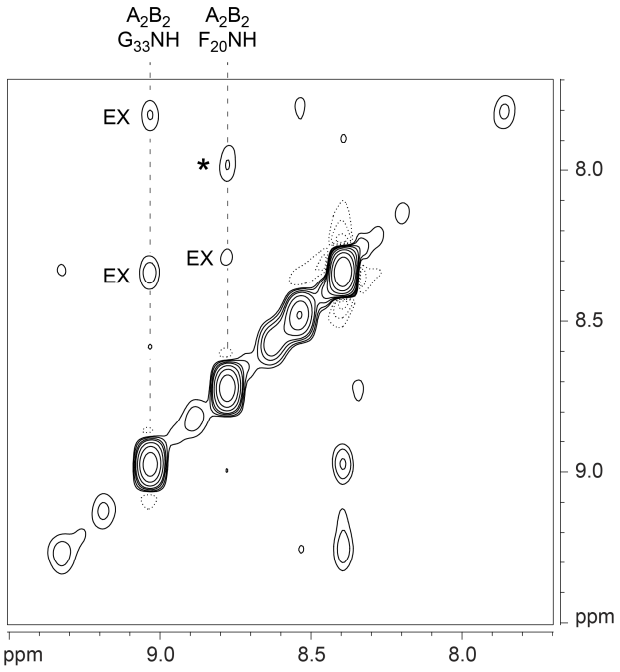

Figure S3.3. ^{15}N-edited NOESY spectrum of the 1:1 mixture of peptides [^{15}N]**1a** and [^{15}N]**1b** at 8.0 mM total concentration in 9:1 H_2O/D_2O at 600 MHz and 293 K. Crosspeaks associated with chemical exchange between the monomers and tetramers are labeled EX. The asterisk (*) indicates a crosspeak from a minor unidentified species associated with the A_2B_2 heterotetramer.

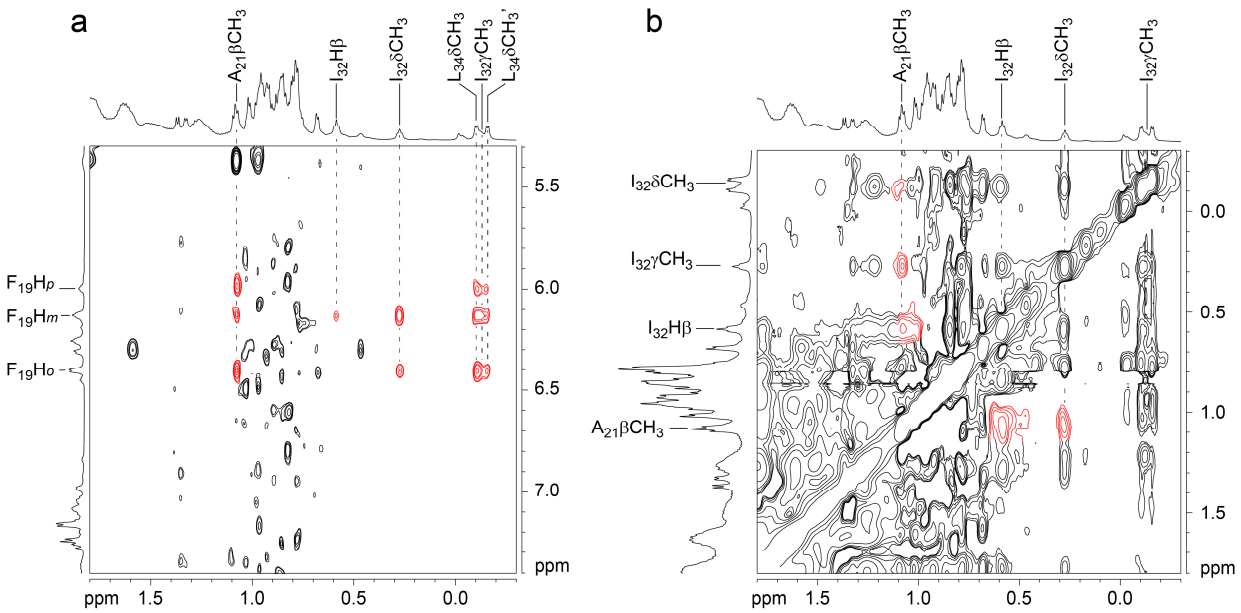

Figure S3.4. Expansions of the ^{1}H NMR NOESY spectrum of the 1:1 mixture of peptides **1a** and **1b** at 8.0 mM total concentration in 9:1 H_2O/D_2O at 600 MHz and 293 K. Key interlayer NOEs between A·A and B·B homodimers from the A_2B_2 heterotetramer are highlighted in red. $F_{19}Ho$, $F_{19}Hm$, and $F_{19}Hp$, correspond to the ortho, meta, and para protons of F_{19}.

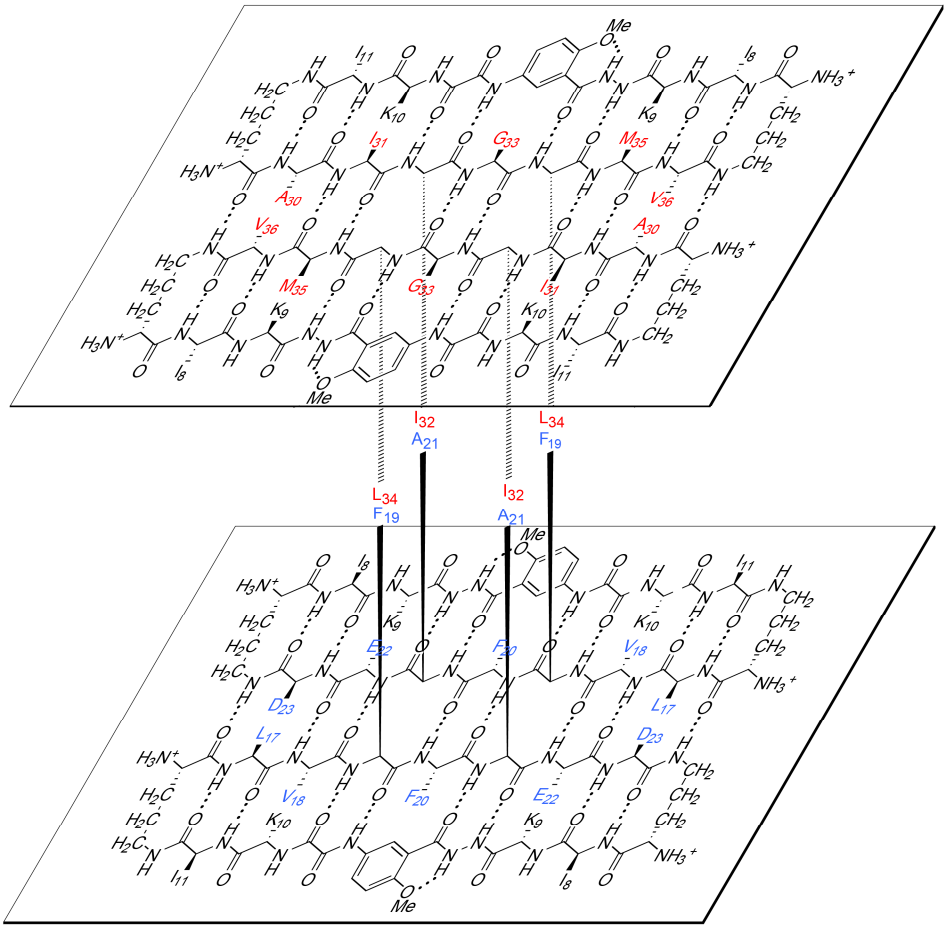

Figure S3.5. A_2B_2 heterotetramer consisting of two hydrogen-bonded homodimers of peptides **1a** and **1b**. Contacts between the side chains of F_{19} and L_{34} and between the side chains of A_{21} and I_{32} are shown, reflecting observed NOEs.

3.II. MATERIALS AND METHODS

Synthesis of Peptides 1

Synthesis and purification of peptides **1a** and **1b**, and [^{15}N]**1a** and [^{15}N]**1b** were performed as described in the preceding chapter.[1]

Fmoc-Protection of ^{15}N-Labeled Amino Acids

Fmoc-protection of ^{15}N-labeled glycine and phenylalanine was performed as described in the preceding chapter.[1,2]

NMR Spectroscopy of Peptides 1

Sample Preparation. NMR spectroscopy of peptides **1a** and **1b** was performed in D_2O (D, 99.96%; Cambridge Isotope Laboratories, Inc.). The solutions were prepared by dissolving a weighed portion of the peptide in the appropriate volume of solvent. The molecular weights of the peptides were calculated as the TFA salts with all amino groups assumed to be protonated (**1a**, M.W. 2223.85 g/mol and **1b**, M.W. 2099.91 g/mol). The solutions were allowed to stand for 24 h to allow complete hydrogen to deuterium exchange of the amide NH protons.

^{1}H NMR, TOCSY, and NOESY Data Collection. NMR spectra were recorded on a Bruker 600 MHz spectrometer with a TBI probe. Presaturation water suppression was applied as needed. TOCSY spectra were recorded with 2048 points in the f_2 dimension and 512 increments in the f_1 dimension with a 150-ms spin-lock mixing time. NOESY spectra were recorded with 2048 points in the f_2 dimension and 512 increments in the f_1 dimension with a 150-ms mixing time.

^{1}H NMR, TOCSY, and NOESY Data Processing. NMR spectra were processed with Bruker XwinNMR software. Automatic baseline correction was applied in both dimensions after phasing the spectra. TOCSY spectra were Fourier transformed to a final matrix size of 2048 x 2048 real points using a Qsinc weighting function (GB = 0.05) and forward linear prediction. NOESY spectra were Fourier transformed to a final matrix size of 2048 x 2048 real points using a Qsinc weighting function (GB = 0.05) and forward linear prediction.

Diffusion-Ordered Spectroscopy (DOSY) Experiments. DOSY experiments were performed on a Bruker 500 MHz spectrometer equipped with a TCI cryoprobe, with a diffusion delay (Δ) of 75-ms and a diffusion gradient length (δ) of 2.5-ms. Sixteen sets of FIDs were recorded with the gradient strength incremented from 5%–95% using a linear ramp. The combined FIDs were Fourier transformed in Bruker's TopSpin™ software to give a pseudo-2D spectrum. After phasing and performing baseline correction, each pseudo-2D spectrum was processed with logarithmic scaling on the Y-axis. The Y-axis was calibrated to the diffusion coefficient of the residual HOD peak in D_2O (1.9×10^{-9} m^2/s at 298 K).[3] The diffusion coefficients of the peptides were read and converted from logarithmic values to linear values.

NMR Spectroscopy of Peptides [^{15}N]1

Sample Preparation. NMR spectroscopy of peptides [^{15}N]**1a** and [^{15}N]**1b** was performed in 9:1 H_2O/D_2O. The solutions were prepared by dissolving a weighed portion of the peptide in the appropriate volume of solvent. The molecular weights of the peptides were calculated as the TFA salts with all amino groups assumed to be protonated ([^{15}N]**1a**, M.W. 2224.85 g/mol and

[^{15}N]**1b**, M.W. 2100.91 g/mol). 4,4-Dimethyl-4-silapentane-1-ammonium trifluoroacetate (DSA) was added as an internal standard for referencing chemical shifts.[4]

^{1}H NMR, ^{1}H,^{15}N HSQC, ^{1}H,^{15}N TOCSY-HSQC (^{15}N-edited TOCSY), and ^{1}H,^{15}N NOESY-HSQC (^{15}N-edited NOESY) Data Collection. NMR spectra were recorded on a Bruker 600 MHz spectrometer with either a TBI probe or a BBFO cryoprobe. Gradient water suppression was applied as needed. ^{1}H,^{15}N HSQC spectra were recorded with 1024 points in the f_2 dimension and 512 increments in the f_1 dimension. ^{1}H,^{15}N TOCSY-HSQC spectra were recorded with a 150-ms spin-lock mixing time, and with 2048 points in the f_3 dimension (^{1}H), one increment in the f_2 dimension (^{15}N), and 512 increments in the f_1 dimension (^{1}H). ^{1}H,^{15}N NOESY-HSQC spectra were recorded with a 150-ms mixing time, and with 2048 points in the f_3 dimension (^{1}H), 1 increment in the f_2 dimension (^{15}N), and 1024 increments in the f_1 dimension (^{1}H).

^{1}H NMR, ^{1}H,^{15}N HSQC, ^{1}H,^{15}N TOCSY-HSQC (^{15}N-edited TOCSY), and ^{1}H,^{15}N NOESY-HSQC (^{15}N-edited NOESY) Data Processing. NMR spectra were Fourier transformed in Bruker XwinNMR software with forward linear prediction and a Qsinc weighting function. Automatic baseline correction was applied in both dimensions after phasing the spectra. The ^{1}H,^{15}N HSQC spectra were processed to a final matrix size of 2048 x 1024 real points and with GB = 0.1 in the f_2 dimension. The ^{1}H,^{15}N TOCSY-HSQC spectra were processed to a final 2D matrix size of 2048 x 1024 real points (f_3, f_1) and with GB = 0.05 in both dimensions. The ^{1}H,^{15}N NOESY-HSQC spectra were processed to a final 2D matrix size of 4096 x 2048 real points (f_3, f_1) and with GB = 0.05 in both dimensions.

Molecular Modeling of Peptides 1a and 1b.

Molecular models of the A_2B_2 heterotetramers were generated using the models and methods from the preceding chapter.[1] The A_4 and B_4 homotetramers of peptides **1a** and **1b** were imported into PyMOL: Peptide monomers were selected to construct the A·A and B·B homodimer subunits within the A·A/B·B topological isomer. Peptide monomers were selected to construct the two A·B heterodimer subunits within the A·B/A·B topological isomer. The dimer subunits were oriented so that the side chains of L_{17}, F_{19}, A_{21}, and D_{23} and the side chains of A_{30}, I_{32}, L_{34}, and V_{36} formed the hydrophobic core of the A_2B_2 heterotetramers.

The coordinates were exported from PyMOL as a .pdb file. The file was imported into MacroModel with the Maestro user interface. Atom types and bond orders were edited as needed to correct errors in bond type and charge. Distance constraints were applied to reflect the folding and dimerization of the macrocycles. Four interlayer distance constraints between the δ-methyl group of Ile_{11} and the methoxy group of Hao were applied to reflect the observed interlayer contacts. Minimization was performed with the MMFFs force field and GB/SA water solvation. All constraints were removed and minimization was repeated to generate a minimum-energy conformation (local minimum). The coordinates were exported in .pdb file format and imported into PyMOL.

Job's Method of Continuous Variation

Nine samples of peptides [^{15}N]**1a** and [^{15}N]**1b** were prepared at 8.0 mM total concentration with mole fractions of peptide [^{15}N]**1b** = 0.00, 0.125, 0.25, 0.375, 0.50, 0.625, 0.75, 0.875, and 1.00. An ^{1}H,^{15}N HSQC spectrum at 600 MHz and 293 K was recorded for each mixture using the data collection and data processing parameters described above. These spectra are shown on pages S40-48.

The spectra were reprocessed in Bruker's TopSpin™ software using a Qsine weighting function to sharpen the crosspeaks for measuring the intensities. One-dimensional ^{15}N spectra from the two-dimensional ^{1}H,^{15}N HSQC spectra were generated by typing "f1sum" in the command line. A stack plot of the ^{15}N spectra is shown on page S49.

The volume integrals of the crosspeaks in the ^{1}H,^{15}N HSQC spectra were measured and normalized to 1.0. Table S3.1 summarizes the volume integrals versus the mole fraction of peptide [^{15}N]**1b**, χ_B.

Table S3.1. Relative integrals of the crosspeaks *1–14* from the ^{1}H,^{15}N HSQC spectra

	A	A_4	B	B_4	A_2B_2		A_3B_1				A_1B_3			
χ_B	*1*	*2*	*3*	*4*	*5*	*6*	*7*	*8*	*9*	*10*	*11*	*12*	*13*	*14*
0.000	0.0664	0.9336	0.0000	0.0000	0.0000	0.0000	0.0000	0.0000	0.0000	0.0000	0.0000	0.0000	0.0000	0.0000
0.125	0.0449	0.6883	0.0608	0.0000	0.0438	0.0435	0.0363	0.0268	0.0427	0.0125	0.0000	0.0000	0.0000	0.0003
0.250	0.0332	0.4359	0.1089	0.0005	0.1309	0.1345	0.0255	0.0421	0.0318	0.0466	0.0031	0.0030	0.0028	0.0012
0.375	0.0281	0.2986	0.1445	0.0042	0.1854	0.1785	0.0424	0.0393	0.0335	0.0239	0.0039	0.0076	0.0064	0.0037
0.500	0.0177	0.1350	0.1987	0.0209	0.2330	0.2310	0.0205	0.0308	0.0262	0.0281	0.0195	0.0158	0.0087	0.0140
0.625	0.0115	0.0608	0.2699	0.0384	0.2423	0.2325	0.0207	0.0206	0.0148	0.0134	0.0278	0.0224	0.0216	0.0033
0.750	0.0082	0.0096	0.3095	0.1466	0.1782	0.1734	0.0037	0.0097	0.0071	0.0055	0.0435	0.0390	0.0293	0.0368
0.875	0.0044	0.0009	0.3820	0.2741	0.0812	0.0783	0.0035	0.0020	0.0000	0.0006	0.0466	0.0351	0.0475	0.0440
1.000	0.0000	0.0000	0.4796	0.5204	0.0000	0.0000	0.0000	0.0000	0.0000	0.0000	0.0000	0.0000	0.0000	0.0000

To generate the Job plot, the relative integrations of the monomers, homotetramers, and heterotetramers were plotted versus the mole fraction χ_B. The normalized integrals of crosspeaks *1* and *2* were used for the relative integrations of the A monomer and A_4 homotetramer, respectively; the normalized integrals of crosspeaks *3* and *4* were used for the relative integrations of the B monomer and B_4 homotetramer, respectively. The sum of the normalized integrals of crosspeaks *5* and *6* was used for the relative integration of the A_2B_2 heterotetramer; the sum of the normalized integrals of crosspeaks *7–10* was used for the relative integration of the A_3B_1 heterotetramer; and the sum of the normalized integrals of crosspeaks *11–14* was used for the relative integration of the A_1B_3 heterotetramer. Table S3.2 summarizes the relative integrations. Figure 8 illustrates the resulting Job plot.

Table S3.2. Relative integrations for the monomers, homotetramers, and heterotetramers

χ_B	A	B	A_4	A_3B_1	A_2B_2	A_1B_3	B_4
0.000	0.0664	0.0000	0.9336	0.0000	0.0000	0.0000	0.0000
0.125	0.0449	0.0608	0.6883	0.1183	0.0873	0.0003	0.0000
0.250	0.0332	0.1089	0.4359	0.1459	0.2654	0.0102	0.0005
0.375	0.0281	0.1445	0.2986	0.1391	0.3639	0.0216	0.0042
0.500	0.0177	0.1987	0.1350	0.1057	0.4640	0.0581	0.0209
0.625	0.0115	0.2699	0.0608	0.0695	0.4748	0.0751	0.0384
0.750	0.0082	0.3095	0.0096	0.0260	0.3516	0.1486	0.1466
0.875	0.0044	0.3820	0.0009	0.0060	0.1595	0.1731	0.2741
1.000	0.0000	0.4796	0.0000	0.0000	0.0000	0.0000	0.5204

3.III. Mathematical Derivations for the Monomer–Homotetramer–Heterotetramer Equilibrium Model

This section describes the mathematical derivations for the monomer–homotetramer–heterotetramer equilibrium model. This model was used for nonlinear least-squares fitting of the Job plot and for generating simulated Job plots. The mathematical derivations are based on those developed by Collum and co-workers in the supporting information of Liou, L. R; McNeil, A. J.; Ramirez, A.; Toombes, G. E. S.; Gruver, J. M.; Collum, D. B. *J. Am. Chem. Soc.* **2008**, *130*, 4859–4868. The following subsections describe (A) the mathematical derivations with general equations; (B) the implementation for homotetramers and heterotetramers; (C) and our implementation for monomers, homotetramers, and heterotetramers.

A. General Equations

In this subsection, I describe the mathematical derivations with general equations. The general equations calculate the concentrations of homooligomers and heterooligomers (that are the same size) as a function of the mole fraction of compounds “A” and “B”:

$$A_N,\ A_{N-1}B_1,\ A_{N-2}B_2,\ A_{N-3}B_3,\ \ldots\ B_N$$

The stoichiometry of the oligomers can be generalized using the term “A_nB_{N-n}”, where the value of N reflects oligomer size; the value of n reflects the number of "A" subunits; and the value of $N-n$ reflects the number of "B" subunits. For example, $N = 4$ and $n = 1$ for an A_1B_3 heterotetramer.

Three main factors influence the relative concentration of oligomers A_nB_{N-n} at equilibrium: multiplicity, free energy, and chemical potential. The equations developed by Collum and co-workers combine these factors for calculating the concentrations of homooligomers and heterooligomers.

1. **Multiplicity (M_n)**: The number of ways the "A" and "B" subunits can be arranged within an oligomer A_nB_{N-n}. Each unique arrangement is called a permutation (ρ). Oligomers that have multiple permutations are present in larger concentrations than oligomers that have only one. The multiplicity or the number of permutations of an oligomer A_nB_{N-n} can be determined with Pascal's triangle or by using binomial theorem, which is shown here:

$$M_n = \frac{N}{(N - n)! \times n!}$$

2. **Free Energy (g_ρ)**: The relative stability of an oligomer permutation ρ. Permutations with the same stoichiometry often have the same relative stability. [In the A_2B_2 heterotetramer of peptides **1a** and **1b**, the A·A/B·B and A·B/A·B topological isomers do not have the same relative stability.] The variable $\phi_{N,n}$ relates the free energy of each permutation to the relative stability.

$$-g_\rho = kT \ln (\phi_{N,n})$$

3. **Chemical Potential (μ_A and μ_B)**: The potential energy associated with the moles of compound "A" and the moles of compound "B" in a mixture. The mole fraction of the compounds reflects the relative chemical potential. The relative chemical potential of μ_A and μ_B shifts as the mole fraction of A and B is varied in a Job's method of continuous variation experiment. For a mixture of tetramers, when the mole fraction of A is greater than the mole fraction of B, the concentration the A_3B_1 heterotetramer is greater than the concentration of the A_1B_3 heterotetramer.

To calculate the concentration of a permutation, the free energy and the chemical potential terms are combined to give the following equation:

$$[\,\rho\,] = C \times \exp\left(\frac{-g_\rho + n_\rho\mu_A + (N - n_\rho)\mu_B}{kT}\right) \quad (1)$$

The free energy g_ρ is the measure of the relative stability of the corresponding permutation ρ; the value of n_ρ is the number of the "A" subunits within the permutation ρ; the value of μ_A is the chemical potential of compound A; the value of μ_B is the chemical potential of compound B. The constant *C* relates oligomerization propensity to the total concentration.

The concentration of an oligomer A_nB_{N-n} is the sum of the concentrations of permutations that have the same stoichiometry ($\rho;n_\rho = n$). For calculating the concentration of an oligomer A_nB_{N-n}, the multiplicity term is combined with the free energy term and chemical potential term to give the following equation:

$$[A_nB_{N-n}] = \sum_{\rho;n_\rho = n} [\,\rho\,] = C \times \exp\left(\frac{n_\rho\mu_A + (N - n_\rho)\mu_B}{kT}\right) \times \sum_{\rho;n_\rho = n} \exp\left(\frac{-g_\rho}{kT}\right) \quad (2)$$

$$= C \times \exp\left(\frac{n_\rho\mu_A + (N - n_\rho)\mu_B}{kT}\right) \times M_n \times \left\langle \exp\left(\frac{-g_\rho}{kT}\right)\right\rangle_{\rho;n_\rho = n} \quad (3)$$

In this equation, the concentrations of permutations ρ that have the same stoichiometry ($\rho;n_\rho = n$) are multiplied by the multiplicity M_n to give the oligomer concentration $[A_nB_{N-n}]$. In a Job's method of continuous variation experiment, the sum of the concentrations of permutations ρ that have the same stoichiometry ($\rho;n_\rho = n$) gives the oligomer concentration $[A_nB_{N-n}]$.

To simplify equation (3), the variables a and b were used to represent the effective chemical potentials μ_A and μ_B, and the variable $\phi_{N,n}$ was used to represent the relative stability of an oligomer A_nB_{N-n}.

$$a = \exp\left(\frac{\mu_A}{kT}\right) \qquad b = \exp\left(\frac{\mu_B}{kT}\right) \qquad \phi_{N,n} = \langle \exp\left(\frac{-g_\rho}{kT}\right)\rangle_{\rho;n_\rho = n}$$

Incidentally, the values of a and b are related to each other such that

$$a + b = 1 \text{ and } \frac{a}{b} = \frac{a}{1 - a}$$

Incorporation of these variables into equation (3) gives the following equation:

$$[A_nB_{N-n}] = C \times M_n \times \phi_{N,n} \times a^n \times b^{N-n} \tag{4}$$

Equation (4) is the general equation for calculating oligomer concentration. To calculate the relative concentration of an oligomer, the concentration is divided by the sum of the concentrations of all the oligomers A_jB_{N-j} :

$$\frac{[A_nB_{N-n}]}{\sum_{j=0}^{N}[A_jB_{N-j}]} = \frac{C \times M_n \times \phi_{N,n} \times a^n \times b^{N-n}}{\sum_{j=0}^{N} C \times M_j \times \phi_{N,j} \times a^j \times b^{N-j}} \tag{5}$$

B. Equations for Homotetramers and Heterotetramers

In this section, I describe the equations for homotetramers and heterotetramers ($N = 4$). Heterotetramers have multiple permutations ρ, which increases the concentrations of the heterotetramers relative to the concentrations of the homotetramers. Table S3.3 summarizes the permutations ρ of the homotetramers and heterotetramers.

Table S3.3. Permutations ρ of the homotetramers and heterotetramers

stoichiometry A_nB_{N-n}	multiplicity M_n	permutation ρ
A_4	1	AAAA
A_3B_1	4	AAAB, AABA, ABAA, AAAB
A_2B_2	6	AABB, ABAB, BAAB, BABA, BBAA, ABBA
A_1B_3	4	ABBB, BABB, BBAB, BBBA
B_4	1	BBBB

The parameters $\phi_{N,n}$ are ascribed to each of the homotetramers and heterotetramers, where the N and n are integers in which the value of N describes the oligomer size and the value of n describes the number of "A" subunits. The value of each $\phi_{N,n}$ reflects the relative stability of each homotetramer or heterotetramer. The parameters $\phi_{4,4}$, $\phi_{4,3}$, $\phi_{4,2}$, $\phi_{4,1}$, and $\phi_{4,0}$ describe the relative stabilities of A_4, A_3B_1, A_2B_2, A_1B_3, and B_4, respectively. The following equations are based on equation (4) and contain these parameters for calculating the concentrations of each homotetramer and heterotetramer:

$$[A_4] = 1 \times C \times \phi_{4,4} \times a^4 \quad (6)$$

$$[A_3B_1] = 4 \times C \times \phi_{4,3} \times a^3 b^1 \quad (7)$$

$$[A_2B_2] = 6 \times C \times \phi_{4,2} \times a^2 b^2 \quad (8)$$

$$[A_1B_3] = 4 \times C \times \phi_{4,1} \times a^1 b^3 \quad (9)$$

$$[B_4] = 1 \times C \times \phi_{4,0} \times b^4 \quad (10)$$

The following equation calculates the relative integration ($I_{N,n}$) by dividing the integration of one tetramer by the sum of the integrations of all tetramers.

$$I_{N,n} = \frac{C \times M_n \times \phi_{N,n} \times a^n \times b^{N-n}}{\sum_{j=0}^{N} C \times M_j \times \phi_{N,j} \times a^j \times b^{N-j}} \tag{11}$$

The following equations calculate the relative integration of each homotetramer and heterotetramer:

$$I_{4,4} = \frac{\phi_{4,4} a^4}{\phi_{4,4} a^4 + 4\phi_{4,3} a^3 b^1 + 6\phi_{4,2} a^2 b^2 + 4\phi_{4,1} a^1 b^3 + \phi_{4,0} b^4} \tag{12}$$

$$I_{4,3} = \frac{4\phi_{4,3} a^3 b^1}{\phi_{4,4} a^4 + 4\phi_{4,3} a^3 b^1 + 6\phi_{4,2} a^2 b^2 + 4\phi_{4,1} a^1 b^3 + \phi_{4,0} b^4} \tag{13}$$

$$I_{4,2} = \frac{6\phi_{4,2} a^2 b^2}{\phi_{4,4} a^4 + 4\phi_{4,3} a^3 b^1 + 6\phi_{4,2} a^2 b^2 + 4\phi_{4,1} a^1 b^3 + \phi_{4,0} b^4} \tag{14}$$

$$I_{4,1} = \frac{4\phi_{4,1} a^1 b^3}{\phi_{4,4} a^4 + 4\phi_{4,3} a^3 b^1 + 6\phi_{4,2} a^2 b^2 + 4\phi_{4,1} a^1 b^3 + \phi_{4,0} b^4} \tag{15}$$

$$I_{4,0} = \frac{\phi_{4,0} b^4}{\phi_{4,4} a^4 + 4\phi_{4,3} a^3 b^1 + 6\phi_{4,2} a^2 b^2 + 4\phi_{4,1} a^1 b^3 + \phi_{4,0} b^4} \tag{16}$$

C. Equations for Monomers, Homotetramers, and Heterotetramers

In this section, I describe how I modified the equations to accommodate the equilibrium of the monomers with the homotetramers and heterotetramers. The result is the equation used for the monomer–homotetramer–heterotetramer equilibrium model for nonlinear least-squares fitting of the Job plot.

$$A,\ B,\ A_4,\ A_3B_1,\ A_2B_2,\ A_1B_3,\ B_4$$

I used the following equations to calculate the concentrations of the monomers as a function of their respective relative stabilities $\phi_{N,n}$ and the chemical potentials a and b.

$$[A] = C \times \phi_{1,1} \times a \tag{17}$$

$$[B] = C \times \phi_{1,0} \times b \tag{18}$$

I used the mass balance equation to accommodate the total concentration of compounds A and B. The total concentration has little or no effect on the equilibria among homotetramers and heterotetramers. By contrast, the total concentration is critical in the equilibria of the monomers with the homotetramers and heterotetramers. The mass balance equation gives the total concentration of compounds A and B ($[A]_{total}$ and $[B]_{total}$) as a function of the monomers, homotetramers, and heterotetramers.

$$[A]_{total} + [B]_{total} = [A] + [B] + 4([A_4] + [A_3B_1] + [A_2B_2] + [A_1B_3] + [B_4]) \tag{19}$$

Substitution of equations (6), (7), (8), (9), (10), (17), and (18) into the mass balance equation gives the following equation:

$$[A]_{total} + [B]_{total} = C(\phi_{1,1}\, a + \phi_{1,0}\, b) + 4C(\phi_{4,4}\, a^4 + 4\phi_{4,3}\, a^3b^1 + 6\phi_{4,2}\, a^2b^2 + 4\phi_{4,1}\, a^1b^3 + \phi_{4,0}\, b^4) \tag{20}$$

Equation (20) was simplified using the following identities, which represent a and b in terms of α and 1 − α:

$$\alpha = a / (a + b) \qquad x = a + b \qquad a = \alpha x \qquad b = (1 - \alpha)x$$

Substitution of $a = \alpha x$ and $b = (1 - \alpha)x$ into equation (20) gives the following equation:

$$[A]_{total} + [B]_{total} = xC(\phi_{1,1}\,\alpha + \phi_{1,0}\,(1 - \alpha)) +$$

$$4x^4C(\phi_{4,4}\,\alpha^4 + 4\phi_{4,3}\,\alpha^3(1 - \alpha)^1 + 6\phi_{4,2}\,\alpha^2(1 - \alpha)^2 + 4\phi_{4,1}\,\alpha^1(1 - \alpha)^3 + \phi_{4,0}\,(1 - \alpha)^4) \qquad (21)$$

Equation (21) was simplified by representing the concentrations of the monomers and tetramers in terms of M_{total} and T_{total}:

$$M_{total} = xC(\phi_{1,1}\,\alpha + \phi_{1,0}\,(1 - \alpha))$$

$$T_{total} = 4x^4C(\phi_{4,4}\,\alpha^4 + 4\phi_{4,3}\,\alpha^3(1 - \alpha)^1 + 6\phi_{4,2}\,\alpha^2(1 - \alpha)^2 + 4\phi_{4,1}\,\alpha^1(1 - \alpha)^3 + \phi_{4,0}\,(1 - \alpha)^4)$$

Substitution of M_{total} and T_{total} into the mass balance equation gives the equation for a monomer−tetramer (monomer−homotetramer−heterotetramer) equilibrium model:

$$[A]_{total} + [B]_{total} = x\,M_{total} + 4x^4\,T_{total} \qquad (22)$$

Setting the equation equal to zero gives the following fourth-order polynomial:

$$x\,M_{total} + 4x^4\,T_{total} - ([A]_{total} + [B]_{total}) = 0 \qquad (23)$$

The fourth-order polynomial was solved for x using Mathematica 10.3 (Wolfram Research, Champaign, IL), which gave a set of four roots (not shown). Each root was evaluated under typical conditions of monomer and tetramer equilibrium (e.g. $M_{total} = 1.4$, $T_{total} = 1.65$, and $([A]_{total} + [B]_{total}) = 8$). The root that gave a non-negative value of x was used as the monomer–homotetramer–heterotetramer equilibrium model.

3.IV. NONLINEAR LEAST-SQUARES FITTING OF THE JOB PLOT

This section describes how I used the monomer–homotetramer–heterotetramer equilibrium model for nonlinear least-squares fitting of the Job Plot. To perform the fit, the model was incorporated into a .m script and executed with a series of scripts in MATLAB 2015b. The scripts are based on those developed by Collum and co-workers in the supporting information of Liou, L. R; McNeil, A. J.; Ramirez, A.; Toombes, G. E. S.; Gruver, J. M.; Collum, D. B. *J. Am. Chem. Soc.* **2008**, *130*, 4859–4868.

The following subsections describe the process of fitting the model to our experimental data (Table S3.2) from the Job's method of continuous variation experiment. The subsections also contain the code from each script along with annotations that describe how the code is used.

> The code is indicated by bracketing the code text with bars along the left- and right-hand side, as shown here.

Annotations for the code appear in between the bracketed text, as shown here.

A. End User Instructions

1. Copy the code from each subsection into its own text file, but do not transfer the annotations. Save each file into the same folder or directory using the following file names:

   data_Monomer_Tetramer.m
   try_fit.m
   refine_fit.m
   multimers.m
   populations_tetramer.m
   populations_monomer.m
   error_of_model.m
2. Open MATLAB and navigate the "Current Folder" of the program to the directory where the .m scripts were saved.
3. Load the data from the data_Monomer_Tetramer.m file into MATLAB. The data can be loaded in one of two ways: by opening the script with MATLAB and clicking "Run" in the window or by typing the file name into the MATLAB command line and pushing enter.

4. Run the try_fit.m script. This script can be run with or without Expt_Errors. To run the script without Expt_Errors, type the following try_fit function into the command line and push enter:

   try_fit(Xb, Ctotal, phi_monomer, peak_assignment_monomer, phi_tetramer, peak_assignment_tetramer, Expt_Populations)
   To run the try_fit.m script with Expt_Errors, type the following try_fit function into the command line and push enter:
   try_fit(Xb, Ctotal, phi_monomer, peak_assignment_monomer, phi_tetramer, peak_assignment_tetramer, Expt_Populations, Expt_Errors)
5. The data points in the figure should resemble the data shown in Figure 8. The curves that overlay the data should resemble the curves from the simulated Job plot in Figure 9e.

6. To run the refine_fit.m script without Expt_Errors, type the following refine_fit function into the command line and push enter:

   refine_fit(Xb,Ctotal,phi_monomer, peak_assignment_monomer, phi_tetramer, peak_assignment_tetramer, Expt_Populations, phi_constant)
   To run the refine_fit.m script with Expt_Errors, type the following refine_fit function into the command line and push enter:
   refine_fit(Xb,Ctotal,phi_monomer, peak_assignment_monomer, phi_tetramer, peak_assignment_tetramer, Expt_Populations, phi_constant, Expt_Errors)
   After the fit, the final phi values shown in the MATLAB terminal are the optimized phi values. These values should be comparable the phi values listed in Figure 8.
7. Make a copy of the file data_Monomer_Tetramer.m to a new file called data_Monomer_Tetramer_new.m. Replace the phi values with the optimized values from the refine_fit.m script.

8. Load the new data file data_Monomer_Tetramer_new.m into MATLAB. Type the try_fit function into the command line and push enter to observe the optimized fit.

B. Definitions

1. **Xb(j)** is the mole fraction χ_B.

2. **Ctotal** is the input for the total concentration of each mixture.

3. **Expt_Populations** is the experimental data input for the relative integrations of the monomers, homotetramers, and heterotetramers (Table S3.2). These data are referred to as the "experimental populations".

4. **Expt_Errors** is the input for the error of the measurements.

5. **peak_assignment_monomer** and **peak_assignment_tetramer** are column identifiers assigned to each monomer and tetramer population.

6. **phi_monomer** and **phi_tetramer** are measures of the relative stabilities of the monomers and tetramers. These values are assigned to each monomer, homotetramer, and heterotetramer population and are used by the monomer–homotetramer–heterotetramer equilibrium model for calculating the relative concentrations of each population.

7. **phi_constant** is the input that dictates whether a phi_monomer or phi_tetramer value remains fixed or is allowed to vary during nonlinear least-squares fitting. A value of 1 allows the corresponding phi to vary; a value of 0 keeps the corresponding phi fixed.

8. **Expt_weights** is the input for the error of each data point and is used for weighting the error of each data point. The data points are weighted equally if nothing is entered.

9. **conc_monomer** and **conc_tetramer** are used for calculating and storing the concentrations for each monomer, homotetramer, and heterotetramer population. [Note that even though the term concentration is used, the scripts are actually calculating the integrations of the monomer and tetramer populations.]

10. **pop_monomer** and **pop_tetramer** are used to temporarily store calculated values for the concentrations (relative integrations) of each monomer or tetramer population. These data are referred to as the calculated (predicted) populations.

11. **Model_Populations** is the final output for the concentrations (relative integrations) of the monomers, homotetramers, and heterotetramers.

12. **mean_error** weighted standard deviation of the residuals over the entire fit.

13. **pop_error(1,j)** is the mean error of experimental populations – calculated populations. The value could be negative, zero, or positive.

14. **pop_error(2,j)** is the root mean square error of experimental populations – calculated populations. The value is always positive.

15. **phi_dimer_new** and **phi_tetramer_new** are the new values of each phi after the fit.

16. **error** is the root mean square error of the new calculated populations.

C. Monomers, Homotetramers, and Tetramers: Data

This script stores the experimental populations and the initial values for performing the fit.

This code clears all stored information in the command line and closes all figures.

```
clear variables;
close all;
clc;
```

This code is the input for the total concentration of the mixtures, which is designated Ctotal. The number of values in Ctotal equal the number of samples studied. In this case, nine samples were studied.

```
Ctotal = [0.008 0.008 0.008 0.008 0.008 0.008 0.008 0.008 0.008];
```

This code is the input the mole fraction χ_B, which is designated Xb.The values entered in Xb equal the mole fraction of each mixture studied. The values are listed from lowest to highest.

```
Xb = [0.00 0.125 0.25 0.375 0.50 0.625 0.75 0.875 1.00];
```

This code is the input for the experimental populations: the relative integrations from the Job's method of continuous variation experiment (Table S3.2). Each column lists the relative integrations of the monomer and tetramer populations in the following order: A, B, A_4, A_3B_1, A_2B_2, A_1B_3, B_4. The columns are separated by a space. Each row lists the relative integrations of the mole fractions Xb listed in the following order: 0.00, 0.125, 0.25, 0.375, 0.50, 0.625, 0.75, 0.875, and 1.00. The rows are separated by a semicolon.

```
Expt_Populations = [
0.0664  0.0000  0.9336  0.0000  0.0000  0.0000  0.0000;
0.0449  0.0608  0.6883  0.1183  0.0873  0.0003  0.0000;
0.0332  0.1089  0.4359  0.1459  0.2654  0.0102  0.0005;
0.0281  0.1445  0.2986  0.1391  0.3639  0.0216  0.0042;
0.0177  0.1987  0.1350  0.1057  0.4640  0.0581  0.0209;
0.0115  0.2699  0.0608  0.0695  0.4748  0.0751  0.0384;
0.0082  0.3095  0.0096  0.0260  0.3516  0.1486  0.1466;
0.0044  0.3820  0.0009  0.0060  0.1595  0.1731  0.2741;
0.0000  0.4796  0.0000  0.0000  0.0000  0.0000  0.5204;];
```

The Expt_Errors input is optional for the fit. These values should be listed for the monomer and tetramer populations in the following order: A, B, A_4, A_3B_1, A_2B_2, A_1B_3, B_4, which is the same order used for the populations in the Expt_Populations input.

```
% Expt_Errors = [;];
```

The peak_assignment_monomer and peak_assignment_tetramer are inputs that designate the column for each monomer or tetramer. For a given monomer or tetramer, the assignment value specifies which column the data should be read from or stored in. The peak_assignment_monomer values are listed in the following order: A, B; the peak_assignment_tetramer values are listed in the following order: A_4, A_3B_1, A_2B_2, A_1B_3, B_4.

```
peak_assignment_monomer = [1 5];
peak_assignment_tetramer = [ 1 2 3 4 5 ];
```

The initial phi values are all set to one.

The phi_monomer values are listed in the following order: A, B; the phi_tetramer values are listed in the following order: A_4, A_3B_1, A_2B_2, A_1B_3, B_4.

```
phi_monomer = [1 1];
phi_tetramer = [1 1 1 1 1];
```

The phi_constants that are set to 1 allow the phi value to be refined with the refine_fit.m script; the phi_constants that are set to 0 keep the value fixed during the refine_fit.m script.

The phi_constant values are listed in the following order: A, B, A_4, A_3B_1, A_2B_2, A_1B_3, B_4. The phi_constant for the A_4 homotetramer was fixed so that the refine_fit.m script gives a unique solution.

```
phi_constant = [1 1 0 1 1 1 1];
```

D. Monomers, Homotetramers, and Tetramers: Try Fit

This script plots the experimental populations, and also plots the populations calculated from the phi values. The two plots are overlayed in a new window. The experimental populations are plotted versus the mole fraction Xb as open circles; the calculated populations are plotted versus the mole fraction Xb as smooth lines. The script also determines the error between the experimental populations and the calculated populations then prints these values in the MATLAB terminal.

```
function try_fit(Xb, Ctotal,...
        phi_monomer, peak_assignment_monomer,...
        phi_tetramer, peak_assignment_tetramer,...
        Expt_Populations, Expt_Errors)
```

This code determines whether Expt_Errors are entered.

```
        if(nargin<8)
           Expt_weights=ones(size(Expt_Populations));
        else
           Expt_weights=1./(Expt_Errors+mean(mean(Expt_Errors)));
        end
```

This code plots the experimental populations of the monomers and tetramers from the Expt_Populations input.

```
        hold on ; cscheme= 'kybmgcrkybmgcr'; axis([0 1 0 1]); xlabel('X_B');
        ylabel('Relative Integration');
        for j=1:size(Expt_Populations,2)
           if (nargin<8)
              plot(Xb, Expt_Populations(:,j),sprintf('%so',cscheme(j)));
           else
              errorbar(Xb, Expt_Populations(:,j), Expt_Errors(:,j),sprintf('%so',cscheme(j)));
           end
        end
```

This code calculates the monomer and tetramer populations using the initial values of the phi's entered.

```
XBc = (0:0.01:1);
Ctotalac = Ctotal(1)*ones(size(XBc));
[conc_monomers, conc_tetramers] = multimers(XBc, Ctotalac,...
                                phi_monomer, phi_tetramer);
```

This code stores the calculated monomer and tetramer populations and stores them in a matrix.

```
pop_tetramer = populations_tetramer(conc_monomers,...
   peak_assignment_monomer, conc_tetramers, peak_assignment_tetramer);

pop_monomer = populations_monomer(conc_monomers,...
   peak_assignment_monomer, conc_tetramers, peak_assignment_tetramer);

pop_tetramer_corrected = pop_tetramer-pop_monomer;
pop_combined = horzcat(pop_monomer(:,1),...
   pop_monomer(:,5),pop_tetramer_corrected);
```

This code plots the calculated populations.

```
for j=1:size(pop_combined,2)
   plot(XBc,pop_combined(:,j),sprintf('%c',cscheme(j)) );
end
```

This code compares the experimental and the calculated populations, then calculates and displays the error.

```
[mean_error, pop_error] = error_of_model(Xb, Ctotal,...
   phi_monomer, peak_assignment_monomer,...
   phi_tetramer, peak_assignment_tetramer,...
   Expt_Populations, Expt_weights);

N = length(horzcat(phi_monomer, phi_tetramer)) - 1;
fprintf(1,'\nThe Mean mismatch is %f percent.\n\n', mean_error*100);

for j=1:size(pop_error, 2)
   fprintf(1,'Predicted value of Population %d exceeds measurement by %f percent\n
and mean square error of %f percent.\n\n',j, pop_error(1,j)*100,pop_error(2,j)*100);
end
```

E. Monomers, Homotetramers, and Tetramers: Refine Fit

This script performs the nonlinear least-squares fitting. The script optimizes the phi values to match the calculated populations to the experimental populations. The script reports the new phi values and the root mean square difference between the calculated and the experimental populations.

```
function [phi_dimer_new, phi_tetramer_new, error] = refine_fit(Xb,Ctotal,...
        phi_monomer, peak_assignment_monomer,...
        phi_tetramer, peak_assignment_tetramer,...
        Expt_Populations, phi_constant, Expt_Errors)
```

This code determines whether Expt_errors are entered.

```
    if (nargin<9)
       Expt_weights = ones(size(Expt_Populations));
    else
       Expt_weights = 1./( Expt_Errors + mean(mean(Expt_Errors)));
    end
```

This code merges the monomer Expt_Populations and the tetramer Expt_Populations into a single input.

```
    phimerge = [phi_monomer, phi_tetramer];
    idx_monomer = [1 2]; idx_tetramer = [3 4 5 6 7];
    param = [1:length(phimerge)];
```

This code sets the initial step size used to optimize the phi values; the initial step size is 10%.

```
    step_size = 0.1*phi_constant.*phimerge(param);
    N_no_progress = 0;
    N_max_trials = 30;
```

This code compares the calculated and experimental populations of the monomers and tetramers, then calculates and displays the error of the model.

```
[error_best, temp] = error_of_model(Xb,Ctotal,...
        phimerge(idx_monomer), peak_assignment_monomer,...
        phimerge(idx_tetramer), peak_assignment_tetramer,...
        Expt_Populations, Expt_weights);

    fprintf(1,'\n Initial Error of Fit = %f percent.\n', error_best * 100);
```

This code is a "for while" loop that reduces the error of the model by optimizing the phi values.

```
    while (N_no_progress < N_max_trials)
        flag = 0;
        for k=1:length(param)
```

This code adjusts the value of phi to the "right" and to the "left".

```
            phi_testr = phimerge;
            phi_testr(param(k))=abs(phimerge(param(k)) + step_size(k));
            [error_testr, temp] = error_of_model(Xb,Ctotal,...
                phi_testr(idx_monomer), peak_assignment_monomer,...
                phi_testr(idx_tetramer), peak_assignment_tetramer,...
                Expt_Populations, Expt_weights);

            phi_testl = phimerge;
            phi_testl(param(k))=abs(phimerge(param(k)) - step_size(k));
            [error_testl, temp] = error_of_model(Xb,Ctotal,...
                phi_testl(idx_monomer), peak_assignment_monomer,...
                phi_testl(idx_tetramer), peak_assignment_tetramer,...
                Expt_Populations, Expt_weights);
```

This code determines which adjustment of phi decreases the error of the model. If either the right or the left value decreases the error, then that value is stored and the loop repeats again. If neither the right or the left value decreases the error, then the step is flagged and the size of the step is reduced.

```
        if (error_testr < error_best)
            error_best = error_testr;
            phimerge = phi_testr;
            step_size(k) = step_size(k) * 1.5;
            N_no_progress = 0;

        elseif (error_testl < error_best)
            error_best = error_testl;
            phimerge = phi_testl;
            step_size(k) = step_size(k) * 1.5;
            N_no_progress = 0;

        else
            flag = flag + 1;
        end
    end

    if (flag >= length(param))
        step_size = step_size * (0.75 + 0.25 * rand);
        N_no_progress = N_no_progress + 1;
    end
```

This code displays the new fit after each phi has been adjusted

```
    fprintf(1,'\n\n Error - %f , Last Good Step - %d , Mean Step Size - %f'...
    ,error_best, N_no_progress, 100*mean(step_size) );
    fprintf('\n     Phi Monomer - '); fprintf(1,'%f ', phimerge(idx_monomer));
    fprintf(1,'\n     Phi Tetramer - '); fprintf(1,'%f ',phimerge(idx_tetramer));

    end

    error = error_best;
    phi_monomer_new = phimerge(idx_monomer);
    phi_tetramer_new = phimerge(idx_tetramer);
```

F. Monomers, Homotetramers, and Tetramers: Multimers

For each mole fraction Xb, this script calculates the concentrations (relative integrations) of the monomer and tetramer populations using the inputs: Xb, Ctotal, phi_monomer, and phi_tetramer.

```
function [conc_monomer, conc_tetramer] = multimers(Xb, Ctotal,...
      phi_monomer, phi_tetramer)

   for j=1:length(Xb)
      [conc_monomer(j,:), conc_tetramer(j,:)] = bisect(Xb(j), Ctotal(j),...
       phi_monomer, phi_tetramer);
   end
```

This code is the bisection function, which optimizes the "relative chemical potential" until the value reflects the mole fraction of the experimental mole fraction.

```
function [conc_monomer, conc_tetramer] = bisect(Xb, Ctotal,...
       phi_monomer, phi_tetramer)

   tolerance = 1e-6;
   bmax = 1; bmin = 0;
   [Xmin, conc_monomer, conc_tetramer] = Cparametric(bmin,...
       phi_monomer, phi_tetramer, Ctotal);
   [Xmax, conc_monomer, conc_tetramer] = Cparametric(bmax,...
       phi_monomer, phi_tetramer, Ctotal);

   while ((Xmax - Xb) > tolerance)
       btest = (bmin + bmax) / 2;
   [Xtest, conc_monomer, conc_tetramer] = Cparametric(btest, phi_monomer,...
       phi_tetramer, Ctotal);

      if (Xtest > Xb)
         bmax = btest; Xmax = Xtest;
      else
         bmin = btest; Xmin = Xtest;
      end
end
```

This code is the mathematical model for the monomer and tetramer equilibrium.

```
function [Xb, conc_monomer, conc_tetramer] = Cparametric(b, phi_monomer, phi_tetramer,
Ctotal )

        a = 1 - b;

        Tscale = 1e9;

        Mtotal = (phi_monomer(1)*a + phi_monomer(2)*b);
        Ttotal = Tscale * (phi_tetramer(1) * a^4 + 4 * phi_tetramer(2) * a^3 * b +...
            6 * phi_tetramer(3) * a * a * b * b + 4 * phi_tetramer(4) * a * b^3 +...
            phi_tetramer(5)*b^4);


        Chi = ((1/2)*sqrt(-((9*Ttotal*Mtotal^2+sqrt(3)*sqrt(27*Ttotal^2*Mtotal^4+...
            1024*Ttotal^3*Ctotal^3))^(1/3)/(2*6^(2/3)*Ttotal))+Mtotal/(sqrt(2)*...
            Ttotal*sqrt((9*Ttotal*Mtotal^2+sqrt(3)*sqrt(27*Ttotal^2*Mtotal^4+1024*...
            Ttotal^3*Ctotal^3))^(1/3)/(6^(2/3)*Ttotal)-(4*2^(2/3)*Ctotal)/(3^(1/3)*...
            (9*Ttotal*Mtotal^2+sqrt(3)*sqrt(27*Ttotal^2*Mtotal^4+1024*Ttotal^3*...
            Ctotal^3))^(1/3))))+(2*2^(2/3)*Ctotal)/(3^(1/3)*(9*Ttotal*Mtotal^2+...
            sqrt(3)*sqrt(27*Ttotal^2*Mtotal^4+1024*Ttotal^3*Ctotal^3))^(1/3)))-...
            sqrt((9*Ttotal*Mtotal^2+sqrt(3)*sqrt(27*Ttotal^2*Mtotal^4+1024*Ttotal^3*...
            Ctotal^3))^(1/3)/(6^(2/3)*Ttotal)-(4*2^(2/3)*Ctotal)/(3^(1/3)*(9*Ttotal*...
            Mtotal^2+sqrt(3)*sqrt(27*Ttotal^2*Mtotal^4+1024*Ttotal^3*Ctotal^3))^(1/3)))/...
            (2*sqrt(2)));

        conc_monomer = Chi/Ctotal*[phi_monomer(1)*a, phi_monomer(2)*b];

        conc_tetramer = Tscale * 4 * Chi^4/Ctotal*[phi_tetramer(1)*a*a*a*a,...
            4*phi_tetramer(2)*a*a*a*b, 6*phi_tetramer(3)*a*a*b*b,...
            4*phi_tetramer(4)*a*b*b*b, phi_tetramer(5)*b*b*b*b];


        Xb = sum(conc_monomer.*[0 1])+sum(conc_tetramer.*[0 0.25 0.5 0.75 1]);
```

G. Monomers, Homotetramers, and Tetramers: Tetramer Populations

For all mole fractions Xb in the calculation, the populations_tetramer script stores all of the calculated populations for the tetramers.

```
function result = populations_tetramer(conc_monomer, peak_assignment_monomer,...
   conc_tetramer, peak_assignment_tetramer)

   result = zeros(size(conc_monomer,1), max(max(peak_assignment_monomer),...
   max(peak_assignment_tetramer)));
     N = size(conc_monomer,2);
    for j=1:N
        idx = peak_assignment_monomer(j);
        result(:,idx) = result(:,idx) + conc_monomer(:,j);
    end

    N = size(conc_tetramer,2);

    for j=1:N
        idx = peak_assignment_tetramer(j);
        result(:,idx) = result(:,idx) + conc_tetramer(:,j);
    end
```

H. Monomers, Homotetramers, and Tetramers: Monomer Populations

For all mole fractions Xb in the calculation, the Populations_monomer script stores all of the calculated populations for the tetramers.

```
function pop_monomer = populations_monomer(conc_monomer,...
   peak_assignment_monomer, conc_tetramer, peak_assignment_tetramer)

   result = zeros(size(conc_monomer,1), max(max(peak_assignment_monomer),...
      max(peak_assignment_tetramer)));
   N = size(conc_monomer,2);
   for j=1:N
      idx = peak_assignment_monomer(j);
      result(:,idx) = result(:,idx) + conc_monomer(:,j);
   end

   pop_monomer = result;
   N = size(conc_tetramer,2);

   for j=1:N
      idx = peak_assignment_tetramer(j);
      result(:,idx) = result(:,idx) + conc_tetramer(:,j);
   end
```

I. Monomers, Homotetramers, and Tetramers: Error of Model

This script is called within the try_fit.m and in the refine_fit.m scripts. The script reports the weighted mean error and population error of the fit.

```
function [mean_error, pop_error] = error_of_model(Xb, Ctotal,...
        phi_monomer, peak_assignment_monomer,...
        phi_tetramer, peak_assignment_tetramer,...
        Expt_Populations, Expt_Errors)

         if (nargin<8)
            Expt_weights=ones(size(Expt_Populations));
         else
            Expt_weights = 1./(Expt_Errors + mean(mean(Expt_Errors)));
         end

         [conc_monomers, conc_tetramers] = multimers(Xb,...
            Ctotal, phi_monomer, phi_tetramer);

         pop_tetramer = populations_tetramer(conc_monomers,...
            peak_assignment_monomer, conc_tetramers, peak_assignment_tetramer);

         pop_monomer = populations_monomer(conc_monomers,...
            peak_assignment_monomer, conc_tetramers, peak_assignment_tetramer);

         pop_tetramer_corrected = pop_tetramer-pop_monomer;

         Model_Populations = horzcat(pop_monomer(:,1),...
            pop_monomer(:,5),pop_tetramer_corrected);

         sizeof_Model = size(Model_Populations);
         sizeof_Expt = size(Expt_Populations);

         Model_Populations_Combined = horzcat(conc_monomers, conc_tetramers);

         sizeof_Model_Combined = size(Model_Populations_Combined);

         diff = Model_Populations_Combined-Expt_Populations;

         mean_error = sqrt(sum(sum(diff.*diff.*Expt_weights)) / sum(sum(Expt_weights)));

         pop_error = sum(diff.*Expt_weights,1) ./ sum(Expt_weights,1);
         pop_error(2,:) = sqrt(sum(diff.*diff.*Expt_weights,1) ./ sum(Expt_weights,1));
```

3. V. REFERENCES

1. Truex, N. L.; Wang, Y.; Nowick, J. S. *J. Am. Chem. Soc.* **2016**, *138*, 13882–13890.

2. Podlech, J.; Gurrath, M.; Müller, G. 9-Fluorenylmethoxycarbonyl Group. In *Houben-Weyl Methods of Organic Chemistry*, Goodman, M., Ed. Thieme: Stuttgart, 2003; Vol. E22a, p 61.

3. Longsworth, L. G. *J. Phys. Chem.* **1960**, *64*, 1914–1917.

4. Nowick, J. S.; Khakshoor, O.; Hashemzadeh, M.; Brower, J. O. *Org. Lett.* **2003**, *5*, 3511–3513.

3.V. CHARACTERIZATION DATA

^{1}H NMR DOSY of a 1:1 mixture of peptides **1a** and **1b**
8.0 mM total concentration in D_2O at 500 MHz and 298 K

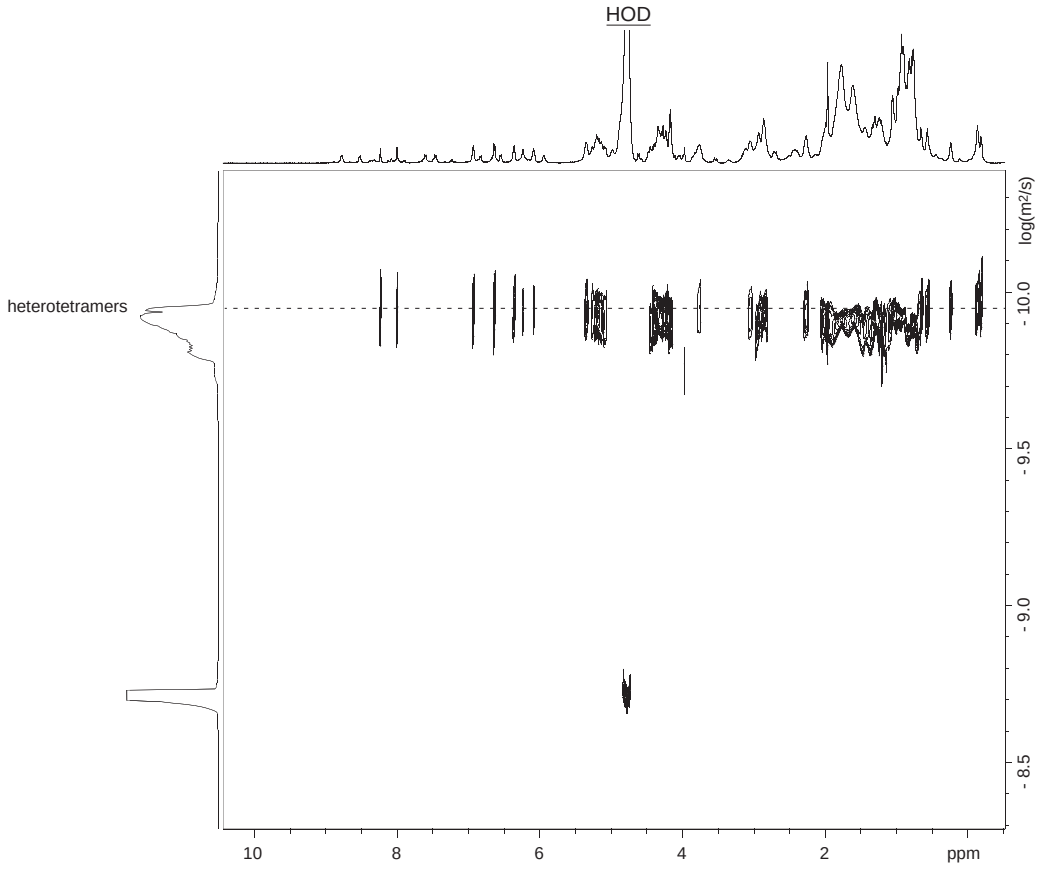

Calculations for the 1:1 mixture of peptides **1a** and **1b** at 8.0 mM total concentration

D_{HOD} = 19.0 x 10^{-10} m^2/s [a]
log (D_{HOD}) = -8.721

$D_{heterotetramers}$: log(D) = -9.943; D = $10^{-9.943}$ = 11.4 ± 1.1 x 10^{-11} m^2/s

[a]Longsworth, L. G. *J. Phys. Chem.* **1960**, *64*, 1914−1917.

$^{1}H,^{15}N$ HSQC of peptides [^{15}N]**1a** and [^{15}N]**1b** at 600 MHz and 293 K
$\chi_B{}^{a}$ = 0.00; 8.0 mM total concentration in 9:1 H_2O/D_2O

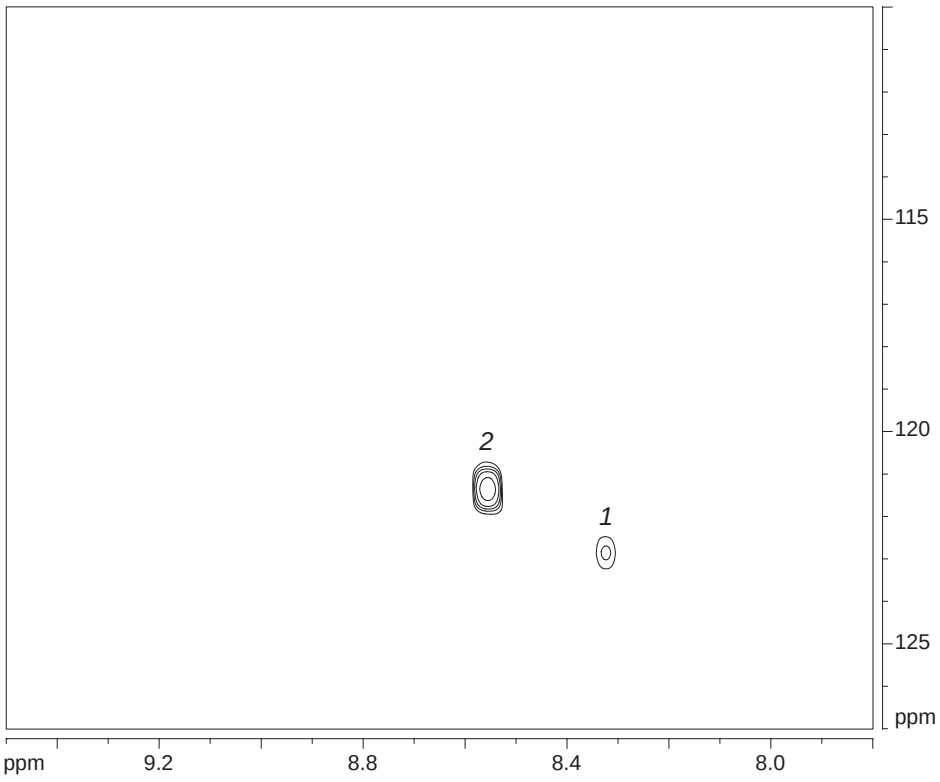

[a] χ_B designates the mole fraction of peptide [^{15}N]**1b**.

$^{1}H,^{15}N$ HSQC of peptides [^{15}N]**1a** and [^{15}N]**1b** at 600 MHz and 293 K
$\chi_B{}^{a}$ = 0.125; 8.0 mM total concentration in 9:1 H_2O/D_2O

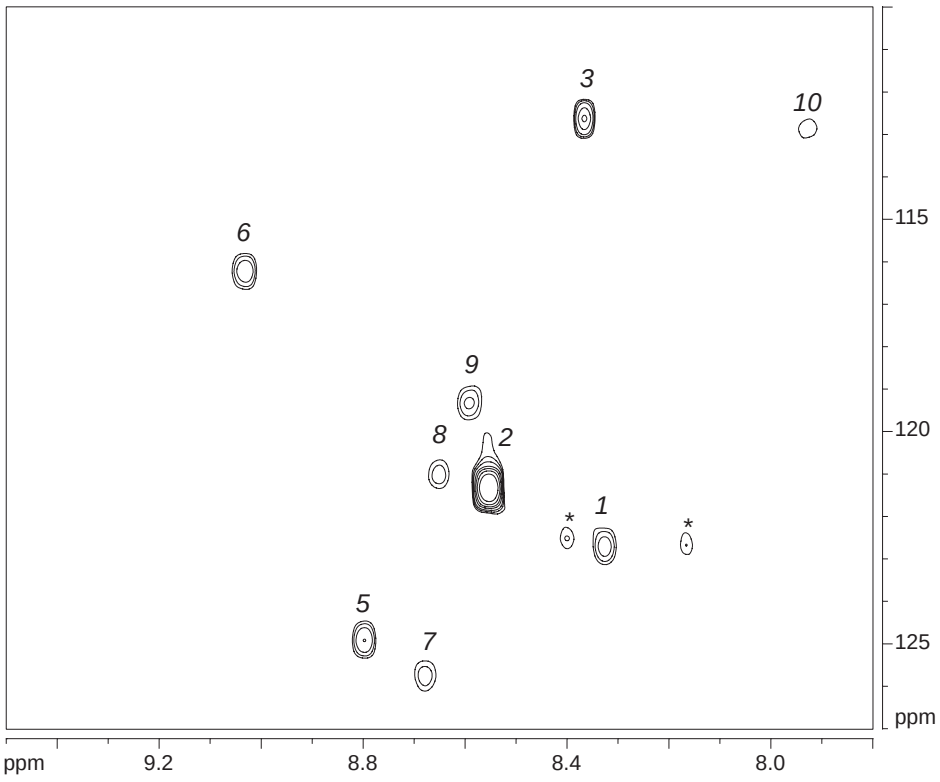

[a] χ_B designates the mole fraction of peptide [^{15}N]**1b**.
The asterisks (*) indicate crosspeaks associated with minor unidentified species.

$^{1}H,^{15}N$ HSQC of peptides [^{15}N]**1a** and [^{15}N]**1b** at 600 MHz and 293 K
$\chi_B{}^{a}$ = 0.25; 8.0 mM total concentration in 9:1 H_2O/D_2O

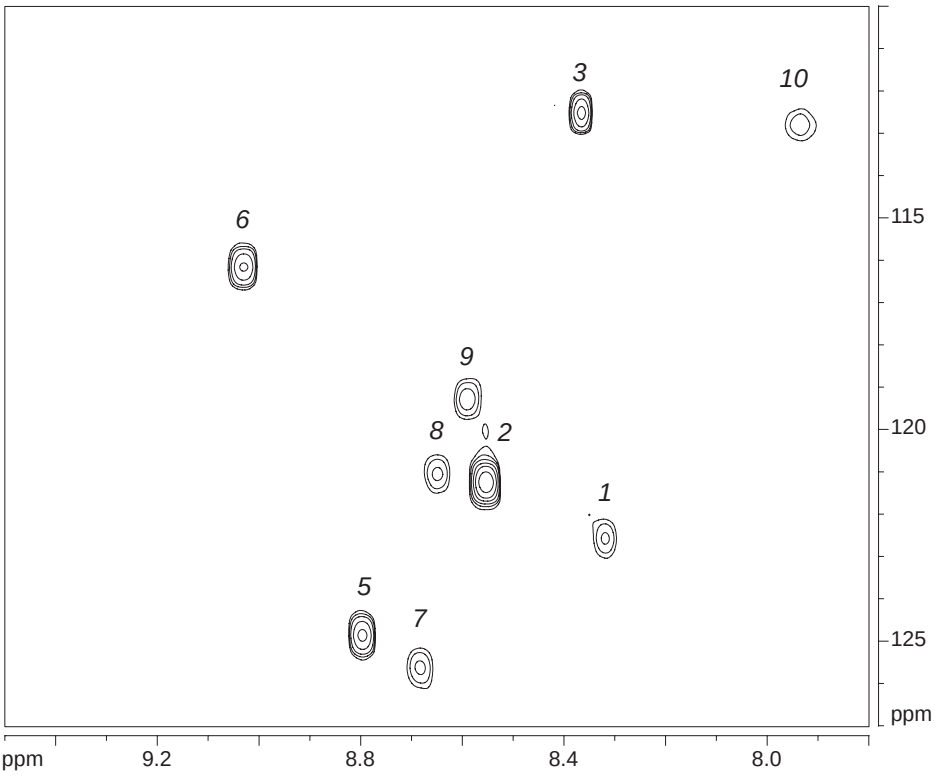

[a] χ_B designates the mole fraction of peptide [^{15}N]**1b**.

$^{1}H,^{15}N$ HSQC of peptides [^{15}N]**1a** and [^{15}N]**1b** at 600 MHz and 293 K
$\chi_B{}^{a}$ = 0.375; 8.0 mM total concentration in 9:1 H_2O/D_2O

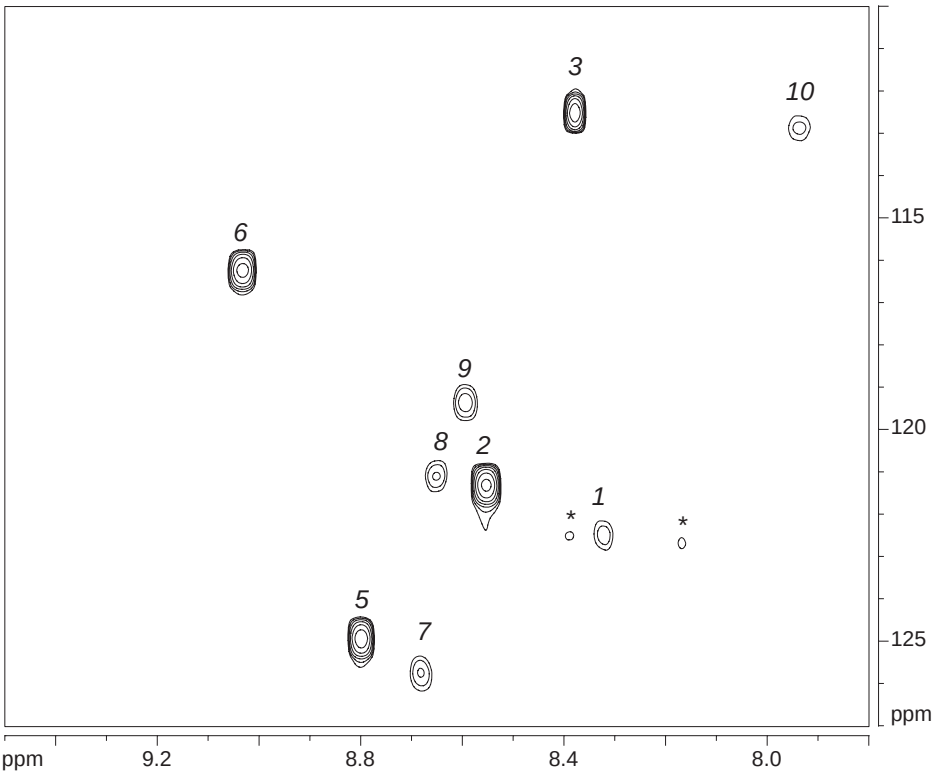

[a] χ_B designates the mole fraction of peptide [^{15}N]**1b**.
The asterisks (*) indicate crosspeaks associated with minor unidentified species.

$^{1}H,^{15}N$ HSQC of peptides [^{15}N]**1a** and [^{15}N]**1b** at 600 MHz and 293 K
$\chi_B{}^{a}$ = 0.50; 8.0 mM total concentration in 9:1 H_2O/D_2O

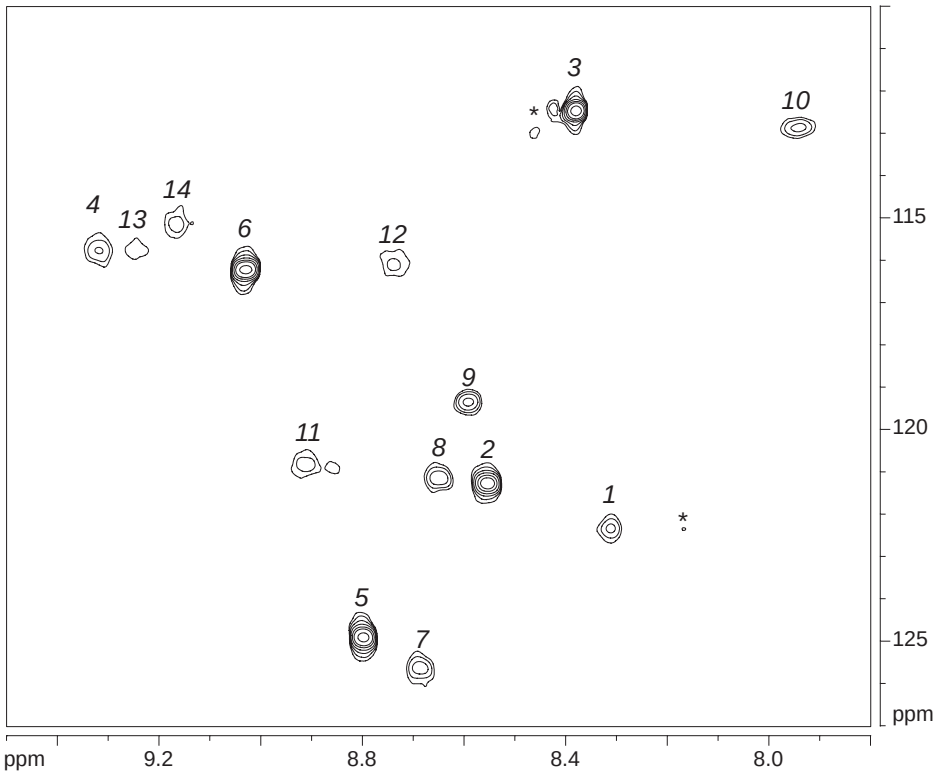

[a] χ_B designates the mole fraction of peptide [^{15}N]**1b**.
The asterisks (*) indicate crosspeaks associated with minor unidentified species.

$^{1}H,^{15}N$ HSQC of peptides [^{15}N]**1a** and [^{15}N]**1b** at 600 MHz and 293 K
$\chi_B{}^{a}$ = 0.625; 8.0 mM total concentration in 9:1 H_2O/D_2O

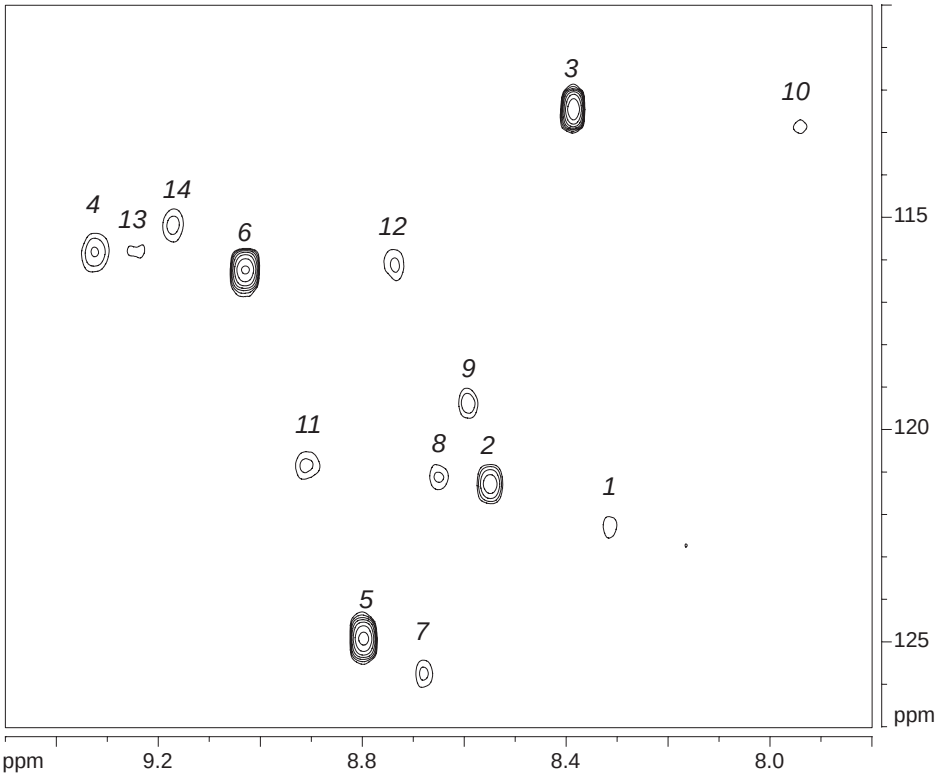

[a] χ_B designates the mole fraction of peptide [^{15}N]**1b**.

$^{1}H,^{15}N$ HSQC of peptides [^{15}N]**1a** and [^{15}N]**1b** at 600 MHz and 293 K
$\chi_B{}^{a}$ = 0.75; 8.0 mM total concentration in 9:1 H_2O/D_2O

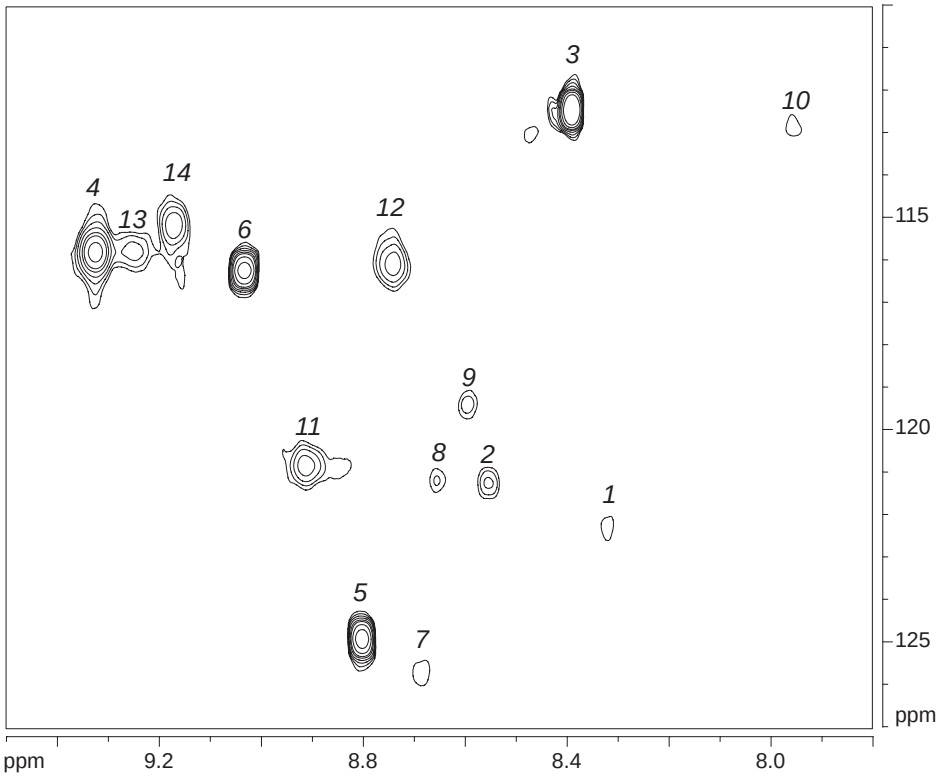

[a] χ_B designates the mole fraction of peptide [^{15}N]**1b**.

$^{1}H,^{15}N$ HSQC of peptides [^{15}N]**1a** and [^{15}N]**1b** at 600 MHz and 293 K
$\chi_B{}^{a}$ = 0.875; 8.0 mM total concentration in 9:1 H_2O/D_2O

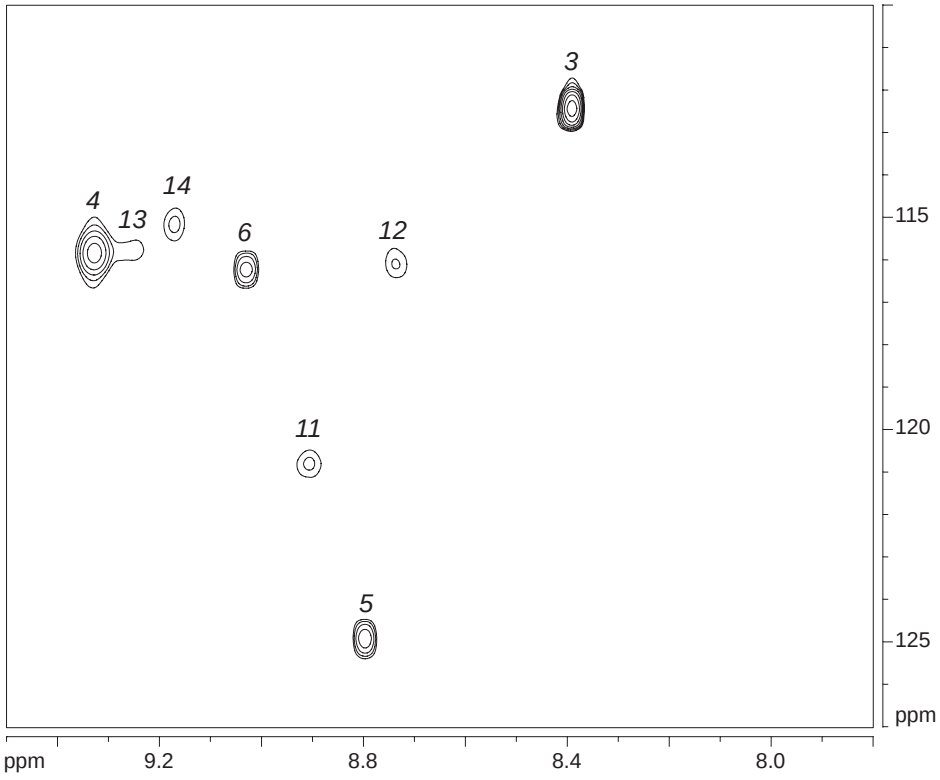

[a] χ_B designates the mole fraction of peptide [^{15}N]**1b**.

$^{1}H,^{15}N$ HSQC of peptides [^{15}N]**1a** and [^{15}N]**1b** at 600 MHz and 293 K
$\chi_B{}^{a}$ = 1.00; 8.0 mM total concentration in 9:1 H_2O/D_2O

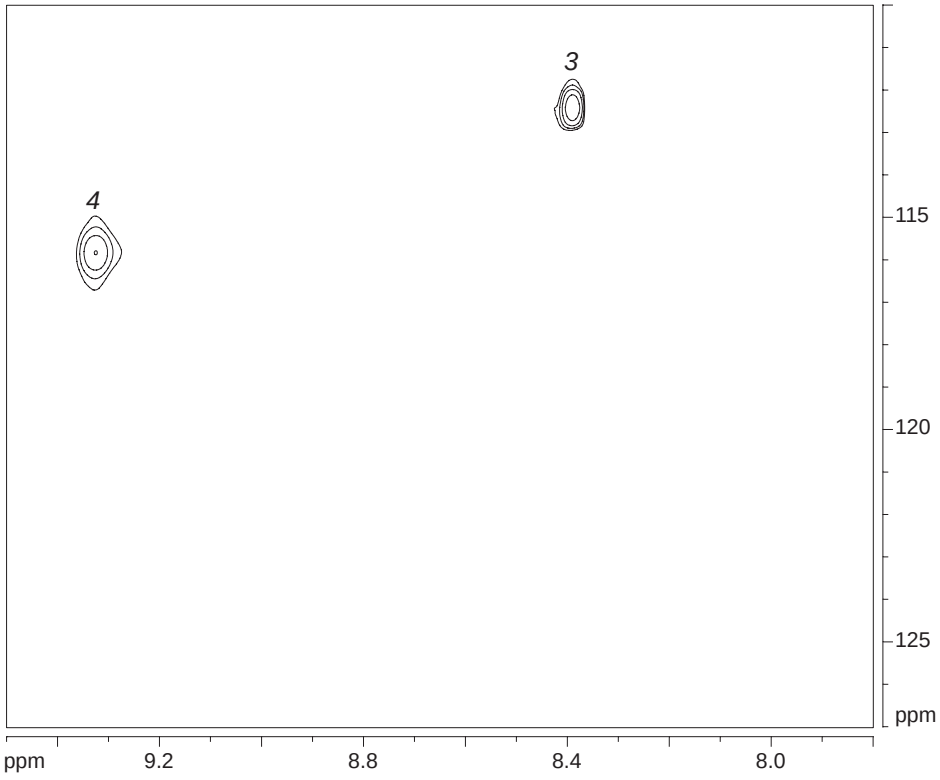

[a] χ_B designates the mole fraction of peptide [^{15}N]**1b**.

$^{1}H,^{15}N$ HSQC of peptides [^{15}N]**1a** and [^{15}N]**1b** in 9:1 H_2O/D_2O at 600 MHz and 293 K
Stack of ^{15}N spectra from the f_1 projections of the $^{1}H,^{15}N$ HSQC spectra

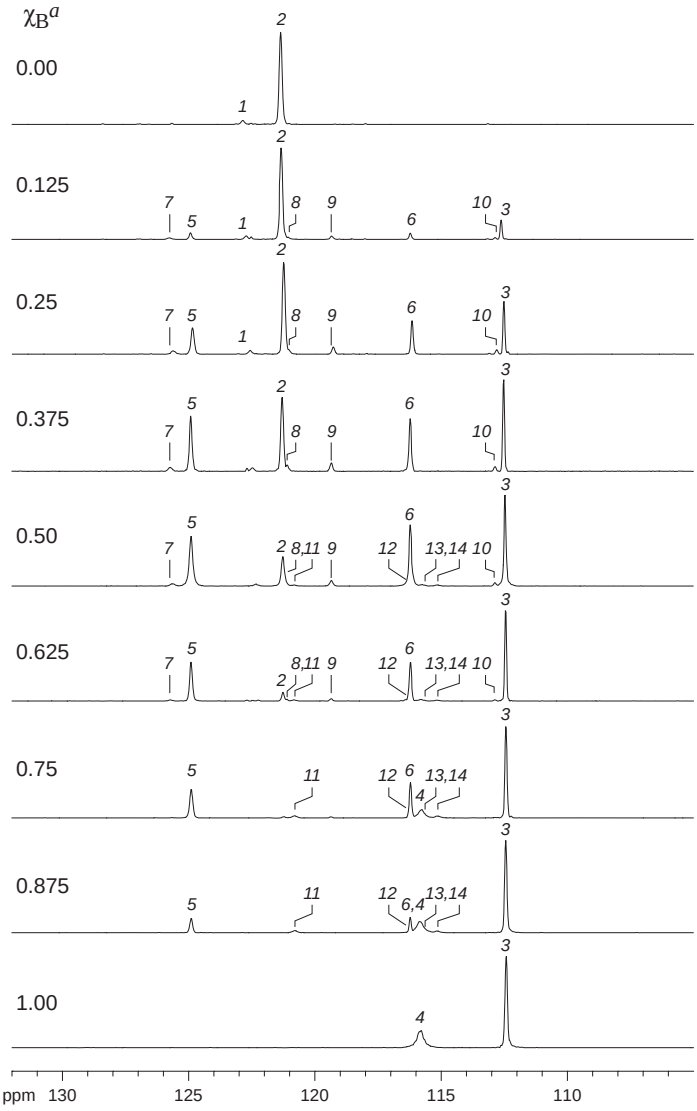

[a] χ_B designates the mole fraction of peptide [^{15}N]**1b**.

CHAPTER 4

Efforts to Correlate the Structure, Solution-Phase Behavior, and Toxicity of Peptides Derived from $A\beta_{17–36}$

INTRODUCTION

Aggregation of the β-amyloid peptide (Aβ) to form oligomers and fibrils is central to the pathology of Alzheimer's disease. The fibrils are insoluble deposits of Aβ that consist of layers of β-sheets, with extensive intermolecular hydrogen bonds and hydrophobic contacts. The oligomers are also rich in β-sheet structure, but they consist of dimers and trimers that can further assemble to give higher-order oligomers.[1,2,3,4,5] While the fibrils represent the thermodynamic endpoint of Aβ aggregation, the oligomers have a fundamental role in causing synaptic dysfunction and neurodegeneration.[6,7,8]

The importance of Aβ oligomers in Alzheimer's disease pathology underscores the significance for obtaining their high-resolution structures. Aβ oligomers form a polymorphic and heterogeneous mixture of aggregates that are difficult to characterize and study.[9,10,11] Many of the oligomers show toxicity toward neuronal cells, but efforts to isolate and characterize these oligomers have provided limited structural information.[10] To date, little is known about the structures of Aβ oligomers at high resolution. As a result, the mechanisms are not fully understood by which the oligomers form and contribute to Alzheimer's disease pathology.[9,10]

Our laboratory has been using macrocyclic β-sheet peptides to shed light on the oligomers formed by Aβ and other peptides and proteins.[12,13,14,15,16,17,18] In 2014, our laboratory introduced macrocyclic β-sheet peptides derived from a β-hairpin of $A\beta_{17–36}$. We incorporated the fragments $A\beta_{17–23}$ (LVFFAED) and $A\beta_{30–36}$ (AIIGLMV) into the upper and lower strands of a macrocyclic β-sheet peptide, and connected the two strands with δ-linked ornithine ($^{\delta}$Orn) turn units. These turn units allow β-sheet folding between the two strands (Figure 4.1).[19] The peptides also contain a single N-methyl amino acid, which prevents uncontrolled aggregation. We began studies of peptide $\mathbf{1_{Met}}$, which embodies these design features, but we found that this peptide

exhibited limited solubility in aqueous solution. Our laboratory then incorporated an ornithine (α-linked) residue to give peptide **1**$_{\mathbf{Orn}}$, which we envisioned as a homologue of peptide **1**$_{\mathbf{Met}}$ that would have better solubility.

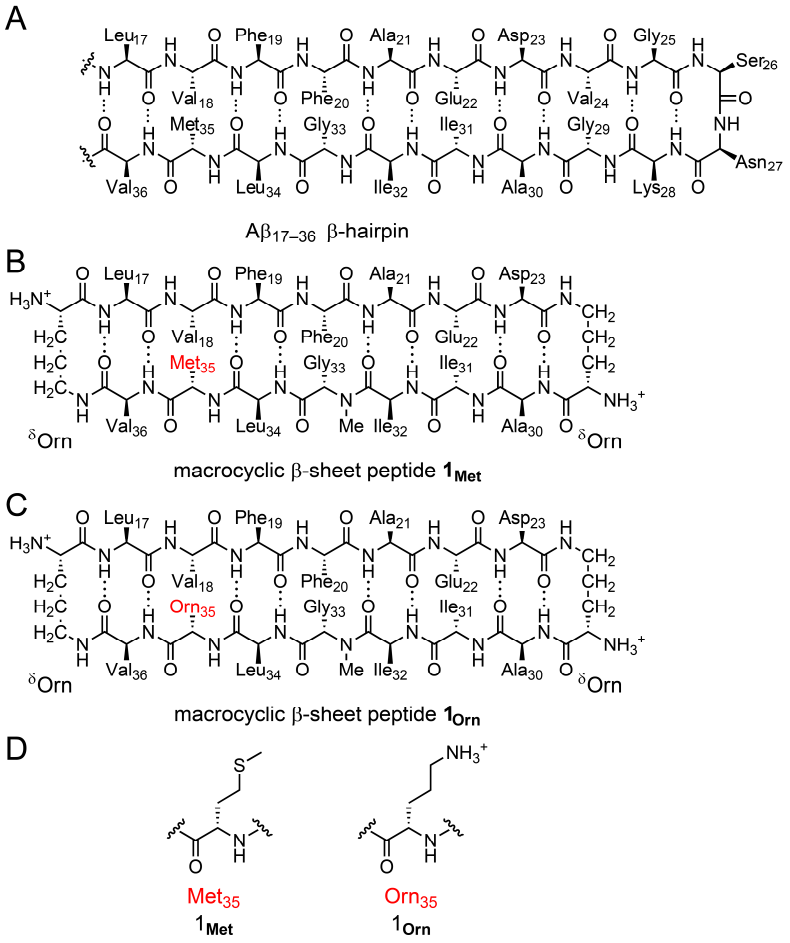

Figure 4.1. Chemical structures of an Aβ$_{17–36}$ β-hairpin and peptides **1**$_{\mathbf{Met}}$ and **1**$_{\mathbf{Orn}}$ (A–C). Met$_{35}$ and Orn$_{35}$ residues illustrating the relationship between peptides **1**$_{\mathbf{Met}}$ and **1**$_{\mathbf{Orn}}$ (D).

Previous X-ray crystallography studies of peptide **1**$_{\mathbf{Orn}}$ showed that this peptide can form trimers, hexamers, and dodecamers.[12] These oligomers inspired our laboratory to design related analogues derived from Aβ, including covalently-stabilized trimers, larger β-hairpins, and alternative pairings of Aβ residues.[14,17,18] X-ray crystallography studies of these peptides show that they can form various sizes and morphologies of dimers, trimers, hexamers, dodecamers, and other higher-order oligomers.

Solution-phase biophysical and biological studies of macrocyclic β-sheet peptides have begun to reveal relationships between oligomerization and toxicity. In a related study of a macrocyclic β-sheet peptide derived from $A\beta_{16–36}$, our laboratory used X-ray crystallography and SDS-PAGE to show that this peptide can form stable hexamers, and used biological studies showed that these hexamers are toxic to neuronal cells.[20] When our laboratory similarly attempted to study the solution-phase behavior and toxicity of peptide $\mathbf{1_{Orn}}$, we found that peptide $\mathbf{1_{Orn}}$ was largely monomeric. As a result, the biological properties of peptide $\mathbf{1_{Orn}}$ were not explored.

Inspired by the oligomerization and toxicity of the macrocyclic β-sheet peptide derived from $A\beta_{16–36}$, I decided to revisit the study of the peptides derived from $A\beta_{17–36}$, peptides $\mathbf{1_{Orn}}$ and $\mathbf{1_{Met}}$. I begin this study by elucidating the X-ray crystallographic structure of peptide $\mathbf{1_{Met}}$. After I established that peptide $\mathbf{1_{Met}}$ adopts the same X-ray crystallographic structure as peptide $\mathbf{1_{Orn}}$, I then attempt to determine whether peptides $\mathbf{1_{Met}}$ and $\mathbf{1_{Orn}}$ form oligomers in solution. I also evaluate the toxicity of these two peptides. Throughout the course of these studies, I compared the oligomers formed by peptides $\mathbf{1_{Met}}$ and $\mathbf{1_{Orn}}$ with those of trimer **2** (Figure 4.2). Trimer **2**, which our laboratory previously characterized, is a covalently-stabilized trimer that assembles in solution to form a dimer.[17] The monomer and dimer of trimer **2** are comparable in molecular weight to a trimer and hexamer formed by peptides $\mathbf{1_{Met}}$ and $\mathbf{1_{Orn}}$.

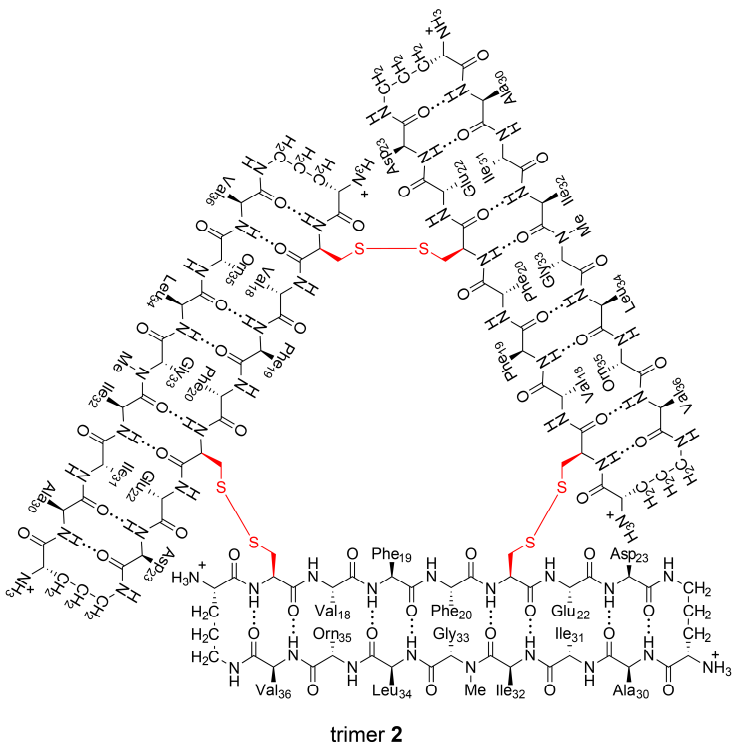

Figure 4.2. Chemical structure of trimer **2**.[17]

I conclude this chapter with ^{1}H NMR spectroscopy studies of peptides $\mathbf{1}_{\mathbf{Met}}$, $\mathbf{1}_{\mathbf{Orn}}$, and trimer **2**. I found that peptide $\mathbf{1}_{\mathbf{Met}}$ was not soluble at an adequate concentration to produce sufficient NMR signals, while peptide $\mathbf{1}_{\mathbf{Orn}}$ and trimer **2** were easily soluble for NMR studies. The ^{1}H NMR spectra of peptide $\mathbf{1}_{\mathbf{Orn}}$ and of trimer **2** showed that oligomers form, but the oligomer spectra were largely indecipherable. Diffusion-ordered spectroscopy (DOSY) revealed that peptide $\mathbf{1}_{\mathbf{Orn}}$ and trimer **2** form oligomers consistent with dodecamers and tetramers, respectively. To promote the formation of a well-defined dodecamer, I also designed analogues of peptide $\mathbf{1}_{\mathbf{Orn}}$ (peptides **3** and **4**) and studied them by ^{1}H NMR spectroscopy and DOSY.

RESULTS AND DISCUSSION

X-ray Crystallographic Structure of Peptide $\mathbf{1}_{\mathbf{Met}}$. Although peptide $\mathbf{1}_{\mathbf{Met}}$ exhibits limited solubility, I found that after sonication this peptide is soluble in a solution without buffer at about 5 mg/mL. This concentration proved sufficient for growing crystals of peptide $\mathbf{1}_{\mathbf{Met}}$ for X-ray

crystallography. Diffraction data of peptide $\mathbf{1}_{\mathbf{Met}}$ were collected in house on a Rigaku MicroMax 007HF X-ray diffractometer at 1.54 Å wavelength. The data were collected to 2.03 Å resolution, processed in XDS, and solved by isomorphous replacement using the structure of peptide $\mathbf{1}_{\mathbf{Orn}}$ (PDB ID: 4NTR). The structure of peptide $\mathbf{1}_{\mathbf{Met}}$ was processed and refined in the R3 space group. The asymmetric unit contains 16 peptides that adopt folded β-sheets with seven to eight intramolecular hydrogen bonds. The structures of peptides $\mathbf{1}_{\mathbf{Met}}$ and $\mathbf{1}_{\mathbf{Orn}}$ are nearly identical, with a root-mean squared deviation of < 1 Å. Figure 4.3 shows monomer subunits from the structures of peptides $\mathbf{1}_{\mathbf{Met}}$ and $\mathbf{1}_{\mathbf{Orn}}$.

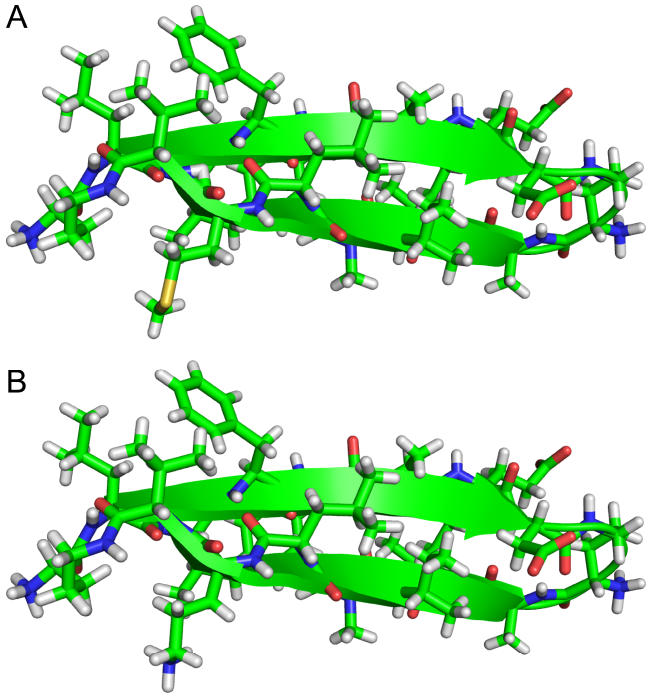

Figure 4.3. Monomer subunits from the X-ray crystallographic structures of peptide $\mathbf{1}_{\mathbf{Met}}$ (A) and peptide $\mathbf{1}_{\mathbf{Orn}}$ (B, PDB ID: 4NTR).

The X-ray crystallographic structure shows peptide $\mathbf{1}_{\mathbf{Met}}$ assembles to form triangular trimers, which further assemble into hexamers and dodecamers. The alternating side chains of peptide $\mathbf{1}_{\mathbf{Met}}$ make up two surfaces—called the major and minor surfaces. The major surface consists of the side chains of Leu_{17}, Phe_{19}, Ala_{21}, Asp_{23}, Ala_{30}, Ile_{32}, Leu_{34}, and Val_{36}; the minor surface consists of the

side chains of Val_{18}, Phe_{20}, Ile_{31}, Gly_{33}, and Met_{35}. In the trimer assembly, these residues also create major and minor surfaces. Figure 4.4 shows these two surfaces of the trimer.

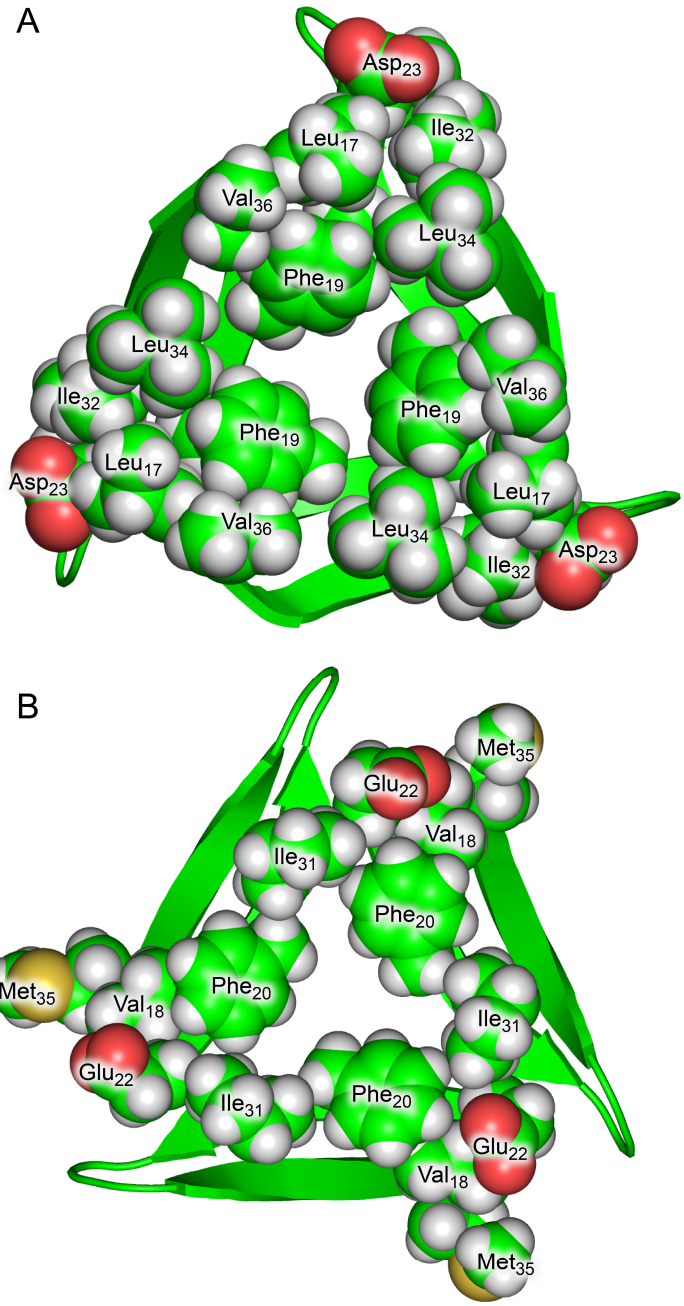

Figure 4.4. Trimer of peptide $\mathbf{1_{Met}}$ showing select residues as spheres. (A) Major surface showing the residues Leu_{17}, Phe_{19}, Asp_{23}, Ile_{32}, Leu_{34}, and Val_{36}. (B) Minor surface showing the residues Val_{18}, Phe_{20}, Glu_{22}, Ile_{31}, and Met_{35}.

The trimer is held together with intermolecular hydrogen-bonds and hydrophobic contacts at the interface of each peptide (Figure 4.5A). This interface shows a pair of hydrogen bonds between Val_{18} and Glu_{22}. This interface also shows a group of hydrophobic contacts. On the major surface of the trimer, these hydrophobic contacts come from the side chains of Leu_{17}, Phe_{19}, and Val_{36} from one peptide and the side chains of Ala_{21}, Ile_{32}, and Leu_{34} from the adjacent peptide. On the minor surface, these hydrophobic contacts come from the side chains of Val_{18} and Phe_{20} from one peptide and the side chain of Ile_{31} from the adjacent peptide. Three ordered water molecules are located in the center of the trimer, forming hydrogen bonds to the backbone NH and CO groups of Phe_{20}. The hexamer is composed of two trimers of peptide $\mathbf{1_{Met}}$ that laminate together on their minor surfaces to form a sandwich-like hexamer (Figure 4.5B). The two trimers are staggered by about 60°. The side chains of Val_{18}, Phe_{20}, and Ile_{32} point toward the center of the hexamer, forming a hydrophobic interface. The dodecamer is composed of four trimers that come together at the vertices of a tetrahedron (Figure 4.5C). The dodecamer is held together through hydrophobic contacts and a salt bridge at the interface of the four trimers. The salt bridge forms between an Asp_{23} and an α-amine of a δ-linked ornithine. The hydrophobic contacts form between the side chains of Leu_{17}, Phe_{19}, Val_{36}, Leu_{34}.

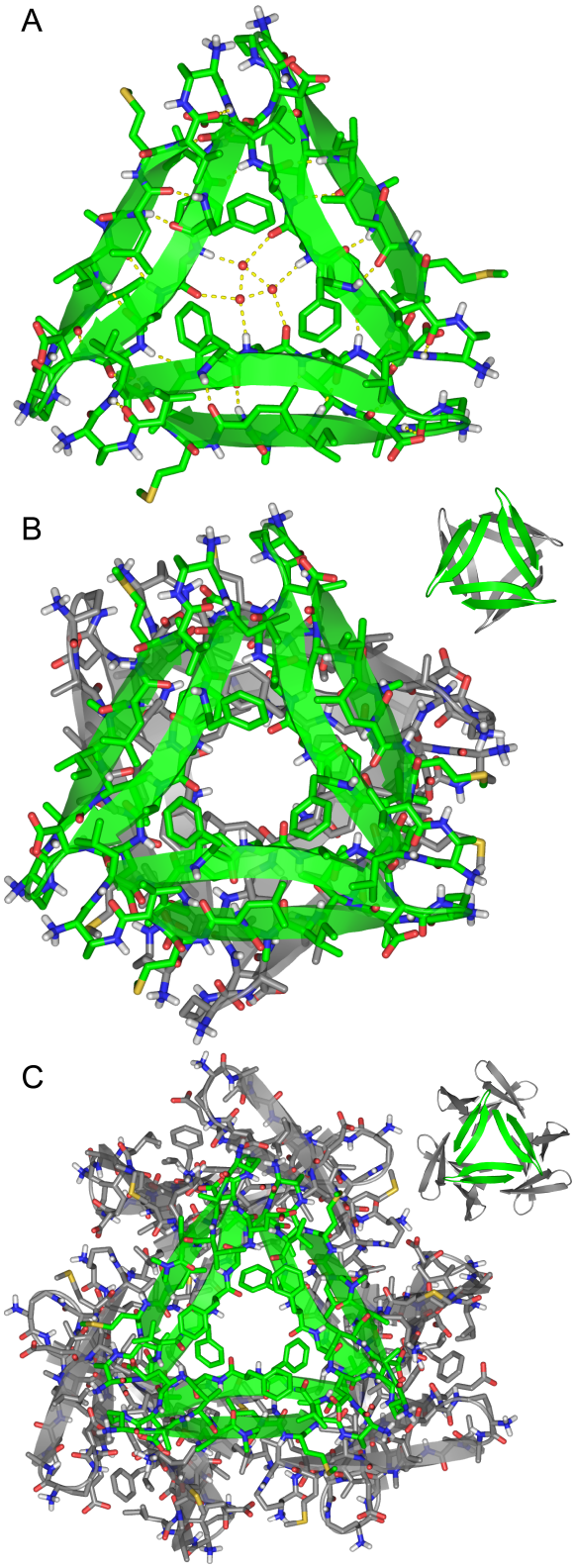

Figure 4.5. X-ray crystallographic structure of peptide $\mathbf{1}_{\mathbf{Met}}$. Triangular trimer with the three ordered water molecules shown in the center (A). The hexamer (B) and dodecamer (C) that are observed in the crystal lattice.

Solution-Phase Biophysical Studies of peptides $\mathbf{1_{Met}}$ and $\mathbf{1_{Orn}}$. Solution-phase biophysical studies of peptides $\mathbf{1_{Met}}$ and $\mathbf{1_{Orn}}$ are important for evaluating whether these peptides fold and oligomerize in aqueous solution. The following subsections evaluate and compare the folding and oligomerization of peptides $\mathbf{1_{Met}}$ and $\mathbf{1_{Orn}}$ by circular dichroism spectroscopy and SDS-PAGE.

Circular Dichroism Spectroscopy. Circular dichroism spectroscopy provides a simple way to evaluate folding. The spectrum of peptide $\mathbf{1_{Met}}$ at 150 μM in 10 mM potassium phosphate buffer at pH 7.4 shows a positive band at about 195 nm and a pronounced negative band at about 218 nm. The spectrum of peptide $\mathbf{1_{Orn}}$ shows only a negative band at about 200 nm. Figure 4.6 shows the circular dichroism spectra of peptides $\mathbf{1_{Met}}$ and $\mathbf{1_{Orn}}$.

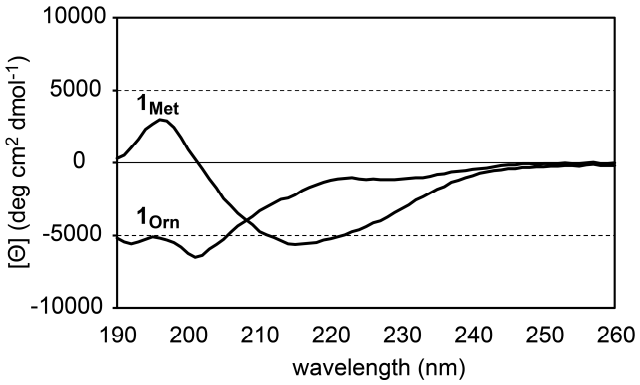

Figure 4.6. Circular dichroism spectra of peptides $\mathbf{1_{Met}}$ and $\mathbf{1_{Orn}}$. The spectra were acquired at 150 uM in 10 mM potassium phosphate buffer at pH 7.4.

Even though the sequences of peptides $\mathbf{1_{Met}}$ and $\mathbf{1_{Orn}}$ are nearly the same, the circular dichroism spectra are clearly not. The spectrum of peptide $\mathbf{1_{Met}}$ reflects that of a folded β-hairpin, but the spectrum of peptide $\mathbf{1_{Orn}}$ reflects that of an unstructured peptide. These spectra illustrate the influence of a single amino acid on β-sheet folding. Peptide $\mathbf{1_{Met}}$ contains the hydrophobic methionine residue, which is well-known to promote β-sheet folding.[21,22] For peptide $\mathbf{1_{Orn}}$, the hydrophilicity and charge of the ornithine residue appears to disrupt folding.

SDS-PAGE. SDS-PAGE is a common method to study mixtures of Aβ oligomers, because this method can separate different oligomers based on molecular weight. Here, I use SDS-PAGE to compare the oligomerization of peptides $\mathbf{1}_{\mathbf{Met}}$ and $\mathbf{1}_{\mathbf{Orn}}$ with trimer **2** (Figure 4.7). Tricine SDS-PAGE followed by silver staining shows that peptides $\mathbf{1}_{\mathbf{Met}}$ and $\mathbf{1}_{\mathbf{Orn}}$ migrate as single bands that are nearly identical, which appear at a molecular weight between 1.7 and 3.8 kDa. Trimer **2** migrates as two bands: a lower band at about 5.3 kDa and a higher band at about 10.6 kDa.

The molecular weights of the bands of peptides $\mathbf{1}_{\mathbf{Met}}$ and $\mathbf{1}_{\mathbf{Orn}}$ are consistent with species that are monomers or possibly dimers. The molecular weights of the trimer **2** bands are consistent with a monomer and dimer, respectively. These bands of trimer **2** migrate at molecular weights that are much larger than those of peptides $\mathbf{1}_{\mathbf{Met}}$ and $\mathbf{1}_{\mathbf{Orn}}$, which further shows that peptides $\mathbf{1}_{\mathbf{Met}}$ and $\mathbf{1}_{\mathbf{Orn}}$ migrate as either monomers or dimers, but not trimers.

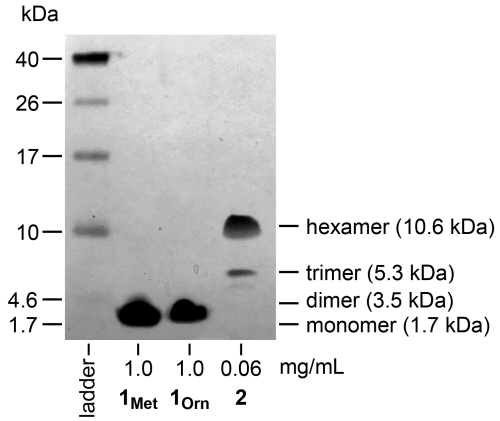

Figure 4.7. Silver-stained SDS-PAGE gel of peptide $\mathbf{1}_{\mathbf{Met}}$, peptide $\mathbf{1}_{\mathbf{Orn}}$, and trimer **2** in Tris buffer at pH 6.8 with 2% (w/v) SDS. Molecular weights calculated for the monomer, dimer, trimer, and hexamer are listed in parentheses.

Toxicity Studies of peptides $\mathbf{1_{Met}}$ and $\mathbf{1_{Orn}}$. Evaluating the toxicity of Aβ oligomers toward neuronal cells is important for studying oligomerization and neurodegeneration relationships. Here, I evaluate the toxicity of peptides $\mathbf{1_{Met}}$ and $\mathbf{1_{Orn}}$ toward the neuronally derived SH-SY5Y cells using a lactate dehydrogenase (LDH) release assay (Figure 4.8). The LDH assay showed that peptide $\mathbf{1_{Met}}$ induces no LDH release at concentrations as high as 200 μM. In contrast, peptide $\mathbf{1_{Orn}}$ increases LDH release in a dose-dependent fashion at 100, 150, and 200 μM.

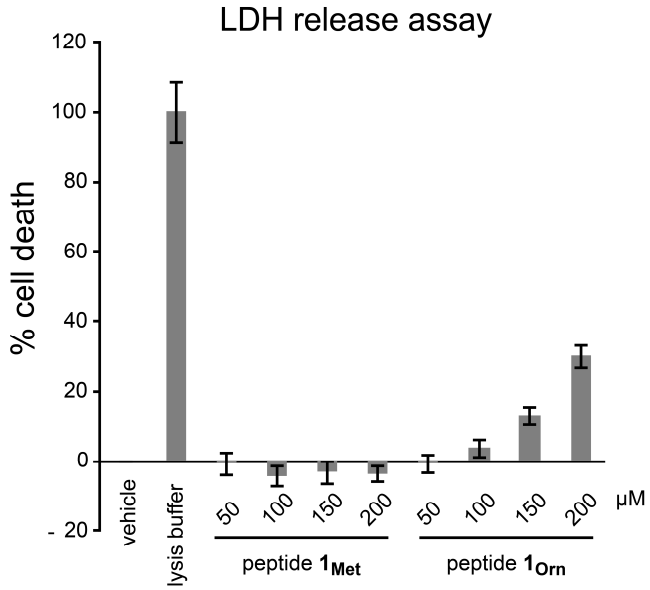

Figure 4.8. LDH release assay for peptides $\mathbf{1_{Orn}}$ and $\mathbf{1_{Met}}$ on SH-SY5Y cells (mean +/- SD, n=5).

Our laboratory has shown previously with peptides derived from Aβ and α-synuclein that oligomerization is important for toxicity.[15,17,20] The LDH release assay of peptides $\mathbf{1_{Met}}$ and $\mathbf{1_{Orn}}$ suggests that these two peptides differ in their solution-phase assembly, because $\mathbf{1_{Orn}}$ is toxic but $\mathbf{1_{Met}}$ is not. Although the lack of toxicity of peptide $\mathbf{1_{Met}}$ may be the result of precipitation or fibril formation, precipitation was not observed in any of the wells in the 96-well plate. Since no difference in solution-phase assembly of peptides $\mathbf{1_{Met}}$ and $\mathbf{1_{Orn}}$ was observed by SDS-PAGE, additional techniques are needed to further study oligomerization.

^{1}H NMR Spectroscopy. I used ^{1}H NMR spectroscopy to further evaluate whether oligomers of peptide $\mathbf{1_{Orn}}$ form in solution. The spectra show that peptide $\mathbf{1_{Orn}}$ oligomerizes in D_2O with 25 mM CD_3COOD and 25 mM CD_3COONa at 500 MHz and 298 K (Figure 4.9). At concentrations less than 0.5 mM, the resonances of peptide $\mathbf{1_{Orn}}$ are sharp and distinct, indicating that the peptide is largely monomeric at these concentrations. At concentrations above 1 mM, the resonances are broadened due to oligomer formation. The oligomer resonances lack distinct features, particularly in the regions of the methyl protons (< 1.1 ppm), the α-protons (4.0 – 5.3 ppm), and the aromatic protons (6.5 – 7.4 ppm). The broad resonances are either due to exchange or the formation of a mixture of oligomers. The broad resonances also indicate that these oligomers do not form stable hydrogen bonds and hydrophobic contacts.

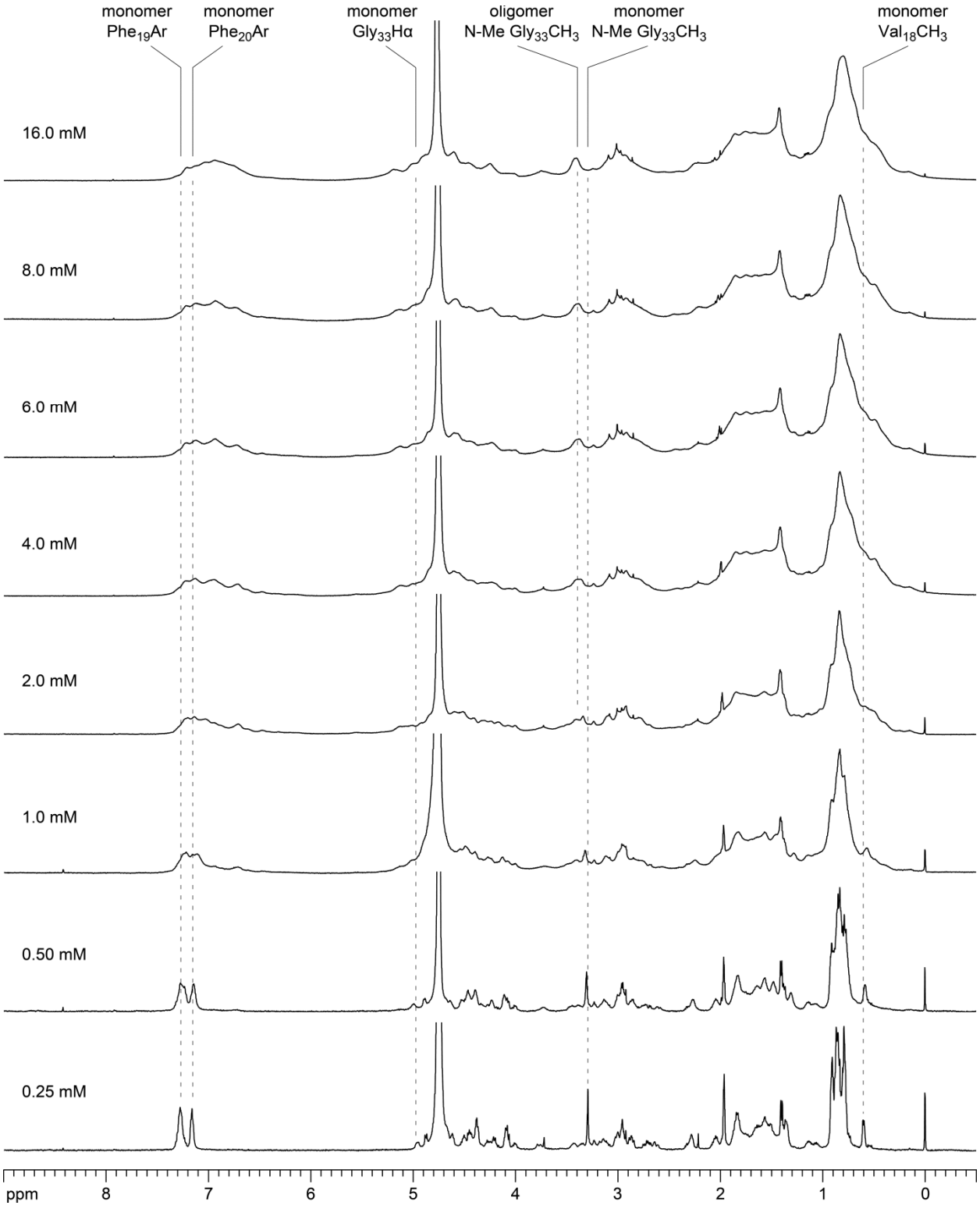

Figure 4.9. ^{1}H NMR spectra of peptide $\mathbf{1_{Orn}}$ at various concentrations in D_2O with 25 mM CD_3COOD and 25 mM CD_3COONa at 500 MHz and 298 K.

I prepared two analogues of peptide $\mathbf{1_{Orn}}$ to interrogate the oligomerization of this peptide (Figure 4.10). I envisioned that incorporating polar residues in place of Val_{18} and Phe_{20} would disrupt the crystallographic hexamer, permitting the formation of a well-defined trimer and dodecamer. These residues would display on the minor surface and disrupt interactions between two trimers within a hexamer (Figure 4.10A). Peptide **3** is a single-mutant analogue that contains Tyr_{20} (Figure 4.10B). Peptide **4** is a double-mutant analogue that contains Thr_{18} and Tyr_{20} (Figure 4.10C).

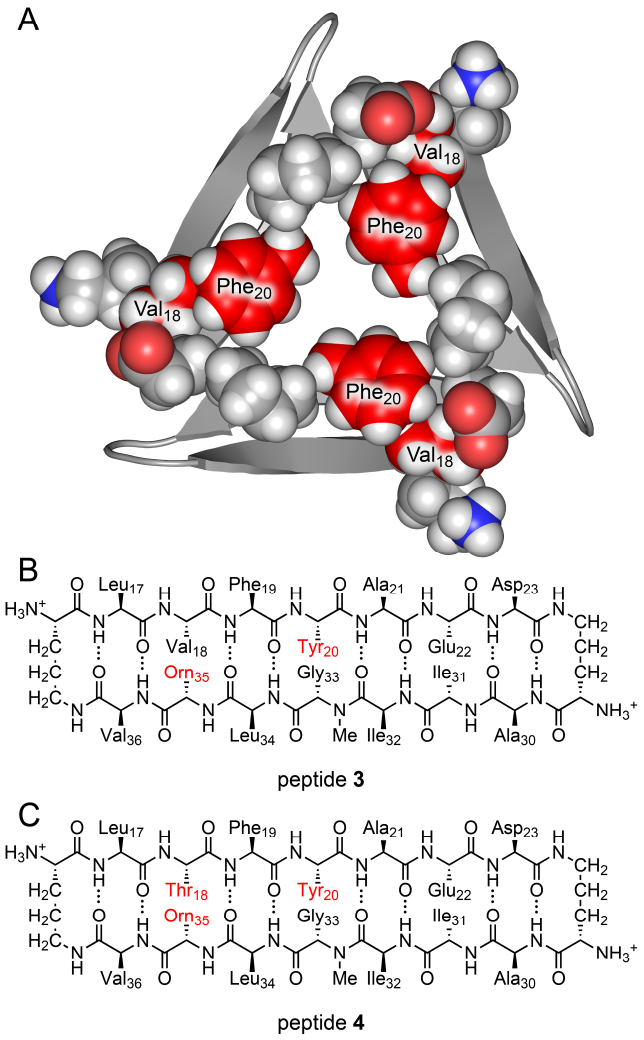

Figure 4.10. X-ray crystallographic structure of the trimer formed by peptide $\mathbf{1_{Orn}}$ (A, PDB 4NTR). Chemical structures of macrocyclic β-sheet peptides **3** and **4** (B and C).

The ^{1}H NMR spectra of peptides **3** and **4** at 8 mM show broad resonances, but are less broad than that of peptide $\mathbf{1_{Orn}}$. The broad resonances indicate that peptides **3** and **4** oligomerize in solution (Figure 4.11). These spectra also indicate that the polar Thr_{18} and Tyr_{20} residues facilitate the formation of oligomers that are more well defined, which suggests that peptides **3** and **4** are promising candidates for future studies by 2D ^{1}H NMR spectroscopy.

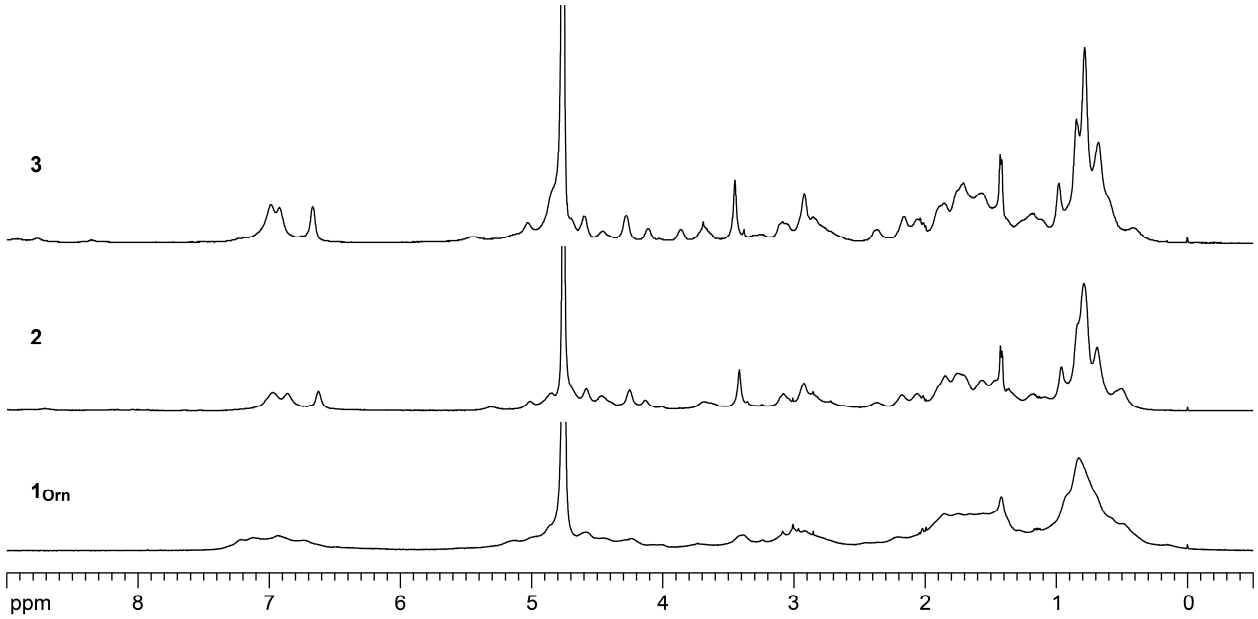

Figure 4.11. ^{1}H NMR spectra of peptides $\mathbf{1_{Orn}}$, **3**, and **4** at 8 mM in D_2O with 25 mM CD_3COOD and 25 mM CD_3COONa at 500 MHz and 298 K.

Diffusion-Ordered Spectroscopy (DOSY). DOSY measures the diffusion coefficient (*D*) of a molecule, which reflects the molecular weight.[23,24,25,26,27] The diffusion coefficient of an oligomer provides information on the size of the oligomer that forms.[28] Although SDS-PAGE and size-exclusion chromatography also provide information on size, these experiments can disrupt oligomers. The DOSY experiment does not. Here, I use DOSY to study the oligomers formed by peptides $\mathbf{1_{Orn}}$, **3**, and **4** and trimer **2** at various concentrations.

DOSY studies of peptide $\mathbf{1_{Orn}}$ at various concentrations show that an oligomer forms that is consistent with a dodecemer (Table 4.1). At 0.25 mM, peptide $\mathbf{1_{Orn}}$ gives a diffusion

coefficient of about 20.4×10^{-11} m^2/s. This diffusion coefficient is associated with the monomer. The diffusion coefficient decreases to 13.2, 9.3, and 8.6×10^{-11} m^2/s upon increasing the concentration to 2.0, 4.0, and 16.0 mM. The steady decrease in diffusion coefficients indicates fast exchange between monomer and oligomer on the NMR time scale.[29]

Table 4.1. Diffusion coefficients (*D*) in D_2O at 298 K

	$MW_{monomer}$[a] (Da)	MW_{trimer}[a] (Da)	conc. (mM)	*D* (10^{-11} m^2/s)	oligomer state
1_{Orn}	1760	5280	0.25	20.4 ± 1.0	monomer
			0.5	18.2 ± 1.2	
			2.0	13.2 ± 1.0	trimer
			4.0	9.3 ± 1.1	
			6.0	9.1 ± 0.8	
			8.0	9.1 ± 1.0	
			16.0	8.6 ± 1.3	dodecamer
2	5297[b]		0.15	8.6 ± 1.7	tetramer[c]
3	1778		8.0	12.2 ± 0.5	tetramer
4	1762		8.0	15.8 ± 0.9	dimer

[a]Molecular weight calculated for the neutral (uncharged) peptide.
[b]Molecular weight calculated for the neutral (uncharged) cross-linked trimer.
[c]Oligomer state of the cross-linked trimer

The diffusion coefficient at 2.0 mM is about 0.65 times the monomer, which is consistent with the value of a trimer. The diffusion coefficients at 4.0, 6.0, and 8.0 mM are about 0.45 times that of the monomer, which indicates the formation of a higher-order oligomer that is much larger than a hexamer (0.55) but smaller than a decamer (0.46). The diffusion coefficient at 16.0 mM is about 0.42 times the monomer, which is comparable to the anticipated (0.44) ratio for a dodecemer.

I used DOSY NMR to study the oligomers formed by trimer **2** to confirm the size of the dodecamer formed by peptide **1_{Orn}**. DOSY studies show that trimer **2** forms an oligomer consistent with a tetramer. The tetramer can also be thought of as a dodecamer of the monomer subunits. The DOSY spectrum of trimer **2** at 0.15 mM shows a single set of resonances, with a diffusion coefficient of about 8.6×10^{-11} m^2/s. This diffusion coefficient is comparable to the value of peptide **1_{Orn}** at 16.0 mM (8.6×10^{-11} m^2/s), indicating that the oligomers have a similar molecular weight.

DOSY studies show that peptides **3** and **4** have a lower propensity to oligomerize than peptide $\mathbf{1_{Orn}}$. At 8.0 mM, peptide **3** gives a diffusion coefficient of about 12.2×10^{-11} m^2/s and peptide **4** gives a diffusion coefficient of about 15.8×10^{-11} m^2/s. These diffusion coefficients are about 0.59 and 0.77 times that of a monomer, which are values consistent with a tetramer and dimer. These diffusion coefficients may also reflect larger oligomers in fast exchange with monomer, indicating lower association constants of peptides **3** and **4** than that of peptide $\mathbf{1_{Orn}}$.

To summarize the DOSY studies, the diffusion coefficients of peptides $\mathbf{1_{Orn}}$, **3**, and **4**, and trimer **2** show that these peptides oligomerize in solution. Peptide $\mathbf{1_{Orn}}$ and trimer **2** form dodecamers and tetramers, which is intriguing since neither of these oligomers were observed by SDS-PAGE. The oligomerization of peptide $\mathbf{1_{Orn}}$ may be important for the toxicity observed in the LDH assay. Even though the LDH assay was performed at micromolar concentrations of peptide $\mathbf{1_{Orn}}$ and the dodecamer forms at millimolar concentrations, smaller oligomers may form within the cellular environment that induce toxicity.

CONCLUSION

Characterizing the structures, biophysical properties, and biological properties of Aβ oligomers is vital for gaining a better understanding of Alzheimer's disease pathology. This chapter provides new information on the biophysical and biological properties of oligomers formed by peptides derived from $A\beta_{17–36}$. In this chapter, I evaluated the solution-phase assembly and biological properties of peptides $\mathbf{1_{Met}}$ and $\mathbf{1_{Orn}}$, using ^{1}H NMR spectroscopy, biophysical studies, and biological studies.

I used X-ray crystallography to establish that peptide $\mathbf{1_{Met}}$ crystallizes in the same fashion as peptide $\mathbf{1_{Orn}}$, forming trimers, hexamers, and dodecamers in the crystal lattice. This finding is significant, because peptide $\mathbf{1_{Met}}$ lacks the ornithine mutation and thus is a better mimic of Aβ.

The crystal structure also establishes that the trimers, hexamers, and dodecamers can tolerate both Met_{35} and Orn_{35} residues, which suggests that position 35 may even tolerate mutations to spectroscopic probes, fluorescent dyes, and other unnatural amino acids.

Although the structures of peptides $\mathbf{1_{Met}}$ and $\mathbf{1_{Orn}}$ are nearly identical, their behavior in solution is different. SDS-PAGE studies showed that peptides $\mathbf{1_{Met}}$ and $\mathbf{1_{Orn}}$ are largely monomeric. Circular dichroism showed that peptide $\mathbf{1_{Met}}$ adopts a well-folded β-hairpin, while peptide $\mathbf{1_{Orn}}$ is largely unstructured. An LDH assay shows that only peptide $\mathbf{1_{Orn}}$ is toxic to cells and that peptide $\mathbf{1_{Met}}$ is not. This assay suggests that peptide $\mathbf{1_{Orn}}$ forms oligomers in the cell media that were not revealed by SDS-PAGE.

The ^{1}H NMR studies of peptides $\mathbf{1_{Met}}$, $\mathbf{1_{Orn}}$, **3**, and **4**, and trimer **2** are the first major effort to characterize *N*-methylated macrocyclic β-sheet peptides by ^{1}H NMR spectroscopy. The ^{1}H NMR studies showed that peptide $\mathbf{1_{Orn}}$ oligomerizes in solution, which provides an explanation for the toxicity observed in the LDH release assay. DOSY studies showed that the oligomers of peptide $\mathbf{1_{Orn}}$ form dimers or trimers at low-millimolar concentrations, but appear to form a dodecamer at higher concentrations. DOSY studies also showed that trimer **2** oligomerizes to form a tetramer in solution, which has a comparable molecular weight to the dodecamer of peptide $\mathbf{1_{Orn}}$. The dodecamer of peptide $\mathbf{1_{Orn}}$ and the tetramer of trimer **2** were not observed previously by other methods. These NMR studies show that DOSY is a useful tool for evaluating the oligomers of *N*-methylated peptides. These NMR studies also provide a basis for using NMR to characterize oligomers formed by other *N*-methylated macrocyclic β-sheet peptides.

ACKNOWLEDGMENTS

I thank Dr. Huiying Li for the helpful advice and assistance, the Laser Spectroscopy Facility at the University of California, Irvine for assistance with the circular dichroism measurements, the National Institutes of Health (NIH) for funding (Grant GM097562), and the Stanford Synchotron Radiation Lightsource (SSRL) and the Berkeley Center for Structural Biology (BCSB) of the Advanced Light Source (ALS) for synchotron data collection. The Use of the Stanford Synchotron Radiation Lightsource (SSRL) is jointly supported by the Department of Energy and the NIGMS. The BCSB is jointly supported by the NIH, NIGMS, and the Howard Hughes Medical Institute. The ALS is supported by the Director, Office of Science, Office of Basic Energy Sciences, of the U.S. Department of Energy under Contract No. DE-AC02-05CH11231.

REFERENCES AND NOTES

1. Hoyer, W.; Gronwall, C.; Jonsson, A.; Stahl, S.; Hard, T. *Proc. Natl. Acad. Sci. U.S.A.* **2008**, *105*, 5099–5104.
2. Sandberg, A.; Luheshi, L. M.; Söllvander, S.; Pereira de Barros, T.; Macao, B.; Knowles, T. P. J.; Biverstål, H.; Lendel, C.; Ekholm-Petterson, F.; Dubnovitsky, A.; Lannfelt, L.; Dobson, C. M.; Härd, T. *Proc. Natl. Acad. Sci. U.S.A.* **2010**, *107*, 15595–15600.
3. Lendel, C.; Bjerring, M.; Dubnovitsky, A.; Kelly, R. T.; Filippov, A.; Antzutkin, O. N.; Nielsen, N. C.; Hard, T. *Angew. Chem., Intl. Ed.* **2014**, *53*, 12756–12760.
4. Yu, L.; Edalji, R.; Harlan, J. E.; Holzman, T. F.; Lopez, A. P.; Labkovsky, B.; Hillen, H.; Barghorn, S.; Ebert, U.; Richardson, P. L.; Miesbauer, L.; Solomon, L.; Bartley, D.; Walter, K.; Johnson, R. W.; Hajduk, P. J.; Olejniczak, E. T. *Biochemistry* **2009**, *48*, 1870–1877.
5. Do, T. D.; LaPointe, N. E.; Nelson, R.; Krotee, P.; Hayden, E. Y.; Ulrich, B.; Quan, S.; Feinstein, S. C.; Teplow, D. B.; Eisenberg, D.; Shea, J.-E.; Bowers, M. T. *J. Am. Chem. Soc.* **2016**, *138*, 549–557.
6. Walsh, D. M.; Selkoe, D. J. *J. Neurochem.* **2007**, *101*, 1172–1184.
7. Haass, C.; Selkoe, D. J. *Nat. Rev. Mol. Cell Biol.* **2007**, *8*, 101–112.
8. Kirkitadze, M. D.; Bitan, G.; Teplow, D. B. *J. Neurosci. Res.* **2002**, *69*, 567–577.
9. Teplow, D. B. *Alzheimers Res. Ther.* **2013**, *5*, 1–39.
10. Benilova, I.; Karran, E.; De Strooper, B. *Nat. Neurosci.* **2012**, *15*, 349–357.
11. Larson, M. E.; Lesne, S. E. *J. Neurochem.* **2012**, *120*, 125–139.
12. Spencer, R. K.; Li, H.; Nowick, J. S. *J. Am. Chem. Soc.* **2014**, *136*, 5595–5598.

13. Spencer, R. K.; Kreutzer, A. G.; Salveson, P. J.; Li, H.; Nowick, J. S. *J. Am. Chem. Soc.* **2015**, *137*, 6304–6311.

14. Kreutzer, A. G.; Hamza, I. L.; Spencer, R. K.; Nowick, J. S. *J. Am. Chem. Soc.* **2016**, *138*, 4634–4642.

15. Salveson, P. J.; Spencer, R. K.; Nowick, J. S. *J. Am. Chem. Soc.* **2016**, *138*, 4458–4467.

16. Yoo, S.; Kreutzer, A. G.; Truex, N. L.; Nowick, J. S. *Chem. Sci.* **2016**, *7*, 6946–6951.

17. Kreutzer, A. G.; Yoo, S.; Spencer, R. K.; Nowick, J. S. *J. Am. Chem. Soc.* **2017**, *139*, 966–975.

18. Salveson, P. J.; Spencer, R. K.; Kreutzer, A. G.; Nowick, J. S. *Org. Lett.* **2017**, *19*, 3462–3465.

19. Pham, J. D.; Spencer, R. K.; Chen, K. H.; Nowick, J. S. *J. Am. Chem. Soc.* **2014**, *136*, 12682–12690.

20. Kreutzer, A. G.; Spencer, R. K.; McKnelly, K. J.; Yoo, S.; Hamza, I. L.; Salveson, P. J.; Nowick, J. S. *Biochemistry* **2017**, *56*, 6061–6071.

21. Minor, D. L., Jr.; Kim, P. S. *Nature* **1994**, *367*, 660–663.

22. Chou, P. Y.; Fasman, G. D. *Biochemistry* **2002**, *13*, 222–245.

23. Polson, A. *J. Phys. Colloid. Chem.* **1950**, *54*, 649–652.

24. Teller, D. C.; Swanson, E.; de Haën, C. *Methods Enzymol.* **1979**, *61*, 104–124.

25. Yao, S.; Howlett, G. J.; Norton, R. S. *J. Biomol. NMR* **2000**, *16*, 109–119.

26. Cohen, Y.; Avram, L.; Frish, L. *Angew. Chem., Intl. Ed.* **2005**, *44*, 520–554.

27. Cohen, Y.; Avram, L.; Evan-Salem, T.; Slovak, S.; Shemesh, N.; Frish, L. Diffusion NMR in Supramolecular Chemistry and Complexed Systems. In *Analytical Methods in Supramolecular Chemistry*, Wiley-VCH Verlag GmbH & Co. KGaA: 2012; pp 197–285.

28. The ratio of oligomer and monomer diffusion coefficients reflects the oligomerization state of the oligomer. Dimers and trimers will have diffusion coefficients of about 0.75−0.79 and 0.66−0.69 times that of a monomer. Hexamers and dodecamers will have diffusion coefficients of about 0.55 and 0.44 times that of a monomer. A trimer can only marginally be distinguished from a trimer on the basis of diffusion coefficients measured by DOSY, but a hexamer could easily be distinguished from a dodecamer.

29. Teilum, K.; Kunze, M. B.; Erlendsson, S.; Kragelund, B. B. *Protein Sci.* **2017**, *26*, 436–451.

SUPPORTING INFORMATION FOR

Efforts to Correlate Structure, Solution-Phase Behavior, and Toxicity of Peptides Derived from $A\beta_{17–36}$

4.I. MATERIALS AND METHODS

General

N,*N*-Dimethylformamide (DMF), 2,4,6-collidine, *N*-methylmorpholine (NMM), and piperidine were purchased from Alfa Aesar and used without further purification. HPLC grade acetonitrile (CH_3CN) was purchased from Fisher Scientific and used without further purification. Methylene chloride (CH_2Cl_2) was purchased from Fisher Scientific, stored under argon, and passed through a column of alumina before use.[1] Boc-Orn(Fmoc)-OH, HCTU, HBTU and HOBt were purchased from GL Biochem Ltd (Shanghai). 2-Chlorotrityl chloride resin and Fmoc protected amino acids were purchased from Chem-Impex International. *N*,*N*-Diisopropylethylamine (DIPEA), trifluoroacetic acid (TFA), and triisopropylsilane (TIPS) were purchased from Oakwood Chemical. Deuterium oxide (D, 99.96%) was purchased from Cambridge Isotope Laboratories, Inc.

Synthesis of Peptides $\mathbf{1_{Met}}$, $\mathbf{1_{Orn}}$, 3, and 4

Synthesis and purification of peptides $\mathbf{1_{Met}}$, $\mathbf{1_{Orn}}$, **3,** and **4**, were performed as described previously.[2,3,4,5,6,7,8,9,10]

Synthesis of Trimer 2

Synthesis, purification, and oxidation of trimer **2** were performed as described previously.[9]

Crystallization of Peptide $\mathbf{1}_{\mathbf{Met}}$.

Initial crystallization conditions for peptide $\mathbf{1}_{\mathbf{Met}}$ were based on the crystallization conditions previously published for peptide $\mathbf{1}_{\mathbf{Orn}}$, 0.1 M HEPES at pH 6.75 and 31% v/v Jeffamine M-600 [3]. These conditions for were optimized for peptide $\mathbf{1}_{\mathbf{Met}}$ using a 4x6 matrix Hampton VDX 24-well plate. In the optimized 24-well plate, the pH of HEPES in each row was varied by ± 0.1 pH units (6.3, 6.4, 6.5, and 6.6) and the Jeffamine concentration in each column was varied by ± 0.25% (24%, 24.25%, 24.5%, 24.75%, 25%, 25.25%, 25.5%). The first well in the 4x6 matrix (A1) was prepared by combining 100 μL of 1 M HEPES at pH 6.3, 480 μL of 50% (v/v) Jeffamine M-600 at pH 7.0, and 420 μL of 18 MΩ water to give a total volume of 1 mL. The conditions for the other wells were prepared in the same fashion by combining the appropriate amounts of 1 M HEPES buffer, 50% Jeffamine at pH 7.0, and 18 MΩ water to give a total volume of 1 mL.

Three hanging-drops were prepared per borosilicate glass slide by combining a solution of peptide $\mathbf{1}_{\mathbf{Met}}$ (1 μL, 5 mg/mL) and the well solution (1 μL) in a ratio of 1:1, 2:1, and 1:2. Each slide was then inverted and placed on the corresponding well, using the silicone grease surrounding the well to create a hermetic seal. Large crystals grew after about 24 h. Crystals suitable for X-ray crystallography were harvested with a nylon loop attached to a copper pin and flash frozen in liquid nitrogen prior to data collection.

NMR Spectroscopy of Peptides

Sample Preparation. NMR spectroscopy of the macrocyclic β-sheet peptides was performed in D2O (D, 99.96%; Cambridge Isotope Laboratories, Inc.) with 25 mM CD3COOD (D, 99.5%; Cambridge Isotope Laboratories, Inc.) and 25 mM CD3COONa (D, 99%; Cambridge Isotope Laboratories, Inc.). Each solution contained 0.06 mM 4,4-dimethyl-4-silapentane-1-ammonium trifluoroacetate (DSA) as an internal standard for referencing chemical shifts. The solutions were prepared by dissolving a weighed portion of the peptide in the appropriate volume of solvent. The molecular weights of the peptides were calculated as the TFA salts with all amino groups assumed to be protonated. The solutions were allowed to stand for at least 1 h to allow complete hydrogen to deuterium exchange of the amide NH protons.

^{1}H NMR, TOCSY and ROESY Data Collection. NMR spectra were recorded on a Bruker 500 MHz spectrometer with a TCI probe. Presaturation water suppression was applied as needed. TOCSY spectra were recorded with 2048 points in the f_2 dimension and 512 increments in the f_1 dimension with a 150-ms spin-lock mixing time. ROESY spectra were recorded with 2048 points in the f_2 dimension and 512 increments in the f_1 dimension with a 200-ms spin-lock mixing time.

^{1}H NMR, TOCSY and ROESY Data Processing. NMR spectra were processed with Bruker XwinNMR software. Automatic baseline correction was applied in both dimensions after phasing the spectra. TOCSY and ROESY spectra were Fourier transformed to a final matrix size of 2048 x 1024 real points using a Qsine weighting function and forward linear prediction. NOESY spectra were Fourier transformed to a final matrix size of 2048 x 2048 real points using a Qsine weighting function and forward linear prediction.

Diffusion-Ordered Spectroscopy (DOSY) Experiments. DOSY experiments were performed on a Bruker 500 MHz spectrometer equipped with a TCI cryoprobe, with a diffusion delay (Δ) of 75-ms and a diffusion gradient length (δ) of 2.5-ms. Sixteen sets of FIDs were recorded with the gradient strength incremented from 5%–95% using a linear ramp. The combined FIDs were Fourier transformed in Bruker's TopSpin^{TM} software to give a pseudo-2D spectrum. After phasing and performing baseline correction, each pseudo-2D spectrum was processed with logarithmic scaling on the Y-axis. The Y-axis was calibrated to the diffusion coefficient of the residual HOD peak in D_2O (1.9×10^{-9} m^2/s at 298 K). The diffusion coefficients of the peptides were read and converted from logarithmic values to linear values.

SDS-PAGE of Peptides $\mathbf{1_{Met}}$, $\mathbf{1_{Orn}}$, and Trimer 2.

Reagents and gels for SDS-PAGE were prepared according to recipes and procedures for Tricine–SDS-PAGE as described by Schägger, H. in *Nat. Protoc.* **2006**, *1*, 16–22.[11] The migration of the peptides was compared with a molecular weight protein ladder (SpectraTM Multicolor Low Range Protein Ladder, ThermoFisher Scientific, catalog #: 26628). The peptides in the gel were visualized by staining them with silver nitrate, which was performed using the procedures and reagents described by Simpson, R. J. *CSH Protoc.*, **2007**.[12] Fresh solutions were prepared each time of the 0.02% (w/v) sodium thiosulfate, 0.1% (w/v) silver nitrate solution, and developing solution.

Sample preparation. SDS-PAGE of peptides $\mathbf{1_{Met}}$, $\mathbf{1_{Orn}}$, and trimer **2** was performed with aliquots from 10 mg/mL stock solutions. The solutions were diluted with 18 MΩ water to create

2-mg/mL solutions of peptides $\mathbf{1}_{\mathbf{Met}}$ and $\mathbf{1}_{\mathbf{Orn}}$ and a 0.12-mg/mL solution of trimer 2. The 2-mg/mL and 0.12-mg/mL solutions were further diluted with a 2X SDS-PAGE loading buffer (100 mM Tris buffer at pH 6.8, 20% (v/v) glycerol, and 4% SDS) to a final concentration of 1 mg/mL for peptides $\mathbf{1}_{\mathbf{Met}}$ and $\mathbf{1}_{\mathbf{Orn}}$, and 0.06 mg/mL for trimer **2**. 5.0 μL of each solution was added into the lanes of a 4% polyacrylamide stacking gel with a 16% polyacrylamide running gel. 2.0 μL of the protein ladder was added into an adjacent lane. The gel was run at a constant 90 volts.

Gel Staining. After electrophoresis, the gel was removed from the casting glass and agitated gently in fixing solution [50% (v/v) methanol and 5% (v/v) acetic acid in deionized water] for 20 min. The fixing solution was then discarded and the gel was agitated gently in 50% (v/v) aqueous methanol for 10 min. The 50% methanol was discarded and the gel was agitated gently in deionized water for 10 min. The water was discarded and the gel was agitated gently in 0.02% (w/v) sodium thiosulfate in 18 MΩ water for 1 min. The sodium thiosulfate was discarded and the gel was rinsed twice with deionized water for 1 min. After the last rinse, the gel was submerged in chilled 0.1% (w/v) silver nitrate in 18 MΩ water and rocked at 4 °C for 20 min. The silver nitrate solution was then discarded and the gel was rinsed twice with 18 MΩ water for 1 min. To develop the gel, the gel was incubated in developing solution (2% (w/v) sodium carbonate, 0.04% (w/v) formaldehyde until the desired intensity of staining was reached (ca. 1–3 min). The development was then stopped by discarding the developing solution and submerging the gel in 5% aqueous acetic acid.

LDH release assays.

The LDH release assay was performed using the Pierce LDH Cytotoxicity Assay Kit from Thermo Scientific. Experiments were performed in replicates of five, and an additional 10 wells were used for controls. Cells were cultured in the inner 60 wells (rows B–G, columns 2–11) of the 96-well plate. DMEM:F12 media (100 μL) was added to the outer wells (rows A and H and columns 1 and 12), in order to ensure the greatest reproducibility of data generated from the inner wells.

Sample Preparation. Preparation of stock solutions of peptides $\mathbf{1}_{\mathbf{Met}}$ and $\mathbf{1}_{\mathbf{Orn}}$. 10-mg/mL stock solutions of peptides $\mathbf{1}_{\mathbf{Met}}$ and $\mathbf{1}_{\mathbf{Orn}}$ were prepared gravimetrically by dissolving 1.0 mg of each compound in 100 μL of deionized water that was filtered through a 0.2 μm syringe filter. The stock solution was used to create 2-, 1.5, 1.0, and 0.5 mM working solutions of peptides $\mathbf{1}_{\mathbf{Met}}$ and $\mathbf{1}_{\mathbf{Orn}}$.

Tissue Culture. Preparation of SH-SY5Y cells for LDH release assays. SH-SY5Y cells were plated in a 96-well plate at 15,000 cells per well. Cells were incubated in 100 μL of a 1:1 mixture of DMEM:F12 media supplemented with 10% fetal bovine serum, 100 U/mL penicillin, and 100 μg/mL streptomycin at 37 °C in a 5% CO_2 atmosphere and allowed to adhere to the bottom of the plate for 24 hours.

Cell Treatment. After 24 hours, the culture media was removed and replaced with 90 μL of serum-free DMEM:F12 media. A 10-μL aliquot of the working solution of peptides $\mathbf{1}_{\mathbf{Met}}$ and $\mathbf{1}_{\mathbf{Orn}}$ was added to each well, for well concentrations of 200, 150, 100, and 50 μM. Experiments were run in replicates of five. Five wells were used as controls and received 10-μL aliquots of

deionized water (vehicle). Another five wells were left untreated, to be subsequently used as controls with lysis buffer for the LDH release assay. Cells were incubated at 37 °C in a 5% CO2 atmosphere for 72 hours.

LDH release assay. After 72 hours, 10 μL of 10x lysis buffer—included with the assay kit—was added to the five untreated wells, and the cells were incubated for an additional 45 min. After 45 min, a 50-μL aliquot of the supernatant media from each well was transferred to a new 96-well plate and 50 μL of LDH substrate solution, prepared according to manufacturer's protocol, was added to each well. The treated plates were stored in the dark for 30 min.

Measuring Cell Death. The absorbance of each well was measured at 490 and 680 nm (A490 and A680). Data were processed by calculating the differential absorbance for each well (A490−A680) and comparing those values to those of the lysis buffer controls and the untreated controls:

% cell death = [(A490−A680)compound − (A490−A680)vehicle]／[(A490−A680)lysis − (A490−A680)vehicle]

4.II. REFERENCES

1. Pangborn, A. B.; Giardello, M. A.; Grubbs, R. H.; Rosen, R. K.; Timmers, F. J. *Organometallics* **1996**, *15*, 1518–1520.
2. Spencer, R.; Chen, K. H.; Manuel, G.; Nowick, J. S. *Eur. J. Org. Chem.* **2013**, 3523–3528.
3. Spencer, R. K.; Li, H.; Nowick, J. S. *J. Am. Chem. Soc.* **2014**, *136*, 5595–5598.
4. Spencer, R. K.; Kreutzer, A. G.; Salveson, P. J.; Li, H.; Nowick, J. S. *J. Am. Chem. Soc.* **2015**, *137*, 6304–6311.
5. Kreutzer, A. G.; Hamza, I. L.; Spencer, R. K.; Nowick, J. S. *J. Am. Chem. Soc.* **2016**, *138*, 4634–4642.
6. Salveson, P. J.; Spencer, R. K.; Nowick, J. S. *J. Am. Chem. Soc.* **2016**, *138*, 4458–4467.
7. Yoo, S.; Kreutzer, A. G.; Truex, N. L.; Nowick, J. S. *Chem. Sci.* **2016**, *7*, 6946–6951.
8. Kreutzer, A. G.; Spencer, R. K.; McKnelly, K. J.; Yoo, S.; Hamza, I. L.; Salveson, P. J.; Nowick, J. S. *Biochemistry* **2017**.
9. Kreutzer, A. G.; Yoo, S.; Spencer, R. K.; Nowick, J. S. *J. Am. Chem. Soc.* **2017**, *139*, 966–975.
10. Salveson, P. J.; Spencer, R. K.; Kreutzer, A. G.; Nowick, J. S. *Org. Lett.* **2017**, *19*, 3462–3465.
11. Schägger, H. *Nature protocols* **2006**, *1*, 16.
12. Simpson, R. J. *CSH protocols* **2007**, *2007*, pdb prot4727.

4.III. CHARACTERIZATION DATA

RP-HPLC of peptide **1_{Met}**

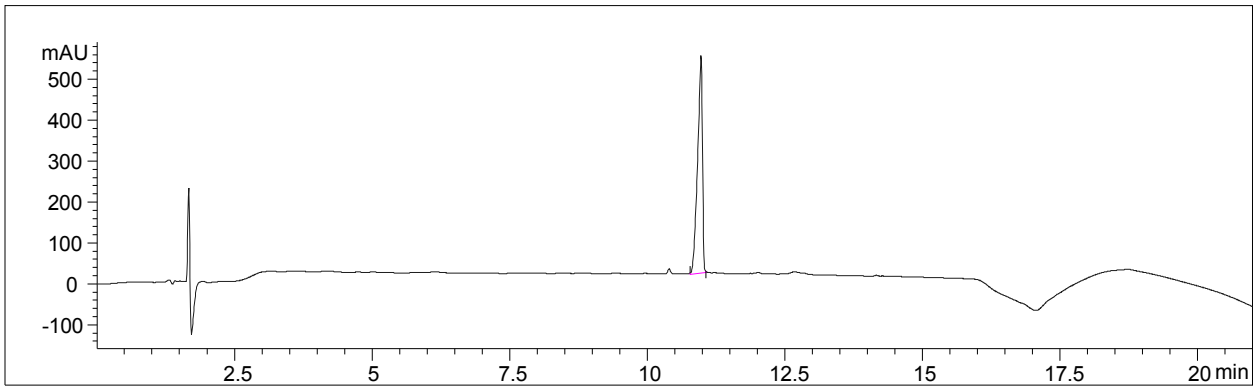

Peak #	RetTime [min]	Type	Width [min]	Area mAU*s	Height [mAU]	Area %
1	10.975	BV	0.1013	3232.95288	531.77228	100.0000
Totals :				3232.95288	531.77228	

column:	Aeris XB-C18 2.6µ
dimensions:	150 mm x 4.6 mm
mobile phase:	A: H_2O, 0.1% TFA B: CH_3CN, 0.1% TFA
gradient:	A/B (95:5) to (0:67) in 15 min
flow rate:	1.0 mL/min
detection:	VWD, wavelength = 214 nm
temperature:	298 K

MS (ESI) of peptide **1_{Met}**

24-Oct-2017
13:31:19

NT_V_171024_1Met_1-1 10 (0.184) Sm (SG, 2x3.00); Cm (8:12)

TOF MS ES+
1.17e3

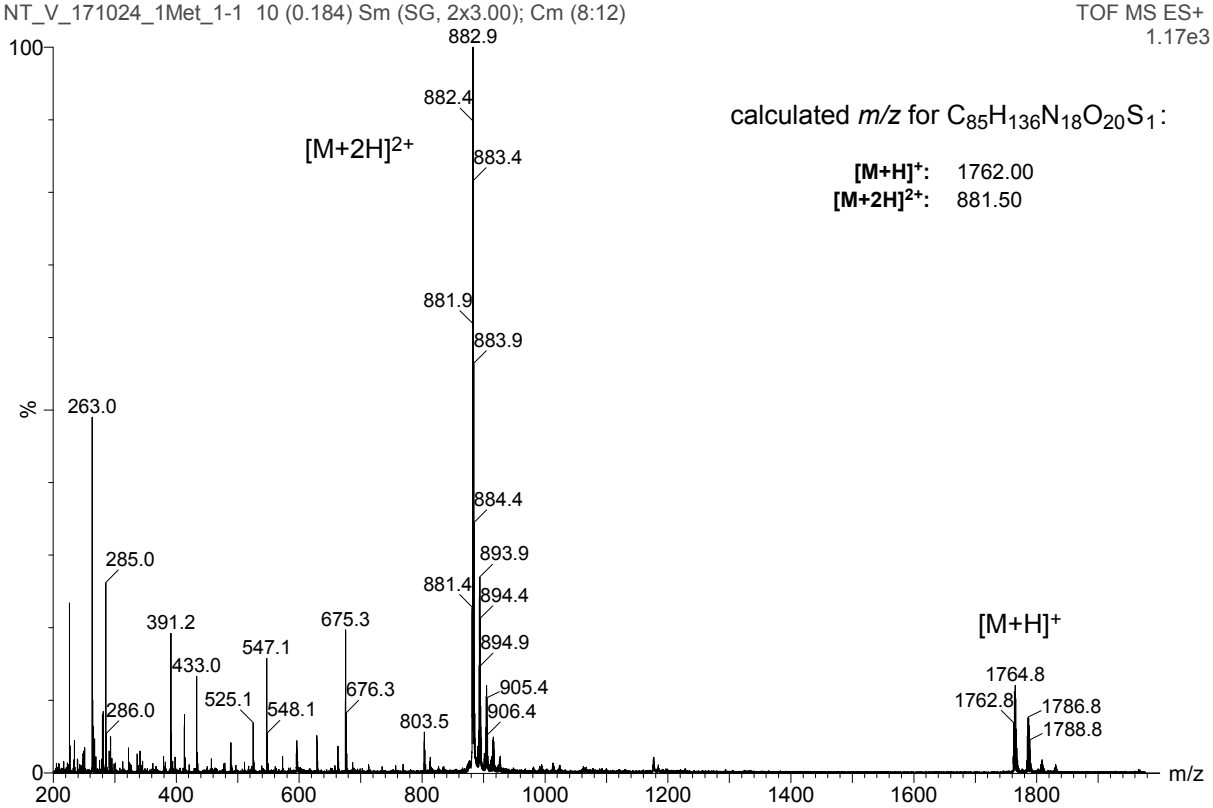

calculated *m/z* for $C_{85}H_{136}N_{18}O_{20}S_1$:

$[M+H]^+$:	1762.00
$[M+2H]^{2+}$:	881.50

MS (ESI) of peptide **1_{Met}**

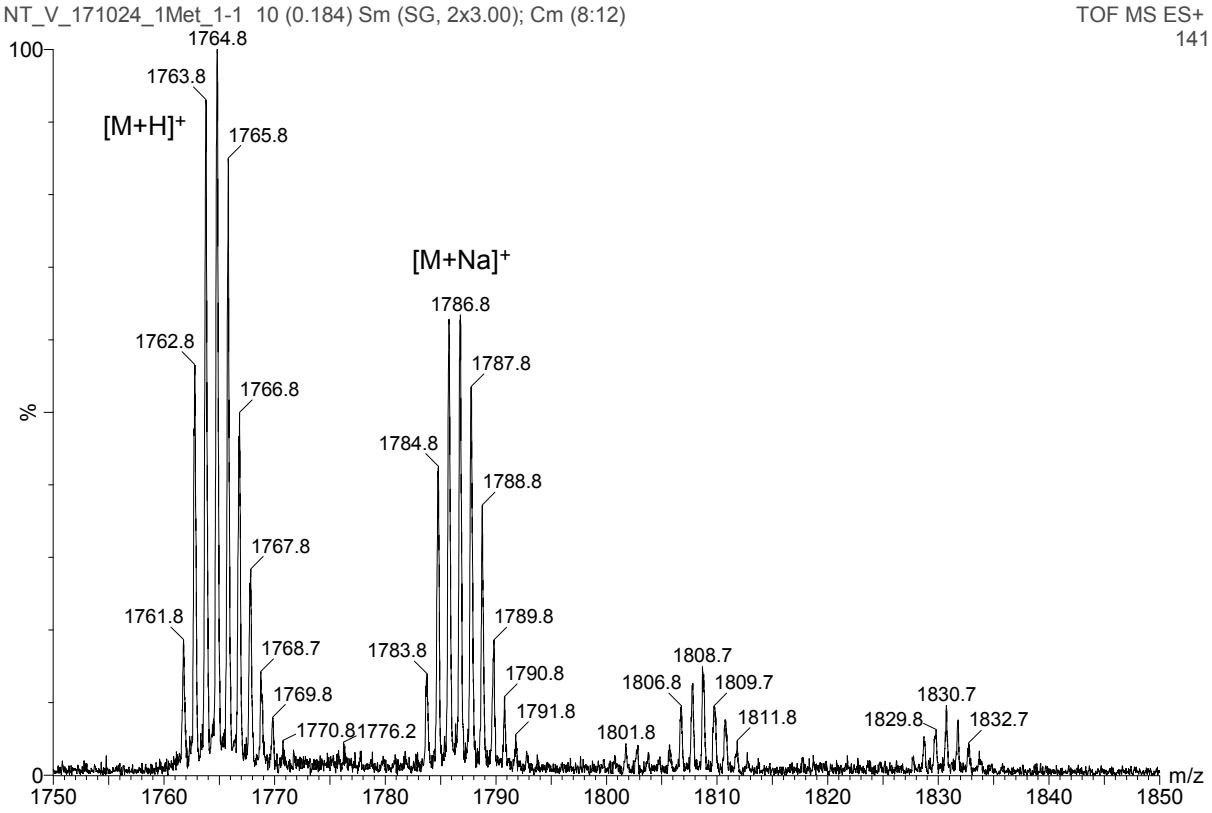

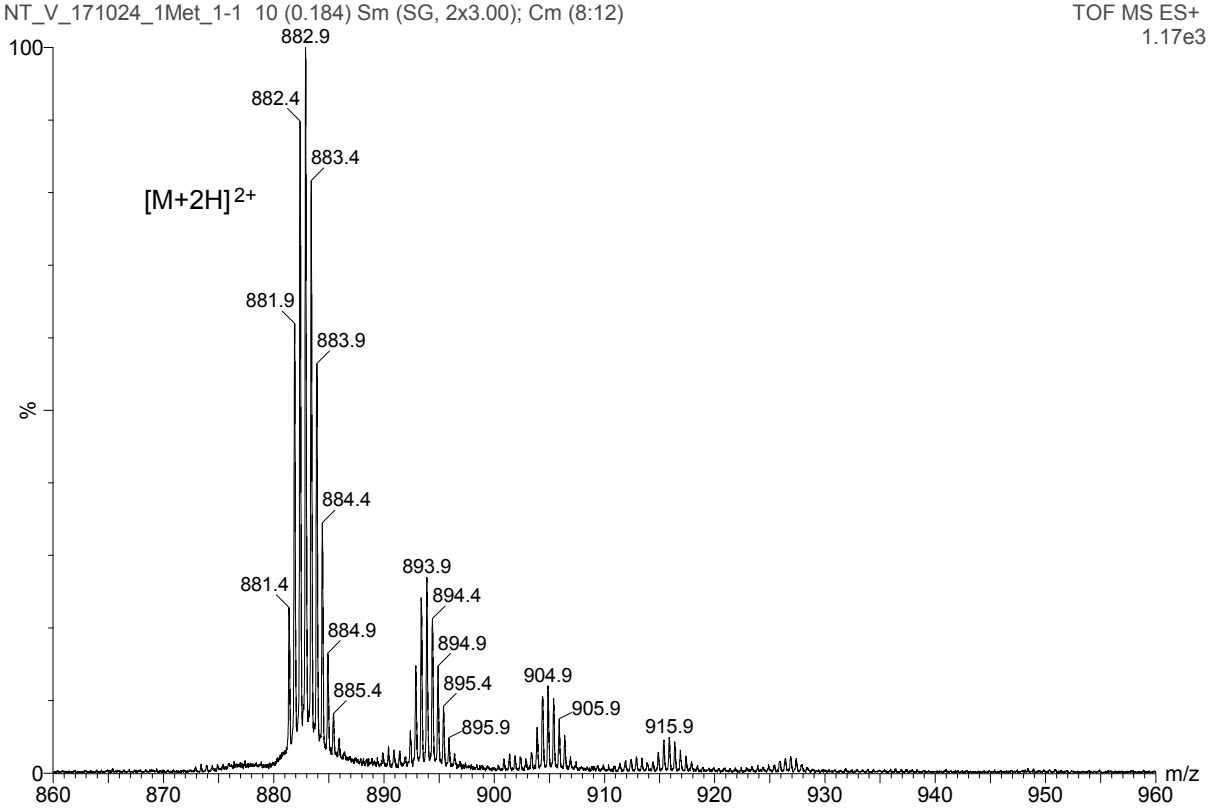

^{1}H NMR of peptide **1$_{Met}$**, *0.5 mM in D_2O with 50 mM acetate buffer at 500 MHz and 293 K

Precipitation was observed in the NMR tube, resulting in a lower sample concentration.
The asterisk (*) indicates that the sample concentration is only nominally 0.5 mM.

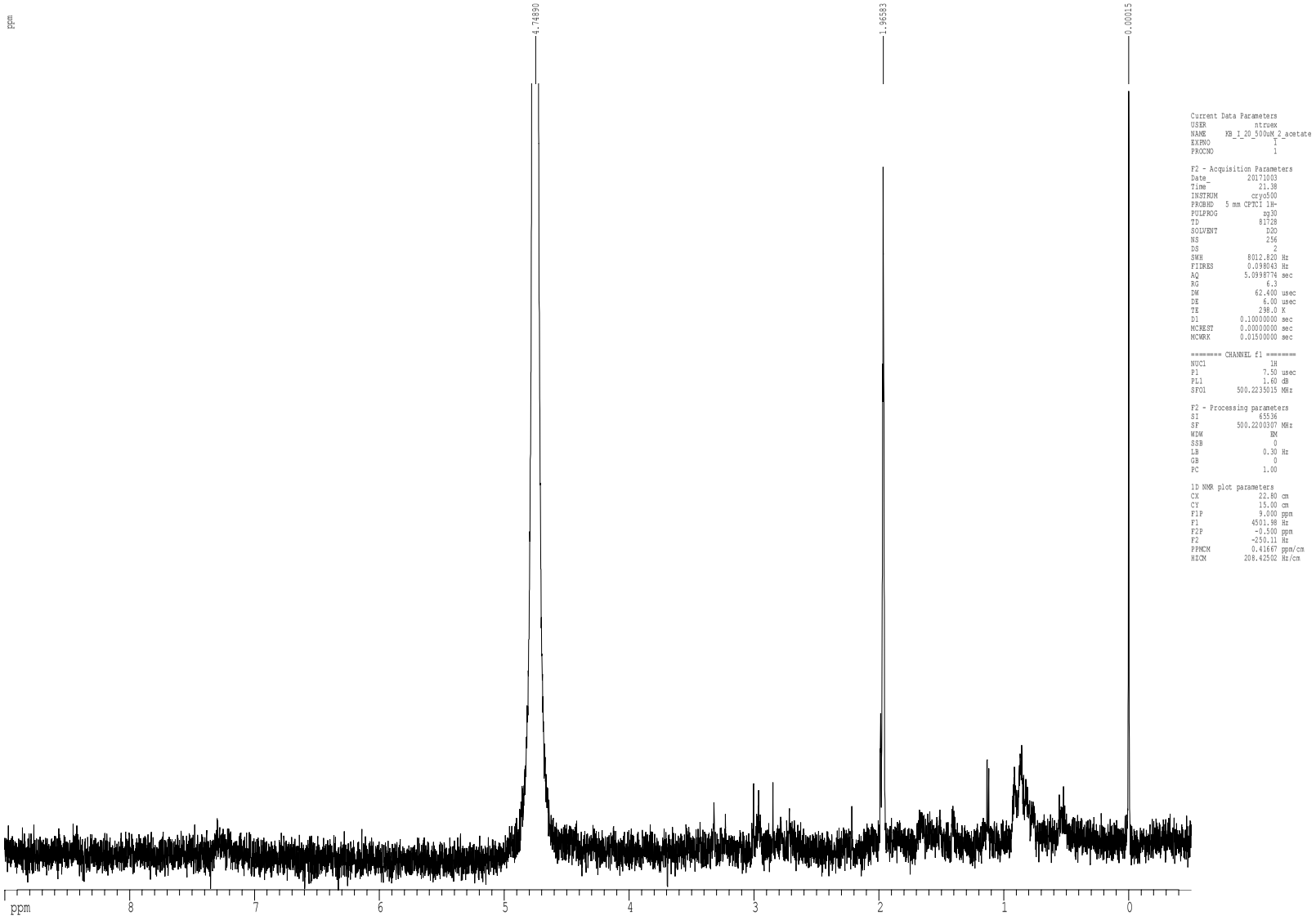


```
Current Data Parameters
USER                ntruex
NAME      KB_1_20_500uM_2_acetate
EXPNO                    1
PROCNO                   1

F2 - Acquisition Parameters
Date_           20171003
Time             21.38
INSTRUM          cryo500
PROBHD   5 mm CPTCI 1H-
PULPROG             zg30
TD                 81728
SOLVENT              H2O
NS                   256
DS                     2
SWH              8012.820 Hz
FIDRES           0.098043 Hz
AQ               5.09987744 sec
RG                   6.3
DW                  62.400 usec
DE                   6.00 usec
TE                  298.0 K
D1            0.10000000 sec
MCREST        0.00000000 sec
MCWRK         0.01500000 sec

======= CHANNEL f1 ======
NUC1                 1H
P1                  7.50 usec
PL1                 1.60 dB
SFO1         500.2235015 MHz

F2 - Processing parameters
SI                  65536
SF           500.2200307 MHz
WDW                  EM
SSB                     0
LB                   0.30 Hz
GB                      0
PC                   1.00

1D NMR plot parameters
CX                  22.80 cm
CY                  15.00 cm
F1P                 9.000 ppm
F1                4501.98 Hz
F2P                -0.500 ppm
F2                 -250.11 Hz
PPMCM              0.41667 ppm/cm
HZCM             208.42502 Hz/cm
```

RP-HPLC of peptide **1_{Orn}**

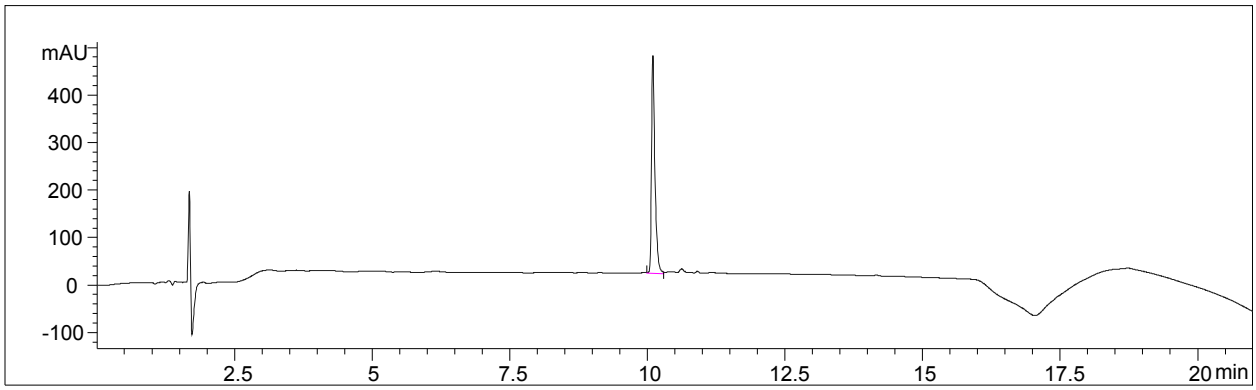

Peak #	RetTime [min]	Type	Width [min]	Area mAU*s	Height [mAU]	Area %
1	10.100	MM	0.0724	1998.96826	460.10202	100.0000
Totals :				1998.96826	460.10202	

column:	Aeris XB-C18 2.6µ
dimensions:	150 mm x 4.6 mm
mobile phase:	A: H_2O, 0.1% TFA B: CH_3CN, 0.1% TFA
gradient:	A/B (95:5) to (0:67) in 15 min
flow rate:	1.0 mL/min
detection:	VWD, wavelength = 214 nm
temperature:	298 K

MS (ESI) of peptide **1_{Orn}**

24-Oct-2017
13:29:17

NT_V_171024_1Orn_2-1 11 (0.202) Sm (SG, 2x3.00); Cm (9:18)

TOF MS ES+
3.92e3

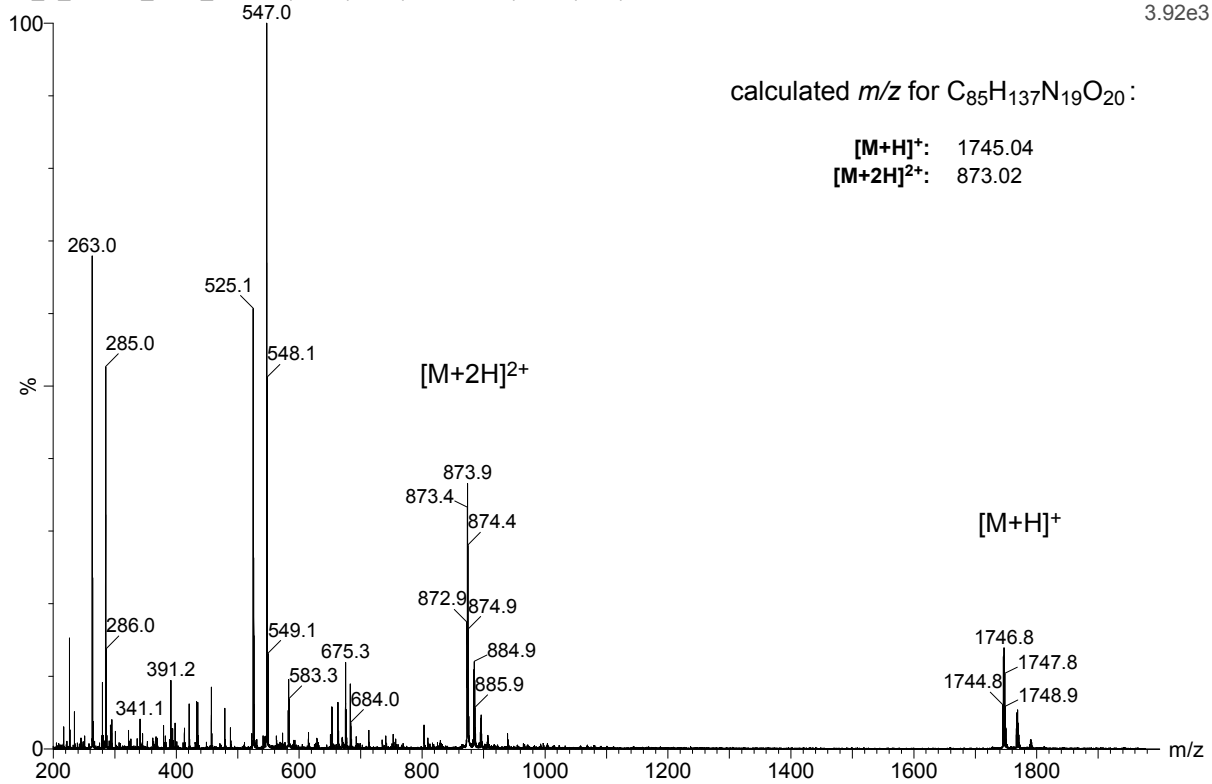

calculated *m/z* for $C_{85}H_{137}N_{19}O_{20}$:

$[M+H]^+$:	1745.04
$[M+2H]^{2+}$:	873.02

MS (ESI) of peptide $\mathbf{1_{Orn}}$

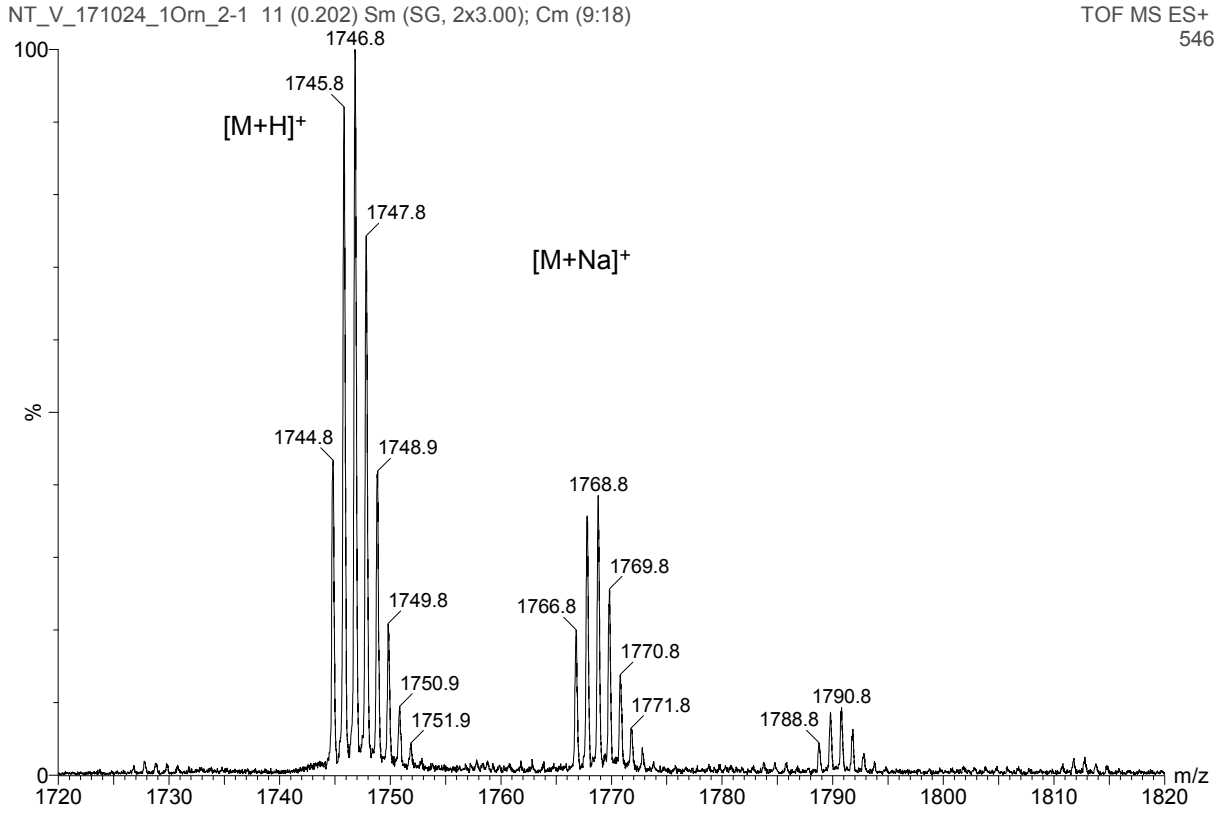

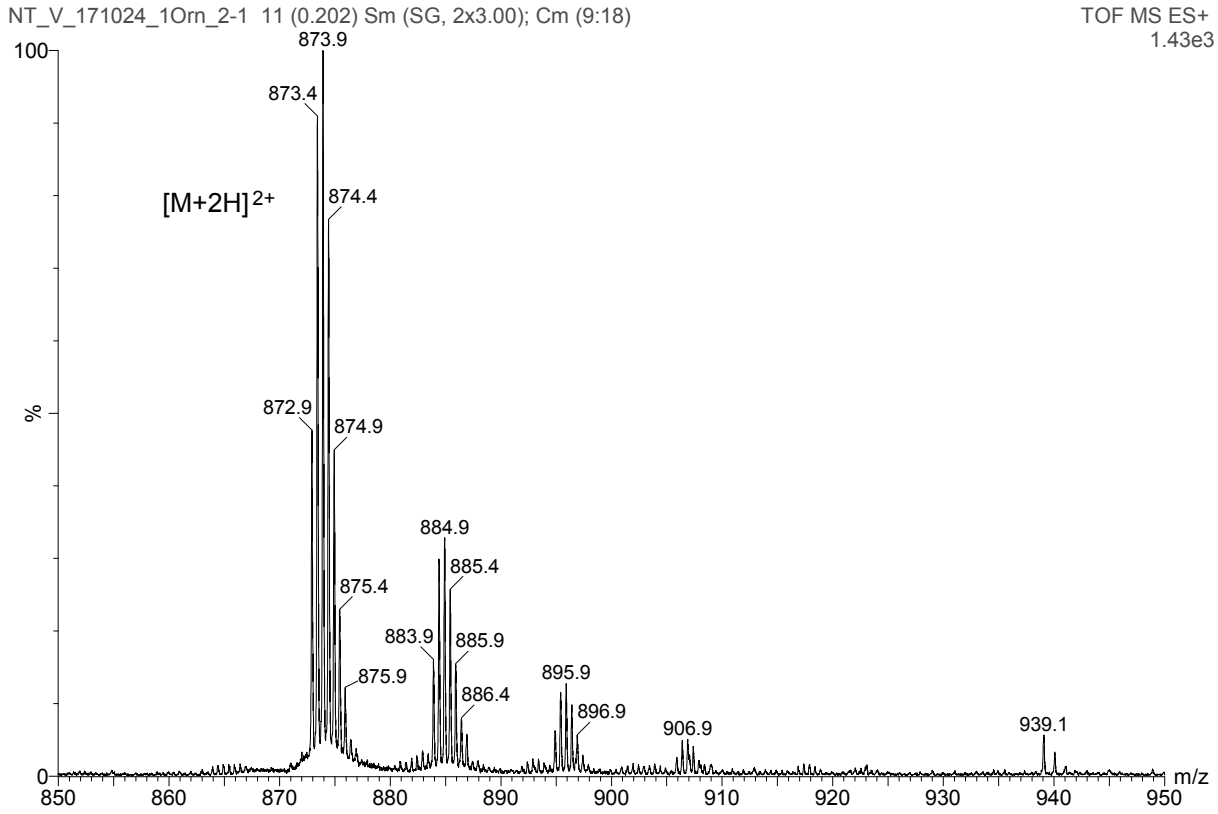

^{1}H NMR of peptide **1orn**, 0.25 mM in D_2O with 50 mM acetate buffer at 500 MHz and 293 K

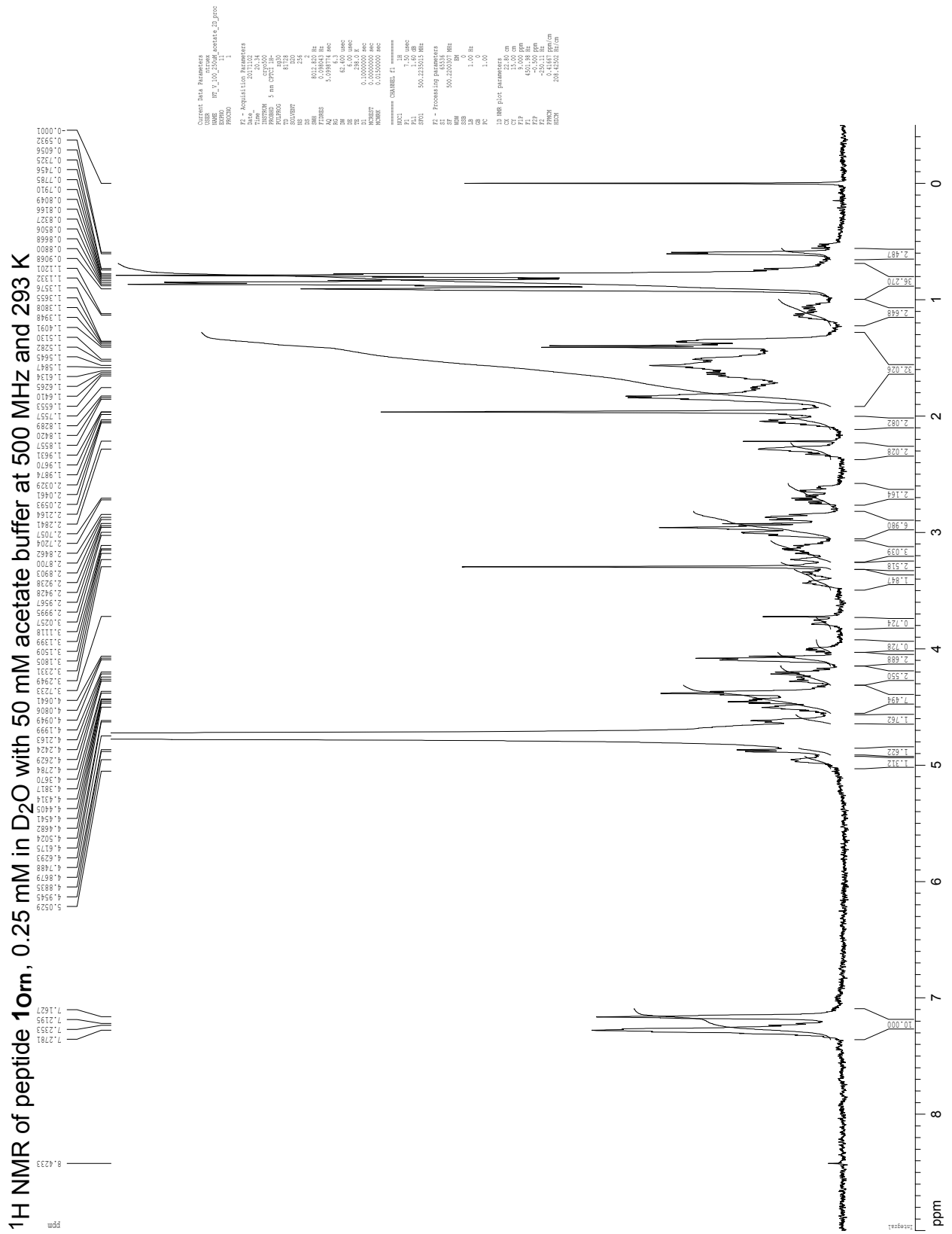

^{1}H NMR of peptide **1orn**, 0.25 mM in D_2O with 50 mM acetate buffer at 500 MHz and 293 K

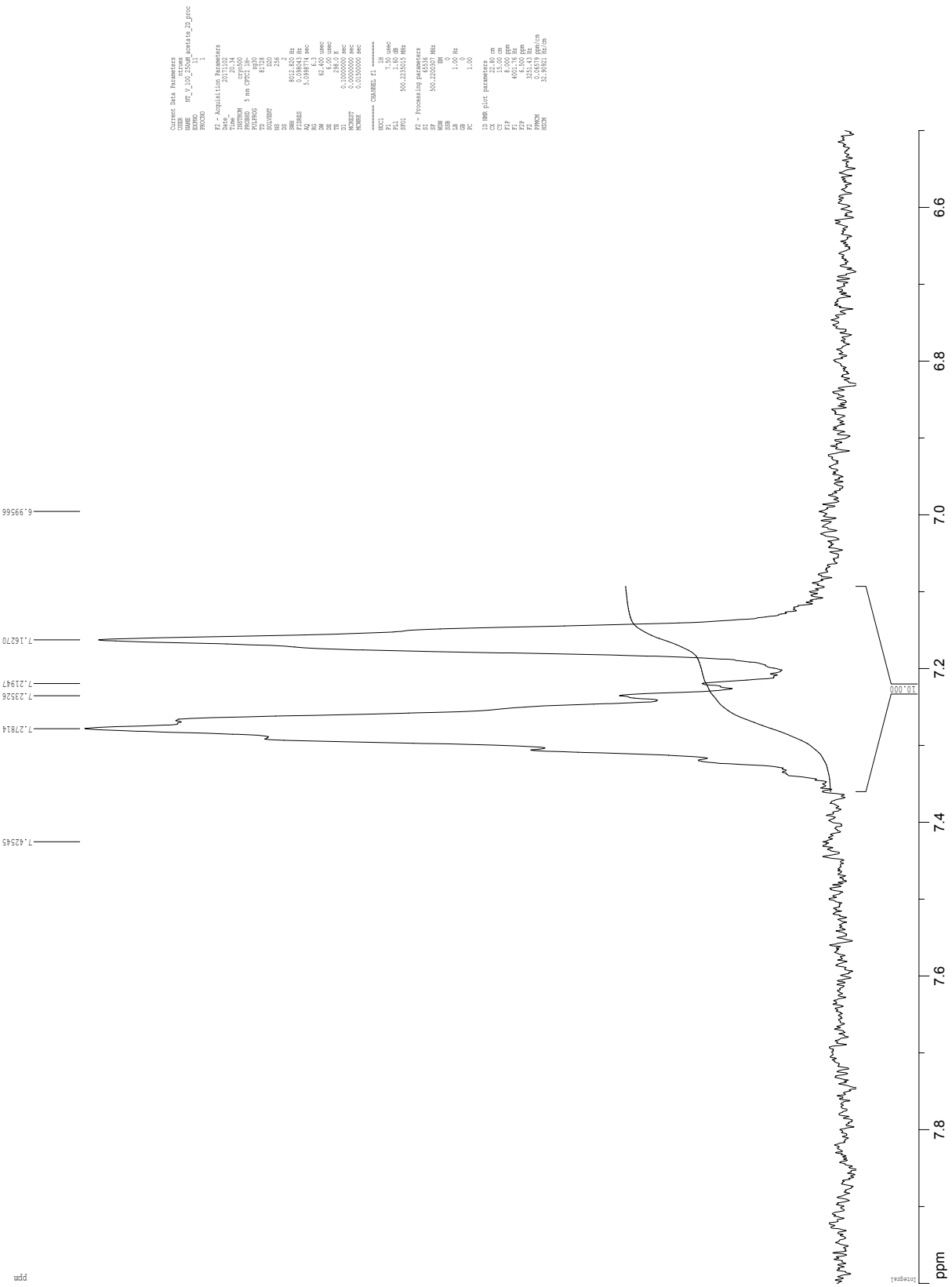

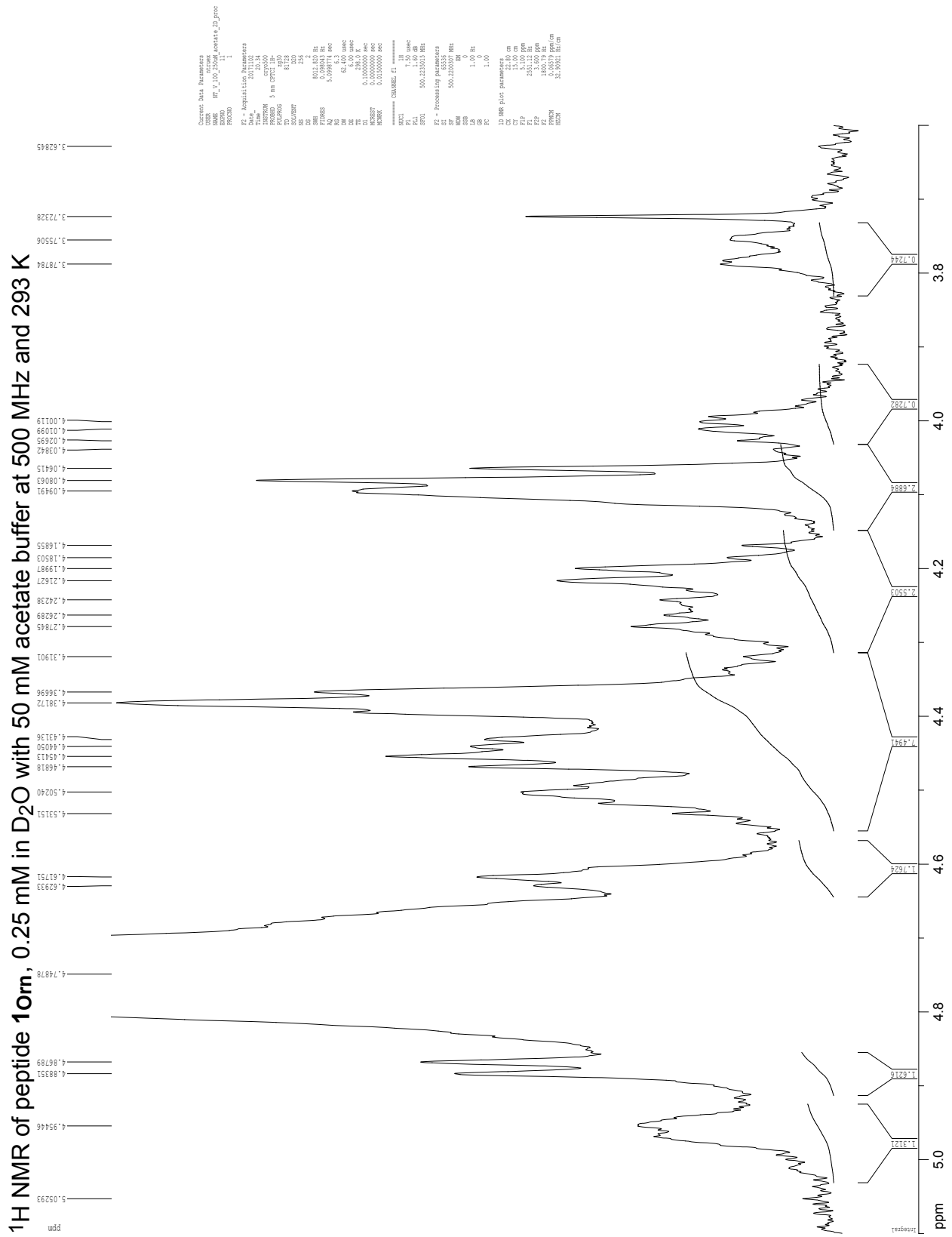
1H NMR of peptide 1orn, 0.25 mM in D2O with 50 mM acetate buffer at 500 MHz and 293 K
ppm
5.0
4.8
4.6
4.4
4.2
4.0
3.8
integral
1.3121
1.6216
1.7624
7.4941
2.5505
2.8884
0.7282
0.7244

^{1}H NMR of peptide **1Orn**, 0.25 mM in D_2O with 50 mM acetate buffer at 500 MHz and 293 K

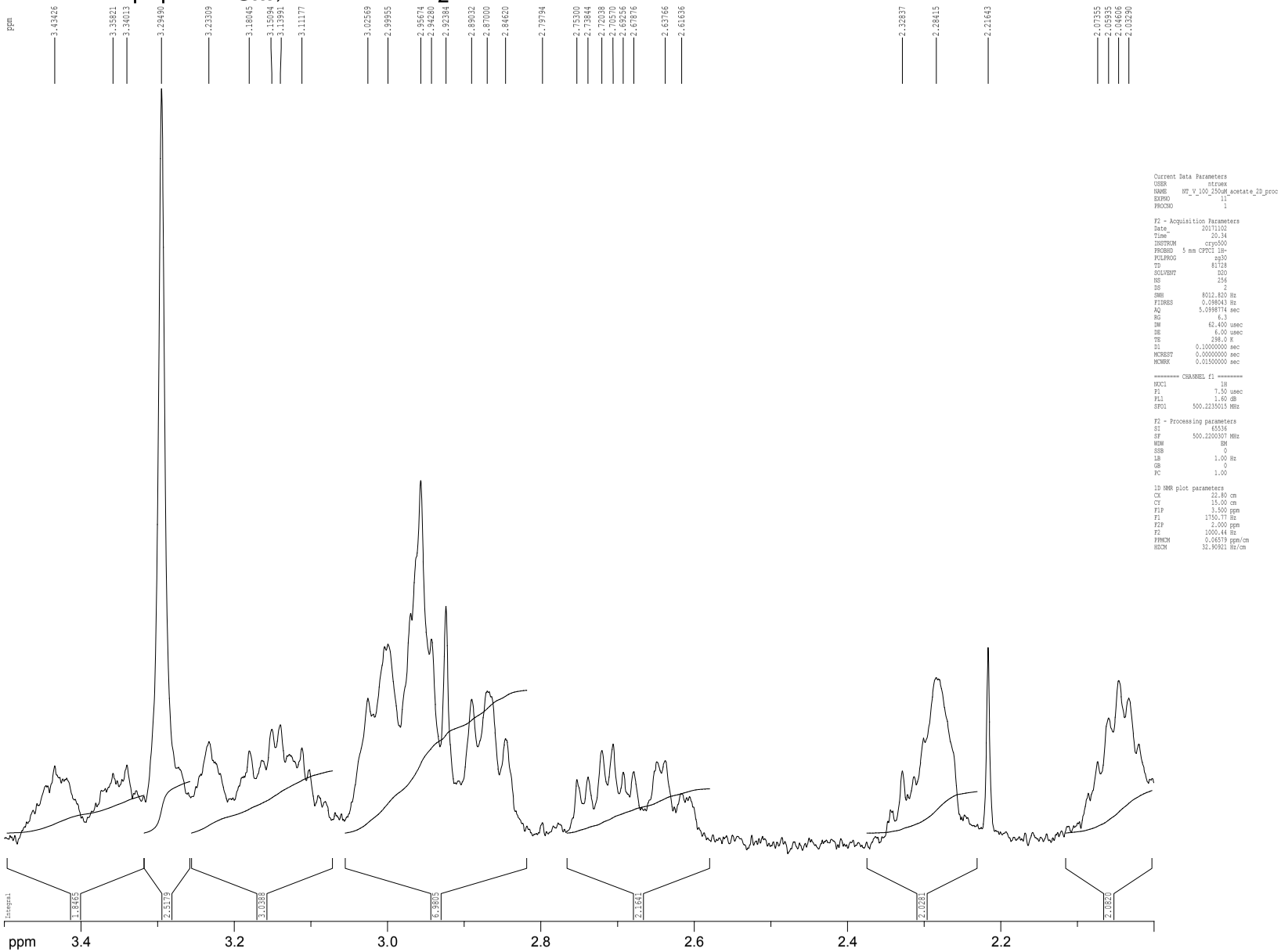

^{1}H NMR of peptide **1Orn**, 0.25 mM in D_2O with 50 mM acetate buffer at 500 MHz and 293 K

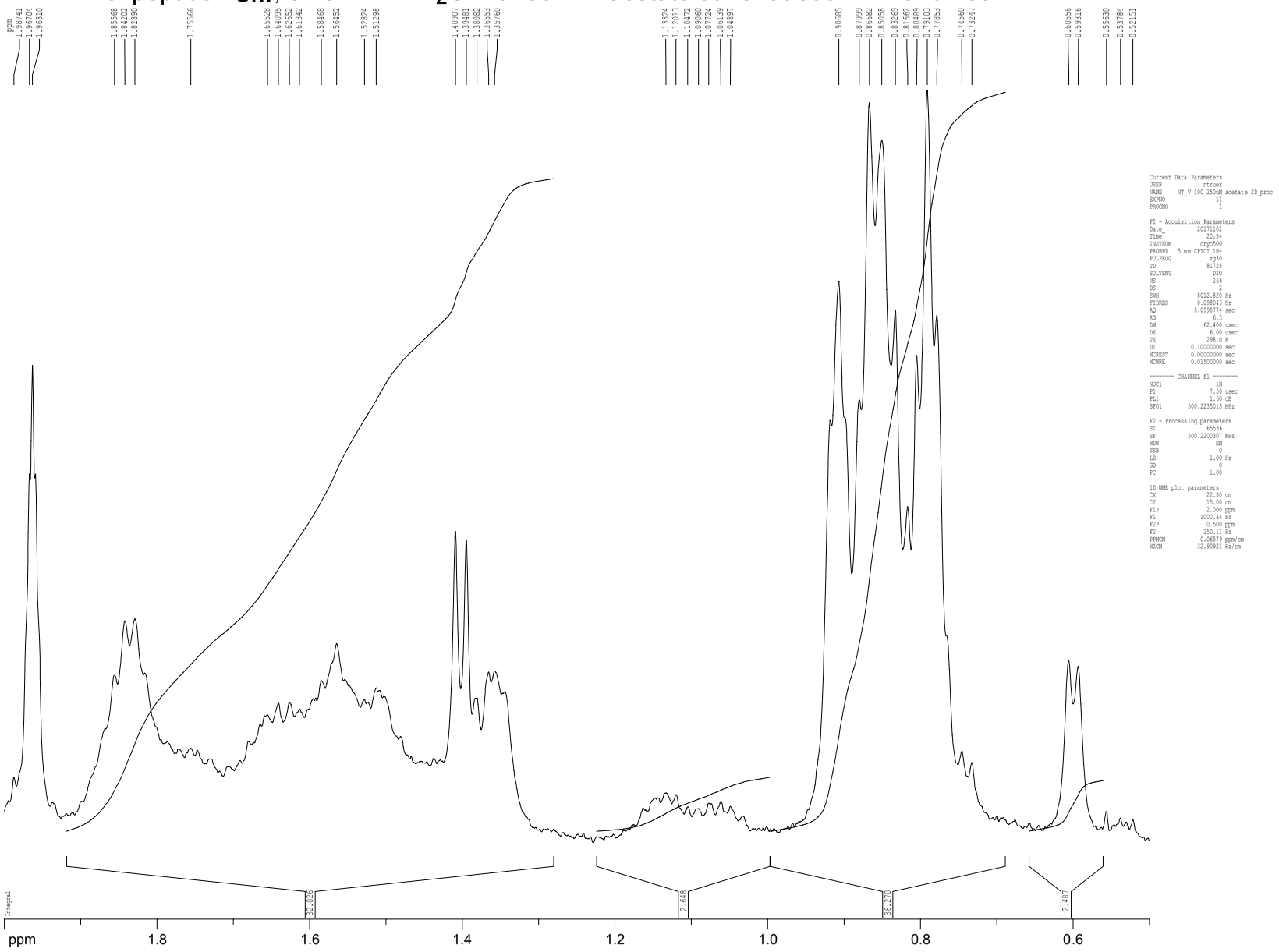

^{1}H NMR 2D TOCSY of peptide **1$_{Orn}$** with presaturation suppression of the HOD peak
0.25 mM in D_2O at 500 MHz and 298 K with 150-ms spin-lock mixing time

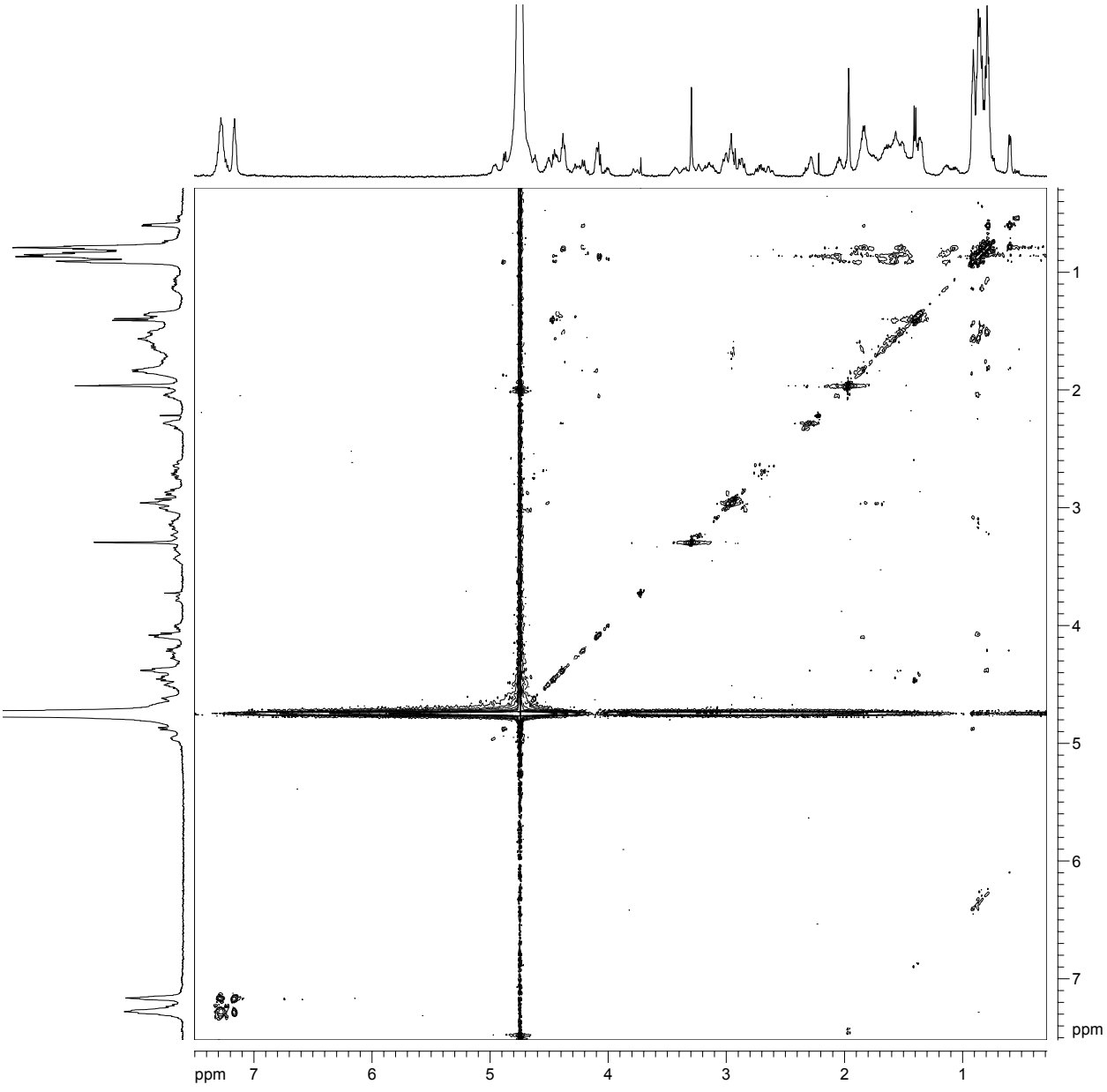

^{1}H NMR 2D TOCSY of peptide **1$_{Orn}$** with presaturation suppression of the HOD peak
0.25 mM in D_2O at 500 MHz and 298 K with 150-ms spin-lock mixing time

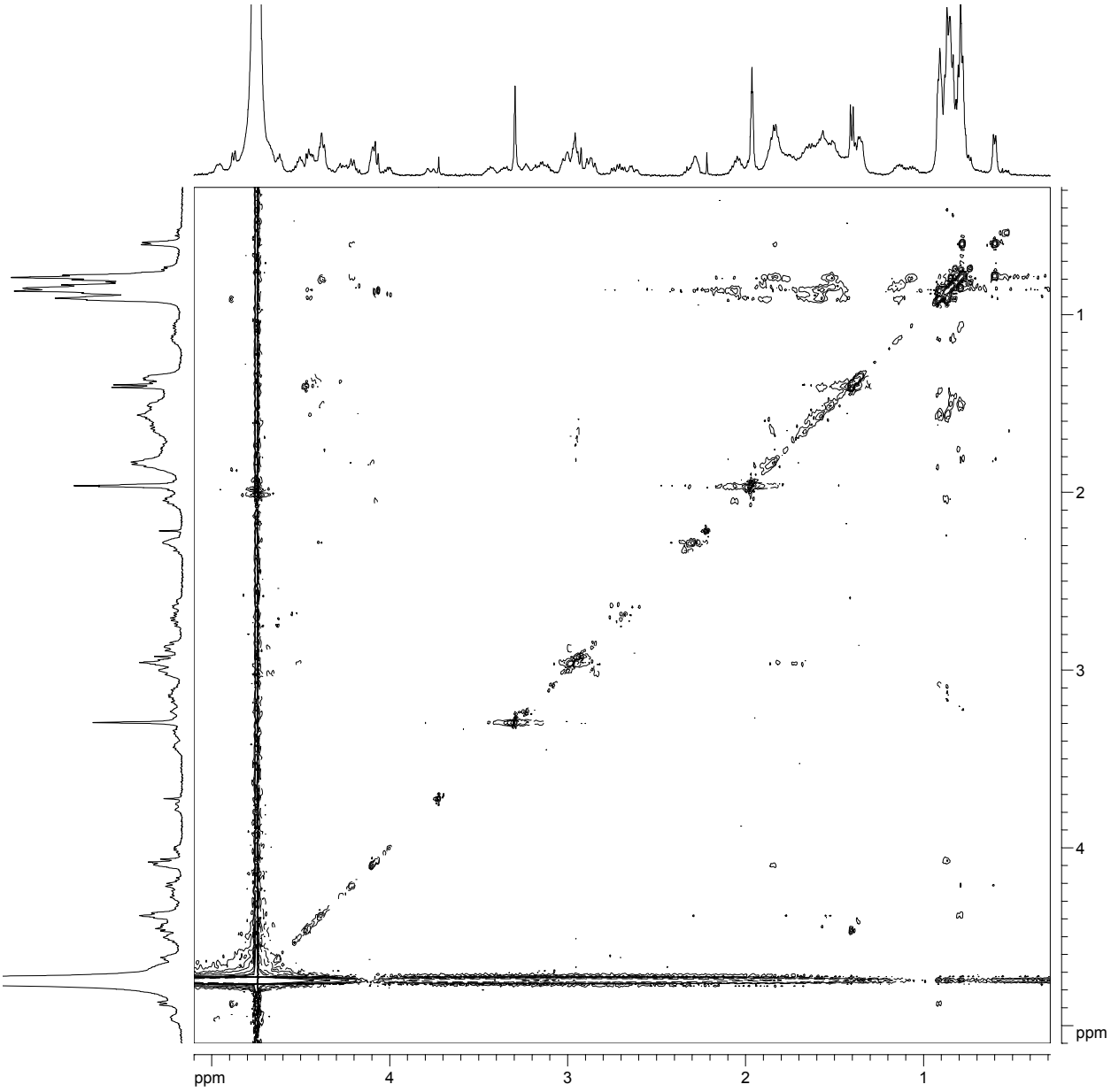

^{1}H NMR 2D ROESY of peptide **1$_{Orn}$** with presaturation suppression of the HOD peak
0.25 mM in D_2O at 500 MHz and 298 K with 150-ms spin-lock mixing time

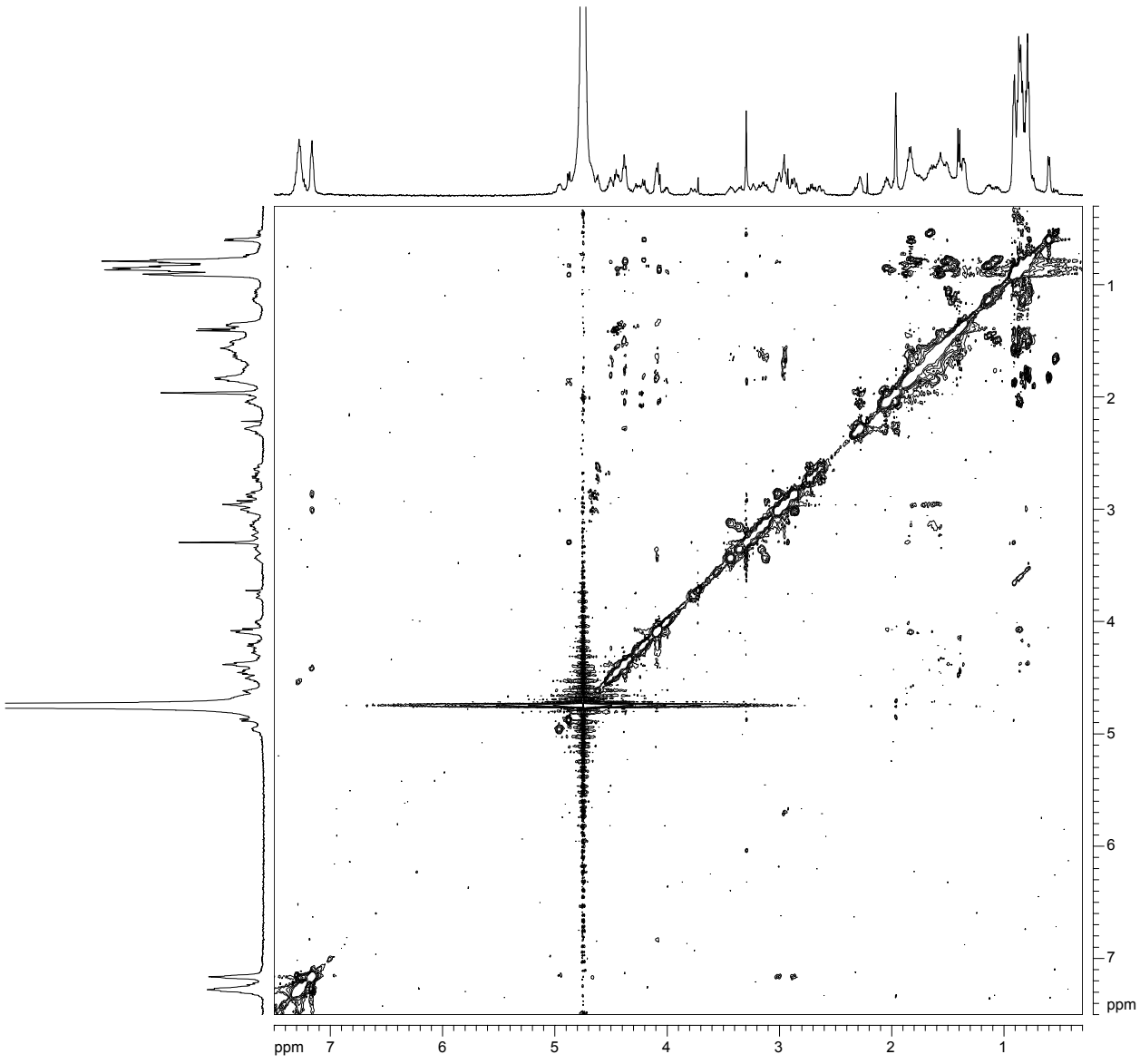

^{1}H NMR 2D ROESY of peptide **1$_{Orn}$** with presaturation suppression of the HOD peak
0.25 mM in D_2O at 500 MHz and 298 K with 150-ms spin-lock mixing time

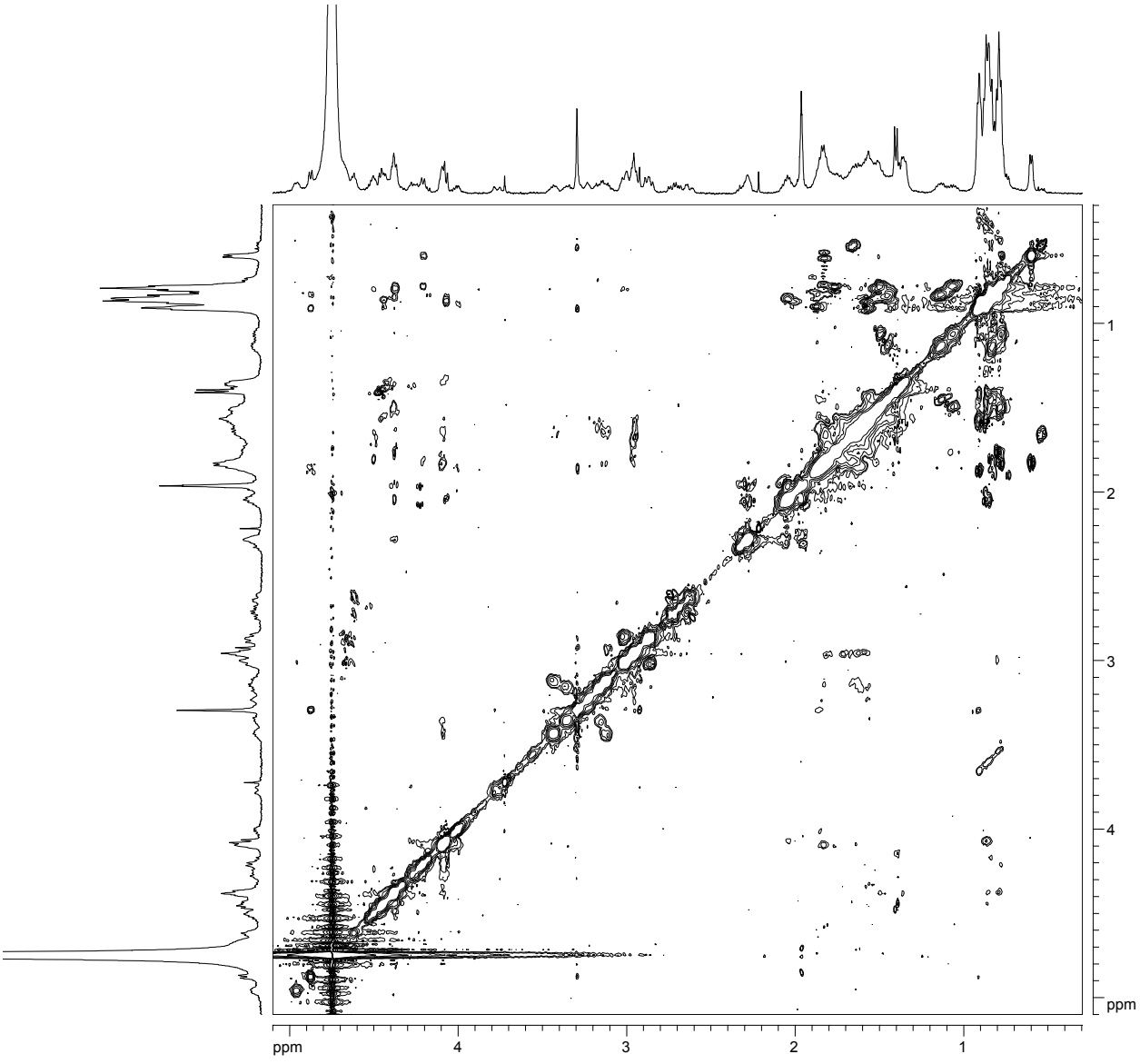

^{1}H NMR DOSY of macrocyclic β-sheet peptide **1$_{Orn}$** at 500 MHz and 298 K
0.25 mM in 50 mM deuterioacetate buffer in D_2O

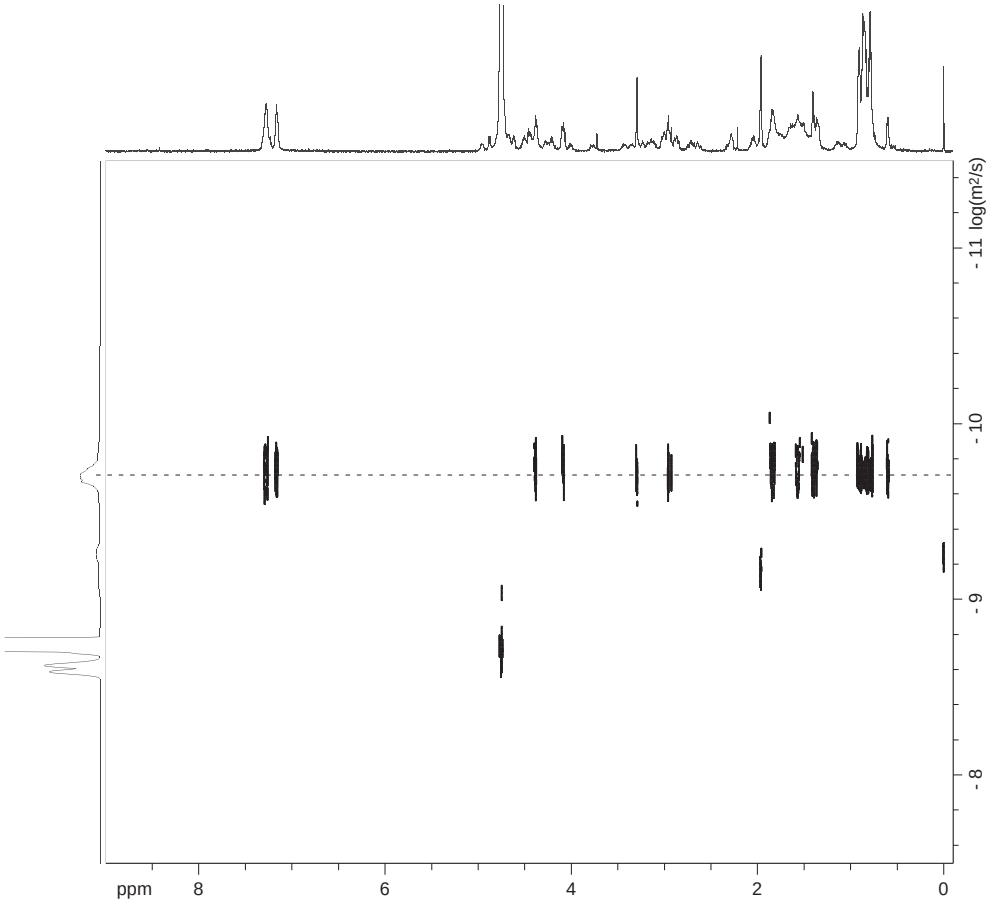

Calculations for macrocyclic β-sheet peptide **1$_{Orn}$** at 0.25 mM

D_{HOD} = 19.0 x 10^{-10} m^2/s [a]
log (D_{HOD}) = -8.721

$D_{monomer}$: log(D) = -9.69; D = $10^{-9.69}$ = 20.4 ± 1.0 x 10^{-11} m^2/s

[a]Longsworth, L. G. *J. Phys. Chem.* **1960**, *64*, 1914−1917.

^{1}H NMR DOSY of macrocyclic β-sheet peptide **1$_{Orn}$** at 500 MHz and 298 K
0.5 mM in 50 mM deuterioacetate buffer in D_2O

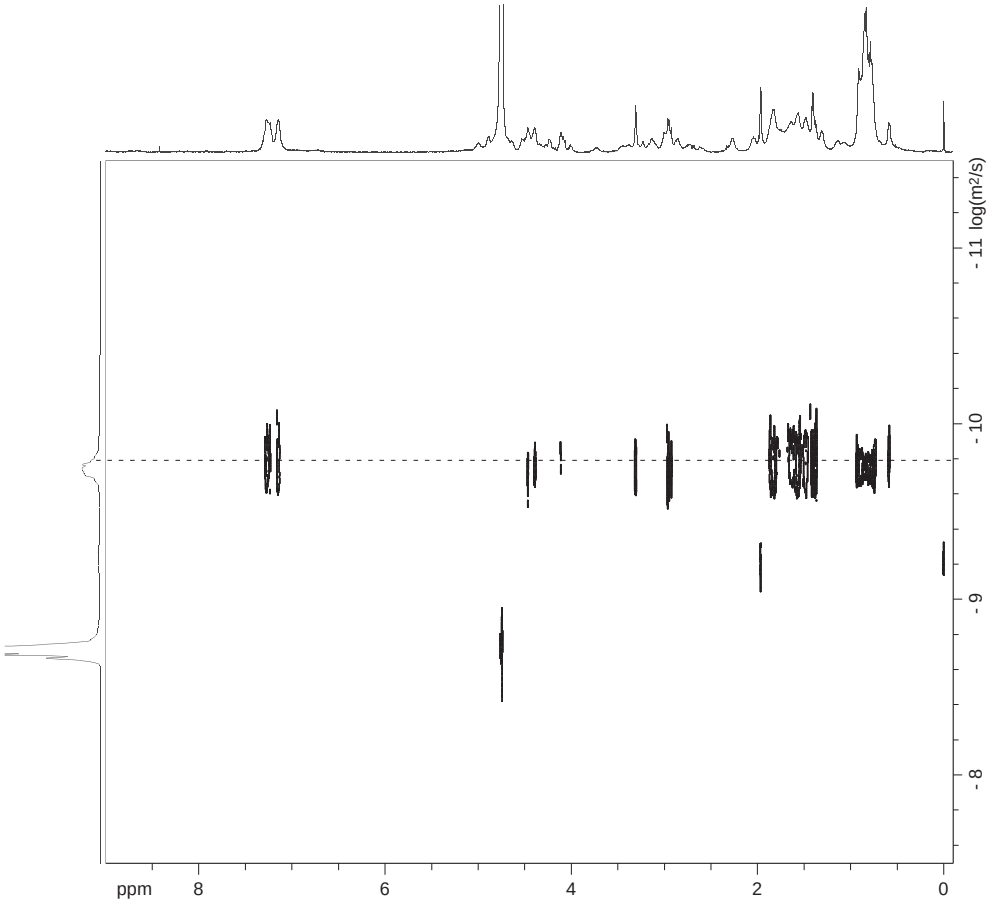

Calculations for macrocyclic β-sheet peptide **1$_{Orn}$** at 0.5 mM

D_{HOD} = 19.0 x 10^{-10} m^2/s [a]
log (D_{HOD}) = -8.721

$D_{oligomer}$: log(D) = -9.74; D = $10^{-9.74}$ = 18.2 ± 1.2 x 10^{-11} m^2/s

[a]Longsworth, L. G. *J. Phys. Chem.* **1960**, *64*, 1914−1917.

^{1}H NMR DOSY of macrocyclic β-sheet peptide **1$_{Orn}$** at 500 MHz and 298 K
2 mM in 50 mM deuterioacetate buffer in D_2O

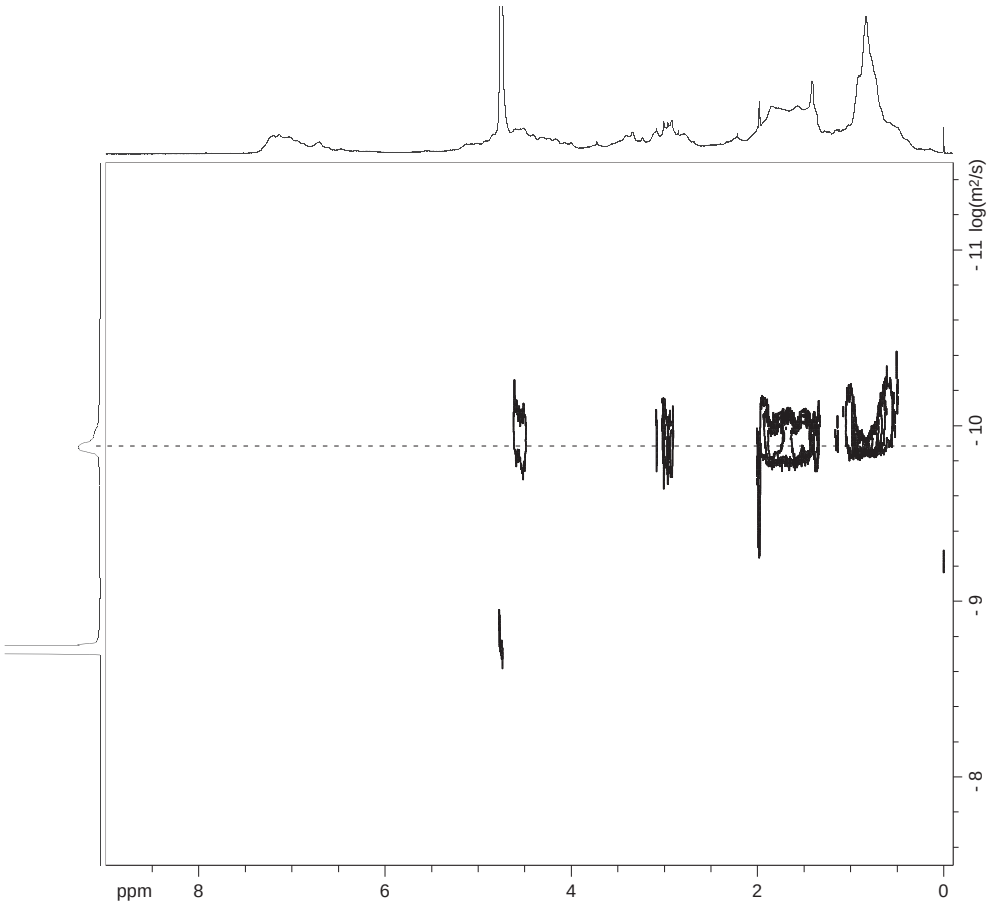

Calculations for macrocyclic β-sheet peptide **1$_{Orn}$** at 2 mM

D_{HOD} = 19.0 x 10^{-10} m^2/s [a]
log (D_{HOD}) = -8.721

$D_{oligomer}$: log(D) = -9.88; D = $10^{-9.88}$ = 13.2 ± 1.0 x 10^{-11} m^2/s

[a]Longsworth, L. G. *J. Phys. Chem.* **1960**, *64*, 1914−1917.

^{1}H NMR DOSY of macrocyclic β-sheet peptide **1$_{Orn}$** at 500 MHz and 298 K
4 mM in 50 mM deuterioacetate buffer in D_2O

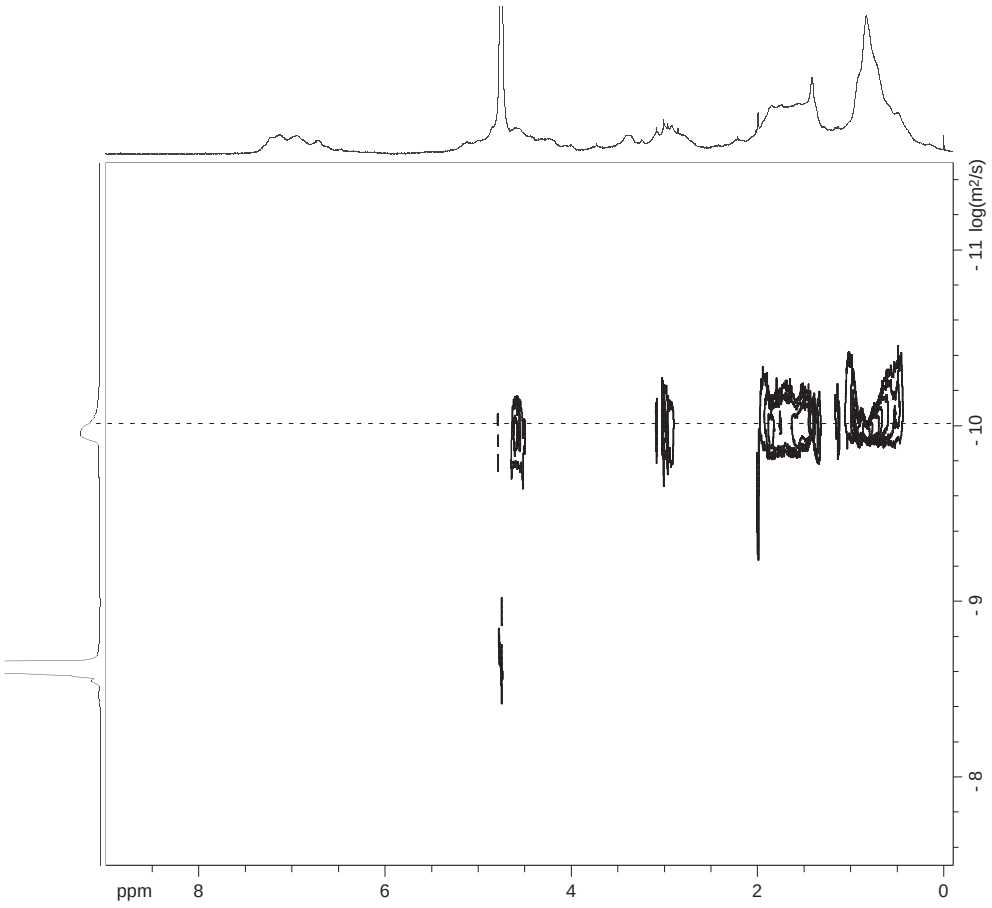

Calculations for macrocyclic β-sheet peptide **1$_{Orn}$** at 4 mM

D_{HOD} = 19.0 x 10^{-10} m^2/s [a]
log (D_{HOD}) = -8.721

$D_{oligomer}$: log(D) = -10.03; D = $10^{-10.03}$ = 9.3 ± 1.1 x 10^{-11} m^2/s

[a]Longsworth, L. G. *J. Phys. Chem.* **1960**, *64*, 1914−1917.

^{1}H NMR DOSY of macrocyclic β-sheet peptide **1$_{Orn}$** at 500 MHz and 298 K
6 mM in 50 mM deuterioacetate buffer in D_2O

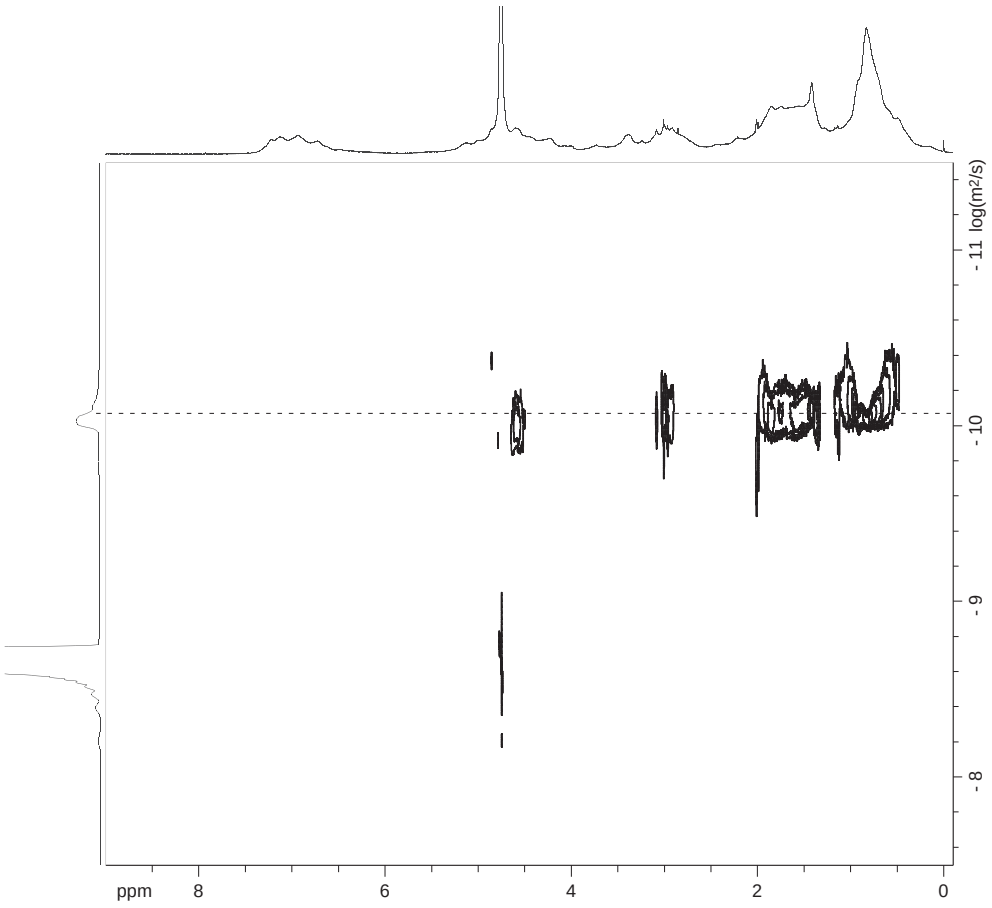

Calculations for macrocyclic β-sheet peptide **1$_{Orn}$** at 6 mM

D_{HOD} = 19.0 x 10^{-10} m^2/s [a]
log (D_{HOD}) = -8.721

$D_{oligomer}$: log(D) = -10.04; D = $10^{-10.04}$ = 9.1 ± 0.9 x 10^{-11} m^2/s

[a]Longsworth, L. G. *J. Phys. Chem.* **1960**, *64*, 1914−1917.

^{1}H NMR DOSY of macrocyclic β-sheet peptide **1$_{Orn}$** at 500 MHz and 298 K
8 mM in 50 mM deuterioacetate buffer in D_2O

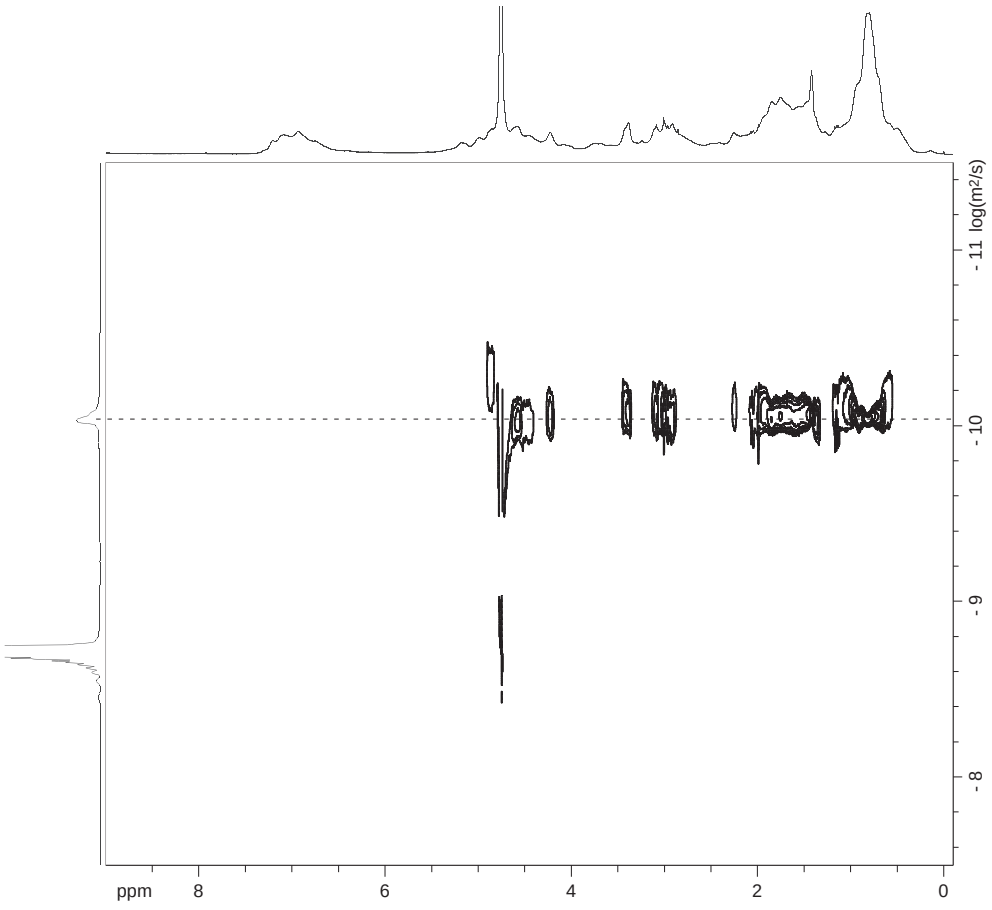

Calculations for macrocyclic β-sheet peptide **1$_{Orn}$** at 8 mM

D_{HOD} = 19.0 x 10^{-10} m^2/s [a]
log (D_{HOD}) = -8.721

$D_{oligomer}$: log(D) = -10.04; D = $10^{-10.04}$ = 9.1 ± 1.0 x 10^{-11} m^2/s

[a]Longsworth, L. G. *J. Phys. Chem.* **1960**, *64*, 1914−1917.

^{1}H NMR DOSY of macrocyclic β-sheet peptide **1$_{Orn}$** at 500 MHz and 298 K
16 mM in 50 mM deuterioacetate buffer in D_2O

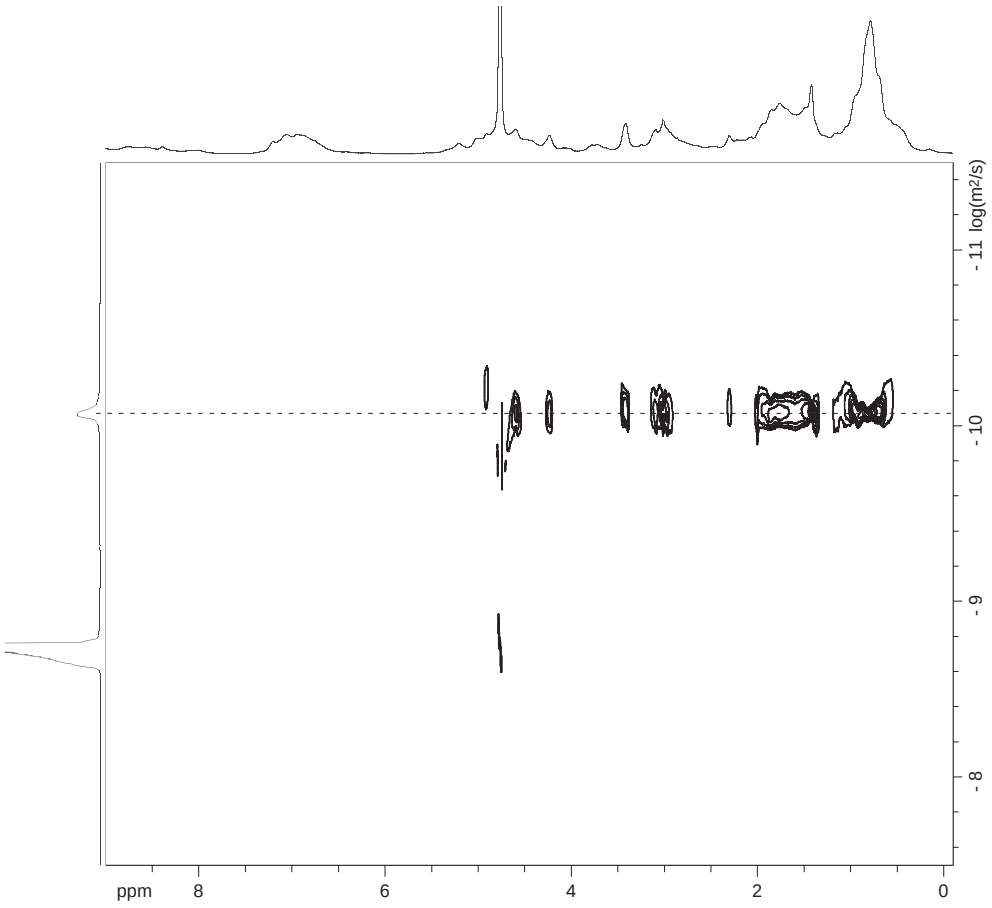

Calculations for macrocyclic β-sheet peptide **1$_{Orn}$** at 16 mM

D_{HOD} = 19.0 x 10^{-10} m^2/s [a]
log (D_{HOD}) = -8.721

$D_{oligomer}$: log(D) = -10.068; D = $10^{-10.068}$ = 9.1 ± 1.3 x 10^{-11} m^2/s

[a]Longsworth, L. G. *J. Phys. Chem.* **1960**, *64*, 1914−1917.

^{1}H NMR of trimer **2**, 0.15 mM in D_2O with 50 mM acetate buffer at 500 MHz and 293 K

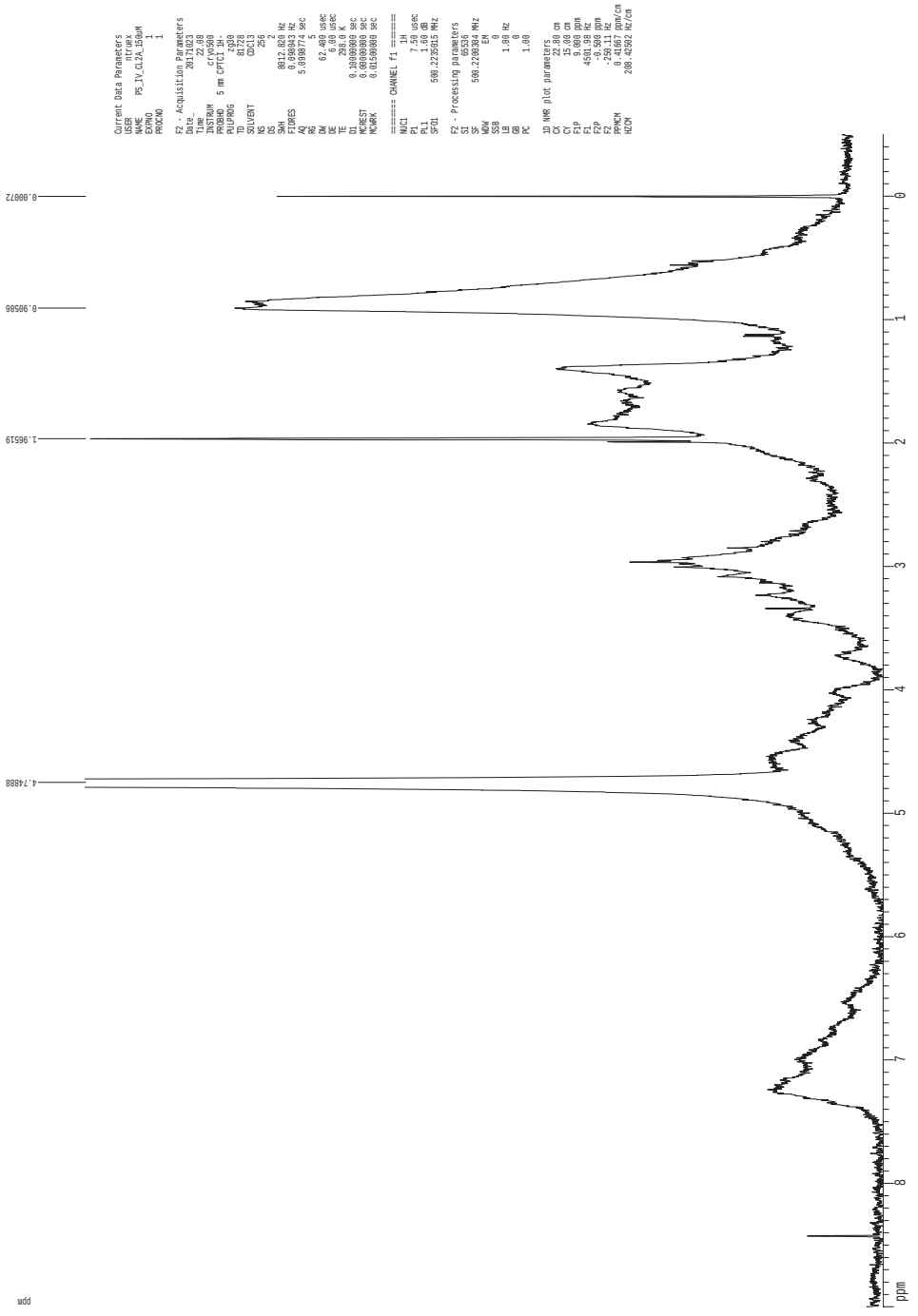

^{1}H NMR DOSY of macrocyclic β-sheet trimer **2** at 500 MHz and 298 K
0.15 mM in 50 mM deuterioacetate buffer in D_2O

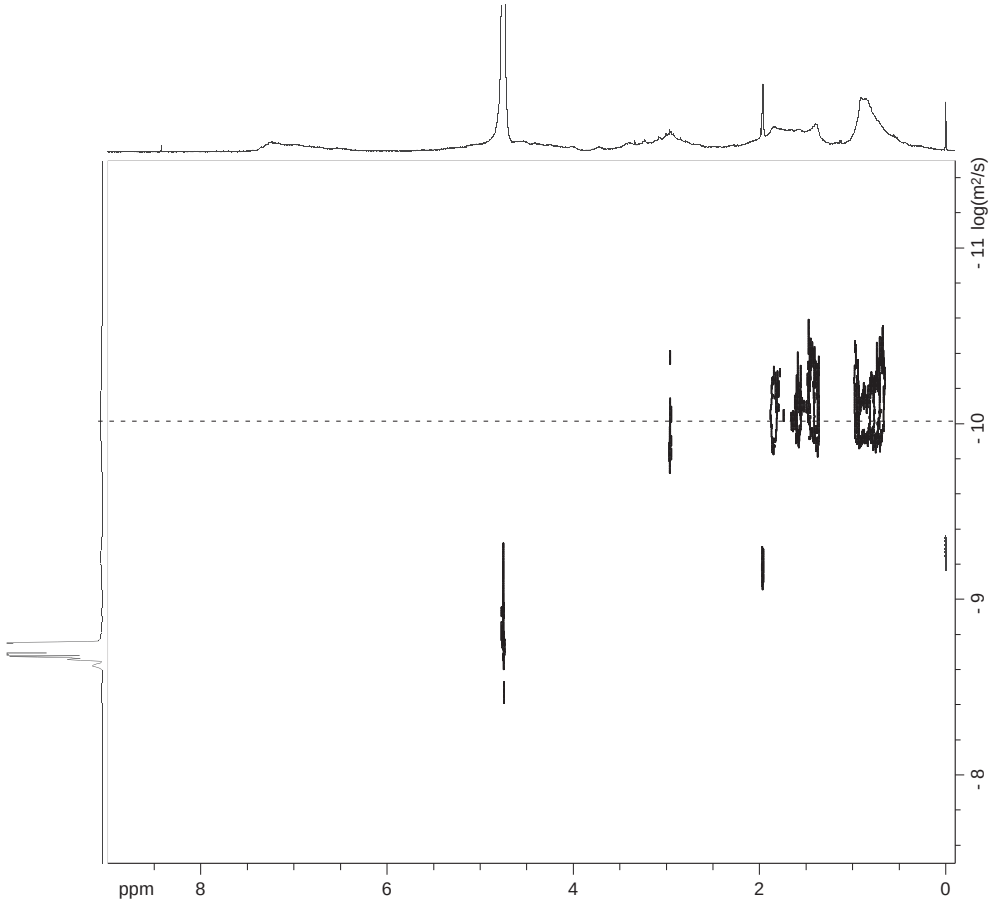

Calculations for macrocyclic β-sheet trimer **2** at 0.15 mM

D_{HOD} = 19.0 x 10^{-10} m^2/s [a]
log (D_{HOD}) = -8.721

$D_{oligomer}$: log(D) = -10.065; D = $10^{-10.065}$ = 8.6 ± 1.7 x 10^{-11} m^2/s

[a]Longsworth, L. G. *J. Phys. Chem.* **1960**, *64*, 1914−1917.

^{1}H NMR DOSY of macrocyclic β-sheet peptide **3** at 500 MHz and 298 K
8 mM in 50 mM deuterioacetate buffer in D_2O

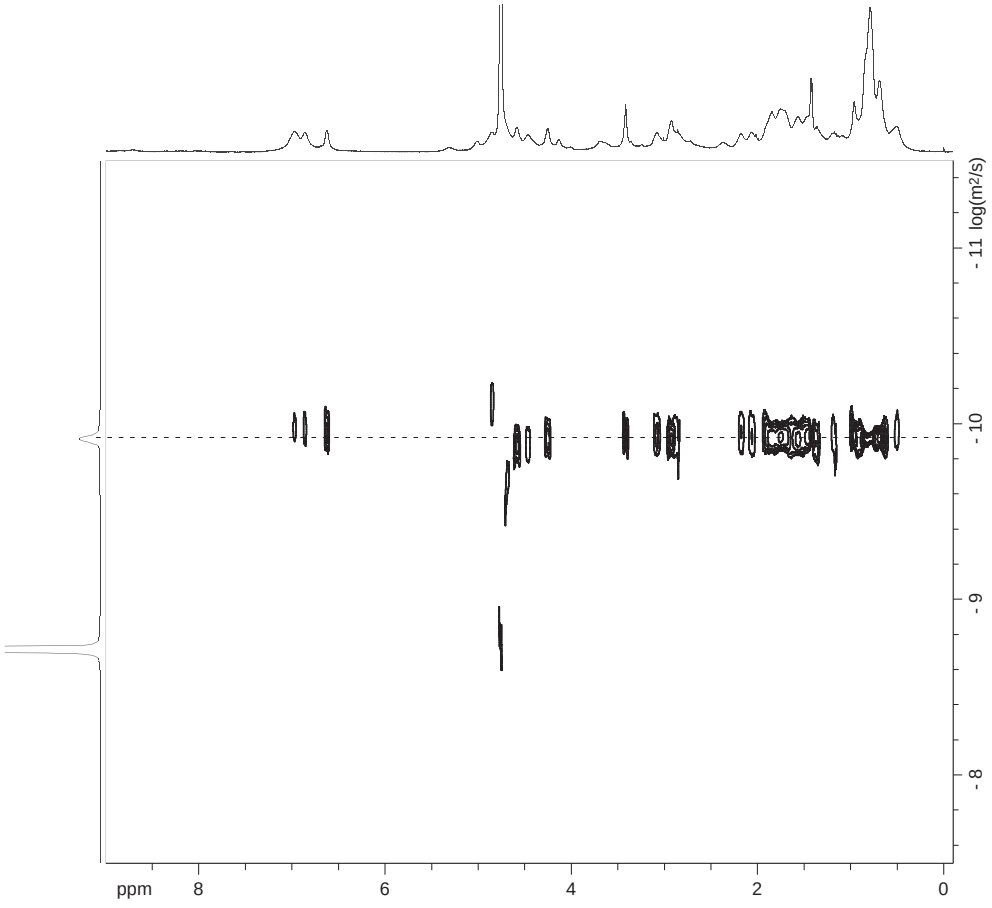

Calculations for macrocyclic β-sheet peptide **3** at 8 mM

D_{HOD} = 19.0 x 10^{-10} m^2/s [a]
log (D_{HOD}) = -8.721

$D_{oligomer}$: log(D) = -9.914; D = $10^{-9.914}$ = 12.2 ± 0.5 x 10^{-11} m^2/s

[a]Longsworth, L. G. *J. Phys. Chem.* **1960**, *64*, 1914−1917.

^{1}H NMR DOSY of macrocyclic β-sheet peptide **4** at 500 MHz and 298 K
8 mM in 50 mM deuterioacetate buffer in D_2O

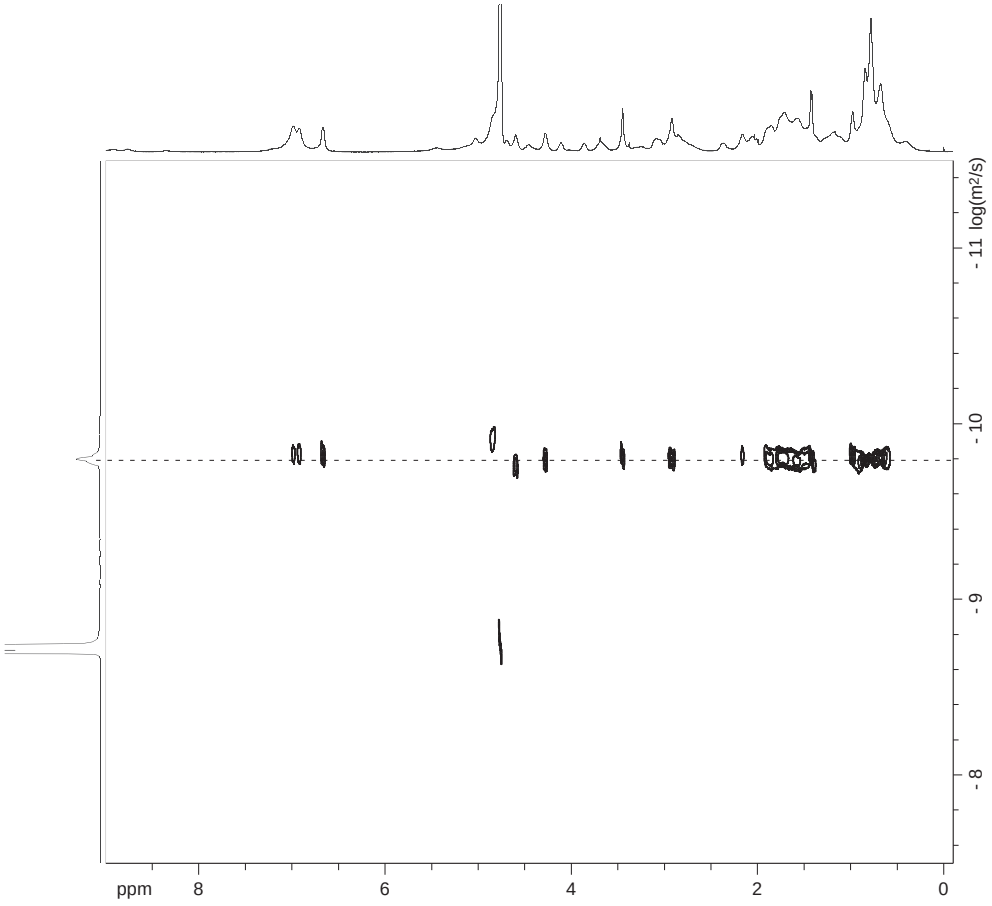

Calculations for macrocyclic β-sheet peptide **4** at 8 mM

D_{HOD} = 19.0 x 10^{-10} m^2/s [a]
log (D_{HOD}) = -8.721

$D_{oligomer}$: log(D) = -9.8; D = $10^{-9.8}$ = 15.8 ± 0.9 x 10^{-11} m^2/s

[a]Longsworth, L. G. *J. Phys. Chem.* **1960**, *64*, 1914−1917.